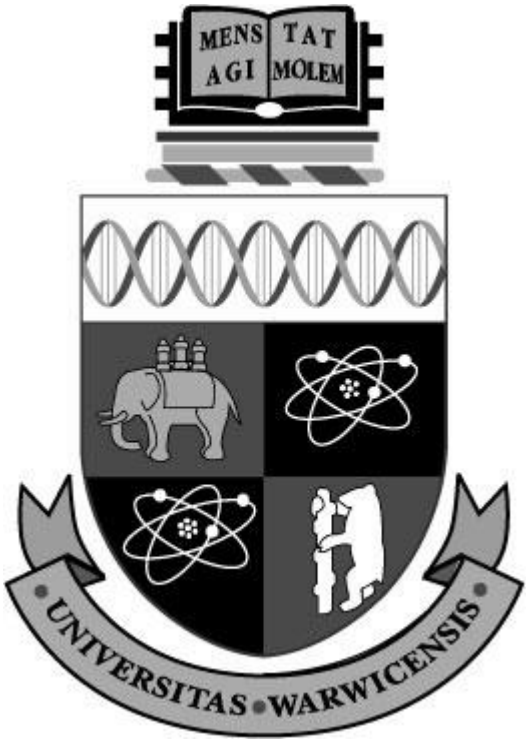

Adaptive Modulation Schemes for Optical Wireless Communication Systems

By

Yu Zeng

A thesis submitted in partial fulfilment of the requirements for the degree of

Doctor of Philosophy in Engineering

School of Engineering

University of Warwick

April 2010

Table of Contents

LIST OF ABBREVIATIONS

AIr	advanced infrared
AP	access point
APD	avalanche photodiode
AWGN	additive white Gaussian noise
BA	bandwidth allocator
BER	bit error rate
CDMA	code division multiple access
CRC	cyclic redundancy check
DFIR	diffuse infrared
DH-PIM	dual header pulse interval modulation
DR	data rate
DPPM	differential pulse position modulation
DAPPM	differential amplitude pulse position modulation
FC	fuzzy control
FCC	federal communications commission
FDMA	frequency division multiple access
FEC	forward error correction
FL	fuzzy logic
FLS	fuzzy logic system
EM	electromagnetic
FOV	field-of-view
FR	fuzzy rule
FS	fuzzy set
HP	hewlett-packard
HPF	high-pass filtering
i.i.d	independent and identically distributed
IM/DD	intensity modulation with direct detection
IR	infrared
IrDA	infrared data association
ISI	inter symbol interference
ISO	international organization for standardization
LAN	local area network
LED	lighting emitting diode
LO	logic operation
LOS	line-of-sight
MAC	medium access control
MAP	maximum a posteriory
MDPIM	Multilevel digital pulse interval modulation
MF	membership function
MPPM	multiple pulse position modulation
MPAPM	multiple pulse amplitude and position modulation
NRZ-OOK	none return to zero OOK

OOK	on-off keying
OW	optical wirless
PAPM	pulse amplitude and position modulation
PIN	the diode with an intrinsic layer between the P and N-type regions
PPM	pulse position modulation
QoS	quality of service
RC	repetition codes
RCPC	rate-compatible punctured convolution codes
RF	radio frequency
RS	reed-solomon
RZ-OOK	return to zero OOK
SNR	signal to noise ratio
SYNC	synchronization
TDMA	time division multiple access
TH	threshold detection
ToS	type of service
TSK	Takagi-Sugeno-Kang model
VoIP	voice over IP
XOR	exclusive or

LIST OF MATHEMATIC AND GREEK SYMBOLS

=	equal to
≠	not equal to
<	less than
>	greater than
≪	much less than
≫	much greater than
≤	less than or equal to
≥	greater than or equal to
∝	is proportional to
|...|	absolute value
!	factorial (e.g. $n!$ means the product $1 \times 2 \times ... \times n$)
~	probability distribution (e.g. X ~ D, means the random variable X has the probability distribution D).
≈	approximately equal
∵	because
∴	therefore
^	exponentiation
{,}	set brackets
{|}	set builder notation
∈	an element of
⊂	subset
⊃	superset
↔	if and only if
⊗	convolution
∑	summation
∏	product
∫	integral
$\bar{X}$	mean value of X
∞	infinity

$A_1,\ A_2$	constants that relate the interference amplitude to P_m
A_R	detector effective surface area
ΔA	reflector elements area
a	impulse response parameter
b_k	input bits
b_i	first amplitude parameters of low frequency components
C_{cs}	set of all possible chip sequences combinations
C_U^o	original upper bound of channel capacity
C_U	updated upper bound of channel capacity
C_L	updated lower bound of channel capacity
c	speed of light in vacuum

c_i	second amplitude parameters of low frequency components
D_j	reflector element treated as detector
D_{rms}	root mean square (RMS) delay spread
d_{Ej}	distance between source to element j
d_{jR}	distance between j to detector
d_{jj}	amplitude parameters of high frequency components
E_u	energy of minimal amplitude pulse
$\bar{E}$	average energy of one chip
f_h	fundamental frequency of the high frequency component
H	ceiling height
$h(t)$	channel impulse response.
$h^{(k-1)}$	previous $(k-1)$ impulse response between element j and D
h_k	channel impulse response of kth pulse
k	number of reflections on room surface
k_{ps}	length of previous sequence
L_{PAM}	amplitude order of PAM
L_{PPM}	pulse position number of PPM
M	number of amplitude levels of M-n-PAPM
M_{re}	number of reflector elements within detector FOV
M_{dr}	data set resolution number
$m(t)$	interference signal at the output of the photodiode
m	ambient light energy
N_0	power spectral density of the white Gaussian noise
N_{ti}	total number of input variables
n_{AWGN}	energy of the additive white Gaussian noise
n	pulse position numbers of M-n-PAPM
n_{rm}	radiation lobe mode number
$\hat{\boldsymbol{n}}_j$	normalised reflector orientation
$\hat{\boldsymbol{n}}_S$	normalised source orientation vector
$\hat{\boldsymbol{n}}_R$	normalised receiver orientation
$\bar{P}$	average transmitted optical power
P_m	average optical power of the interfering signal
P_j	optical power arrived on element j
P_S	total source optical power
P_{at}	average transmitted optical power
P_{ar-OOK}	average received optical power of OOK
$P_{success}$	probability of detection success
P_x	Gaussian normal distribution
$Q(x)$	customary Q-function of digital telecommunications
R	distance between the source and receiver
R_b	data rate
R_j	surface reflection pattern
R_{pr}	photodiode responsivity (A/W)
$R(\emptyset)$	optical power per unit solid angle originated from the source

$\mathcal{R}\{\}$	optical receiving element
$\boldsymbol{r}_S$	source position in three dimensional Cartesian coordinate
$\boldsymbol{r}_R$	receiver position in three dimensional Cartesian coordinate
$S\{\}$	optical source element
S_σ	optical signal to noise ratio
Δs	spatial resolution
s	optical signal power contribution
$\vec{\boldsymbol{s}}_j$	position vector of reflector j with area ΔA and FOV=90^o
T_c	time interval
$u(t)$	Heaviside unit step function
V_k	artificial light interference to signal power ratio
X	all possible chip sequences
$x(t)$	input optical power
$y(t)$	total photocurrent produced by the photodetector
z	energy accepted by the photodetector

$\emptyset$	angle between incident path and $\widehat{\boldsymbol{n}}_S$
$\emptyset_{s\widehat{\boldsymbol{n}}_S}$	angle between source $\widehat{\boldsymbol{n}}_S$ and $(\boldsymbol{r}_R - \boldsymbol{r}_S)$
$\emptyset_{Ej}$	emitting angles
θ	detector threshold
$\theta_{r\widehat{\boldsymbol{n}}_R}$	angle between receiver $\widehat{\boldsymbol{n}}_R$ and $(\boldsymbol{r}_s - \boldsymbol{r}_R)$
θ_{ji}	incident angles
θ_{jj}	phase parameters of high frequency components
δ	Dirac delta function
σ	Gaussian noise variance
ρ	surface reflection coefficient
ρ_j	reflection coefficient of surface j
$\mathcal{E}_j$	reflector element treated as emitter
ζ_i	first phase parameters of low frequency components
φ_i	second phase parameters of low frequency components
γ	fraction factor between RZ-OOK and NRZ-OOK
λ	ratio between peak and average intensity
β_k	pulse power after channel inference
μ_A	membership functions
π	ratio of a circle's circumference to its diameter

LIST OF FIGURES

CHAPTER 1

CHAPTER 2

CHAPTER 3

CHAPTER 4

CHAPTER 5

CHAPTER 6

LIST OF TABLES

ACKNOWLEDGEMENTS

I would like to thank my supervisors, Prof. Roger Green and Dr. Mark Leeson for their support and encouragement over the years. I wouldn't imagine what I can achieve without Prof. Roger Green and Dr. Mark Leeson. I would also like to thank Prof. Fary Ghassemlooy and Dr. Christos Mias to act as my external examiner and internal examiner. Thanks for the professional guidance you have provided during my examinations.

Thanks goes to the following people from the School of Engineering, University of Warwick for their assistance during my PhD: Dr. Zur Abu Bakar, Dr. Loh Tianhong, Dr. Roberto Ramirez-Iniguez, Dr. Xiaoming Jian, Dr. Lei Sun, Dr. Lei Xue, Dr. Philip Shepherd, Dr. Dean Hamilton and Mr. Shaobo Sun, Dr. Matthew Higgins, Miss Harita Joshi, Mr.Bo Zhao, Ms. Yanling Zhai for being my group mates and all the fruitful discussions.

Special thanks go to all my friends, who have supported me thought the easy and hard times, especially Jackie Cai. Last, I would like to thank for my parents, for their understanding, patience and continues support during my years at Warwick, who make it possible for me to complete this PhD.

DECLARATION

This thesis is presented in accordance with the regulations for the degree of doctor of philosophy. All work reported has been carried out by the author unless otherwise stated. This thesis has not been submitted for a degree at another university.

LIST OF PUBLICATIONS

Journals:

1. H.F.Rashvand, Y.Zeng, R.J.Green and M.S.Leeson, "Lookup Table Error Correcting Multiple Pulse PPM Codes for Wireless Optical Communication Channels" IET Communications Special Issue on Optical Wireless Communication Systems, Volume 2, Issue 1, pages 27-34, January 2008

2. Y.Zeng, R.J.Green, S.B.Sun and M.S.Leeson, "Tunable Pulse Amplitude and Position Modulation Technique for Reliable Optical Wireless Communication Channels" Journal of Communications, Academy Publishers, Vol. 2, No. 2, pages 22-28, March 2007

Conference:

1. Y.Zeng, R.J.Green and M.S.Leeson, "Multiple pulse amplitude and position modulation for the optical wireless channel" the IEEE ICTON 2008 10th International Conference on Transparent Optical Networks, Volume 4, pages 193-196 (We.C4.4), Athens, Greece, June 22-26, 2008

2.. Y.Zeng, R.J.Green and M.S.Leeson, "Adaptive Pulse Amplitude and Position Modulation for Optical Wireless Channels" at the The 2nd IEE International Conference on Access Technologies, pages 13-16, Abington Hall, Cambridge, UK, 21st to 22nd June 2006,

3. Y.Zeng, R.J.Green, "Modulation Adaptive System for Wireless Infrared Channels" at the 5th annual Postgraduate Symposium on the Convergence of Telecommunications, Networking and Broadcasting (PGNET 2004), pages 74-77, University of Liverpool, Liverpool, UK, 28-29 June 2004

Abstract

High-speed wireless optical communication links have become more popular for personal mobile applications. This is a consequence of the increasing demand from the personal information service boom. Compared to the radio frequency domain, optical wireless communication offers much higher speeds and bit rates per unit power consumption. As stated by the official infrared standard IrDA optical communication enjoys much lower power consumption than Bluetooth, with an inherent security feature while in Line of Sight (LOS) applications. There are also drawbacks such as the infrared radiation cannot penetrate walls as radio frequencies do and interference from the background contribute to the channel dispersions.

Focus on the modulation aspects of the optical wireless communication, this thesis try to improve the channel immunity by utilising optimised modulation to the channel. Modulation schemes such as on off keying (OOK), pulse amplitude modulation (PAM) and pulse position modulation (PPM) and pulse position and amplitude modulation PAPM schemes have been validated. The combined power and bandwidth requirements suggest that the adaptive modulation schemes can provide reliability when deployed in a real time channel, resulting in improved system performance.

As a result, an adaptive modulation technique is proposed. Extensive simulations of severe noise distraction have been carried out to validate the new scheme. The simulation results indicate that the new scheme can provide increased immunity against channel noise fluctuation at a relatively low complexity. The scheme obtained formed a basis to support reliable mobile optical wireless communication applications.

The adaptive scheme also takes the real time channel conditions into account, which is different from existing schemes. Guaranteed system performance can be secured without compromising power and bandwidth efficiency. This is also a new approach to realise reliable optical wireless links. Fuzzy logic control module has been developed to match the adaptive pattern.

Chapter 1

Introduction

1.1 Overview

The increasing demand for bandwidth had driven researchers to explore new technologies to accommodate more data throughput over the decades [1-7]. As the conventional radio frequency (RF) domain becomes heavily congested, the search for an alternative information transmission medium took priority [8-10]. Optical wireless communication attracted considerable attention from the academic community [10-14]. Starting from short distances and low speed experimental links, the optical wireless communication domain became a viable addition to communication systems, and showed promising prospects [15-21]. Suggested by

diverse application requirements, the future communication framework can benefit from a combined RF and optical infrastructure [22].

In optical communications, there were two mainstream areas: fixed optical fibre and free space optical (FSO) links. The former found most applications in long distance communications. For example, the optical fibres with attenuation less than 20dB/km were demonstrated in 1970 [23]. Optical fibre gradually replaced copper wire in consumer markets; service providers, such as the Internet service providers (ISPs), cable television (CATV), and telephone companies already utilised it widely [24]. To deliver the required connectivity, these service providers faced challenges in reaching the individual customers, namely the 'last mile' problem [25].

Several solutions were suggested, including worldwide interoperability for microwave access (WiMAX), power line communication (PLC) and line of sight (LOS) optical links [26-28]. The maximum data throughput was certainly limited by the available bandwidth. Especially within an office environment, different devices need as much bandwidth as possible, whilst also being vulnerable to severe interference.

The free space optical wireless link mainly been applied in short range (less than 2 kilometres) and inter-building data connections complementary to existing RF networks. Although challenged by several competitive RF bands, including the industrial, scientific and medical (ISM) radio bands, and the local multipoint distribution service (LMDS) bands [29], optical wireless showed the promising

features of higher data throughput and immunity to the interference usually suffered by RF systems. Table 1.1 presented a comparison of ISM, LMDS and optical wireless systems [30].

Table 1.1. Comparison of ISM, LMDS and FSO systems
(table adapted from [30])

System	**ISM Band**	**LMDS**	**Optical Wireless**
Frequency	2.4GHz	24-40GHz	30-60THz
Licensed	No	Yes	No
Multipoint Topology	Omni or Sectored	Omni or Sectored	Virtual Multipoint
Cell Radius	8-15km	2-3km	1-2km
Downstream Bandwidth	3-8Mbps per sector (per frequency)	155Mbps per sector	1.5Gbps per user
Upstream Bandwidth	3Mbps peak per user	3-10Mbps per user	1.5Gbps per user
Symmetric	No	No	Yes
Protocol Independence	No	No	Yes
Fade Mechanism	Heavy Rain	Rain	Thick Fog, Snow
Initial Investment for few subscribers	High	High	Low
Investment for 50-100 subscribers per cell	Medium	Medium	Medium

From the above table, the optical wireless (OW) channel surpassed the RF system in following aspects: the downstream bandwidth per user/sector/frequency of OW system was nearly 10 times that of the LDMS system and up to 500 times that of the ISM system. The upstream bandwidth was similar to that of the downstream bandwidth. In the cell radius comparison, the OW system provided the shortest distance coverage, where ISM and LDMS systems can achieve a range which as 7.5 and 1.5 times further than the OW system respectively. Noticeably, weather conditions had an impact on the reliability of the channel, which could affect the transmission data rate.

The presence of bandwidth limitations resulted in the need for significant contributions by means of information processing procedures, which suggested that effective modulation techniques was the key to achieve higher transmission throughput. Reliability issues were also considered vital for established

connections. Thus, the communication system can be treated as a multi-task process; the resulting system model depended on the key requirements posed by different situations.

To summarise, this chapter narrowed down the discussion from general communication knowledge to the motivation behind this PhD project. It provided the background to the key challenges arising from the literature review and explained the methodologies used to obtain simulation results.

1.2 Optical Wireless Communication

The origin of optical wireless communication can be traced back to ancient times when fire beacons were used to transmit simple message over long distances [21]. It was the pioneering research work done by F.R.Gfeller and U.Bapst in 1979 that inspired the technical community to explore further the potential of the indoor optical wireless communication [10].

In comparison to RF, optical wireless communication enjoyed benefits such as: lower implementation cost, higher security, unregulated spectrum and operational safety. On the other hand, the channel can be severely interfered with by background noise: shot noise induced by the background ambient light (radiation from the sun if the system operated near a window or outside) and the interference induced by artificial light sources [31]. (See Table 1.2 for a comparison between RF and IM/DD infrared systems for indoor wireless communications [15]). IR systems can suffer from multipath distortion (in a diffuse system). In comparison, though, directed line-of-sight (LOS) IR systems had the potential to achieve a data

rate of a few gigabits per second and higher [32]. More details of the channel type were discussed in Chapter 2.

Table 1.2 Comparison between radio and IM/DD infrared systems for indoor wireless communications (table adapted from [15])

Property of Medium	Radio	IM/DD Infrared	Implication for IR
Bandwidth Regulated?	Yes	No	Approval not required. Worldwide compatibility
Passes Through Walls?	Yes	No	Less coverage.
			More easily secured. Independent links in different rooms.
Multipath Fading?	Yes	No	Simple link design.
Multipath Distortion?	Yes	Yes	
Path Loss	High	High	
Dominant Noise	Other Users	Background Light	Limited range.
Input X(t) Represents	Amplitude	Power	Difficult to operate outdoors
SNR Proportional to	$\int \lvert X(t)\rvert^2 \, dt$	$\int \lvert X(t)\rvert^2 dt$	High transmitter power requirement.
Average Power Proportional to	$\int \lvert X(t)\rvert^2 dt$	$\int X(t) dt$	Choose waveform X(t) with high peak-to-average ratio.

Apart from points listed in Table 1.2, another benefit to use IR over RF was from the health concerns. Side effects caused by exposure to electromagnetic (EM) radiation were still ongoing research topics [33]. Since human nervous system receive and interpret information via electrical signals [34], possible carcinogenic, reproductive and neurological effects may indeed develop due to exposure to intense EM radiations [35].

Since the 90s, extensive research efforts had been focused on improving the channel performance. This included modulation [36-43], coding and equalization [44-47], diversity detection [48-50], multiple access [51], channel characterization and modelling [52, 53], optical component design [54-56], prototype communication links [16, 57, 58] etc. There were activities also welcomed by the beginning of the official interest group, the Infrared Data Association (IrDA) in

1993 [32]. The IrDA had been influenced by industry partners in defining protocols and standards. One of the most challenging tasks was to increase the data rate of the IR link.

1.2.1 System Structure

Optical wireless communication systems consisted of a transmission unit and a receiving unit. In the transmission unit, a light emitting source (LED or LD) was modulated by a time-varying electrical current (EC) signals generated from the system input. In the receiving unit, photodiodes (PIN or APD) were used to generate EC signals according to the instantaneous optical power received from the EC signals of the transmission. Amplifier and filter modules were also used in both units to improve the system throughput and immunity to noise.

As discussed above, due to the physical properties of the link, most optical wireless systems employed intensity modulation and direct detection (IM/DD). Figure 1.1 showed a typical Infrared link using IM/DD [15]. $X(t)$ represents the instantaneous optical power from the emitter, $Y(t)$ indicates the instantaneous current generated by the photodetector. Since the surface of the photodetector was millions of square wavelengths at the received optical signal wavelength, the optical link will not suffer from multipath fading effects that usually experienced by the RF system [12].

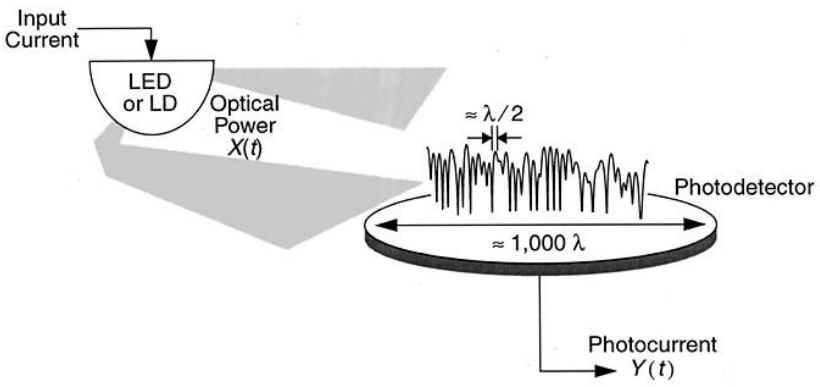

Figure 1.1 Transmission and reception in an infrared link with IM/DD (figure adapted from [12])

According to transmitter and receiver calibration, the optical link can be classified as LOS or diffuse (non-LOS). In LOS links, the transmitter and receiver were aligned to give the maximum power efficiency. Compared to the diffuse system, LOS offered higher transmission speed due to the lower path loss and narrow field of view (FOV) of the optical receiver [59]. The LOS system can also be deployed in outdoor applications. Although optical filters and perfect alignment were needed for the outdoor system, a commercial product, the CableFree Gigabit G1500™, can provide 1.5Gbps FSO link at a distance of 1.5Km [60]. The major drawback of LOS systems was that they were susceptible to physical blockage of the established links, and thus difficult to apply in mobility situations.

The diffuse link, on the other hand, can provide more robustness for the optical channel at a cost of reduced power and bandwidth efficiency. The transmitter and receiver in a diffuse system established a connection by reflecting light from the ceiling or other diffusely reflecting surfaces [15]. The users of a diffuse system need not consider the alignment between transmitter and receiver. A constant connection can be maintained, as long as the user was covered by the transmitter

signals illumination. The diffuse systems usually feature wide FOV receivers [61]. The first diffuse indoor diffuse Infrared wireless system was built by IBM in 1979, which achieved a data rate of 64kb/s and 125kb/s using phase shift keying (PSK), and baseband pulse code modulation (PCM), respectively [10]. A 50Mb/s diffuse link was achieved by researchers at Berkeley in 1994 which employed OOK modulation and a decision feedback equaliser to mitigate the inter symbol interference (ISI) [58].

According to orientation between the transmitter and receiver, the optical link can also be divided into 3 categories: Directed, Hybrid and Nondirected. The directed link refereed to the case when the transmitter and receivers were pointing in the same direction in a LOS or a diffuse (Non-LOS) system. A hybrid link can provide some degree of directionality but the receiver employed a wide angle FOV to receive the optical signal. In the nondirected scenario, both transmitter and receiver had a wide angle of FOV [15]. A detailed classification of optical wireless links can be seen in Figure 1.2.

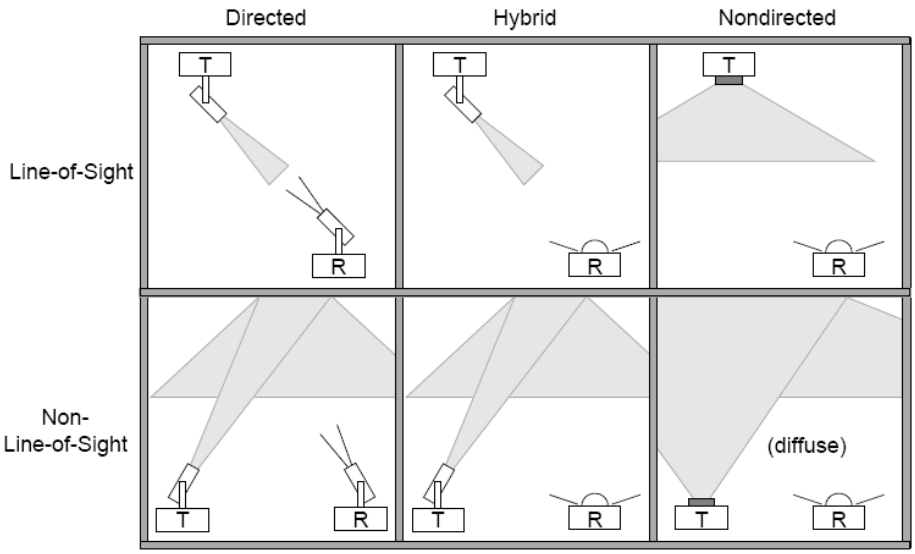

Figure 1.2 Classification of optical wireless link
(figure adapted from [15])

1.2.2 Optoelectronic Components

1.2.2.1 Transmitter Optical Component

As indicated in Figure 1.1, the transmitter of an optical wireless system usually included a LED or LD which typically operated in a wavelength range from 780 - 950 nm [21]. This was due to the availability of the majority low cost optoelectronic components which fell within this wavelength range. According to different requirements, the LED and LD can be applied to various optical wireless links. Sometime the LDs were preferred over LED, as LDs usually had higher optical power outputs, broader modulation bandwidth, and nowadays, fairly linear electrical to optical signal conversion above the lasing threshold. Linearity can help more sophisticated modulation schemes e.g. multi-subcarrier and multilevel modulations [62]. Due to eye safety, a LD can easily damage human eyes if used directly. In comparison, the LEDs were relatively safer to operate. More importantly, the cost of an LED was usually less than that of a LD, making it a

good choice for mass production and for quick adoption to the consumer market. Table 1.3 listed detailed comparisons between LEDs and LDs.

Table 1.3 Comparison of LEDs and LDs (table adapted from [15, 21])

Characteristic	LED	LD
Optical Spectral Width	25 – 100 nm	$<10^{-5}$ – 5 nm
Modulation Bandwidth	Tens of kHz to Hundreds of MHz	Tens of kHz to Tens of GHz
Special Circuitry Required	None	Threshold and Temperature Compensation Circuitry
Eye Safety	Considered Eye Safe	Must be Rendered Eye Safe
Reliability	High	Moderate
E/O Conversion Efficiency	10-20%	30-70%
Cost	Low	Moderate to High

1.2.2.2 Receiver Optical Component

The receivers in an optical wireless system adopted PIN diodes or avalanche photodiodes (APD). PIN diodes were employed in most applications, this was due to their low bias voltage requirements and tolerance to temperature fluctuations [63]. APDs were usually 10 to 15 dB more sensitive than PINs, and this came at the cost of high cost, high bias voltage requirements, and temperature-dependant gain [15].

1.3 Project Motivation

As mentioned earlier, the optical wireless channel was limited by channel constraints such as the maximum allowable optical power and available bandwidth. Modulation schemes well suited to conventional channel were not necessarily perform well for the optical wireless channel. In terms of combined power and bandwidth efficiency, on off keying (OOK), pulse amplitude modulation (PAM) and pulse position modulation (PPM) were found to be good candidates for the IM/DD model [12, 15]. Many modulation schemes were based

on the PPM, this including the multiple PPM (MPPM) [43], overlapping PPM (OPPM), differential PPM (DPPM) [37], differential amplitude PPM (DAPPM) [64], digital pulse interval modulation (DPIM) [65] and spectral efficient modulation scheme such as the adaptively biased QAM (AB-QAM) [66] and 2-Level 2-Pulse-Position Modulation (2L2PPM) [67] were reported.

The effects of ISI in diffuse links and the ambient light noise from background illumination need to be considered when validating performance of optical wireless systems [68, 69], which was usually ignored by most optical wireless system researchers for model simplicity. Although techniques such as the use of equalisation filters can be effective to reduce the ISI, yet were not optimised for dynamic ISI interference, and usually came at cost of system complexity [12, 70].

In order to maintain the channel throughput under combined channel impairments, an adaptive pulse amplitude and position modulation scheme was proposed [71]. The resulting modulation system can utilise pulse amplitude and position adaptation according to system requirements. This had shed some light on actively employing modulation techniques to combat channel degradation. Simulation and analysis results had shown the proposed adaptive modulation scheme can provide excellent solutions for improving channel throughput and can maintain system reliability under interferences. A fuzzy logic control module were developed to assist the adaptation process, the control process was simpler compared to other artificial control techniques. Yet the obtained model was extremely efficient in control pattern recognition through training.

1.4 Thesis Structure

This thesis was organised as follows:

The first chapter was the introduction, mainly providing the background and a literature review on related topics. It also suggested the main problem to be solved throughout the thesis, and discussed the possible solutions.

The second chapter concentrates on the channel models and channel interference. Channel topologies together with artificial light model were discussed. Two major types of noise source: the ISI caused by multipath dispersion and background ambient light noise interference introduced by artificial light source were analysed. Mathematic expressions and quantified noise parameters were discussed and derived.

The third chapter began with the analysis of popular modulation schemes that had been selected as candidate schemes for optical wireless communications. The combined power and bandwidth properties, signalling structures and error performance were covered. This also prepared the backgrounds for Chapter 4.

The fourth chapter discussed the proposed adaptive modulation scheme. Comparisons with other modulation schemes were demonstrated, e.g. the combined power and bandwidth performance, the transmission data error rate under constant power and eye safety constraints. Moreover, the data rate recovery ability, under moderate and severe channel conditions, was further investigated.

The fifth chapter addressed the application of fuzzy logic control concept for the adaptive modulation. Followed by brief introductions of the artificial intelligence, the control algorithms were explained. Example fuzzy inference models were constructed. Adaptive neuro-fuzzy inference system (ANFIS) models were also developed for the control pattern recognition.

The sixth chapter looked into the reliability issues of the optical channel. Adaptive modulation schemes under combined channel interference were further demonstrated by using the fuzzy logic control technique, the resulting system had shown the capability of maintaining system stability under either or both of the two types channel interferences induced by multipath ISI and background ambient light.

The seventh chapter covered the conclusions and suggestions for future work. Important results and methodology obtained from previous chapters were summarised, and the possibilities for future directions were discussed.

Chapter 2

Channel Model

2.1 Introduction

The appropriate channel model for the optical wireless system depends on the relative background optical noise levels where the system was deployed [12, 52,

72]. In the case of low background interference, the channel can be modelled by a Poisson process. This was due to the random nature of the photons emitted from the light source. When the background noise was high enough and comparable with the optical signals, (in some cases this referred to optical signals other than the source which operating at the same wavelength) the channel can be approximately modelled by an additive white Gaussian noise (AWGN) model [15]. The exact channel model can be approached by combining both Poisson and Gaussian distribution contributions. To obtain the combined formula, one key step was to calculate the summation of Poisson and Gaussian stochastic variables. The probability density expression for such a sum was easy to write down, but as it contained an infinite summation, which made it numerically impractical [72].

As discussed in Chapter 1, the optical wireless channel was an intensity modulation and direct detection (IM/DD) channel. The typical optical wireless system structure can be found in Figure 2.1.

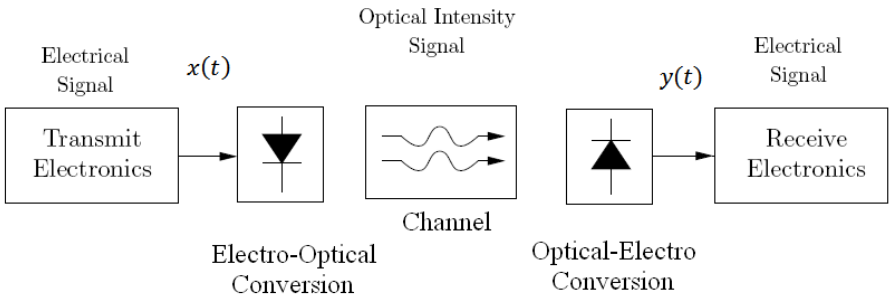

Figure 2.1 Optical wireless system diagram (figure adapted from [21])

The equivalent channel model can be illustrated in Figure 2.2, where $x(t)$ is the input optical power, and $y(t)$ is the total photocurrent produced by the

photodetector, R_{pr} is the responsivity of the photodiode, and $h(t)$ is the channel impulse response.

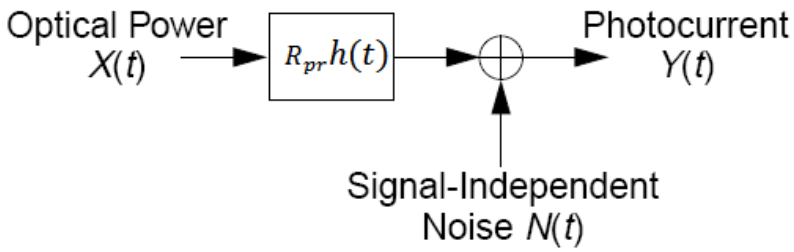

Figure 2.2 Equivalent channel model (figure adapted from [12])

Using the Gaussian model, the output current at the receiver $y(t)$ was given by:

$$y(t) = R_{pr}\, x(t) \otimes h(t) + n(t) \tag{2.1}$$

Where the symbol "⊗" denotes convolution, since the optical signal was non-negative and the average transmitted optical power P_{at} must be constrained due to eye and skin safety, so $x(t)$ must satisfy the following:

$$x(t) \geq 0\,, \qquad \lim_{T\to\infty} \frac{1}{2T} \int_{-T}^{T} x(t)dt \leq P_{at} \tag{2.2}$$

These constraints greatly influenced the choice of signal design, channel model and modulation selection. Note that in equation (2.2) the input $x(t)$ represented power, not amplitude. This was different to the conventional RF wireless channel, where the power $\int x^2(t)dt$ thus the mean square of the signal amplitude of the channel input was limited. These unique constraints made the wireless Infrared

channel distinguished from the conventional linear Gaussian noise channel. The resulting channel combines the filtered Gaussian noise characteristics of conventional wire based channels with the IM/DD constraints of fibre-optic systems [12]. Modulation schemes that were well suited to the conventional channel may not be strong candidates for wireless optical channels. More details on modulation will be discussed in Chapter 3.

2.2 Literature Review

2.2.1 Channel Capacity

The channel capacity was the highest rate in bits per channel use at which information can be sent with arbitrarily low probability of error [29]. The capacity of discrete-time memoryless channel subject to various input constraints had been studied followed by Shannon's information theory [73]. The most common input constraints for the optical wireless channel were average power and bandwidth. Since the early work of Gfeller into the optical wireless communication [10], the capacity of the optical wireless communication channel had been an attractive topic [12, 15, 74-76]. Recently a tighter higher and lower bound were reported for the low signal to noise power (SNR) case [77]. Figure 2.3 showed the lower and upper bounds together with L-PAM modulation with L= 2, 4 and 8, where C_U^o, C_U and C_L were the original upper bound, updated upper and lower bound respectively.

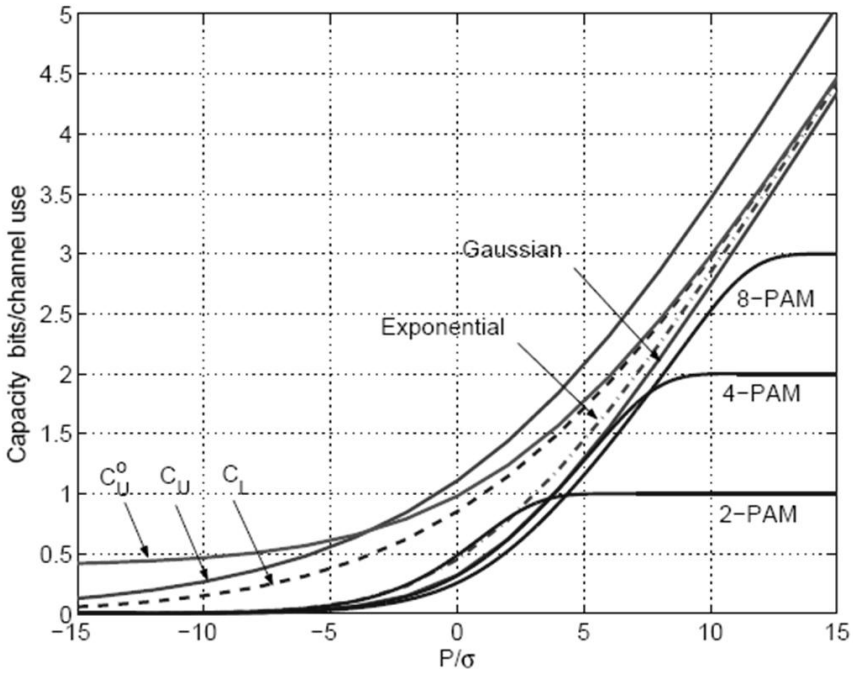

Figure 2.3 Capacity bounds and mutual information for continuous one-sided exponential, Gaussian and discrete uniform PAM (figure adapted from [77])

The capacity bound for L-PPM modulation had also been demonstrated in [78]. Figure 2.4 showed the capacity bounds for L-PPM modulation on AWGN channel using the Monte Carlo method, where L took the value from 2 up to 256.

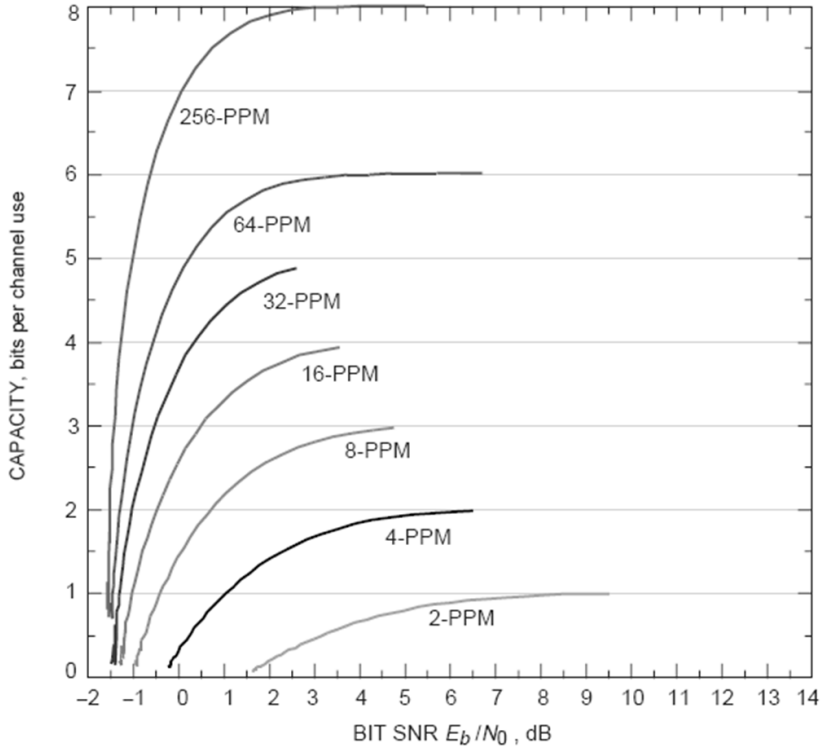

Figure 2.4 PPM capacity on the AWGN channel, determined by Monte Carlo simulation (figure adapted from [78])

From Figure 2.3 and Figure 2.4, the achievable capacity bound increased with the modulation order.

2.2.1.1 Eye Safety

One main constraint of the optical wireless channel came from the eye and skin safety regulations. As in all light wave communications, the optical wireless channel exhibited a potential danger of eye hazard when the optical energy of the transmission signal exceeds certain levels. There were several international organizations that had published eye safety regulations to protect people from eye injury while operating high energy optical sources. These included the International Electrotechnical Commission (IEC) based in Switzerland and the

American National Standards Institute (ANSI) in the America. Potential damages caused by different wavelength laser can be found in Table 2.1 [79].

Table 2.1 Types of radiation and their likely effects on the human eye (table adapted from [79])

Name	Wavelength	Eye Damage	Example of Laser Type
Ultra-Violet 'C'	100 – 280 nm	Cornea	Argon Fluoride 193 nm
Ultra-Violet 'B'	280 – 315 nm	Cornea	
Ultra-Violet 'A'	315 – 400 nm	Cornea & Lens	Nitrogen 337 nm
Visible	400 – 760 nm	Cornea & Retina	Ruby 694nm (Red)/ Helium/Neon 633 nm (Red). Neodymium YAG Freq Doubled 532 nm (Green). Argon 485-515 nm (Blue-Green)
Infra-Red 'A'	760 nm – 1.4 μm	Cornea & Retina	Gallium Arsenide, 850 nm Neodymium YAG 1.064 μm
Infra-Red 'B'	1.4 - 3.0 μm	Cornea	Erbium, 1.612 μm
Infra-Red 'C'	3.0 μm - 1mm	Cornea	Carbon Dioxide (CO_2), 10.6 μm

2.2.1.2 Classes of Lasers

Laser sources were classified, for simplicity, into four classes from I to IV. Table 2.2 showed the different classes, and the definition of each class was described below [13]:

Table 2.2 Laser safety classifications for a point-source emitter (figure adapted from [13])

	650 nm (visible)	880 nm (infrared)	1310 nm (infrared)	1550 nm (infrared)
Class 1	Up to 0.2 mW	Up to 0.5 mW	Up to 8.8 mW	Up to 10 mW
Class 2	0.2 – 1 mW	N/A	N/A	N/A
Class 3A	1 – 5 mW	0.5 – 2.5 mW	8.8 – 4.5 mW	10 – 50 mW
Class 3B	5 – 500 mW	2.5 – 500 mW	45 – 500 mW	50 – 500 mW

Class I was the lowest class of laser and lasers in this class were believed to be unable to cause eye damage even when shone directly into the eye for an extended

period of time. Class II lasers emited low-power, visible radiation that probably cannot cause damage within 0.25 seconds if shone directly into the eye. Class III lasers were those that can create a hazard in less than 0.25 seconds. These can cause permanent damage to the naked eye. Class IV lasers had such high power levels that they can create dangerous levels of radiation even after reflection from dull surfaces [79].

2.2.2 Channel Topologies

Following the discussions in Chapter 1, different channel topologies can be approximated by mathematical models. LOS and diffuse models were discussed in this section. In respect to the IR channel modelling, Gfeller and Bapst first treated the diffuse IR link as a ceiling illumination model, and indicated that the received optical power was independent of position and angular orientation of the photodetector [10]. Analysis for double reflection was reported by Hash *et al* [80]. Barry extended the simulation model to count for any number of reflections [81].

The Lambertian model was usually adapted as the propagation model used to model the wireless optical channel. The optical source (transmitter) can be modelled by the following [12]:

$$R(\emptyset) = \frac{n_{rm}+1}{2\pi} P_S cos^{n_{rm}}(\emptyset), \quad \emptyset \in [-\frac{\pi}{2}, \frac{\pi}{2}] \tag{2.3}$$

$R(\emptyset)$ is defined as the optical power per unit solid angle originated from the source with unit source orientation vector $\hat{\boldsymbol{n}}_S$, P_S is the total source optical power, n_{rm} is the radiation lobe mode number, the source radiation pattern become more

directional when n_{rm} increases, this can be observed in Figure 2.5. $\emptyset$ is the angle between incident path and normalised source orientation $\hat{\boldsymbol{n}}_S$. Figure 2.5 showed a typical relationship between source and the receiver. The source and receiver can be denoted using their parameters $S = \{\boldsymbol{r}_S, \hat{\boldsymbol{n}}_S, n_{rm}; P_s\}$, $\mathcal{R} = \{\boldsymbol{r}_R, \hat{\boldsymbol{n}}_R, \mathrm{A}_R, \mathrm{FOV}\}$. S and $\mathcal{R}$ are optical source and receiving element respectively, Where $\boldsymbol{r}_S$ and $\boldsymbol{r}_R$ is source and receiver position in three dimensional Cartesian coordinate with $[x, y, z]$. $\hat{\boldsymbol{n}}_R$ is the normalised receiver orientation, A_R is detector effective surface area, FOV is detector field of view.

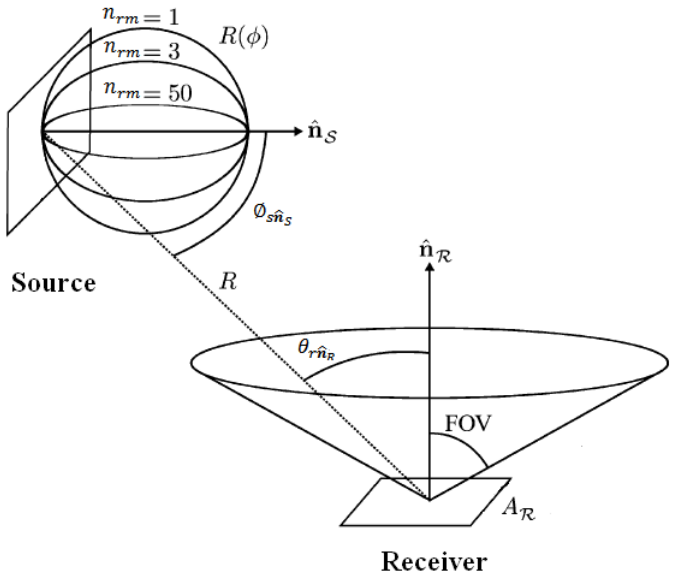

Figure 2.5 Geometry of optical source and detector
(figure adapted from [50])

2.2.3 Propagation Model

Figure 2.5 also showed the geometry set up of optical source, detector (receiver). If the distance R between transmitter and receiver was larger than the detector size,

e.g. $R^2 \gg A_R$, the received irradiance can be treated constant over surface of detector, thus the optical pulse energy in a LOS system can arrive at the receiver about the same time. The impulse response can be expressed as [12]:

$$h^{(0)}(t; S, \mathcal{R}) = \frac{n_{rm}+1}{2\pi} cos^{n_{rm}}\left(\emptyset_{s\hat{\boldsymbol{n}}_S}\right) \frac{\cos\left(\theta_{r\hat{\boldsymbol{n}}_R}\right) A_R}{R^2} \, rect(\theta_{r\hat{\boldsymbol{n}}_R}/FOV)\delta(t - R/c) \quad (2.4)$$

For $h^{(0)}$, (0) indicate no reflections between S and $\mathcal{R}$, $\delta(t - R/c)$ is delayed Dirac delta function, c is speed of light in vacuum, R is the distance between the source and receiver, $R = \|\boldsymbol{r}_s - \boldsymbol{r}_R\|$, $\theta_{r\hat{\boldsymbol{n}}_R}$ is the angle between receiver $\hat{\boldsymbol{n}}_R$ and $(\boldsymbol{r}_s - \boldsymbol{r}_R)$, $\emptyset_{s\hat{\boldsymbol{n}}_S}$ is the angle between $\hat{\boldsymbol{n}}_S$ and $(\boldsymbol{r}_R - \boldsymbol{r}_S)$, where $\cos\left(\theta_{r\hat{\boldsymbol{n}}_R}\right) = \hat{\boldsymbol{n}}_R \cdot (\boldsymbol{r}_s - \boldsymbol{r}_R)/R$, $\cos\left(\emptyset_{s\hat{\boldsymbol{n}}_S}\right) = \hat{\boldsymbol{n}}_S \cdot (\boldsymbol{r}_R - \boldsymbol{r}_S)/R$. The rectangular function $rect(x)$ is to make sure only the incident light from transmitter that within receiver's FOV were counted for calculation, energy that fall outside the FOV will not contribute to the total energy received by the detector, defined as, $rect(x) = \begin{cases} 1 & for\ |x| \le 1 \\ 0 & for |x| > 1 \end{cases}$. In equation (2.4), it was assumed that $\emptyset_{s\hat{\boldsymbol{n}}_S} < 90^o$, $\theta_{r\hat{\boldsymbol{n}}_R} \le FOV$ and $R^2 \gg A_R$, which was generally true for a typical room setup [12].

2.2.3.1 Single Reflection Model

When there was only one reflection between transmitter and receiver, the propagation model was the single reflection model. Figure 2.6 illustrated the model structure. Actual transmitter and receiver can use any reflecting surface, e.g. walls, floors. The ceiling bounce model was the most commonly used for Infrared channel modelling. To calculate the impulse response, the ceiling surface was

divided into a large set of small areas ΔA, refer to as reflector elements [82]. These areas were first considered as individual collecting elements as indicated in previous section, and optical power received can be obtained using the source and detector model. Each element was then act as a point source that re-emits the collected signal scaled by the surface reflection coefficient ρ ($\rho \leq 1$). By summarising each of the reflector elements, the one reflection impulse response can be expressed as [82]:

$$h^{(1)}(t; S, \mathcal{R})$$
$$= \sum_{j=1}^{M_{re}} \rho \frac{(n_{rm}+1)A_d \Delta A}{2\pi d_{Ej}^2 d_{jR}^2} cos^{n_{rm}}\left(\emptyset_{Ej}\right) \cos\left(\theta_{ji}\right) R(\theta_{ji}, \emptyset_j, S)\, \delta(t - \frac{(d_{Ej}+d_{jR})}{c}) \quad (2.5)$$

Where M_{re} is number of reflector elements within detector FOV, $\emptyset_{Ej}$ and θ_{ji} are emitting and incident angles, d_{Ej} and d_{jR} are distance between source to element j and j to detector respectively. $\Delta A = \Delta s \times \Delta s$, Δs is the spatial resolution. $R(\theta_{ji}, \emptyset_j, S)$ is surface reflection pattern. Note same assumption hold for the single reflection model, e.g. $d_{jR} \gg \sqrt{A_D}$.

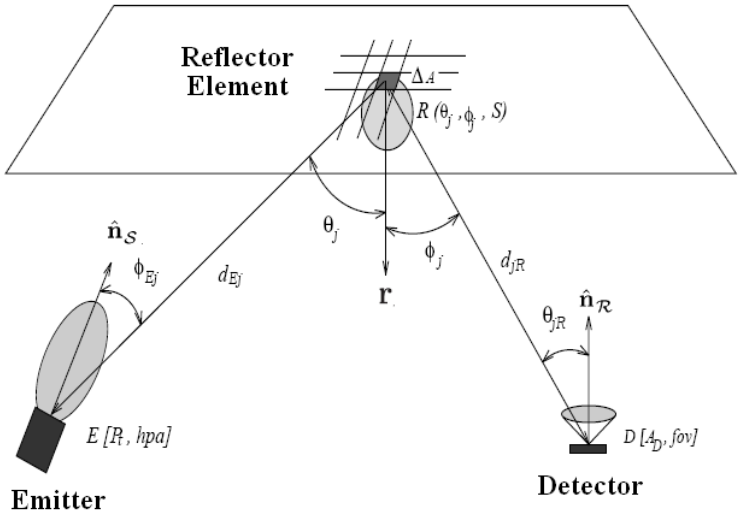

Figure 2.6 Single reflection propagation model
(figure adapted from [82])

2.2.3.2 Multiple Reflection Model

Same method can be extended to the multiple reflection case, where the optical pulse reflected on room surface *k* times before arriving at the receiver, Figure 2.7 demonstrated a multiple reflection model.

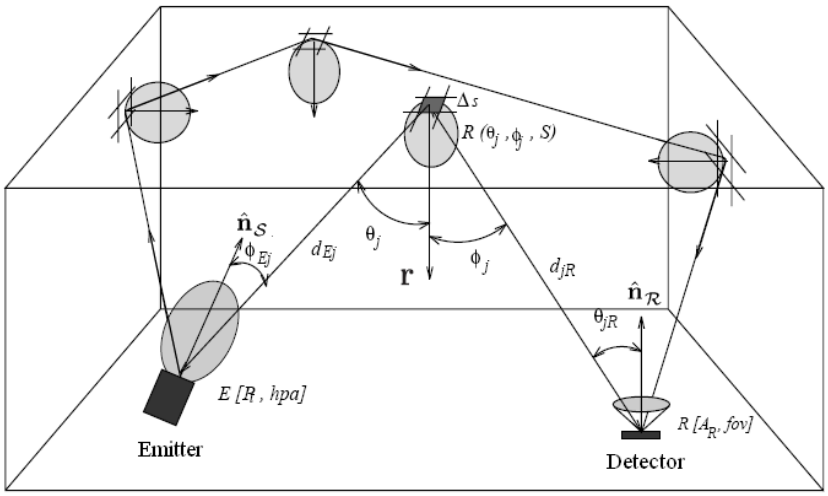

Figure 2.7 Multiple reflection model
(figure adapted from [82])

The impulse response of a multiple reflection model can be expressed as a recursive algorithm to count any number of reflections as [12, 82]:

$$h^{(k)}(t;\mathcal{E},D)=\frac{n_{rm}+1}{2\pi}\sum_{j=1}^{M_{re}}\rho_j\cos^{n_{rm}}\left(\emptyset_j\right)\frac{D\left(\theta_{ji},90^{\mathrm{o}}\right)}{d_{Ej}^2}h^{(k-1)}(t-\frac{d_{Ej}}{c};\mathcal{E}_j,D)\,\Delta A \tag{2.6}$$

Where $D_j=\{\vec{\boldsymbol{s}}_j;\hat{\boldsymbol{n}}_j;\Delta A,90^{\mathrm{o}}\}$ is when reflector element acted as detector, and $\mathcal{E}_j=\{\vec{\boldsymbol{s}}_j;\hat{\boldsymbol{n}}_j;P_j,R_j(\theta_i,\theta_o)\}$ is when reflector element acted as emitter. $\vec{\boldsymbol{s}}_j$ is position vector of reflector j with area ΔA and FOV= 90^{o} , $\hat{\boldsymbol{n}}_j$ is reflector normalised orientation, P_j is power arrived on element j and $R_j(\theta_i,\theta_o)$ is the surface reflection pattern. ρ_j is the reflection coefficient of j. $h^{(k-1)}(t;\mathcal{E}_j,D)$ is the previous $(k-1)$ impulse response between element j and D.

2.2.4 Channel Interferences

2.2.4.1 Multipath ISI

The main interferences for Infrared communication channel including background noise and multipath inter symbol interferences (ISI). The multipath ISI was mainly limited by transmitter and receiver geometry. The following figures were two scenarios of the multipath effects. First case showed multipath propagation can cause distortion to the receiver when LOS path was available. Second case showed when LOS path was not available (e.g. blocked), the multipath propagation can be used to maintain communication through reflections.

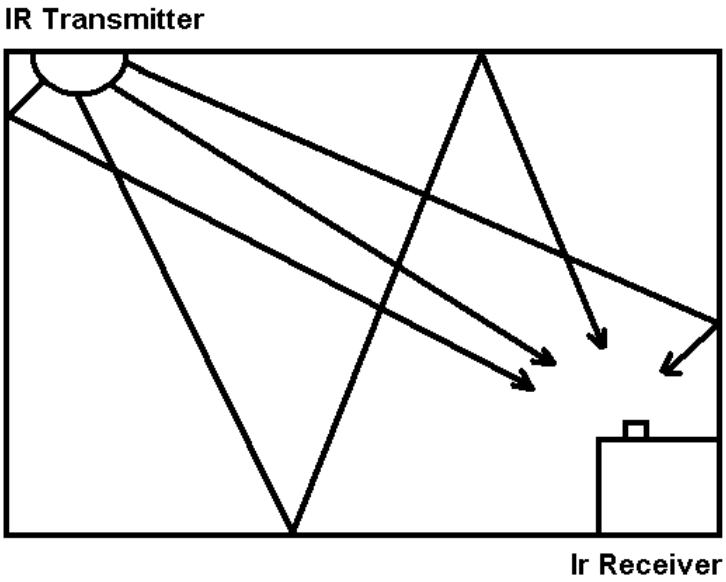

Figure 2.8 Propagation model distorted by multipath effects

Figure 2.8 showed a multi-path data link when LOS is available. In this case, the multipath contribution distorted the received optical pulse as late arrived pulses also contributed to the detected optical power at the receiver.

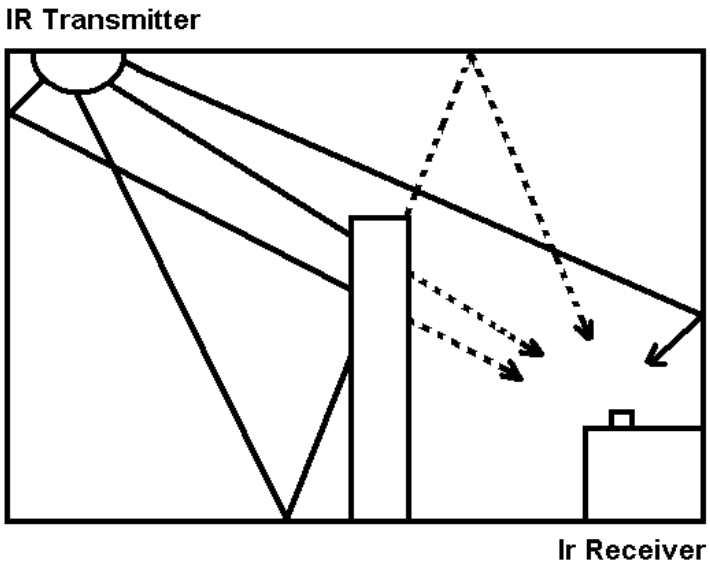

Figure 2.9 Propagation model employing multipath effects

Figure 2.9 showed that an office separator can block most of the transmitted IR signals. The receiver can only communicate with the transmitter through a multi-path link. In this case, the multi-path links can cover areas that cannot be reached through a LOS links.

2.2.4.2 Impulse Response Comparison

An example 5m×3m×2m room can be used to demonstrate the single and multiple reflection prorogation models. Detailed room geometry and transmitter to receiver locations can be found in Appendix II-1, and name this room A. There was no separator between transmitter and receiver in room A. Consider a same size room B, place a separator between transmitter and receiver, choose floor reflectivity of room B to be higher than room A, to allow better higher order reflections. Detailed geometry and separator locations for room B can be found in Appendix II-2. The impulse response of room A and room B can be found in following Figure 2.10 and Figure 2.11.

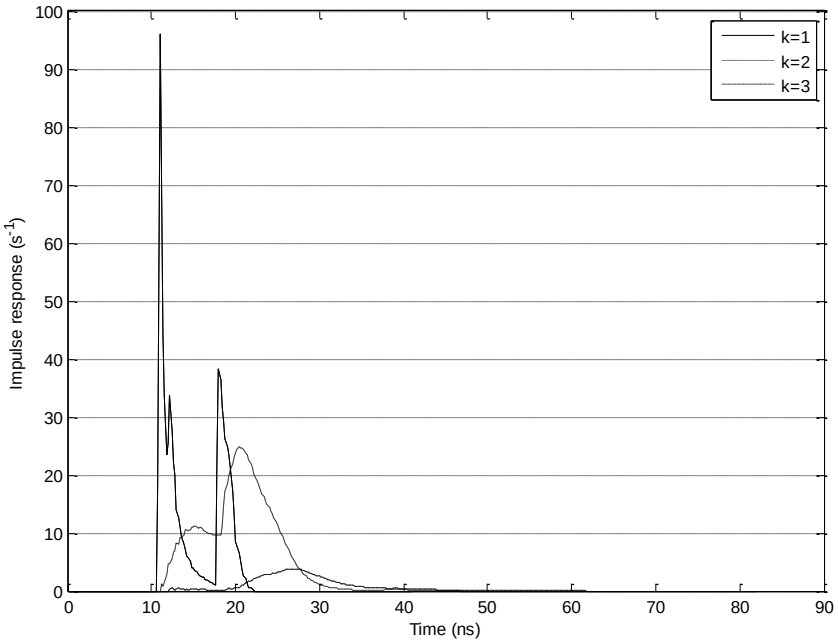

Figure 2.10 Impulse response of room A (K=1, 2, 3) (unblocked)

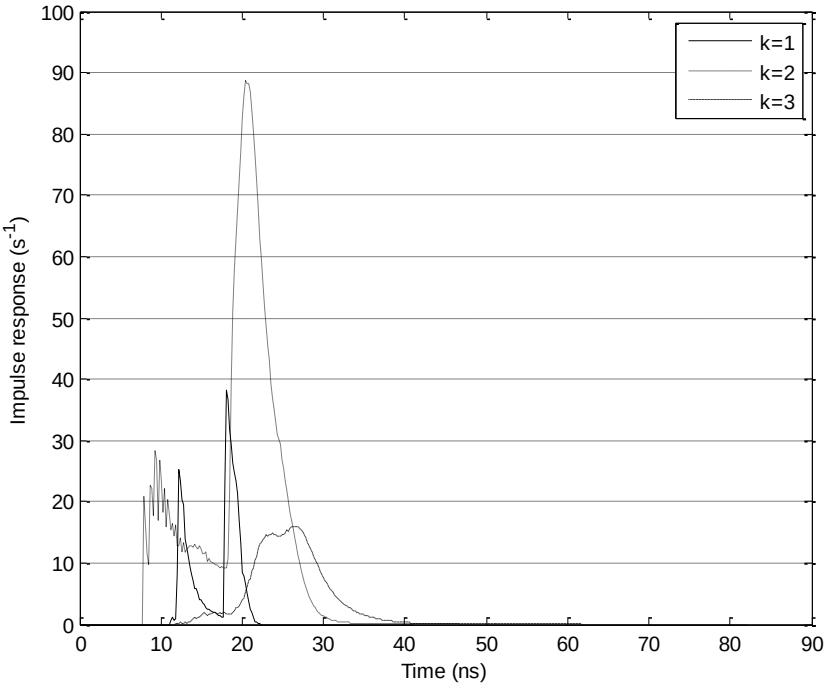

Figure 2.11 Impulse response of room A (K=1, 2, 3) (blocked)

From Figure 2.10, it can be demonstrated that as number of bounces increase, the received optical power decreased significantly after the reflection from room surface. Since there was no separator between the transmitter and receiver, optical wireless communication systems in room A relied on signals with lower reflection orders (e.g. k=1). Although contributions from second and third reflections count towards the total received optical energy at the receiver, compared to first order reflection, they were not significant. It was a totally different scenario for room B. In Figure 2.11, by placing a separator between transmitter and receiver, most of the first order reflection energy was blocked. A more reflective floor also helped shifting the received energy to the second order reflection. Thus for room B, communication systems can establish connections using second order reflections. Appling the same system in room A to room B would results in substantial system degradation if system parameters remain the same. This was because the contribution of the received optical energy had been shifted due to the blockage.

From above two figures, it had been demonstrated that channel impulse response can be significantly different even with the same geometry (e.g. size of two rooms were same) and transmitter-receiver locations. This suggested that the impact of multipath reflection cannot be neglected when validating modulation schemes. Channel dynamics need to be considered when designing optical communication systems.

For the multiple reflection model, in order to get more accurate approximation of the impulse response $h(t)$, the reflection orders k was preferred to count as many reflections as possible, while the time needed to calculate $h(t)$ also increases

exponentially with k [12], even with latest computers, the calculation time was still considerably long for higher order reflections.

2.2.4.3 Ceiling Bounce Model

Carruthers *et al* proposed a simplified iterative based algorithm which required only 1/90 calculation time compared to Barry's method with 3 reflections [83]. In this thesis, Carruthers's method was adapted for calculation of the impulse response of a given set up geometry; the ceiling bounce model can be demonstrated in Figure 2.12.

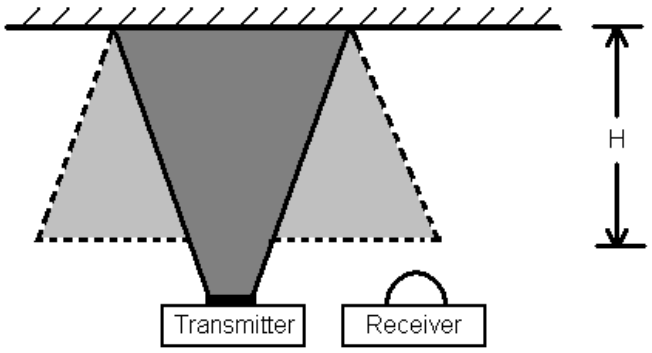

Figure 2.12 Ceiling bounce model (figure adapted from [64])

This model can be expressed by the path loss and delay spread [53]:-

$$h(t) = \frac{6a^6}{(t+a)^7}u(t) \tag{2.7}$$

$$D_{rms} = \frac{a}{12}\sqrt{\frac{13}{11}} \tag{2.8}$$

Where $h(t)$ is the channel impulse response, $u(t)$ is Heaviside unit step function, $u(t) = \begin{cases} 0, & t < 0 \\ 1, & t > 0 \end{cases}$, a depends on the relative location of the transmitter and receiver, when the transmitter and receiver were collocated, $a = 2H/c$, where H is the ceiling height , c is speed of light, D_{rms} is the root mean square (RMS) delay spread. In this thesis, it was assumed that the transmitter and receiver were collocated, as discussions will not loss generality with this assumption regarding to non collocated cases. From equation (2.7), the channel impulse response can be quantified by the ceiling height, thus H can be used to reflect severity of the ISI caused by multipath propagation.

2.2.4.4 Background Light Interference

The background noise caused by the ambient light from sun light and artificial light can be intense. The background light noise can affect optical wireless system that employing the Infrared spectrum; this can be demonstrated in following Figure 2.13.

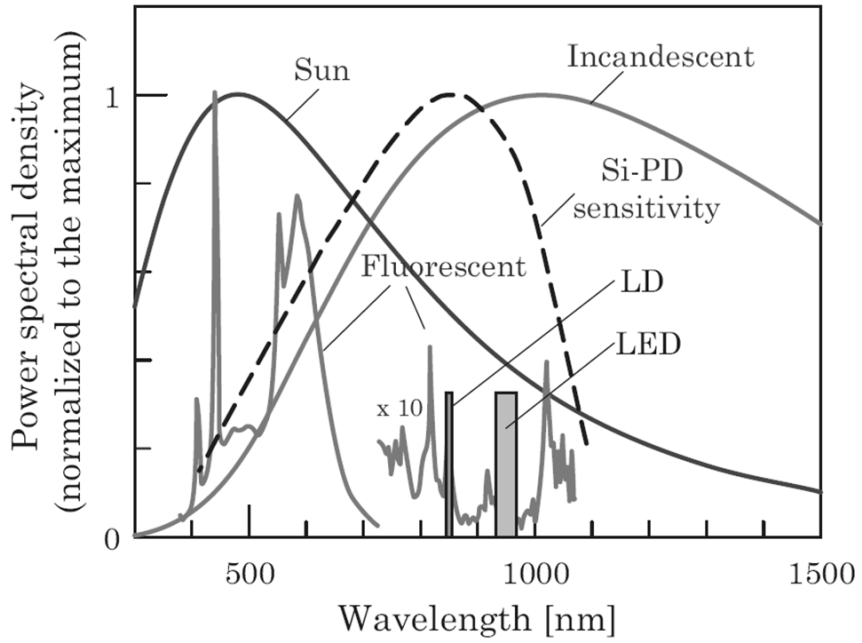

Figure 2.13 Background radiation with Si-photodiode responsivity
(figure adapted from [10] [12])

Figure 2.13 showed the background radiation power spectral density of sunlight, incandescent and florescent lighting. The Si-Photodiode responsivity was also indicated with dotted lines. This showed the Infrared optical channel can suffer intense distortion caused by the background ambient noise. The sunlight and incandescent light exhibited less periodic characteristics than the florescent light. Thus an optical filter can be used to effectively block much of these two types of radiation. The florescent lamps can be grouped into two categories: lamps driven by conventional ballast and electronic ballast (also known as the energy saving lamp). The latter became more popular as the energy saving feature. The incandescent and florescent lamps exhibited different spectrum. The artificial lamp radiation pattern can be found in following Figure 2.14 [84].

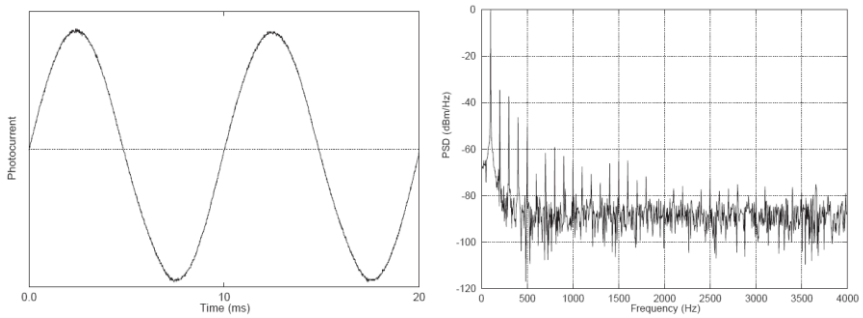

(a)

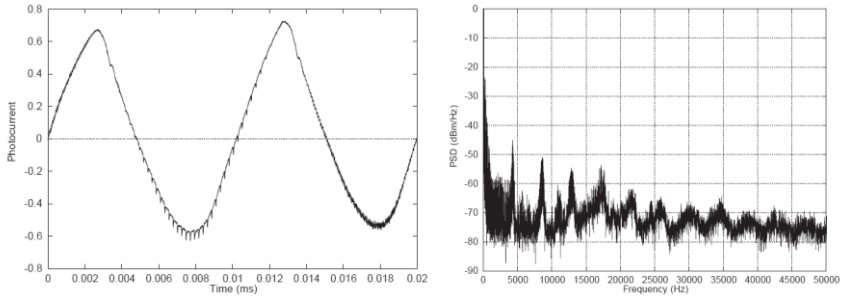

(b)

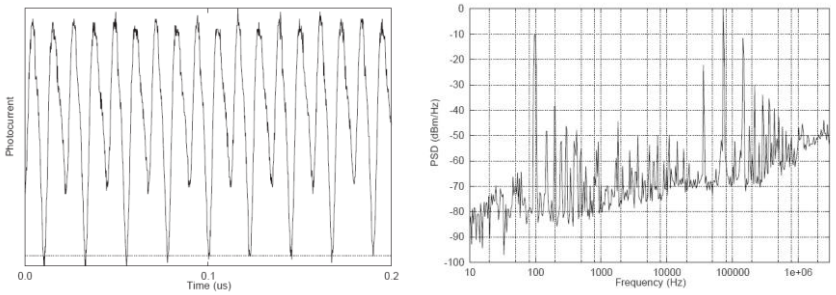

(c)

Figure 2.14 Typical artificial light interference time waveform and spectrum of (a) Incandescent lamp (b) Fluorescent lamps driven by conventional ballast and (c) Fluorescent lamp driven by electronic ballast (energy saving lamp) (figure adapted from [84])

It can be observed from Figure 2.14 that radiation from electronic ballast driven florescent lamps had a stronger periodic nature.

2.2.4.5 Fluorescent Light Interference Model

According to Moreira *et al* [85], two significant frequency bands can be observed: 1. Low frequency component that was similar to the conventional ballast driven fluorescent lamp; 2. High frequency component, generated by the electronic ballast switching circuit. The frequency also ranged from tens KHz to more than 1MHz. The mathematical model of the florescent lamp driven by electronic ballast can be expressed by the following [68, 85]:

$$m(t) = R_{pr} P_m + \frac{R_{pr} P_m}{A_1} \sum_{i=1}^{20} [b_i cos(2\pi(100i - 50)t + \zeta_i) + c_i cos(2\pi 100it + \varphi_i)] + \frac{R_{pr} P_m}{A_2} \left[d_0 \cos(2\pi f_h t + \theta_0) + \sum_{jj=1}^{11} d_{jj} cos\left(2\pi 2j f_h t + \theta_{jj}\right) \right] \quad (2.9)$$

Where $m(t)$ is the interfering signal at the output of the photodiode, R_{pr} is the photodiode responsivity (A/W), P_m is average optical power of the interfering signal. A_1, A_2 are constants that relate the interference amplitude to P_m and have typical value of 5.9 and 2.1 respectively, f_h is the fundamental frequency of the high frequency component and takes the value of 37.5 kHz. b_i, c_i were low frequency components that can be expressed by the following [85]:

$$b_i = 10^{(-13.1 \ln(100i - 50) + 27.1)/20}, 1 \ll i \ll 20 \quad (2.10)$$

$$c_i = 10^{(-20.8 \ln(100i) + 92.4)/20}, 1 \ll i \ll 20 \quad (2.11)$$

ζ_i , φ_i are phase parameters of low frequency components and d_{jj} , θ_{jj} are high frequency components, their typical values can be found in the following Table 2.3 and Table 2.4:

Table 2.3 Typical values for phase parameter ζ_i and φ_i
(table adapted from [85])

i	ζ_i	φ_i	i	ζ_i	φ_i
1	4.65	0	11	1.26	6
2	2.86	0.08	12	1.29	6.17
3	5.43	6	13	1.28	5.69
4	3.9	5.31	14	0.63	5.37
5	2	2.27	15	6.06	4
6	5.98	5.7	16	5.49	3.69
7	2.38	2.07	17	4.45	1.86
8	4.35	3.44	18	3.24	1.38
9	5.87	5.01	19	2.07	5.91
10	0.7	6.01	20	0.87	4.88

Table 2.4 Typical value for amplitude and phase parameters of high frequency components (table adapted from [85])

j	d_{jj} (dB)	θ_{jj} (rad)	j	d_{jj} (dB)	θ_{jj} (rad)
0	-22.22	5.09	6	-39.3	3.55
1	0	0	7	-42.7	4.15
2	-11.5	2.37	8	-46.4	1.64
3	-30	5.86	9	-48.1	4.51
4	-33.9	2.04	10	-53.1	3.55
5	-35.3	2.75	11	-54.9	1.78

A sample waveform of the interference signal with R_{pr} =1A/W and P_m =1W can be obtained using equation (2.9) and demonstrated in the following Figure 2.15 [68].

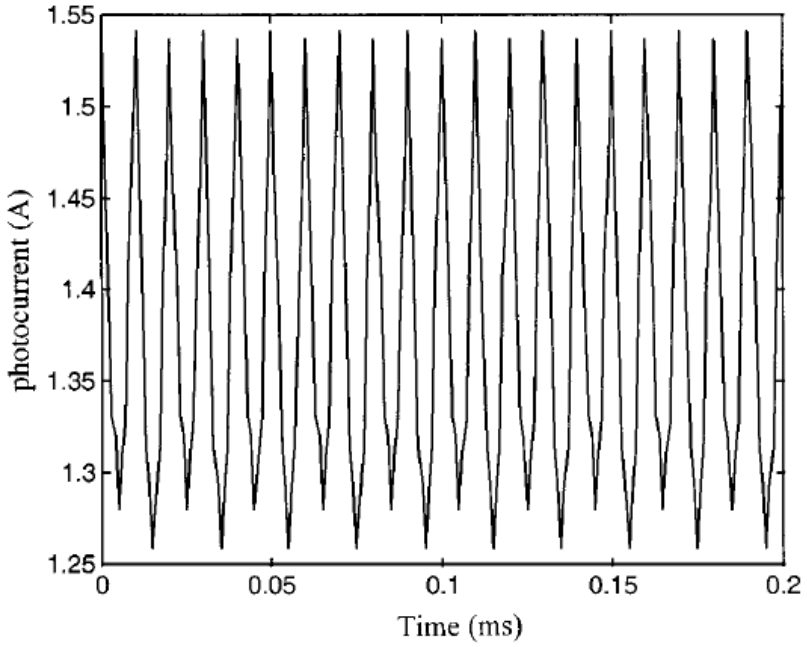

Figure 2.15 Sample interference waveform of incandescent lamp driven by electronic ballast with R_{pr} =1A/W and P_m =1W (figure adapted from [68])

2.2.4.6 Filter Performance Comparison

Electronic highpass filter (HPF) can be used to help reducing the artificial light interference but also introduced extra ISI [31]. The filter cut-off frequency compromised between the interference attenuation and extra ISI that was introduced. The HPF on modulation performance under different interferences was reported by Moreira *et al* [31, 69] and can be found in Figure 2.16 and Figure 2.17.

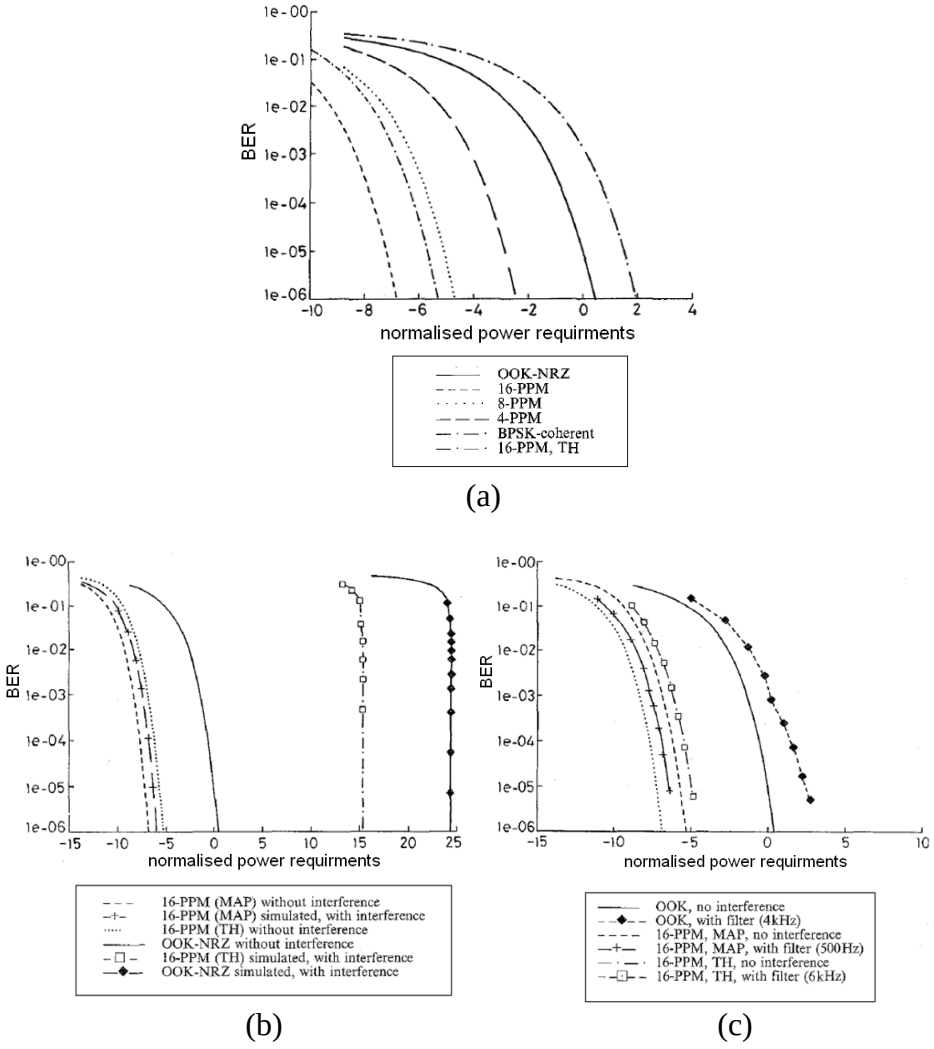

Figure 2.16 Modulation performance in channel limited by (a) shot noise only (b) incandescent light without HPF (c) incandescent light with HPF (figure adapted from [31])

In Figure 2.16, comparing (b) with (a), the incandescent light interferences resulted 24dB penalty for OOK, 16dB for 16-PPM with threshold detection (TH) and 1.5dB for 16-PPM with maximum-a-posterior (MAP) detection for a 1Mbps data link. Comparing (c) with (b), applying HPF can effectively reduce the interference caused by incandescent lamp for both OOK and 16-PPM modulation schemes. Modulation performance comparison under fluorescent light interference can be found in following Figure 2.17.

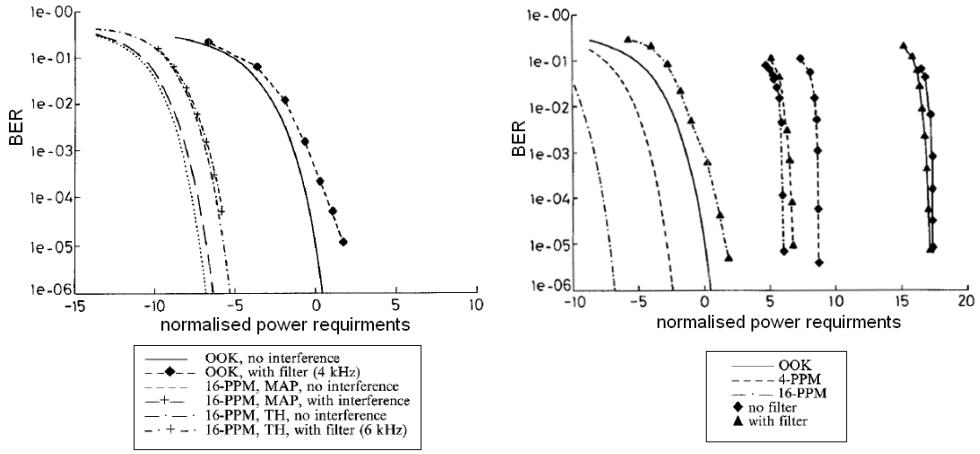

(a) (b)

Figure 2.17 Modulation performances in channel limited by (a) fluorescent light driven by conventional ballast with and without HPF (b) fluorescent light driven by electronic ballast with and without HPF (figure adapted from [31])

In Figure 2.17 (a), interferences of fluorescent light driven by conventional ballast were similar to the incandescent case as demonstrated in Figure 2.16 (c), as this type of interferences can be effectively mitigated by HPF. In Figure 2.17 (b), the interferences introduced by electronic-ballast-driven fluorescent light were difficult to mitigate even using the HPF. Since this type of interference exhibited wider band nature than the incandescent lamp and florescent lamp driven by conventional ballast, it can seriously impair the performance of the OW system and cannot be ignored [85].

Apart from HPF, better BER performance can also be obtained by designing the system modulation/demodulation to achieve a higher average BER first, and then reducing the results to the target BER value through error correction codes (ECC), in conjunction with interleaving [86]. However, ECC method often resulting in reduced transmission data rate [87].

2.3 Problem Definitions

2.3.1 Main Challenges

From previous discussions, the ISI caused by multipath propagation and artificial light interference from fluorescent lamp driven by electronic ballast were two major interferences, and these need to be taken into account when validating modulation schemes. The severity of multipath ISI can be quantified by the distance variable in the ceiling bounce model. HPFs were effective for mitigating interference induced by incandescent light and conventional-ballast-driven fluorescent light but not for the electronic-ballast-driven fluorescent light. The L-PPM modulation scheme presented a good candidate under severe interferences caused by artificial lighting. Yet as were discussed in Chapter 3, the L-PPM modulation scheme was not bandwidth efficient compared to L-PAM and OOK schemes.

The main challenge faced by this thesis was to seek the most optimised modulation scheme that can provide maximum system throughput while capable of withstanding most if not all of the intense channel interferences at a target BER requirement. This defined a dilemmatic situation, modulation schemes such as the L-PPM proved to be less susceptible to artificial lighting interferences but not bandwidth efficient. Bandwidth efficient schemes such as the OOK and L-PAM were prone to artificial lighting interferences. This led to a natural conclusion of a modulation scheme that can combine benefits from both above candidates and able to avoid the drawbacks of each individual scheme. The multilevel pulse amplitude and position modulation (PAPM) thus been selected as the new

candidate modulation scheme to exploit the potential benefits as an adaptive modulation scheme.

2.3.2 Possible Solutions

Similar modulation combinations had been proposed in the literature, such as the differential amplitude pulse position modulation (DAPPM) [64], which combined the differential pulse position modulation (DPPM) and pulse amplitude modulation (PAM). Multilevel digital pulse interval modulation (MDPIM) combined dual header pulse interval modulation (DH-PIM) with PAM [88]. Both DAPPM and MDPIM can increase data throughput due to the PAM element while enjoy the benefits from DAPPM and DPIM elements, such as the inherent symbol synchronisation capability and improved transmission rate and bandwidth requirements. With many new PPM derivatives being reported, the L-PPM scheme still remain attractive for its power efficiency and improved immunity to the fluorescent lamp induced noise [15]. The 4-PPM modulation scheme was adopted by the IrDA in its physical layer specification [89].

In order to compare and validate the PAPM modulation under different types of interferences, detailed analytical model together with BER, SNR and data rate relationships were needed. Wong *et al* [68] had developed an analytical model for studying multipath ISI and electronic-ballast-driven fluorescent light interferences. Yet Wong's model was limited to OOK, 2-PPM and sequence inversion keying (SIK) direct sequence spread spectrum, and the multipath ISI considered was only valid for a specific room set up. Moreira *et al* [31] developed mathematical models for analysing the artificial light interference for OOK and L-PPM of

1Mbps and 10Mbps data links. Further discussions on the electronic-ballast-driven fluorescent light interferences were reported by Narasimhan *et al* [90], SNR and normalised power requirements were also compared with data rate extended to 100Mbps. HPF effectiveness comparisons were carried out in both works. Note the L-PAM model was not mentioned in the context of artificial light interferences.

Appropriate control modules needed to realise the dynamic adaptations for the proposed modulations. This can be facilitated by employing artificial intelligence algorisms. Simulation results needed to be compared with analytical discussions.

2.4 Original Contributions

The contributions presented within this thesis can be summarised into three constituent parts:

1. BER expressions for L-PAM, L-PPM and M-n-PAPM modulation schemes were derived in Chapter 3. The expressions can be used to simulate the combined contributions from both multipath ISI and interference introduced by electronic-ballast-driven fluorescent lights. Since the expressions were provided as general forms, modulation orders and its combinations were not limited. A software package written in Matlab was also developed for calculating the BER versus SNR and data rate. In Chapter 4, analytical models developed for the adaptive PAM, PPM and PAPM modulation schemes were verified in different scenarios. Data rate improvements under variable channel interference were achieved by actively updating modulation parameters according to the BER variations, the simulation results and analytical model match well.

2. Fuzzy logic control modules were constructed to realise the dynamic modulation parameter adaptations in Chapter 5. The fuzzy logic controlled modulation optimisation systems were developed to demonstrate the feasibility of adaptive modulation optimisation under single or multiple interferences. An ANFIS based control system was developed, and its ability to recognise the control pattern through training data set was demonstrated. Amongst the obtained models trained by different algorisms, the hybrid algorism combined with 2-D recursive data set showed perfect match to the original control pattern than other candidates.

3. The adaptive modulation concept developed in this thesis provided some insight on the stabilising issues of high speed OW communication link. In Chapter 6, by adaptive modulation parameters optimisation, system throughput can be improved compared to non-optimising case.

2.5 Summary and Conclusions

Summary

The Infrared communication channel can be characterised by LOS and diffuse prorogation model. Channel noise mainly came from background noise and multipath ISI. The achievable data rate of a channel was restricted to the available bandwidth that a specific channel can provide. The impulse response of the channel was depended on transmitter, receiver location and orientation, dimension of the room where the system was deployed. Eye safety regulations defined the maximum allowed average and peak optical power that can be used in an optical wireless link.

Conclusions

The unique characteristics of the optical wireless channel exhibited challenges and opportunities. Constrains and interferences presented to the channel need to be taken into account when designing communication systems. In order to improve channel throughput, the first step was to set up the appropriate channel model. This included fully understanding the mathematical model of the channel, noise sources and error performance under each or combined interferences. Partially represented channel model cannot be used for validating system performances. Channel behaviours can be described for a specific scenario. Channel frequency response can vary significantly according to transmitter and receiver location. Furthermore, analytical models developed for the optical wireless channel can only be applied to validate the modulation scheme performance when given the exact channel parameters.

In order to improve the channel throughput under the presence of channel limits, next chapter considered different modulation schemes proposed in the literature, and their performance under the constraints imposed by the challenges in designing a robust optical wireless system.

Chapter 3

Modulation for Optical Wireless Channel

3.1 Introduction

The optical channel is quite different from the conventional RF channel. This consequently resulted in a different approach when it came to the modulation design. Modulation schemes which fit well in electromagnetic channels were not necessarily perform well in the optical domain [12]. Modulation techniques remained an active topics amongst both academic researchers and industrial communication system engineers [16, 37-40, 42, 43, 91]. Depending on the nature

of the information source, modulation can be summarised as analogue or digital formats [29]. Depending on the pulse shape or time width, the modulation can be subdivided into amplitude modulation, position modulation or combination of the two. A detailed modulation tree can be found in Figure 3.1 [36]. Important modulation schemes for OW system were introduced in section 3.2. Multilevel modulation schemes were discussed in section 3.3.

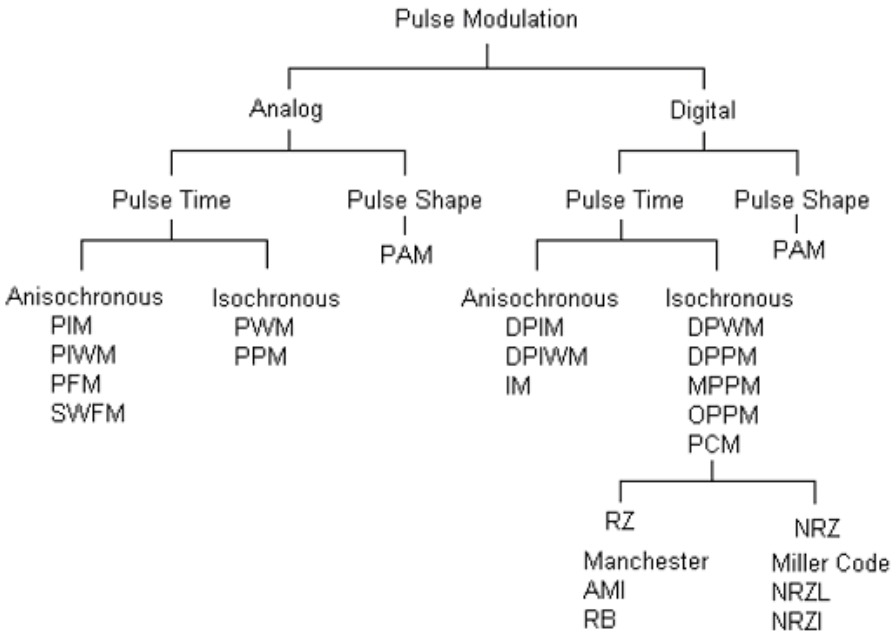

Figure 3.1 Family tree of pulse modulation schemes for optical wireless systems (figure adapted from [10, 36])

In this chapter, special interests were focused on the modulation schemes proposed in the literature by optical system engineers and academic researchers. As discussed in chapter 2, the optical signal can be severely interrupted by channel noise from background lighting and interference due to the multipath distortion. Thus modulation schemes that exhibited both power and bandwidth efficiencies became more attractive. Since the ultimate task for the modulation design was to increase channel throughput, the error performance and throughput

efficiency were taken into consideration when discussing different modulation techniques.

3.2 Modulation Schemes

3.2.1 On-Off-Keying (OOK)

The OOK modulation scheme was one of the simplest modulation techniques. It was commonly used because of its easy implementation. By default, the OOK modulation discussed in this thesis refers to the Non Return to Zero (NRZ) OOK, and this is different from the Return to Zero (RZ) OOK modulation by a fraction of γ, where $\gamma \in (0,1]$ [15]. The RZ-OOK signalling requires $5log_{10}(\gamma)$ (dB) more optical power than NRZ-OOK to achieve the same BER [92]. Figure 3.2 showed the comparison between NRZ-OOK signal and RZ-OOK signal in time space.

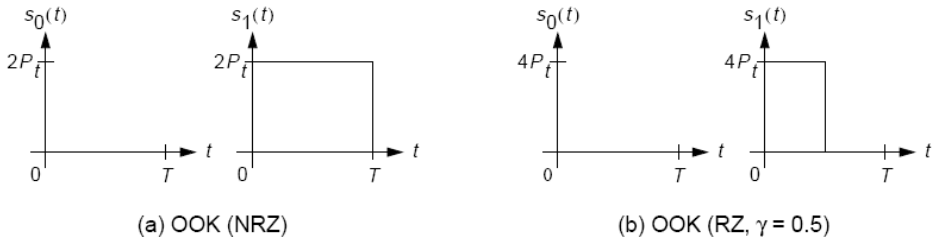

Figure 3.2 Comparison of (a) NRZ-OOK pulse (b) RZ-OOK pulse with duty cycle $\gamma = 0.5$ (figure adapted from [15])

The transmitter operating at a bit rate R_b, emited rectangular pulses of duration $1/R_b$. In order to maintain average transmitted optical power $P_{at} = P$, the transmitter emit optical intensity power $2P$ to represent a bit '1', and no power to represent a bit '0'. Assuming the pulse shape $P(t)$ is close normalized to unity, the transmitted OOK pulse signal can be presented by following [12]:

$$p(t) = \begin{cases} 1 & for \quad t \in [0,T) \\ 0 & elsewhere \end{cases} \tag{3.1}$$

The power spectral density (PSD) of OOK can be calculated using the following equation [21], and its PSD curve can be found in Figure 3.3:

$$S_{OOK}(f) = {P_{at-OOK}}^2 \delta(f) + {P_{at-OOK}}^2 T_{OOK} Sinc^2(\pi f T_{OOK}) \tag{3.2}$$

Where the first and second part of equation (3.2) are the discrete and continuous portions respectively, δ is the Dirac delta function, P_{at-OOK} is the average transmitted optical power, T_{OOK} is the symbol interval, and $sinc(x) = \frac{\sin(x)}{x}$

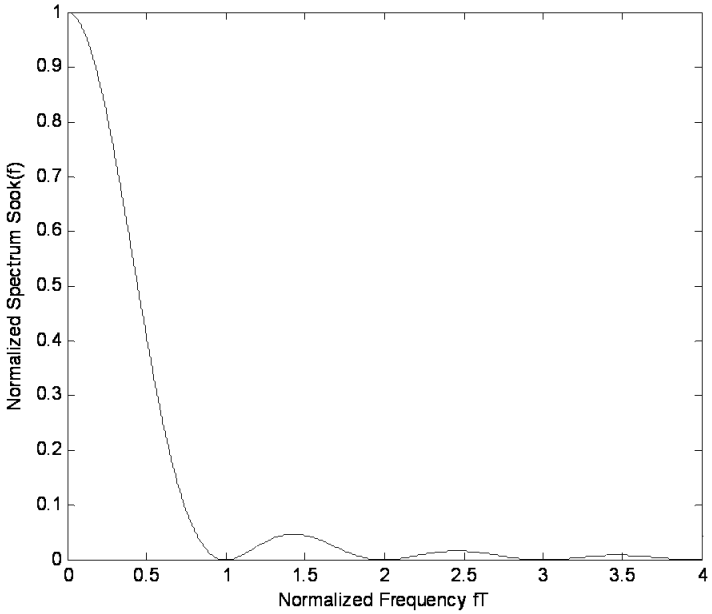

Figure 3.3 The continuous portion of the power spectral density of OOK scheme (figure adapted from [21])

The bandwidth required by OOK is $R_b = 1/T$, the inverse of the pulse width, its bit error rate (BER) is [12]:

$$BER_{OOK} = Q\left(\frac{P_{ar-OOK}}{\sqrt{N_0 R_b}}\right) \tag{3.3}$$

where N_0 is the power spectral density of the white Gaussian noise and $Q(x)$ is the customary Q-function of digital telecommunications. P_{ar-OOK} is the average received optical power. Since $x \in \Re$, and $Q(x)$ is monotonically decreasing, the inverse $Q^{-1}(x)$ where $x \in \{0,1\} \to \Re$ is straightforward to obtain [93]. The power requirement for OOK is [12]:

$$P_{OOK} = \sqrt{N_0 R_b} Q^{-1}(BER_{OOK}) \tag{3.4}$$

Furthermore, the OOK modulation scheme was often treated as a benchmark to other modulation schemes, which can make comparison among different modulation schemes better related.

3.2.2 Pulse Amplitude Modulation (PAM)

The PAM modulation technique belonged to pulse amplitude level modulation scheme. Consider L-level PAM (L-PAM), That is, one of L possible amplitude levels transmitted from the transmitter to represent a specific value. The bandwidth requirement, BER and power requirement for L-PAM is [12]:

$$B_{L-PAM} = \frac{R_b}{\log_2 L_{PAM}} = \frac{1}{\log_2 L_{PAM}} B_{OOK} \tag{3.5}$$

$$BER_{L-PAM} = Q\left(\frac{P_{L-PAM}}{L_{PAM} - 1} \sqrt{\frac{\log_2 L_{PAM}}{N_0 R_b}} \right) \tag{3.6}$$

$$P_{L-PAM} = \frac{L_{PAM} - 1}{\sqrt{\log_2 L_{PAM}}} \cdot \sqrt{N_0 R_0} Q^{-1}(BER_{L-PAM}) \tag{3.7}$$

The time waveforms of 4-PAM modulation can be found in Figure 3.4

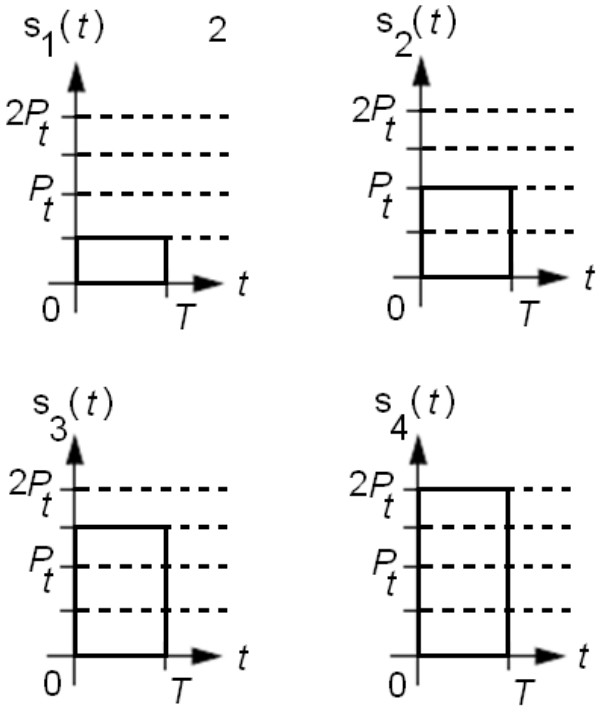

Figure 3.4 Time waveforms of 4-PAM

To compare with the OOK system, when achieving the same BER:

$$BER_{OOK} = BER_{L-PAM} \tag{3.8}$$

The power requirement of the L-PAM is therefore:

$$P_{L-PAM} = \frac{L_{PAM} - 1}{\sqrt{\log_2 L_{PAM}}} P_{OOK} \tag{3.9}$$

The above equation is under the assumptions of a high Signal to Noise Ratio (SNR), moderate values of L_{PAM} ($L_{PAM} \geq 2$), and a given BER.

3.2.3 Pulse Position Modulation (PPM)

In PPM, transmitted optical signals were represented by the location of the pulse within a clock cycle. As a result, synchronisation between transmitter and receiver was required or assumed when comparing PPM schemes with other schemes. In addition, the PPM modulation scheme was also regarded as particular version of an L-position PPM (L-PPM) system. The power and banwidth requirement of an L-PPM system can be approximated by [12]:

$$P_{L-PPM} = \sqrt{\frac{2}{L_{PPM} \log_2 L_{PPM}}} P_{OOK} \tag{3.10}$$

$$B_{L-PPM} = \frac{L_{PPM}}{\log_2 L_{PPM}} B_{OOK} \tag{3.11}$$

Figure 3.5 illustrate a 4-PPM modulation pulse time waveforms.

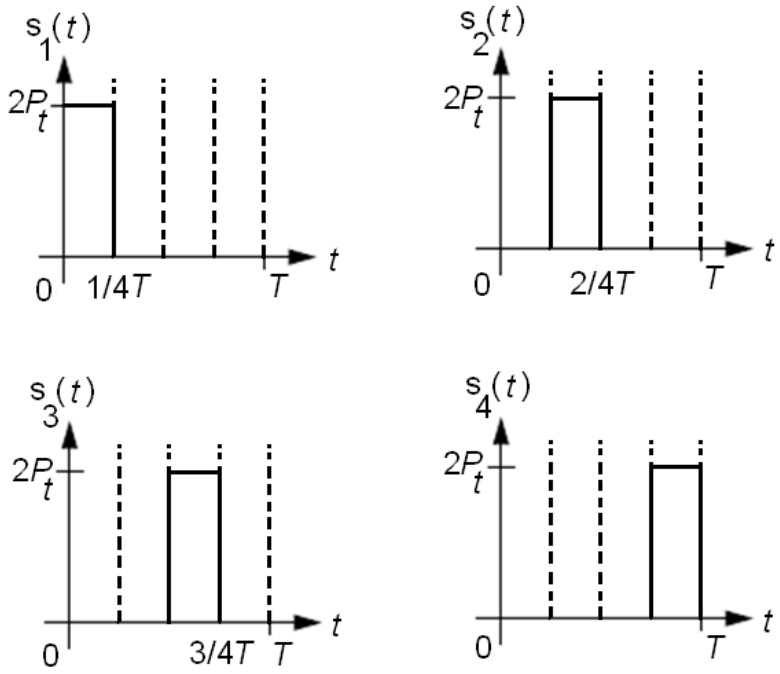

Figure 3.5 Time waveforms of 4-PPM

3.2.4 Pulse Amplitude and Position Modulation (PAPM)

In PAPM modulation, the information was represented both by the amplitude and the position of the pulse. PAPM was a multi-level modulation scheme. It can be expressed as M-n-PAPM, where M is the number of amplitude levels, and n is the pulse numbers within a clock cycle. The bandwidth and power requirement of the M-n-PAPM is [70]:

$$B_{M-n-PAPM} = \frac{n}{\log_2 nM} B_{OOK} \tag{3.12}$$

$$P_{M-n-PAPM} = \sqrt{\frac{2M^2}{n\log_2 nM}} P_{OOK} \tag{3.13}$$

The time waveforms of a 2-4-PAPM can be found in Figure 3.6

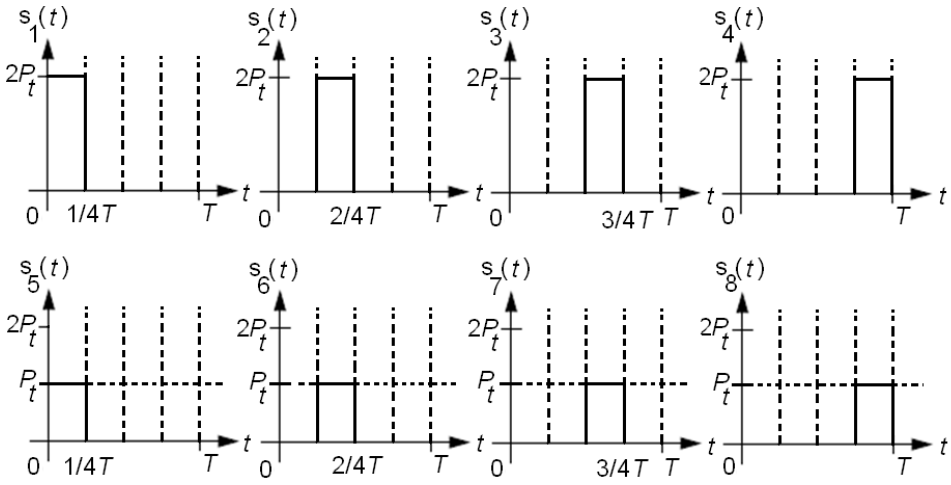

Figure 3.6 Time waveform of 2-4-PAPM

3.3 BER under ISI and Background Ambient Light Noise

In this section, the BER expression for different modulation schemes under both ISI and background ambient light noise can be derived. During an instance of time interval T_c, energy y of kth sample arriving at the threshold detector is [68]:

$$y = z + n_{AWGN}, \qquad z = s + m \tag{3.14}$$

Where z is energy accepted by the photodetector and n_{AWGN} is impulse energy of the additive white Gaussian noise, its variance $\sigma = \sqrt{T_c N_0/2}$, s is contribution of signal and m is contribution from ambient light energy [68]:

$$s = E_u b_k \otimes h = \lambda \bar{E} b_k \otimes h_k \tag{3.15}$$

E_u is energy of minimal amplitude pulse, where $E_u = \lambda \bar{E}$, λ is a ratio between peak and average intensity, $\bar{E}$ is average energy of one chip, $\bar{E} = \bar{P} T_c$, $\bar{P}$ is average transmitted optical power, e.g. for OOK coding scheme, parameter $\lambda = 2$, for L-PPM $\lambda = L$, '$\otimes$' denotes convolution, b_k is the input bits, h_k is the channel impulse response, the relationship between E_u and $\bar{E}$ can be demonstrated in Figure 3.7. Here the impulse response employed was the ceiling bounce model discussed in Chapter 2.

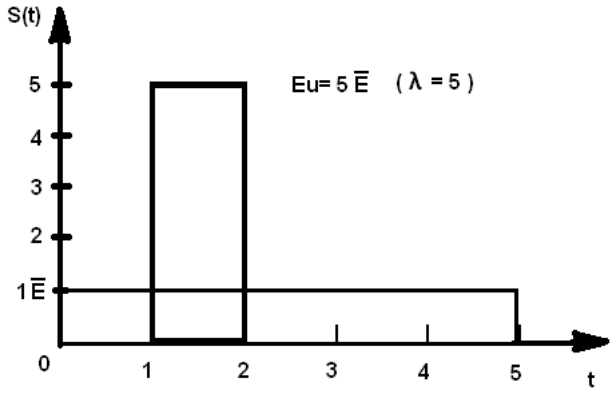

Figure 3.7 Relationships of E_u and $\bar{E}$ of 5-PPM

It is convenient to scale h when $a = 1$, equation (2.7) becomes:

$$h_1(t) = \frac{6}{(t+1)^7} \tag{3.16}$$

To calculate the ambient light interference, the channel impulse response within a time interval were considered, assume at time T_a after channel inference, kth pulse

arrived at the receiver became β_k, within time interval kT_a and $(k+1)T_a$, the resulting impulse response can be calculated using the following

$$\beta_k = \int_{kT_a}^{(k+1)T_a} h_1(t)dt = (t+1)^{-7}\Big|_{(k+1)T_a}^{kT_a} \tag{3.17}$$

Similar to Wong's method [68], in order to consider the impact of ambient light interference, the ambient light noise to signal power ratio (ASR) can be used to indicate the degree of ambient light interference. The ratio can be integrated into equation (3.14) by dividing $\bar{E}$, express y, z, v and n_{AWGN} in units of $\bar{E}$:

$$\begin{gathered} Y = y/\bar{E} \\ Y = Z + N, \qquad Z = S + V \\ S = \frac{s}{\bar{E}} = \lambda b \otimes h, \quad V = ASR = \frac{m}{\bar{E}} \end{gathered} \tag{3.18}$$

The optical signal to noise ratio is defined as:

$$SNR_0 = \frac{R_{pr}\bar{E}}{\sigma} \tag{3.19}$$

Where R_{pr} is photodetector responsivity, substitute $\sigma = \sqrt{T_c N_0/2}$ and $\bar{E} = \bar{P}T_c$ into equation (3.19), the optical SNR_0 can be denoted as

$$S_\sigma = SNR_0 = R_{pr}\bar{P}\sqrt{2T_c/N_0} \tag{3.20}$$

3.3.1 OOK

For given threshold θ, the probability of Y with bit $b_0 = 1$ to fall below threshold θ is $Q\big(S_\sigma(Z-\theta)\big) = Q(S_\sigma(S+V-\theta))$, Figure 3.8 demonstrated the OOK threshold detection, the received pulse of '0' or '1' bit, where [68]

$$S = S^0 = \lambda \sum_{j=0}^{k-1} b_{k-j} h_j \tag{3.21}$$

The probability of Y with bit $b_0 = 0$ to be greater than θ is $Q\big(S_\sigma(\theta - Z)\big) = Q(S_\sigma(\theta - S - V))$, where

$$S = S^1 = \lambda \sum_{j=1}^{k-1} b_{k-j} h_j \tag{3.22}$$

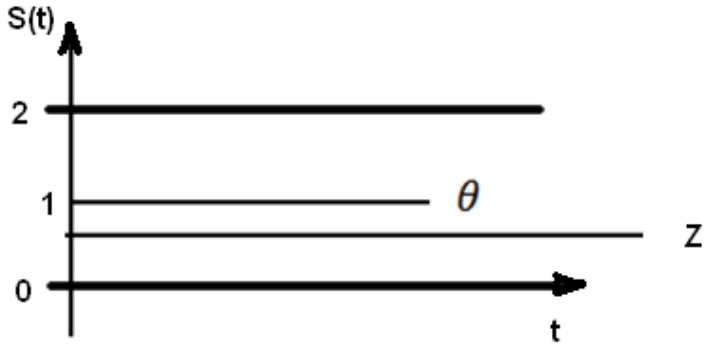

Figure 3.8 OOK detector thresholds

Assume $\theta = 1$, the error probability of OOK can be obtained by counting errors from bit '0' and '1' over all possible pulses and by averaging over the period of

the ambient light interference. The probability can be expressed by the following [68]

$$BER_{OOK}$$

$$= \frac{1}{T_i} \int_{t}^{t+T_i} \left(\frac{1}{2}\right)^k \left[\sum_{\substack{b \\ b_0=0}} Q\left(S_\sigma(1 - S^1 - V_k)\right) + \sum_{\substack{b \\ b_0=1}} Q\left(S_\sigma(S^0 + V_k - 1)\right) \right] dt \tag{3.23}$$

Where T_i is the considered time period of ambient light interference, $\left(\frac{1}{2}\right)^k$ is the probability of b_0 being '1' or '0' within previous pulse sequence of length k, assuming bit '1' and '0' to be equiprobable. The first term in the sum count for $b_0 = 0$ case and second term for $b_0 = 1$, the detection success rate within a pulse sequences can then be obtained from equation (3.23)

$$P_{Success\_OOK} = 1 - BER_{OOK} \tag{3.24}$$

3.3.2 PAM

For PAM case, thresholds θ_i can be used to make decision on received signal power. There were three possible events:

1. Detection success.
2. Over detection failure (over threshold to next level)
3. Under detection failure (not enough power to current level)

This can be denoted by the following equation:

$$BER = \frac{1}{X}\left(\sum_{b}^{b_0=0} P_{over\,,0} + \sum_{\substack{b \\ 0<a<A}}^{b_0=a} \left(P_{over\,,a} + P_{under\,,a}\right) + \sum_{b}^{b_0=A} P_{under\,,A}\right) \quad (3.25)$$

Where $X = (L_{PAM} + 1)^K$, X is all possible chip sequences. P_{over} and P_{under} represent the probability density of its related level denoted by 0, a or A. For probability of error over interference T_i, similar to OOK case, the full probability error for a L-PAM system can be expressed by the following:

$$BER = \frac{1}{T_i}\int_{t}^{t+T_i} \frac{1}{(L_{PAM}+1)^k}\Big[\sum_{\substack{b \\ b_0=0}} Q\left(S_\sigma\left(\tilde{\theta}_0 - S - V_k\right)\right) + \sum_{\substack{b \\ 0<a<A}} Q\left(S_\sigma\left(\tilde{\theta}_a - S - V_k\right)\right) + \sum_{\substack{b \\ 0<a<A}} Q\left(S_\sigma\left(S + V_k - \tilde{\theta}_{a-1}\right)\right) + \sum_{\substack{b \\ b_0=A}} Q\left(S_\sigma\left(S + V_k - \tilde{\theta}_{A-1}\right)\right)\Big]dt \quad (3.26)$$

Where $\tilde{\theta}$ represents the thresholds for different detection levels, V_k is ASR, $S_\sigma = SNR_0 = R\bar{P}\sqrt{2T_c/N_0}$ is the defined optical SNR, $S = \lambda\sum_{j=0}^{k-1} b_{k-j}\,h_j$ is the convolved signal after the optical wireless channel. In fact, OOK can be treated as 2-PAM, as 2-PAM had two levels of amplitude change, if assume the possible levels were '0' and '1', then OOK can be included into L-PAM modulation schemes.

3.3.3 PPM and PAPM

For PAPM signal detection, similar to PPM detector, a maximum-a-posterior (MAP) can first be used to detect the positions of the primary pulse [31]. Then a threshold detector detected the level of the received optical signal. The PPM can be treated as a special case of PAPM when amplitude level was one. Thus it was possible to derive the error probability for these two schemes. Considering a pulse sequence received under ISI and corrupted by ambient light noise, at the receiver, the detected pulse chips can be expressed by the set of event:

$$E_c = \{X \mid X = (x_1, x_2, x_3, \dots, y, \dots, x_n)\} \tag{3.27}$$

Where $y = x_i$, x_n is the last chip of the received pulse. The probability of all outcomes of the detection event can be expressed as following

$$\int P_X dX = 1 \tag{3.28}$$

Assume $-\infty < x_i < +\infty$, and x_i are independent

$$P_X dX = P_{x_1} dx_1 P_{x_2} dx_2 \dots P_y dy \dots P_{x_n} dx_n \tag{3.29}$$

It was assumed that P_x is a Gaussian normal distribution, and its probability density function is then $P_x = \frac{1}{\sigma\sqrt{2\pi}} e^{-\frac{x^2}{2\sigma}}$ where $\sigma = \sqrt{T_c N_0/2}$ is the Gaussian noise variance. Successful detection of m-th amplitude level of the primary symbol was a condition of following two events:

$$x_j < B_j = y + G_j \tag{3.30}$$

$$G^- < y < G^+ \tag{3.31}$$

Where $G_j = z_i - z_j$, G^- and G^+ were defined as following:

$$G^+ = \begin{cases} \theta_m - Z_i, & m < M \\ +\infty, & m = M \end{cases}$$

$$G^- = \begin{cases} \theta_{m-1} - Z_i, & m > 0 \\ -\infty, & m = 0 \end{cases} \tag{3.32}$$

given a fixed y, the probabilities of equation (3.30) are,

$$p_j = \int_{-\infty}^{B_j} P_{x_j} dx_j = \int_{-\infty}^{B_j} \frac{1}{\sigma\sqrt{2\pi}} e^{-\frac{{x_j}^2}{2\sigma}} dx_j = 1 - Q\left(\frac{B_j}{\sigma}\right) \tag{3.33}$$

Detailed derivation can be found in Appendix III-1, the probability of success for both equation (3.30) and equation (3.31) is then

$$P_{success} = \int_{G^-}^{G^+} P_y dy \prod_j \int_{-\infty}^{B_j} P_{x_j} dx_j \tag{3.34}$$

Where $\prod$ is product operation. Substitute equation (3.33) into equation (3.34) yields:

$$P_{success} = \int_{G^-}^{G^+} P_y \prod_j \left(1 - Q\left(\frac{B_j}{\sigma}\right)\right) dy \tag{3.35}$$

The full probability of correct detection Pcd over all possible chips sequences and during one period of ambient light interference is $Pcd = \frac{1}{T_i}\int_{dt}^{T_i} \frac{1}{C_{cs}} \sum_{C_{cs}} P_{success}$. Where C_{cs} is the set of all possible chip sequences combinations, $C_{cs} = (M \cdot n)^{(\frac{k_{ps}}{n}+1)}$, M is the number of amplitude level, n is number of slot number, k_{ps} is length of previous sequence, T_i is the ambient light noise interference period, the detection error P_{de} can then be expressed as:

$$P_{de} = 1 - Pcd = \frac{1}{T_i}\int_{dt}^{T_i} \frac{1}{C_{cs}} \sum_{C_{cs}} (1 - P_{success}) \tag{3.36}$$

3.4 Summary

Modulation schemes preferred for the optical wireless channel were introduced. The combined power and bandwidth efficiency expressions were listed. The detection error probability of the three baseband modulation schemes were listed and derived for optical channel impaired by both ISI and background ambient light noises. The obtained analytical model can be used to count for any modulation order of PAM, PPM and PAPM modulation schemes. This extended the previous mathematical model and provided a useful platform to validate modulation schemes under single or multiple interferences.

Using equations developed in this section, the performance of different modulation schemes can be simulated and compared with analytical methods.

Chapter 4

Adaptive Modulation

4.1 Introduction

Following the discussions in Chapter 3, the desired system performance suggested the optical wireless system can benefit from employing different modulation schemes under different channel conditions. This was similar to an RF system, and a different modulation order had been used to achieve highest throughput according to SNR condition [94]. In this chapter, the performances of modulation schemes were investigated further under interference conditions. Since the trade

off between the bandwidth and power efficiency was non avoidable, modulation schemes can adaptively tune amplitude levels or pulse positions in order to maintain the maximum possible throughput under interferences [95].

As discussed in Chapter 3, the average required power to achieve a certain BER level was dependent on the power spectral density of the AWGN channel and data rate. A practical transmitter-receiver structure model can keep the transmission power constant, although the momentary signal power may vary from the average power. However, the optical wireless link can be distorted by interference from different noise source. Multipath ISI and periodic background ambient noise can contribute to the performance degradation.

Multilevel modulation schemes had the potential ability to maintain a satisfactory system performance under distortion. Rate-compatible punctured convolutional codes (RCPCs) and repetition codes (RCs) had been combined with L-PPM to give a good BER performance at the cost of lower data rates [40]. Apart from the average power requirement, the data rate and the BER were two important parameters for wireless optical links.

Wong et al analysed ISI and ambient noise impact for different modulation techniques under specific channel geometry set ups (a room size of 5m×5m×3m) [68]. Their discussions were limited to include comparison amongst OOK, 2-PPM and SIK only. In this chapter, the performance of popular modulation schemes were discussed under a more general channel model, e.g. not limited to a specific room set up, with modulation schemes extended to include L-PAM, L-PPM and

M-n-PAPM. In terms of combating the ISI and background ambient noise, the proposed adaptive modulation scheme were analysed under different channel impairments. Simulation results were used to validate the performance of the proposed scheme with other candidate for the wireless optical communication channel.

The adaptive modulation scheme here was initially intended to mitigate the data rate drop in a diffuse optical link, where multipath distortion was present [71]. However, the adaptive modulation was not limited to a diffuse model. Modulation techniques developed in this chapter were also suitable for LOS systems, where multipath distortion was not regarded as significant compared to that of diffuse systems, since the interference from ambient light noise can be reduced by increasing the optical pulse intensity, thus increasing the SNR. In the interests of data rate recovery, the optimum modulation scheme parameter under different system degradations can be obtained through searching algorisms. The candidate modulation schemes had been chosen, based on the merit of combined power and bandwidth efficiency, as detailed in Chapter 3. For model simplicity, the following assumptions were made:

a. The channel was an AWGN type
b. Synchronisation was maintained for L-PPM and M-n-PAPM
c. The system operated in an office environment (e.g. moderate radiation from the sun)

4.1.1 Channel Model

As discussed in Chapter 2, concentrating only on a specific channel can lead to loss of generality. The more general and accurate ceiling bounce model was chosen as the channel model for discussion.

The impulse response of the ceiling bounce model can be plotted versus time at a given ceiling height H, in Figure 4.1, $H = 10m$, time step was $1ns$.

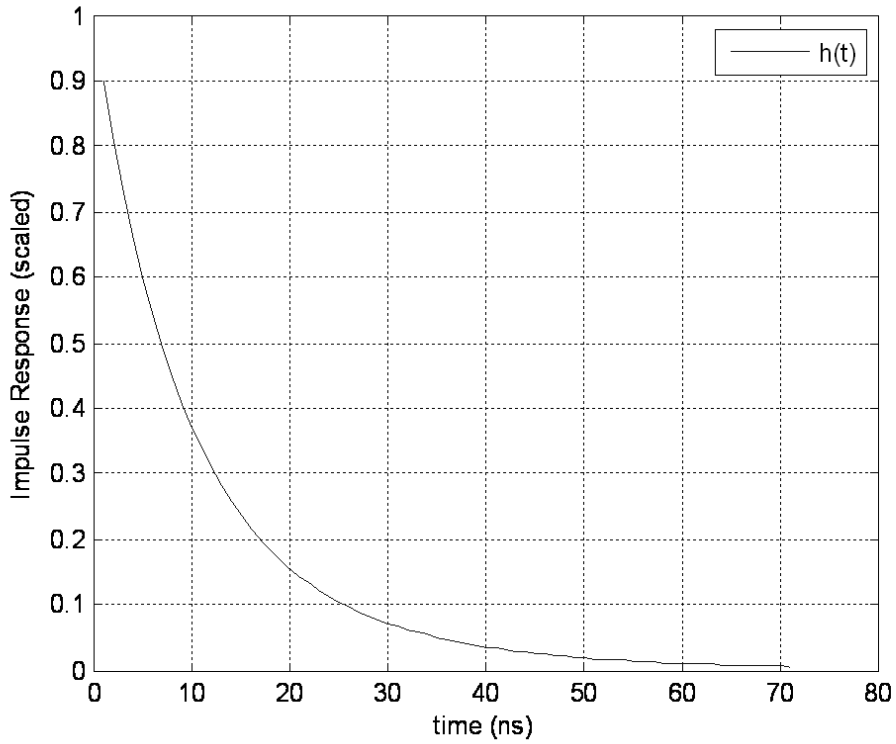

Figure 4.1 Channel impulse response (H=10m)

In Figure 4.1, the energy of the received optical pulse decreases with time, while most energy (e.g. 90%) arrived within $30ns$ in this case, with delayed tails lasting up over to $70ns$. The impulse response was directly related to parameter a according to equation (2.7), and the relationships of the impulse response under different ceiling height can be obtained in Figure 4.2.

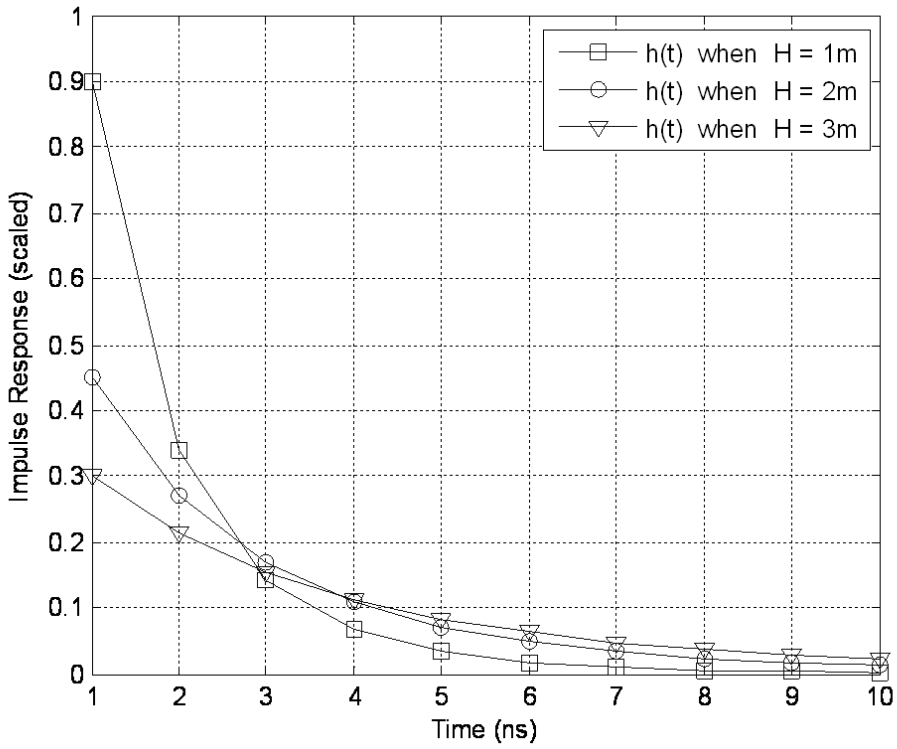

Figure 4.2 Channel impulse response according to H

In Figure 4.2, as H increased, the starting value of $h(t)$ decreased, which indicated that the received optical pulse energy was reduced, the energy under the $h(t)$ curve also shifted to its tail, which suggested that when optical path length increased, the delay of the pulse increased, so the ISI interferences became worse. The reverse happened when H decreased. Thus the ceiling height can be used to reflect ISI severity.

The standard system model was derived from the OOK modulation scheme. First, for given link parameters, a corresponding normalised data rate compensation ratio was derived from the OOK scheme. Second, a multilevel modulation scheme performed a search within its available system status to find its data rate compensation ratios. Finally, comparing these ratios to the normalised OOK ratio,

the system status with best approximation to the normalised ratio represented the optimum candidate for the adaptive modulation scheme.

4.1.2 IrDA BER Requirements

In May 2001, the IrDA serial Infrared physical layer specification (version 1.4) indicated a general industry BER requirement for an IR ready product [89], stating that the "Bit Error Ratio shall be no greater than 10^{-8}, the link shall operate and meet the BER specification over its range." In the more recent IrDA serial Infrared physical layer measurement guidelines (version 1.2.7), published in February 2006 [96], the BER requirement had been relaxed for practical applications, stating "for the purpose of practical testing time and acceptable bit error rate in most "real" applications, 10^{-7} is acceptable for data rates of 0.5M-4M bps, and 10^{-6} is acceptable for data rates of 9.6k-115.2k bps." This reflected that the lifting of the rigorous 10^{-8} standard presented a barrier for some real time applications.

Thus, in the test model two sets of BER test data were used. The first set ranged from 10^{-9} to 10^{-7}, to represent moderate degradation and second set ranged from 10^{-7} to 10^{-4}, to represent severe degradation. The data rate was chosen at 4Mbps and 250Mbps.

4.2 Adaptive Modulation

As discussed in Chapter 3, the L-PAM, L-PPM can be treated as a special case of M-n-PAPM, e.g. when M=1, M-n-PAPM becomes 1-n-PAPM, which was PAPM modulation with one amplitude level, that was, L-PPM in fact. When n=1, M-n-PAPM becomes L-PAM. Thus M-n-PAPM was a unified form of both PAM and PPM. In this section, the adaptive ability of these three modulation schemes was discussed. The Matlab program used to calculate the adaptive factor for L-PAM, L-PPM and M-n-PAPM can be found in Appendix IV-1.

The adaptive modulation scheme was proposed to improve data throughput when the optical wireless channel was distorted due to ISI and intense background ambient light noise [71]. By changing the optical pulse amplitude levels or positions, signal pulse energy and bandwidth requirement can be adjusted. This resulted changes in SNR and data rate respectively, which in turn provides BER improvements at the cost of power consumption or reduced data rate. This approach was different from other techniques, such as spread spectrum, which increased system complexity. Adaptive modulation schemes were especially suitable for high speed indoor wireless optical environment, where communication systems operate under intense background ambient light noise and ISI interference.

The OOK modulation scheme was again treated as a reference when comparing with other schemes. The power compensation ratio was obtained from the BER variation ratio. For moderate degradation, with initial BER=10^{-9} and final BER=10^{-7}, from equation (3.4) the power compensation ratio is given by:

$$\frac{P_{OOK\_i}}{P_{OOK\_f}} = \frac{\sqrt{N_0 R_{OOK\_i}}\,Q^{-1}(BER_{OOK\_i})}{\sqrt{N_0 R_{OOK\_f}}\,Q^{-1}(BER_{OOK\_f})} = \frac{\sqrt{R_{OOK\_i}}\,Q^{-1}(BER_{OOK\_i})}{\sqrt{R_{OOK\_f}}\,Q^{-1}(BER_{OOK\_f})} \quad (4.1)$$

Where P_{OOK_i} and R_{OOK_i} are the initial power requirement and data rate to achieve initial BER_{OOK_i}. P_{OOK_f} and R_{OOK_f} are the power requirement and data rate to achieve the varied final BER_{OOK_f}, and in the case of constant average power, $P_{OOK\_i} = P_{OOK\_f}$, and equation (4.1) becomes:

$$\frac{R_{OOK\_i}}{R_{OOK\_f}} = \left[\frac{Q^{-1}(BER_{OOK\_f})}{Q^{-1}(BER_{OOK\_i})}\right]^2 \quad (4.2)$$

Note equation (4.1) and equation (4.2) were only valid when satisfying the following conditions:

$$\begin{cases} R_{OOK\_i} > 0 \\ R_{OOK\_f} > 0 \end{cases} \quad (4.3)$$

$$\begin{cases} Q^{-1}(BER_{OOK\_i}) \neq 0 \\ Q^{-1}(BER_{OOK\_f}) \neq 0 \end{cases} \quad (4.4)$$

Where (4.2) yields the following:

$$\begin{cases} BER_{OOK\_i} \neq Q(0) \leftrightarrow BER_{OOK\_i} \neq 0.5 \\ BER_{OOK\_f} \neq Q(0) \leftrightarrow BER_{OOK\_f} \neq 0.5 \end{cases} \quad (4.5)$$

For moderate degradation, where $BER_{OOK\_i}=10^{-9}$, $BER_{OOK\_f}=10^{-7}$. For severe degradation conditions, $BER_{OOK\_i}=10^{-7}$, $BER_{OOK\_f}=10^{-4}$. To compare the specific throughput losses caused by the BER variation, the data rate R_{OOK_i}=4Mbps and R_{OOK_i}=250Mbps were substituted into equation (4.2), and the data rate change results can be found in the following Table 4.1

Table 4.1 Data rate degradation of OOK

Moderate Degradation		Severe Degradation	
Initial R_b (Mbps)	Final R_b (Mbps)	Initial R_b (Mbps)	Final R_b (Mbps)
4	5.3	4	7.8
250	332.7	250	488.6

In Table 4.1, with moderate degradation, the data rates changed from 4Mbps and 250Mbps to 5Mbps and 333Mbps respectively, which was 33.1% of throughput variation. For severe degradation, the variation was 95.5%

Comparing data rate variation for systems operating at 4Mbps, the difference between the moderate and severe model was not significant. By contrast, for a system operating at 250Mbps, the data rate loss between the moderate and severe model was large. This suggested that, at higher speed, the OOK modulation scheme was more susceptible to BER variation.

4.2.1 Adaptive L-PAM

The L-PAM modulation required more power to achieve the same level of BER as L-PPM. Thus L-PAM modulation was not preferred in terms of power efficiency [15]. While considering the bandwidth requirements, L-PAM modulation was more efficient than L-PPM, as, by assigning different levels of amplitude to

represent a symbol sequence, the L-PAM signal cannot span its symbol sequence along the time axis, which was the case for L-PPM. This can be demonstrated in Figure 4.3. Higher level PAM was throughput-efficient scheme, as it allowed more data to be transmitted compared to PPM. Detailed procedures and Matlab program for Figure 4.3 can be found in Appendix IV-2.

In Figure 4.3, changing from 2-PAM to 16-PAM reduced the bandwidth requirement by a factor of 1/4, so 16-PAM can transmit 4 times more data than 2-PAM within same time. This came at a cost of 8.8dB power penalty. The power to bandwidth ratio for L-PAM was then 8.8 / (1-0.25) = 11.73 dB per bandwidth unit.

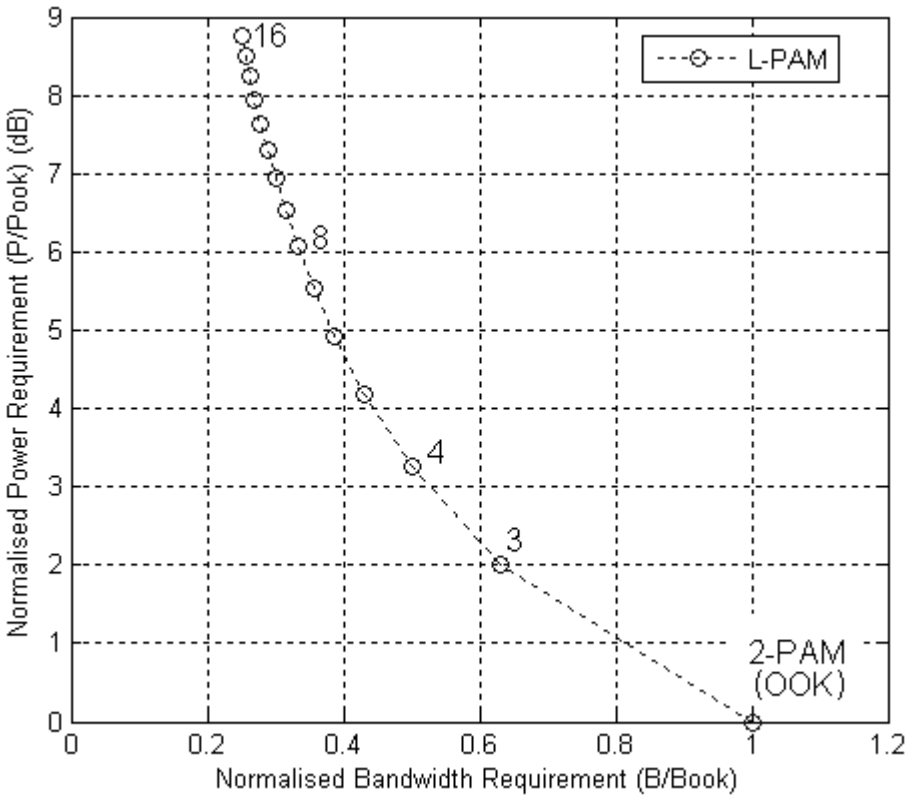

Figure 4.3 Normalised power and bandwidth requirement of L-PAM

From equation (3.7), the average power requirement of L-PAM can be found for a given BER, following equation (4.1); the initial and final state of the L-PAM scheme can be described as:

$$\frac{P_{L-PAM\_i}}{P_{L-PAM\_f}} = \frac{\frac{L_{PAM\_i}-1}{\sqrt{\log_2 L_{PAM\_i}}} \cdot \sqrt{N_0 R_{L-PAM\_i}} Q^{-1}(BER_{L-PAM\_i})}{\frac{L_{PAM\_f}-1}{\sqrt{\log_2 L_{PAM\_f}}} \cdot \sqrt{N_0 R_{L-PAM\_f}} Q^{-1}(BER_{L-PAM\_f})} \quad (4.6)$$

Where $P_{L\text{-}PAM\_i}$, $R_{L\text{-}PAM\_i}$ and L_{PAM_i} indicate the average power requirement, the data rate and amplitude level to achieve $BER_{L\text{-}PAM\_i}$. $P_{L\text{-}PAM\_f}$, $R_{L\text{-}PAM\_f}$ and L_{PAM_f} represent the average power requirement, data rate and amplitude level respectively to achieve $BER_{L\text{-}PAM\_f}$. Following the same discussion as for OOK, the initial error rate, the varied error rate, and the initial data rate satisfy the following:

$$\begin{cases} BER_{L-PAM\_i} = BER_{OOK\_i} \\ BER_{L-PAM\_f} = BER_{OOK\_f} \\ R_{L-PAM\_i} = R_{OOK\_i} \end{cases} \quad (4.7)$$

Keeping the average power requirement constant, equation (4.6) can yield:

$$\because \frac{P_{L-PAM\_i}}{P_{L-PAM\_f}} = 1$$

$$\leftrightarrow \frac{R_{L-PAM\_i}}{R_{L-PAM\_f}} = \left[\frac{\frac{L_{PAM\_f}-1}{\sqrt{\log_2 L_{PAM\_f}}}}{\frac{L_{PAM\_i}-1}{\sqrt{\log_2 L_{PAM\_i}}}} \right]^2 \cdot \left[\frac{Q^{-1}(BER_{L-PAM\_f})}{Q^{-1}(BER_{L-PAM\_i})} \right]^2 \qquad (4.8)$$

From equation (4.8), the data rate ratio was a function of amplitude levels and BER, where the first item in equation (4.8) can be used as a ratio to balance the degradation caused by the variation of the BER.

Comparing equation (4.8) with equation (4.2), the L-PAM scheme provides a ratio factor by changing the amplitude level L_{PAM}. This ratio factor was a function of L_{PAM}. The set formed by L_{PAM} was a subset of the natural number set N with a condition $\{L_{PAM} \mid L_{PAM} \geq 2, L_{PAM} \subset N\}$. By selectively choosing values of L_{PAM_i} and L_{PAM_f}, the ratio factor in equation (4.8) can compensate for the data rate reduction caused by the BER variation.

A test case can be demonstrated by employing a multilevel L-PAM modulation scheme, where the pulse amplitude levels took three values, which can be expressed as $L_{PAM\_i}, L_{PAM\_f} \in \{2,3,4\}$, so from equation (4.8), the adaptive factors can be obtained by substituting L_{PAM} values, and the resulting matrix can be expressed by Table 4.2

Table 4.2 L-PAM value matrix of adaptive factors

$\left[\frac{\frac{L_{PAM\_f}-1}{\sqrt{\log_2 L_{PAM\_f}}}}{\frac{L_{PAM\_i}-1}{\sqrt{\log_2 L_{PAM\_i}}}}\right]^2$		L_{PAM_i}		
		2	3	4
L_{PAM_f}	2	1	0.4	0.2
	3	2.5	1	0.6
	4	4.5	1.8	1

In Table 4.2, the adaptive factor matrix was obtained by changing pulse amplitude levels. The maximum value is 4.5, which was provided by changing the amplitude level from 2 to 4. The minimum value was 0.2, and obtained by changing the amplitude from 4 back to 2. This suggested that a reverse level change will not necessary give the same adaptive ratio. The ratio table was symmetric along the table axis.

For moderate system degradation, which the initial BER=10^{-9} and the final BER=10^{-7}, substituting BER values into (4.8), the degradation factor is thus:

$$\left[\frac{Q^{-1}(BER_{L-PAM\_f})}{Q^{-1}(BER_{L-PAM\_i})}\right]^2 = \left[\frac{Q^{-1}(10^{-7})}{Q^{-1}(10^{-9})}\right]^2 = 0.8 \tag{4.9}$$

Considering this degradation factor, together with the candidate values in Table 4.2, in order to find the optimum adaptive level factor, the inverse of above ratio was compared with every value in Table 4.2. The preferred value made the right

hand side of equation (4.8) approach 1. Thus, subtracting the inverse value of the above ratio, and applying it to every element in Table 4.2, gives Table 4.3

Table 4.3 Comparison of adaptive and interference ratio for L-PAM

$\frac{R_{L-PAM\_i}}{R_{L-PAM\_f}}$ - 1		L_{PAM_i}		
		2	3	4
L_{PAM_f}	2	-0.2	-0.7	-0.8
	3	0.9	-0.2	-0.6
	4	2.4	0.3	-0.2

From Table 4.3, the values along the diagonal were self level comparison, and thus were ignored. Positive values indicated the situation where the adaptive factor was greater than the interference factor, and suggested that the adaptive factor was sufficient to compensate the degradation caused by the BER variation. The negative situations were vice versa. Note the values in Table 4.3 also indicated the quality of the adaptive factors. These values reflected how close the adaptive factors can approach the interference factor. Thus, the absolute values were taken when processing comparisons. The smaller the values, the better the adaptive abilities become. This can be demonstrated in the following Figure 4.4.

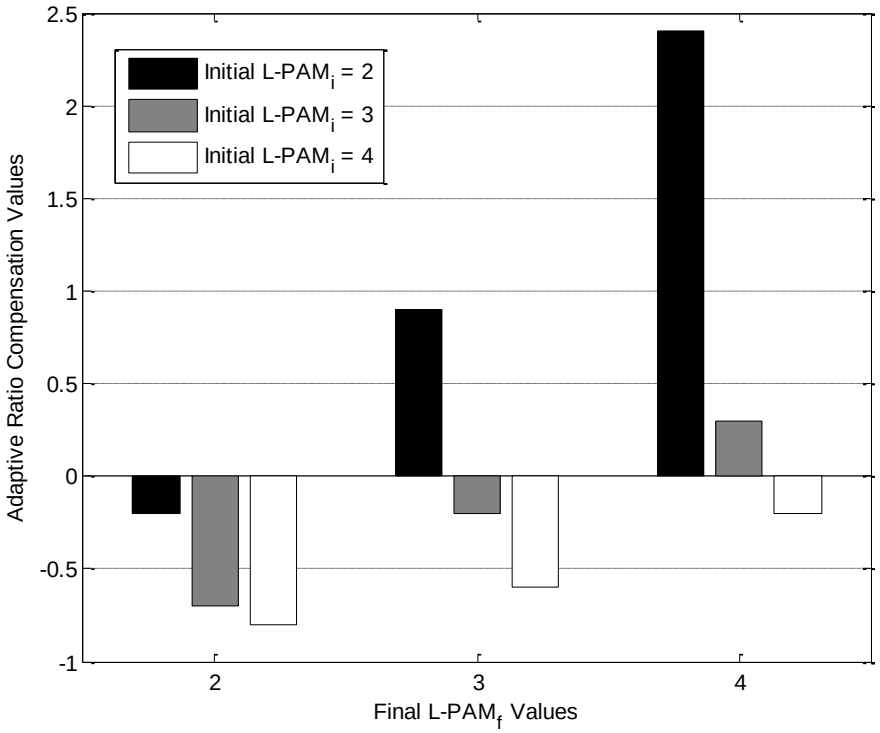

Figure 4.4 Optimum adaptive ratio value search (L-PAM)

In Figure 4.4, apart from the diagonal values, the optimum value can be achieved while the amplitude adapts from 3-level PAM to 4-level PAM. Thus, under moderate BER degradation, the recovered data rate $R_{L\text{-}PAM\_f}$ can be calculated using equation (4.8).

$$\because \frac{R_{L-PAM\_i}}{R_{L-PAM\_f}} = \left[\frac{\frac{L_{PAM\_f}-1}{\sqrt{\log_2 L_{PAM\_f}}}}{\frac{L_{PAM\_i}-1}{\sqrt{\log_2 L_{PAM\_i}}}} \right]^2 \cdot \left[\frac{Q^{-1}(BER_{L-PAM\_f})}{Q^{-1}(BER_{L-PAM\_i})} \right]^2$$

$$\therefore R_{L-PAM\_f} = R_{L-PAM\_i} \cdot \left[\frac{\frac{L_{PAM\_i}-1}{\sqrt{\log_2 L_{PAM\_i}}}}{\frac{L_{PAM\_f}-1}{\sqrt{\log_2 L_{PAM\_f}}}} \right]^2 \cdot \left[\frac{Q^{-1}(BER_{L-PAM\_i})}{Q^{-1}(BER_{L-PAM\_f})} \right]^2 \quad (4.10)$$

L_{PAM_i}=3, L_{PAM_f}=4, $BER_{L\text{-}PAM\_i}=10^{-9}$ and $BER_{L\text{-}PAM\_f}=10^{-7}$ were substituted into equation (4.10) for the final data rate of $R_{L\text{-}PAM\_i}$=4Mbps and $R_{L\text{-}PAM\_i}$=250Mbps respectively. $BER_{L\text{-}PAM\_i}=10^{-7}$ and $BER_{L\text{-}PAM\_i}=10^{-4}$ were substituted for severe degradation, so the data rate recovery may be obtained. The data rate stability of L-PAM is represented in the following Table 4.4.

Table 4.4 Data rate recovery of L-PAM ($L_{PAM} \in \{2,3,4\}$)

Moderate Degradation		Severe Degradation	
Initial R_b (Mbps)	Final R_b (Mbps)	Initial R_b (Mbps)	Final R_b (Mbps)
4	5.3	4	3.6
250	325	250	225

From Table 4.4, the adaptive L-PAM performed similarly to the OOK scheme under moderate BER degradations and lower data rate. However, the adaptive L-PAM outperformed OOK under severe BER degradations, especially when operating at a higher data rate. Thus adaptive L-PAM modulation schemes with $L_{PAM} \in \{2,3,4\}$ can provide data rate recovery compared to OOK. The adaptive L-PAM modulation schemes indicated an improvement of data rate recovery under severe degradation. This resulted in a 30% throughput variation for the 4Mbps link and 90% for the higher 250Mbps. Compared to OOK, L-PAM reduced the variation range.

4.2.2 Adaptive L-PPM

Similar to adaptive L-PAM, by adjusting number of the pulse positions within a symbol sequence, the adaptive L-PPM can realise balancing between power and bandwidth requirements. PPM was a bandwidth-efficient modulation technique compared to OOK and PAM. This can be demonstrated by Figure 4.5. Detailed procedure and Matlab program for Figure 4.5 can be found in Appendix IV-3.

In Figure 4.5, it was seen that by changing from 2-PPM to 16-PPM, the power requirement reduced 7.5dB. This came at a cost of twice the bandwidth requirement. The power to bandwidth ratio for L-PPM was then 7.5 / (4-2) = 3.75 dB per bandwidth unit. This was 3 times more power efficient than PAM.

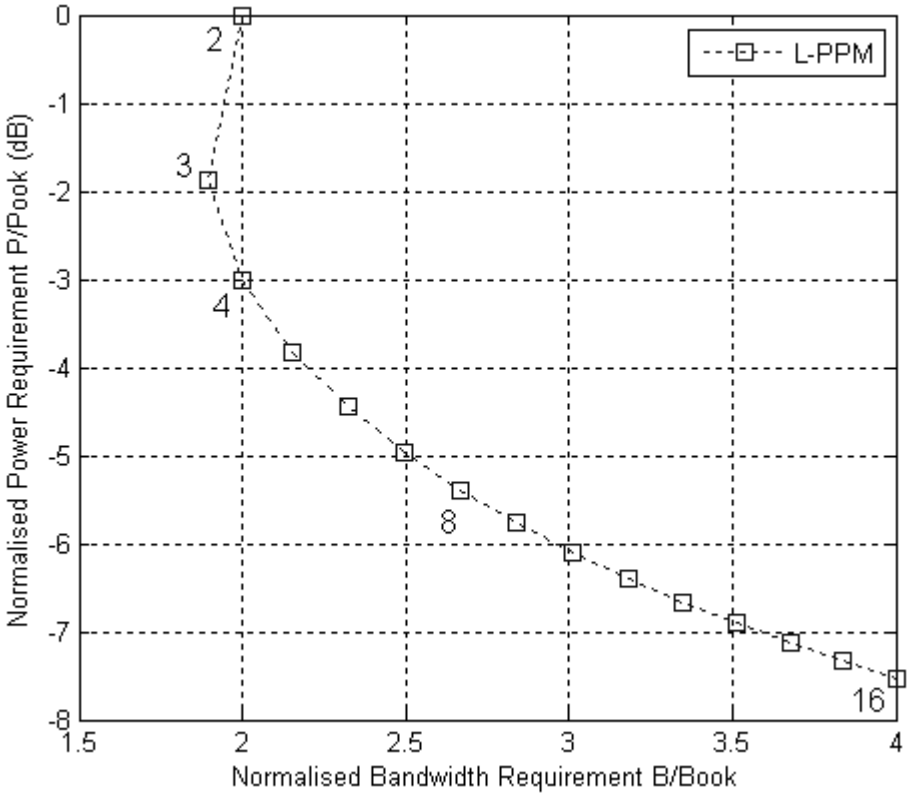

Figure 4.5 Normalised power and bandwidth requirement of L-PPM

The L-PPM modulation scheme was a power efficient scheme, and 4-PPM modulation was adopted in the IrDA standard for 4Mbps data links [89]. In contrast with the L-PAM scheme, under moderate pulse position levels (e.g.$L_{PAM} > 2$), the L-PPM scheme only required half, or even less of the power required by other schemes such as the OOK and PAM. The L-PPM modulation

scheme was not bandwidth efficient [15]. Higher order pulse positions can lead to higher bandwidth consumption.

Next, the data rate recovery abilities for L-PPM were examined. In a similar way to the adaptive L-PAM, the OOK modulation scheme was treated as a benchmark. According to equation (3.10) the average power requirement of L-PPM for a given BER can be represented by relating to OOK as follows:-

$$\frac{P_{L-PPM\_i}}{P_{L-PPM\_f}} = \frac{\sqrt{\frac{2}{L_{PPM\_i} \cdot \log_2 L_{PPM\_i}}} \cdot \sqrt{N_0 R_{L-PPM\_i}} Q^{-1}(BER_{L-PPM\_i})}{\sqrt{\frac{2}{L_{PPM\_f} \cdot \log_2 L_{PPM\_f}}} \cdot \sqrt{N_0 R_{L-PPM\_f}} Q^{-1}(BER_{L-PPM\_f})} \quad (4.11)$$

where $P_{L\text{-}PPM\_i}$, $R_{L\text{-}PPM\_i}$ and L_{PPM_i} indicate the initial average power requirement, data rate and pulse position levels required to achieve $BER_{L\text{-}PPM\_i}$. $P_{L\text{-}PPM\_f}$, $R_{L\text{-}PPM\_f}$ and L_{PPM_f} represent the average power requirement, data rate and pulse position levels required to achieve $BER_{L\text{-}PPM\_f}$. Following the L-PAM discussion, the BER and pulse positions can be related to OOK as follows:-

$$\begin{cases} BER_{L-PPM\_i} = BER_{OOK\_i} \\ BER_{L-PPM\_f} = BER_{OOK\_f} \\ R_{L-PPM\_i} = R_{OOK\_i} \end{cases} \quad (4.12)$$

Since the average power requirement was fixed, equation (4.11) can be rearranged to represent data rate:

$$\frac{R_{L-PPM\_i}}{R_{L-PPM\_f}} = \left[\frac{L_{PPM\_i}\cdot\log_2 L_{PPM\_i}}{L_{PPM\_f}\cdot\log_2 L_{PPM\_f}}\right]\cdot\left[\frac{Q^{-1}(BER_{L-PPM\_f})}{Q^{-1}(BER_{L-PPM\_i})}\right]^2 \quad (4.13)$$

The data rate ratio can be represented by two parts, the adaptive part formed by pulse position levels and variation of system BER. Comparing equation (4.13) with equation (4.8) and equation (4.2), and similar to the adaptive L-PAM, the adaptive L-PPM scheme included the pulse position level L_{PPM} as an adaptive factor. This ratio factor was function of L_{PPM} and it satisfied $\{L_{PPM} \mid L_{PPM} \geq 2, L_{PPM} \subset N\}$. Using same model applied to L-PAM, substituting $L_{PPM\_i}, L_{PPM\_f} \in \{2,3,4\}$ into (4.13), allowed the ratio factor to be represented by Table 4.5 below:

Table 4.5 L-PPM value matrix of adaptive factors

$\left(\frac{L_{PPM\_i}\cdot\log_2 L_{PPM\_i}}{L_{PPM\_f}\cdot\log_2 L_{PPM\_f}}\right)$		L_{PPM_i}		
		2	3	4
L_{PPM_f}	2	1	0.4	0.3
	3	2.4	1	0.6
	4	4	1.7	1

In Table 4.5, the maximum ratio provided by this matrix was 4, which was obtained by shifting L from 2 to 4. The minimum ratio was 0.3 by changing pulse positions from 4 back to 2. Similar to PAM, the adaptive ratio was symmetric along the matrix diagonal. Under moderate system degradation, substituting $BER_{L\text{-}PPM\_i}=10^{-9}$ and $BER_{L\text{-}PPM\_f}=10^{-7}$ into equation (4.13), given the degradation

factor to be same as in equation (4.9). Perform a search to find the optimum adaptive level, multiply equation (4.9) by values in Table 4.5, then Table 4.6 can be obtained.

Table 4.6 Comparison of adaptive and interference ratio for L-PPM

$\frac{R_{L-PPM\_i}}{R_{L-PPM\_f}}$ - 1		L_{PPM_i}		
		2	3	4
L_{PPM_f}	2	-0.25	-0.68	-0.81
	3	0.79	-0.25	-0.55
	4	2.01	0.26	-0.25

Similar to Table 4.3, in Table 4.6, the values along the diagonal were self level comparison, and thus were discarded. Positive values indicated the adaptive factor was sufficient to compensate the degradation caused by the BER variation. The negative values indicated the reverse situation. This can be further demonstrated by Figure 4.6, where the optimum ratio can be compared to other values.

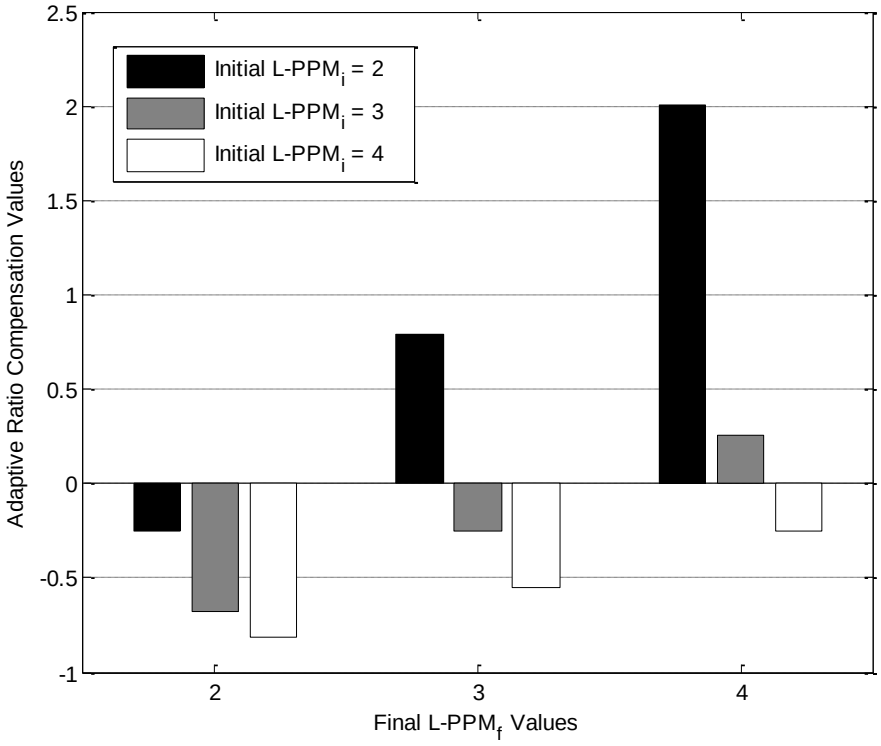

Figure 4.6 Optimum adaptive ratio value search (L-PPM)

From Figure 4.6, the optimum value can be achieved by changing pulse positions from 3-level PPM to 4-level PPM. Note this was similar to the L-PAM model. For moderate degradation, L_{PPM_i}=3, L_{PPM_f}=4, $BER_{L\text{-}PPM\_i}=10^{-9}$ and $BER_{L\text{-}PPM\_f}=10^{-7}$ of $R_{L\text{-}PPM\_i}$=4Mbps and $R_{L\text{-}PPM\_i}$=250Mbps must be substituted into equation (4.13) respectively. For severe degradation, BER was replaced with $BER_{L\text{-}PPM\_i}=10^{-7}$ and $BER_{L\text{-}PPM\_i}=10^{-4}$, so the data rate recovery for adaptive L-PPM can be obtained. Adaptive L-PPM schemes had an improved performance over adaptive L-PAM, Referring to Table 4.1 for OOK and Table 4.4 for adaptive L-PAM, the data rate recovery of adaptive L-PPM can be represented in the following Table 4.7.

Table 4.7 Data rate recovery of L-PPM ($L_{PPM} \in \{2,3,4\}$)

Moderate Degradation		Severe Degradation	
Initial R_b (Mbps)	Final R_b (Mbps)	Initial R_b (Mbps)	Final R_b (Mbps)
4	5.0	4	3.4
250	315	250	215

From Table 4.7, adaptive L-PPM achieved certain improvements compared to OOK and PAM. Comparing Table 4.1, Table 4.4 and Table 4.7, under moderate system degradation, adaptive PPM offered data rate compensation of 0.3Mbps better than OOK and PAM for a 4Mbps link, and 10Mbps better in 250Mbps link. Under severe degradation, for the 4Mbps link, the improvement increased to 4.4Mbps for OOK and a similar 0.2Mbps over adaptive L-PAM. For the 250Mbps link the figures became 273.6Mbps and 10 Mbps for OOK and adaptive L-PAM respectively. The data rate stability of the adaptive L-PPM was significant over the OOK model. The performance enhancement factors exhibited sufficient for higher speed than lower speed counterparts.

4.2.3 Adaptive M-n-PAPM

Now considering adaptive PAPM, similar to discussions for adaptive PAM and PPM, the adaptive PAPM can realise adaptation by changing both amplitude and number of pulse slots. The normalised power and bandwidth requirements can be found in Figure 4.7. Detailed procedures and Matlab program for Figure 4.7 can be found in Appendix IV-4.

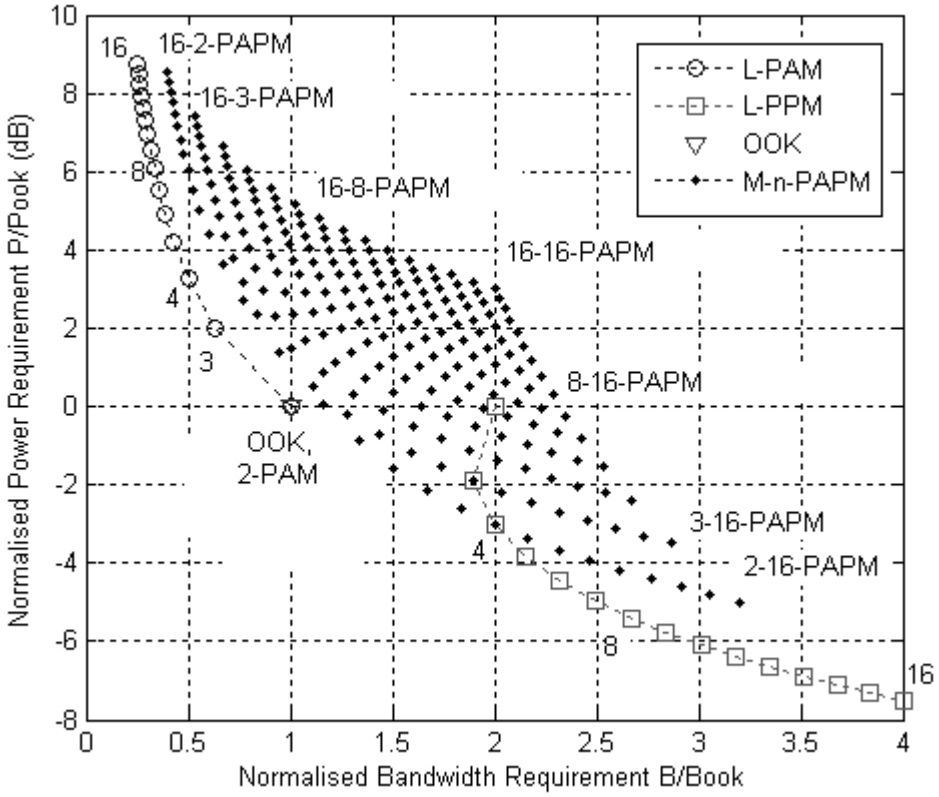

Figure 4.7 Normalised power and bandwidth requirement of M-n-PAPM

The adaptive M-n-PAPM modulation scheme was a combined multilevel modulation scheme based on PAM and PPM. As discussed in Chapter 3, the adaptive M-n-PAPM can provide a candidate solution to fill in the gap formed by PAM and PPM. By adaptively changing system states, the adaptive PAPM can be used to balance between power and bandwidth requirements, which resulted in a different pulse property that can be employed under different interference from the channel [95].

In this section, adaptive M-n-PAPM was discussed using the same models which were applied to OOK, PAM and PPM. The nomenclatures were the same as used in Chapter 3. M represents the amplitude levels and n represents the number of

pulse positions. For M-n-PAPM to be valid, M and n need to satisfy $\{M,n \mid \mathrm{M} \geq 2, \mathrm{n} \geq 2\}$. Similar to adaptive L-PAM and L-PPM, higher level amplitudes and pulse positions can lead to higher power and bandwidth consumption. Again the OOK modulation scheme was treated as a benchmark for comparison. From equation (3.13), the average power requirement of the M-n-PAPM scheme can be found for a given BER:-

$$\frac{P_{M-n-PAPM\_i}}{P_{M-n-PAM\_f}} = \frac{\frac{M_i+1}{\sqrt{n_i \log_2(M_i n_i)}} \cdot \sqrt{N_0 R_{M-n-PAPM\_i}} Q^{-1}(BER_{M-n-PAPM\_i})}{\frac{M_f+1}{\sqrt{n_f \log_2(M_f n_f)}} \cdot \sqrt{N_0 R_{M-n-PAPM\_f}} Q^{-1}(BER_{M-n-PAPM\_f})} \quad (4.14)$$

Where $P_{M\text{-}n\text{-}PAPM\_i}$, $R_{M\text{-}n\text{-}PAPM\_i}$, M_i and n_i indicate the average power requirement, data rate, system amplitude and pulse position level to achieve $BER_{M\text{-}n\text{-}PAPM\_i}$ respectively. $P_{M\text{-}n\text{-}PAPM\_f}$, $R_{M\text{-}n\text{-}PAPM\_f}$, M_f and n_f represent the system parameters to achieve $BER_{M\text{-}n\text{-}PAM\_f}$ respectively. Since the same model conditions applied to the OOK scheme were used, the BER satisfy the following:

$$\begin{cases} BER_{M-n-PAPM\_i} = BER_{OOK\_i} \\ BER_{M-n-PAPM\_f} = BER_{OOK\_f} \\ R_{M-n-PAPM\_i} = R_{OOK\_i} \end{cases} \quad (4.15)$$

Since system operated under constant average power constraint, equation (4.14) can be rearranged to relate data rate with amplitude, pulse position and error rate:

$$\frac{R_{M-n-PAPM\_i}}{R_{M-n-PAPM\_f}} = \left[\frac{\frac{(M_f+1)^2}{n_f \log_2(M_f n_f)}}{\frac{(M_i+1)^2}{n_i \log_2(M_i n_i)}} \right] \cdot \left[\frac{Q^{-1}(BER_{M-n-PAPM\_f})}{Q^{-1}(BER_{M-n-PAPM\_i})} \right]^2 \quad (4.16)$$

Comparing equation (4.16) with other modulations, the adaptive factor of M-n-PAPM was a function of both M and n. This formed the basis for the adaptive M-n-PAPM. The efficiency of the modulation scheme depended on the values selected. Similar to PAM and PPM, the data rate ratio can be represented by a function of amplitude levels and pulse position numbers, together with channel BER in equation (4.16). Based on the formulas obtained, the power and bandwidth efficiency of the adaptive M-n-PAPM can be observed by applying the experimental models. As M-n-PAPM contains two variables, the system states table was thus included more candidate levels. This certainly benefited the optimum value searching process.

Similar to adaptive PAM and PPM, the ratio factor can also be treated as a function of M and n. The resulting set satisfies $\{M,n \mid M,n \geq 2 \quad M,n \subset N\}$. Following the above conditions; a joint level ratio table can be organised by selectively choose value of M_i, n_i and M_f, n_f. The obtained ratio factor was then applied to the model discussed earlier to test the ability of data rate recovery against channel degradation. The adaptive ratio factor can then be determined, as in Table 4.8

Table 4.8 M-n-PAPM value matrix of adaptive factors

$\frac{(M_{\_i}+1)^2}{\frac{n_{\_i}\log_2(M_{\_i}n_{\_i})}{\frac{(M_{\_f}+1)^2}{n_{\_f}\log_2(M_{\_f}n_{\_f})}}}$			Final Value of $M_{\_f}$ and $n_{\_f}$								
			$M_{\_f}=2$			$M_{\_f}=3$			$M_{\_f}=4$		
			$n_{\_f}=2$	$n_{\_f}=3$	$n_{\_f}=4$	$n_{\_f}=2$	$n_{\_f}=3$	$n_{\_f}=4$	$n_{\_f}=2$	$n_{\_f}=3$	$n_{\_f}=4$
Initial Value of $M_{\_i}$ and $n_{\_i}$	$M_{\_i}=2$	$n_{\_i}=2$	1	1.9387	3	0.72702	1.3373	2.0165	0.54	0.96794	1.44
		$n_{\_i}=3$	0.5158	1	1.5474	0.375	0.68979	1.0401	0.27853	0.49927	0.74276
		$n_{\_i}=4$	0.33333	0.64624	1	0.24234	0.44577	0.67218	0.18	0.32265	0.48
	$M_{\_i}=3$	$n_{\_i}=2$	1.3755	2.6667	4.1264	1	1.8394	2.7737	0.74276	1.3314	1.9807
		$n_{\_i}=3$	0.74777	1.4497	2.2433	0.54364	1	1.5079	0.4038	0.7238	1.0768
		$n_{\_i}=4$	0.4959	0.96141	1.4877	0.36053	0.66317	1	0.26779	0.48	0.71409
	$M_{\_i}=4$	$n_{\_i}=2$	1.8519	3.5902	5.5556	1.3463	2.4765	3.7343	1	1.7925	2.6667
		$n_{\_i}=3$	1.0331	2.0029	3.0994	0.7511	1.3816	2.0833	0.55789	1	1.4877
		$n_{\_i}=4$	0.69444	1.3463	2.0833	0.50488	0.92869	1.4004	0.375	0.67218	1

From Table 4.8, the obtained adaptive factor table for adaptive M-n-PAPM contained more values than other modulation schemes. It was 9 times larger than that of both L-PAM and L-PPM. This certainly resulted in a better precision than the other two modulation schemes. Comparing Table 4.2 and Table 4.5, Table 4.8 exhibits some similar properties, e.g. values along diagonal were equal to 1.

Adaptive M-n-PAPM can be observed under moderate system degradation. Substituting the initial BER=10^{-9} and the final BER=10^{-7} into equation (4.18), the moderate degradation factor was same as for PAM and PPM modulations.

Similarly to previous discussions, the optimum adaptive factor made the best possible match for equation (4.16), i.e. it can choose adaptive ratio factors to make the initial and final data rate compatible, thus maximising the data rate compensation. The comparable basis depended on the above BER ratio. The optimum adaptive ratio can be obtained by two steps: Firstly, subtraction of the inverse BER ratio from every element in Table 4.8 was done. Secondly, a minimum search was performed within the results. The minimum data reflected the most optimum system level under the given BER condition. Thus the optimum system level can be identified using this algorithm. Note that values along the diagonal were not considered as valid, as these were self comparison. Applying the above calculation to Table 4.8 results in the following:

Table 4.9 Table 4.9 Comparison of adaptive and interference ratio for M-n-PAM

$\frac{R_{M-n-PAPM\_i}}{R_{M-n-PAPM\_f}}$ - 1			Final Value of $M_{\_f}$ and $n_{\_f}$								
			$M_{\_f} = 2$			$M_{\_f} = 3$			$M_{\_f} = 4$		
			$n_{\_f} = 2$	$n_{\_f} = 3$	$n_{\_f} = 4$	$n_{\_f} = 2$	$n_{\_f} = 3$	$n_{\_f} = 4$	$n_{\_f} = 2$	$n_{\_f} = 3$	$n_{\_f} = 4$
Initial Value of $M_{\_i}$ and $n_{\_i}$	$M_{\_i} = 2$	$n_{\_i} = 2$	1	0.456889	1.254407	-0.45367	0.004949	0.515368	-0.59421	-0.27262	0.082115
		$n_{\_i} = 3$	-0.61239	1	0.162832	-0.7182	-0.48164	-0.21837	-0.79069	-0.62482	-0.44184
		$n_{\_i} = 4$	-0.74951	-0.51437	1	-0.81789	-0.66502	-0.49488	-0.86474	-0.75754	-0.63929
	$M_{\_i} = 3$	$n_{\_i} = 2$	0.033628	1.003917	2.100884	1	0.382283	1.084354	-0.44184	0.00049	0.488424
		$n_{\_i} = 3$	-0.43808	0.089416	0.685775	-0.59147	1	0.133145	-0.69656	-0.45609	-0.19083
		$n_{\_i} = 4$	-0.62735	-0.27753	0.117957	-0.72907	-0.50165	1	-0.79877	-0.63929	-0.46338
	$M_{\_i} = 4$	$n_{\_i} = 2$	0.391609	1.697943	3.174828	0.011729	0.861016	1.806238	1	0.346994	1.003917
		$n_{\_i} = 3$	-0.22364	0.505144	1.329077	-0.43557	0.038234	0.56556	-0.58077	1	0.117957
		$n_{\_i} = 4$	-0.47815	0.011729	0.56556	-0.6206	-0.30212	0.052339	-0.7182	-0.49488	1

In Table 4.9, there were a few values close to 0, which suggested the resulting data rate recovery outperforms the other three modulation schemes. Similarly to the previous discussions, positive values indicated the adaptive factor was greater than the interference factor, where negative values indicated the reverse situation. The absolute value of the subtraction can determine the efficiency of the adaptive factors. It measured how closely the adaptive factors can approach the interference factors. The adaptive efficiency can be demonstrated in the following Figure 4.8 below:-

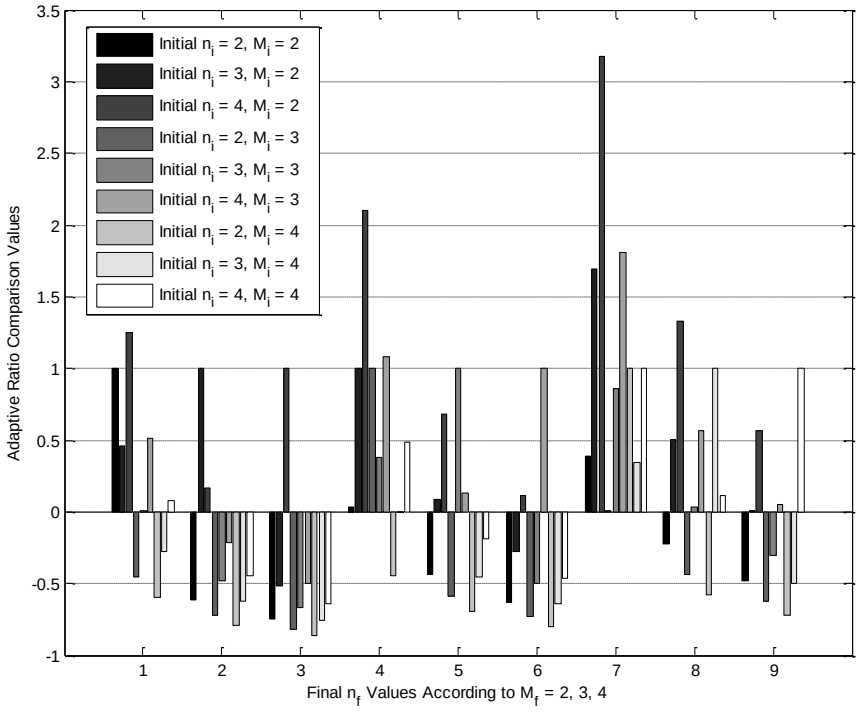

Figure 4.8 Optimum adaptive ratio value search (M-n-PAPM)

In Figure 4.8, the obtained subtraction values provided the candidate system levels. More complicated adaptive tasks can be performed by an adaptive M-n-PAPM scheme. The maximum optimised value can be arrived by searching the minimum absolute value in Table 4.9. The minimum value found by the simulation program

was 4.9×10^{-4}. This was obtained by changing 2-2-PAPM to 3-3-PAPM. The recovered data rate $R_{M\text{-}n\text{-}PAPM\_f}$ can be calculated using equation (4.16). Rearranging equation (4.16) as follows gives:

$$R_{M-n-PAPM\_f} = R_{M-n-PAPM\_i} \cdot \frac{\frac{(M_i+1)^2}{n_i \log_2(M_i n_i)}}{\frac{(M_f+1)^2}{n_f \log_2(M_f n_f)}} \cdot \left(\frac{Q^{-1}(BER_{M-n-PAPM\_i})}{Q^{-1}(BER_{M-n-PAPM\_f})} \right)^2 \quad (4.17)$$

For moderate degradation, $M_{\_i}$=4, $n_{\_i}$=3, $M_{\_f}$=3, $n_{\_f}$=2, $BER_{M\text{-}n\text{-}PAPM\_i}=10^{-9}$ and $BER_{M\text{-}n\text{-}PAPM\_f}=10^{-7}$ were substituted into equation (4.17) under two initial data rates $R_{M\text{-}n\text{-}PAPM\_i}$=4Mbps and $R_{M\text{-}n\text{-}PAPM\_i}$=250Mbps respectively.

For severe degradation, the above operation was again performed with $BER_{M\text{-}n\text{-}PAPM\_i}=10^{-8}$ and $BER_{M\text{-}n\text{-}PAPM\_f}=10^{-6}$. Since the algorithm was the same, this process will not be repeated, and keeping the remaining parameters unchanged, final data rate values can be obtained:

Table 4.10 Data rate recovery of M-n-PAM $M,n\in\{2,3,4\}$

Moderate Degradation		Severe Degradation	
Initial R_b (Mbps)	Final R_b (Mbps)	Initial R_b (Mbps)	Final R_b (Mbps)
4	3.9	4	3.9
250	249	250	248

From the results in the table, referred to Table 4.1, Table 4.4 and Table 4.7 for OOK, L-PAM and L-PPM modulation schemes, the efficiency of data rate recovery for the adaptive M-n-PAPM scheme can be further demonstrated, as in above Table 4.10.

In Table 4.10, the adaptive M-n-PAPM modulation technique provided excellent throughput recovery ability. By selectively employing the pulse amplitude and position levels, the M-n-PAPM was better than the other three modulation schemes. The final data rate recovered by using multilevel PAPM showed a promising potential for adaptive systems. According to Table 4.10, performances under both moderate and severe conditions demonstrated improvements.

4.3 Performance under Multipath ISI

The multipath ISI was dependent on the channel geometry, and was one of the main limiting factors of the data rate. Under situations where strong LOS path exist and contribute more received power than the diffuse path, by increasing the amplitude ratio, the average received optical pulse power can help to improve the BER. Using the BER equation derived in Chapter 3, the BER performance of OOK, L-PAM and L-PPM schemes can be analysed under ISI.

4.3.1 OOK and PAM

a. BER performance according to amplitude levels

Firstly, consider channel noise caused by multipath ISI, with H = 1m, Using equation (3.26), the SNR to BER performance of OOK and L-PAM (L=2, 3, 4, 5) can be obtained, the simulation results can be found in Figure 4.9. Detailed procedure and Matlab program for Figure 4.9 can be found in Appendix IV-5.

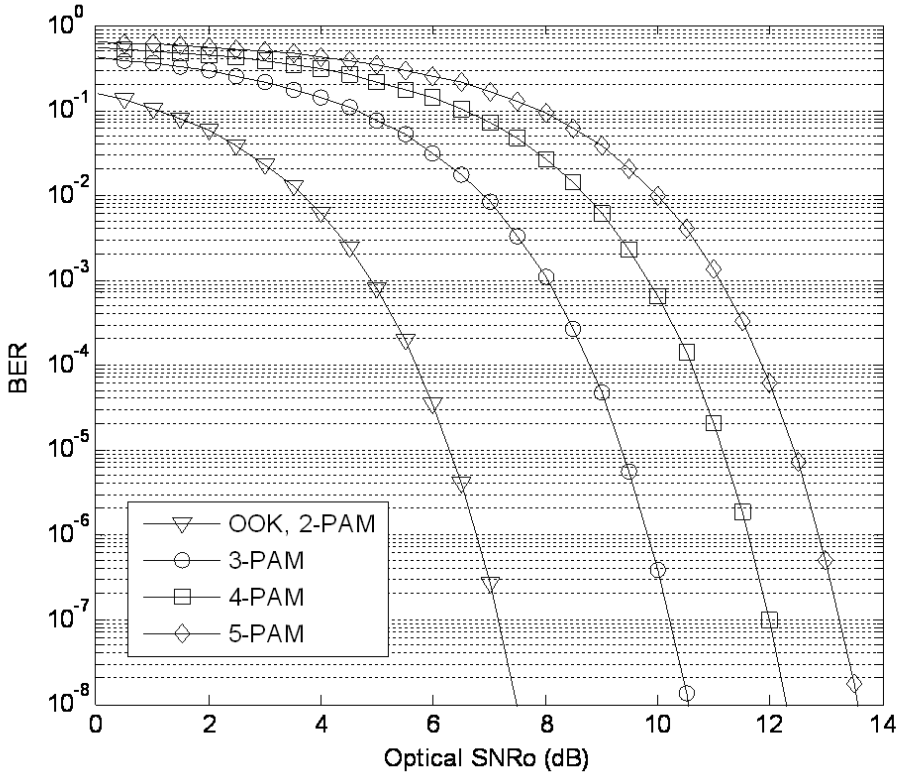

Figure 4.9 OOK and L-PAM SNR vs BER comparison (with L=2, 3, 4, 5)

In Figure 4.9, under same noise conditions, the PAM modulation scheme required more optical power to achieve same level of BER compared with OOK. This suggested that the PAM modulation scheme was not preferred for power limited applications, e.g. mobile device and PDAs, where battery life was essential for operation. However, PAM can be found useful in applications where bandwidth was limited but not the power consumption. Since the PAM modulation scheme required less bandwidth than OOK and PPM (e.g. when $L_{PAM} > 2$), which suggested that the PAM can provide a higher throughput.

b. BER performance according to ceiling height

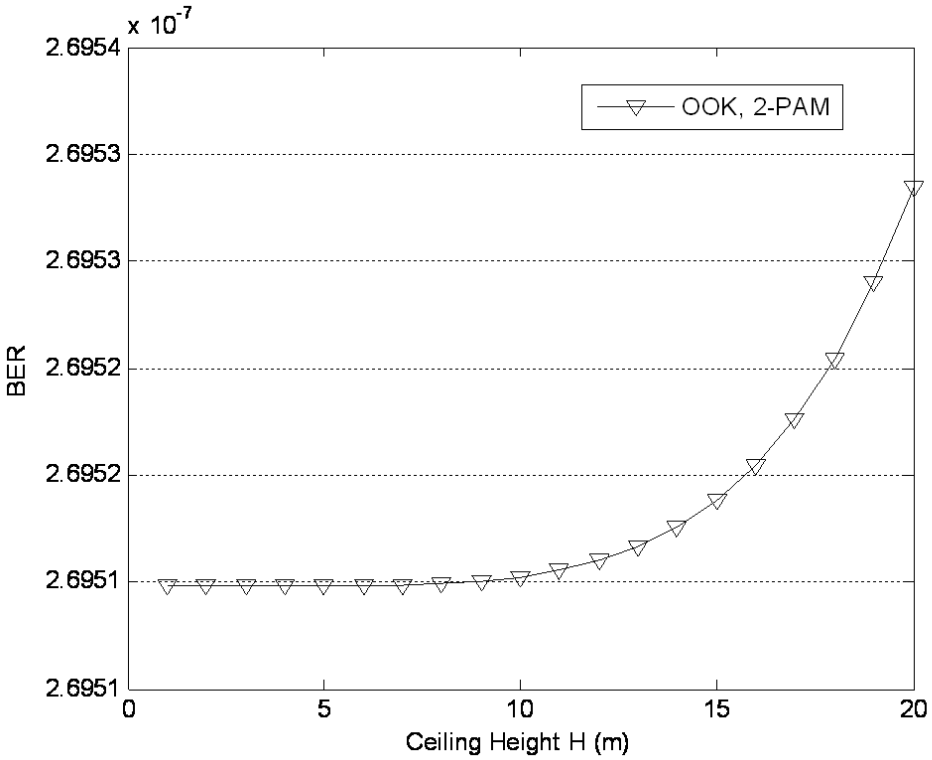

Figure 4.10 BER to ceiling height for OOK and 2-PAM

In this Figure 4.10, the BER increased with ceiling height H, which suggested the impact of ISI on the channel depending on room geometry. Although the H value was larger than for the typical office set up, e.g. room height usually fell in the range of 2-3 metres, this indicated how the BER performance can be affected by the room geometry change at a low data rate, e.g. R_b=1Mb/s. Detailed procedures and Matlab program for Figure 4.10 can be found in Appendix IV-6. At higher data rate, the significance of the contribution from H increased accordingly. This can be illustrated in the following figure.

c. BER performance according to data rate Rb

By increasing data rate up to 280Mb/s, using equation (3.26), the BER performance under different data rate can be obtained. (H=3.5m)

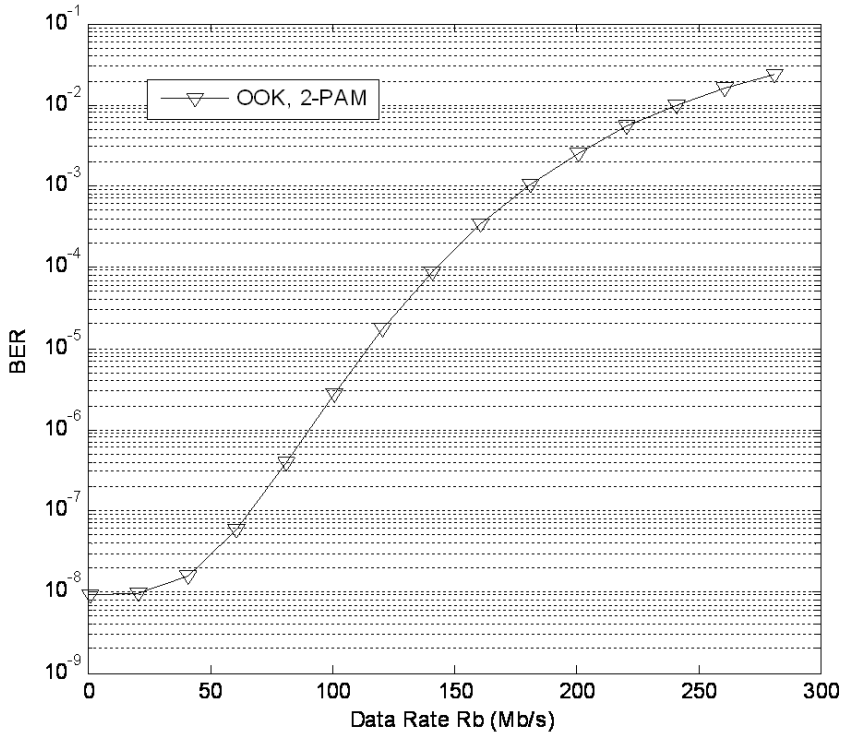

Figure 4.11 BER to data rate for OOK and 2-PAM

In Figure 4.11, the BER increased steadily when the data rate R_b was higher than about 21Mb/s. This suggested at lower data rate (less than the data rate threshold which started increasing the BER), for a given room geometry and SNR value, the OOK and 2-PAM modulation scheme can maintain a required BER with data rate up to the threshold. When the data rate R_b exceeded the threshold, the impact of the ISI cannot be neglected. Detailed procedures and Matlab program for obtaining Figure 4.11 can be found in Appendix IV-7.

The threshold data rate can also be obtained by an analysis method. When an OOK or 2-PAM modulation scheme was employed, each pulse train contained one information bit (‘1’ or ‘0’). Since the room height H=3.5 (m), the shortest time for an optical pulse travelling to and from the ceiling was $T = 2H/c$, where c is speed of light, the highest sampling frequency without ISI interference was then $f = 1/T = c/2H$, thus the maximum available bandwidth was $B = f/2 = c/4H$ =21.4 (MHz). When comparing combined power and bandwidth requirement for different modulation schemes, the normalized bandwidth requirement for both OOK and 2-PAM were 1, that was, $B = R_b$, so the maximum achievable data rate at a given BER was 21.4 (Mb/s), which matched well with the simulation results.

4.3.2 PPM and PAPM

Consider the L-PPM modulation schemes under multipath ISI and short noise only. Using equation (3.35), the BER performance of a 2-PPM modulation system under different data rate can be simulated, similar to OOK and 2-PAM case, H=3.5m. As discussed early, the L-PPM can be treated as special case of M-n-PAPM where M=1. Thus the 2-PPM scheme can be treated as 1-2-PAPM modulation schemes.

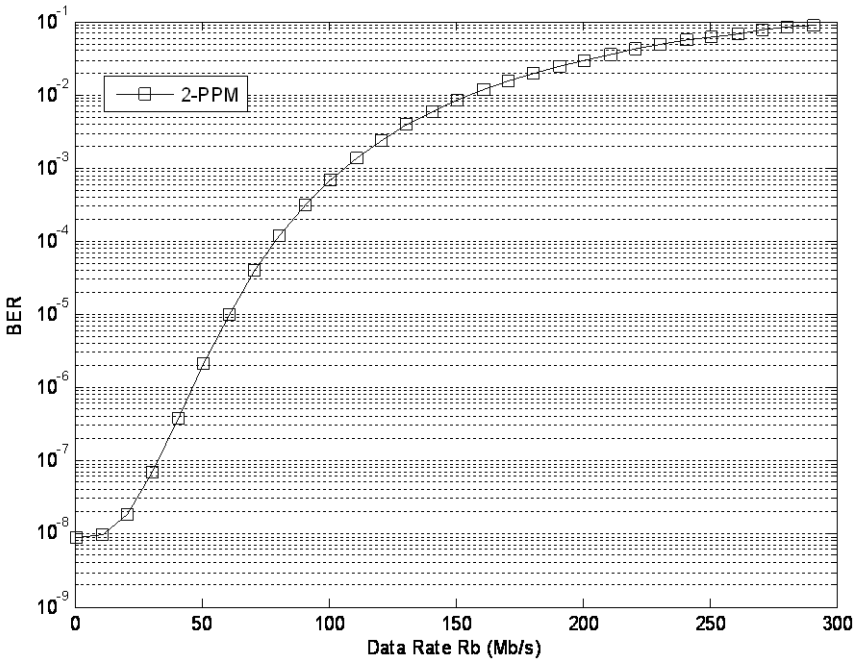

Figure 4.12 BER to data rate for 2-PPM

In Figure 4.12, compared with the OOK and 2-PAM, the 2-PPM can only maintain half of the reliable data rate for a given BER when other channel parameters were same. This was because the 2-PPM required twice the bandwidth of the OOK and 2-PAM according to the work detailed in Chapter 3. The L-PPM modulation scheme required less average power to maintain the same BER level as the OOK and L-PAM (e.g. $L_{PPM} > 2$), which came at a cost of higher bandwidth requirements, thus resulting in a lower data rate. The threshold data rate analysis for 2-PAM still held for the 2-PPM, since the 2-PPM required twice the bandwidth as 2-PAM, so the threshold data rate for 2-PPM was half that of the 2-PAM. $R_b{}' = 21.4/2 = 10.7Mb/s$. The next Figure 4.13 was a zoomed version of the previous Figure 4.12, and this again matched well with the simulation results. Detailed procedures and Matlab programs for Figure 4.12 and Figure 4.13 can be found in Appendix IV-8 and Appendix IV-9 respectively.

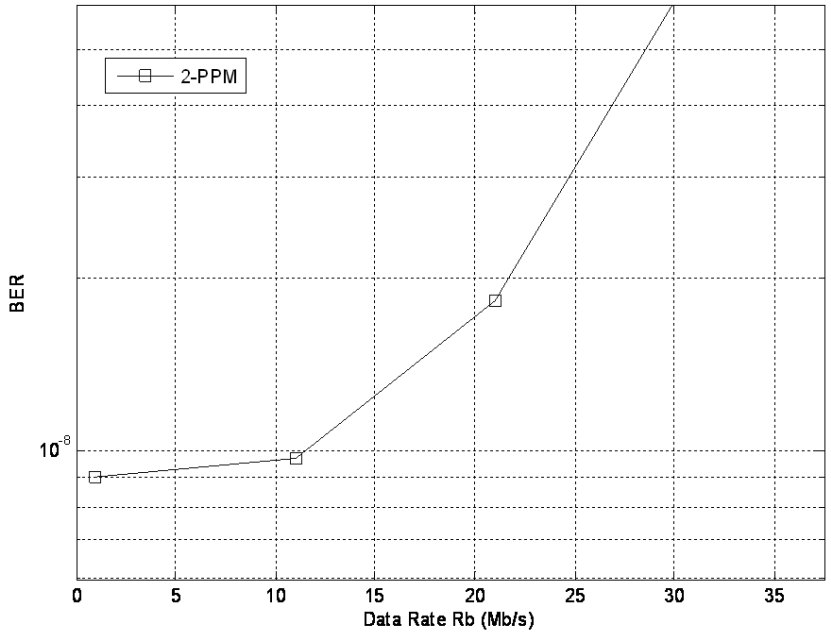

Figure 4.13 Zoomed version of BER to data rate for 2-PPM

4.4 Summary and Conclusions

Summary

In this chapter, simulations were carried out to examine the candidate modulation schemes for the optical wireless channel. By adaptively adjusting the modulation orders; a flexible system infrastructure can be realised. This was different from other adaptive multilevel modulation schemes in terms of simplicity and combined power and bandwidth efficiency [37, 43, 64, 97]. The data rate losses due to channel degradation can be minimised when the optimum modulation depth chosen for the related adaptive ratio factor. The experimental simulations, however, operated whilst following requirements for expected maximum optimisation. The studied system model can be further improved when applying rule-based artificial intelligence control techniques.

The adaptive multilevel M-n-PAPM scheme showed a promising prospect in terms of stabilising data rate and BER under different degradations. The experimental models discussed in this chapter were realistic model, emphasising the practical aspect of the proposed modulation constellation. Nevertheless, this was by no means to limit the discussions on a specific model. More complicated channel models, which can be difficult for non-adaptive modulation to operate, can be utilised by the adaptive modulation techniques discussed here.

Conclusions

In this chapter, the proposed adaptive modulation concepts were validated in the context of stabilising the transmission data rate. This was a new attempt for reducing the interferences presented to the channel by actively updating the modulation orders. In fact, most modulation schemes proposed for the optical wireless channel can be validated as candidates for adaptive modulations. Results presented here can be used to further demonstrate the capability of adaptive modulation using different signal modulation techniques. The analytical model and simulation results helped confirming the feasibility of the adaptive modulation techniques which can be used for the optical wireless channel.

Chapter 5

Fuzzy Logic Control

5.1 Introduction

Artificial intelligence (AI) attracted much attention from both scientists and engineers since it was discussed by John McCarthy in 1956 [98]. It received fast

growth by employing programs and algorithms that can imitate the activities of a human brain such as reasoning, learning and pattern recognition [99].

In the AI hierarchy, there were categories including: logical AI, inference, genetic programming, heuristics, pattern recognition and so forth [100]. Yet more general classifications of AI applications can be divided into three main branches: cognitive robotics, computational intelligence and data mining. These included the sub categories which can be demonstrated in the Figure 5.1 that follows.

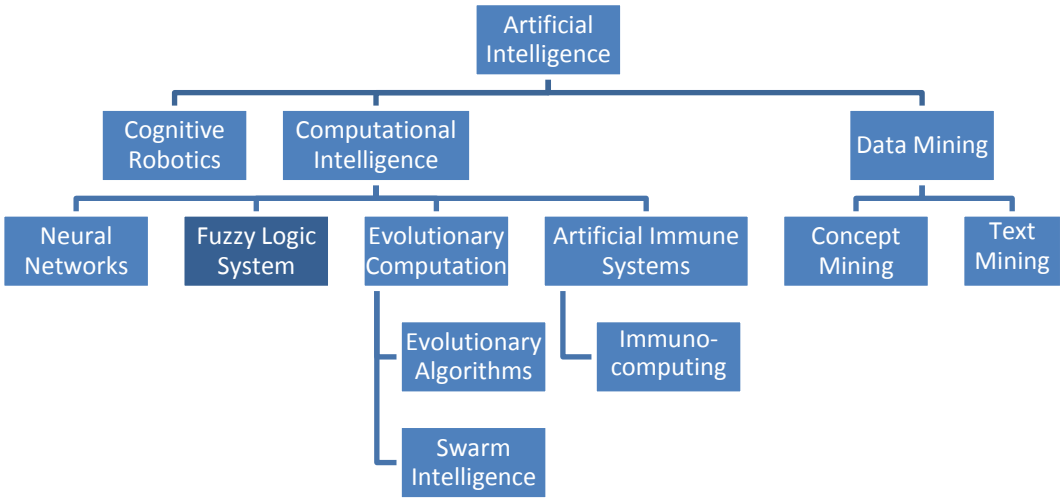

Figure 5.1 General categories of AI (figure adapted from [98])

From the figure, among the AI family, cognitive robotics and data mining emphasised on simulating human brain activity and the learning process respectively [101, 102]. They were commonly used for solving complex problems or assisting in the study of the learning process. Under the computational intelligence category, neural networks produced a similar output in response to their training or learning process [103, 104]. Evolutionary computation involved

an iterative search until a preset target was reached [105]. The artificial immune system can often find applications in medical and biology analysis [106]. The fuzzy logic (FL) control algorithm was a rule based approach which allowed conditions to be expressed in natural language forms [107]. This enabled the transfer of previous experience into automatic control processes. FL also exhibited the simplest structure compared to other AI techniques, delivering a faster response. Hence, FL was a good candidate technique that can be used to assist adaptive modulation.

Following the concepts developed in Chapter 4, the block diagram of a FL controlled adaptive modulation system was shown in Figure 5.2. According to the channel state information obtained at the receiver, (e.g. BER and SNR values) the FL controller made decisions based on predefined adaptation rules. These decisions were then directed back to the adaptive M-n-PAPM modulator so that the modulation order can then be updated according to the channel requirements. Thus the adaptive modulation can be controlled by the FL controller for real-time applications.

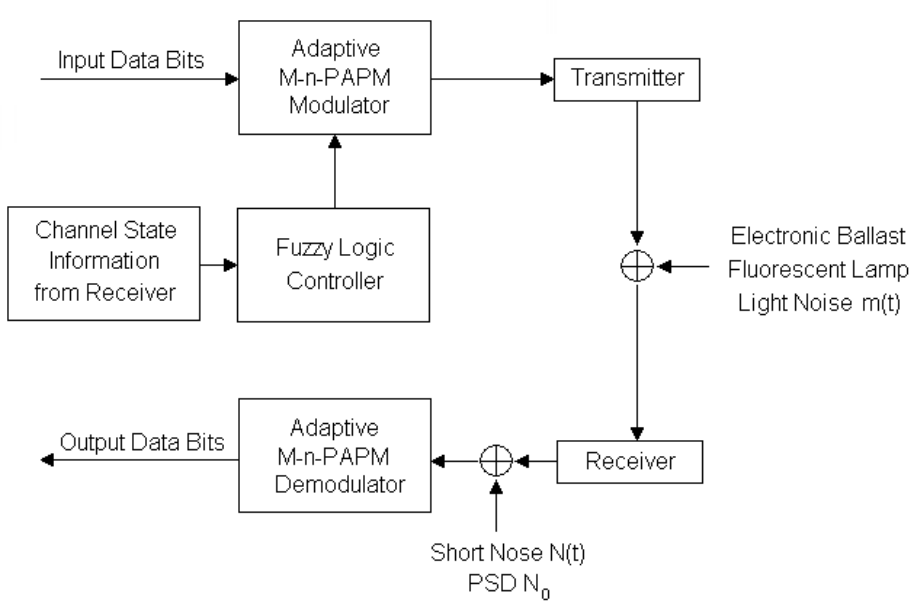

Figure 5.2 Block diagram of FL controlled adaptive modulation system

5.2 System Structure

The FL concept was theorised by Lotfi Zadeh in [108], yet the origins can be traced back to ancient times with most applications of FL being control related systems. A FL control system can be applied to adaptive modulation according to Figure 5.2. In this section, the elements of the fuzzy system were discussed. The following Figure 5.3 represented the basic structures of a fuzzy system:

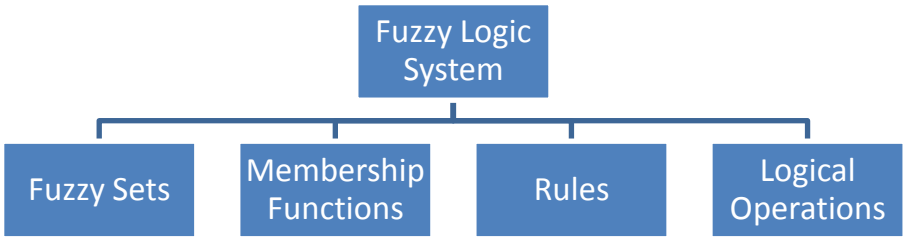

Figure 5.3 Structure of fuzzy system (figure adapted from [107])

5.2.1 Fuzzy Sets

In Figure 5.3, there were four elements in a fuzzy system. Compared to classical sets, fuzzy sets (FS) were sets without a clearly defined boundary, which contained elements with partial degrees of a membership [109]. FSs were important part of FL systems. System states of different modulation schemes and BER conditions of a specific channel can be grouped into different FSs. For example, BER degradation can be grouped into two categories: moderate and severe. The degree of degradation can also be grouped by its variation to the required BER value, e.g. ±10% and ±50% BER variations can be used to represent moderate and severe degradation, respectively.

5.2.2 Membership Function

A membership function (MF) was defined as "A fuzzy set (class) A in X is characterized by a membership (characteristic) function $f_A(x)$ which associates with each point in X a real number in the interval [0,1], with the value of $f_A(x)$ at x representing the 'grade of membership' of x in A" [110]. This can be further demonstrated using a simple formula: "If u is an element in the universe of discourse U, then a fuzzy set A in U is the set of ordered pairs $A = \{(u, \mu_A(u)) : u \in U\}$, where $\mu_A(u)$ is a membership function carrying an element from U into a membership value between 0 (no degree of membership) and 1 (full degree of membership)" [111].

In adaptive modulation, the modulation instructions can be grouped into different groups. For example, 'No Change', 'Change Slow' and 'Change Fast' to indicate

the rate of level change according to BER variation, a sample value can be found in Table 5.1 [71]:

Table 5.1 Modulation parameter change rate

Modulation Parameter	No Change	Change Slow	Change Fast
BER Variation (%)	0	10-50	>50

5.2.3 Fuzzy Set Operation

Since a FS was a superset of conventional (Boolean) logic that were extended to handle the concept of partial truth -- truth values between "completely true" and "completely false", the standard logical definitions in fuzzy logic were defined as following [112]:

truth (not x) = 1.0 - truth (x)

truth (x and y) = minimum (truth(x), truth(y))

truth (x or y) = maximum (truth(x), truth(y))

This can be represented by the following Boolean operations:

Complement: $\mu_{\bar{A}}(x) = 1 - \mu_A(x)$

Intersection: $\mu_{A \cap B}(x) = \min\{\mu_A(x), \mu_B(x)\}$

Union: $\mu_{A \cup B}(x) = \max\{\mu_A(x), \mu_B(x)\}$

Where A and B represented subsets of the universe with membership functions μ_A and μ_B. More detailed fuzzy set operators can be found in Appendix V-1.

Traditional control systems were based on mathematical models, which defined a relationship that transforms the desired state and observe state of the system into inputs. The inputs can alter the future state of that system. FL systems worked the same way but the decisions and the reasoning were replaced by FSs and fuzzy rules [109]. Fuzzy control, which directly used fuzzy rules, can influence the operation of a system by changing inputs to that system via rules which modeled how the system operates [113].

5.2.4 Fuzzy Rules

FL incorporated a simple rule-based 'If X and/or Y then Z' approach to solve control problems rather than attempting to model a system mathematically. This process can simplify the modeling process. It was particularly helpful for system updates, engineers can understand the control system more easily without going through great details [107]. The fuzzy control (FC) system can be illustrated using following block diagram, Figure 5.4 [114].

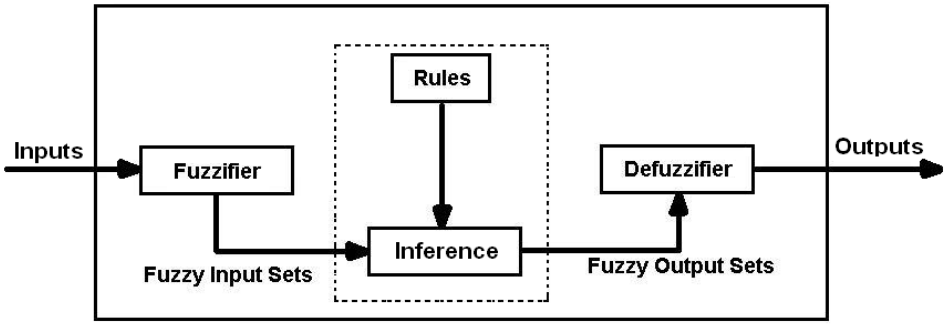

Figure 5.4 Fuzzy logic system block diagram (figure adapted from [109])

In Figure 5.4, the FC system worked in sequential steps: 1.Convert input data to FS (Fuzzify Inputs); 2. Apply fuzzy rules (FR) to FS (Fuzzy Logic Operation); 3.

Convert results to output data (Defuzzify Outputs). The fuzzy inference was the process of formulating the mapping from a given input to an output using fuzzy logic [107]. Detailed fuzzy operations were discussed in next section.

5.3 Adaptive Modulation Control

5.3.1 Model Parameters

For adaptive modulation, the modulation parameter change was based on the discussion in Chapter 4 to find the best fit to maximise the data rate under different BER variation caused by different noise source discussed in Chapter 2. BER values can be grouped by: Minor, Moderate and Severe, which represent changes to one, two and three orders of magnitude, respectively. The BER variation can be normalised as:

$$BER_{unit} = \log_{10}\left(\frac{BER_{final}}{BER_{initial}}\right) \tag{5.1}$$

Where BER_{unit} is the mapped fuzzy control input, $BER_{initial}$ is the initial system BER and BER_{final} is the final system BER. By using equation (5.1), the new BER unit was outlined in Table 5.2.

Table 5.2 BER degradation mapping

Modulation Level Change	Minor	Moderate	Severe
Actual BER Change (compared to original level)	10	100	1000
$\log_{10}\left(\frac{BER_{final}}{BER_{initial}}\right)$	1	2	3

5.3.2 BER Variation to Modulation Level

Following the discussions in previous sections, the FC system can give instructions to the modulator based on the feedback from the channel. The instructions for adapting can be treated as system output. The rules for FC system can be set as following rules, name this system A.

1. If BER variation is minor then required level change is zero.
2. If BER variation is moderate then required level change is minor.
3. If BER variation is severe then required level change is large.

The rules defined range for the BER variation (input) and the required level change (output). The BER variation range took the unit value given in Table 5.2. The required level change referred to the value range given in Figure 4.8, e.g. between [0, 5]. The membership functions of BER variation and level change can be obtained according to its value range. By mapping BER variation and level change values from inputs to degree of memberships, the input data were converted to FS inputs as demonstrated in the previous Figure 5.4. This relationship can be further demonstrated in Figure 5.5.

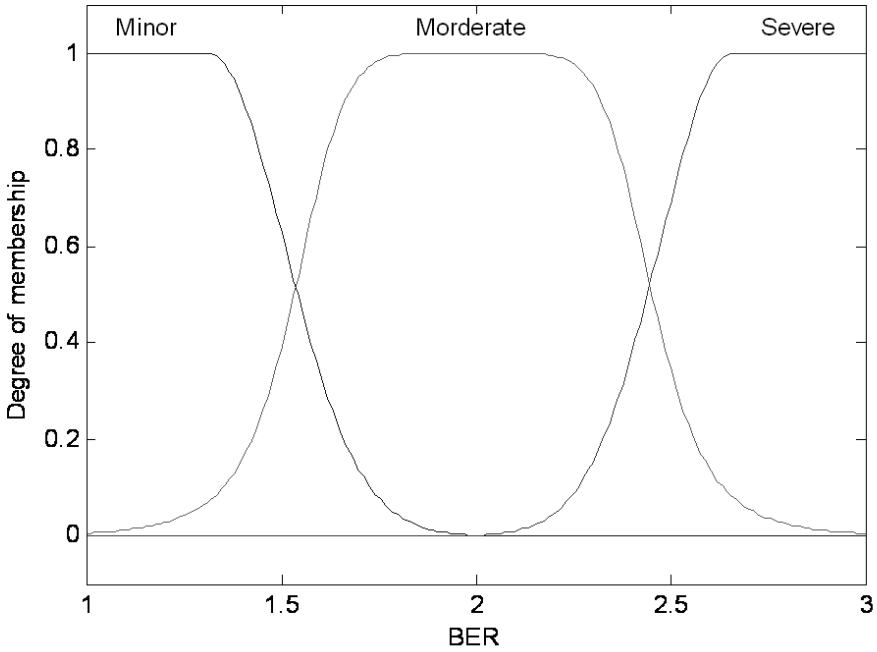

Figure 5.5 BER variations to fuzzy set mapping

From Figure 5.5, the input BER variation value in the range [1, 3] was mapped into FSs by its related three membership functions. The obtained degree of membership (y axis) reflected which category the input BER variation belonged to. For example, if the BER variation was 1, according to its membership function, the resulting fuzzy set input was 1, which is the 'Minor' case. Increasing the BER variation value from 1 to 2, decreased the contribution from the 'Minor' and increased the 'Moderate' contribution from 0 to 1. This was also true for the 'Severe' case, which suggested that depending on the input BER variation value and its membership functions, the obtained fuzzy sets can represent input value according to preset membership functions.

The output of the fuzzy control system was the level change requirement defined in the group as 'zero', 'minor' and 'large'. The level change requirement value

can be obtained by mapping the input fuzzy sets using similar method as the BER variation. The differences were the level changing range. This can be presented in Figure 5.6. The resulting fuzzy system block diagram was shown in Figure 5.7.

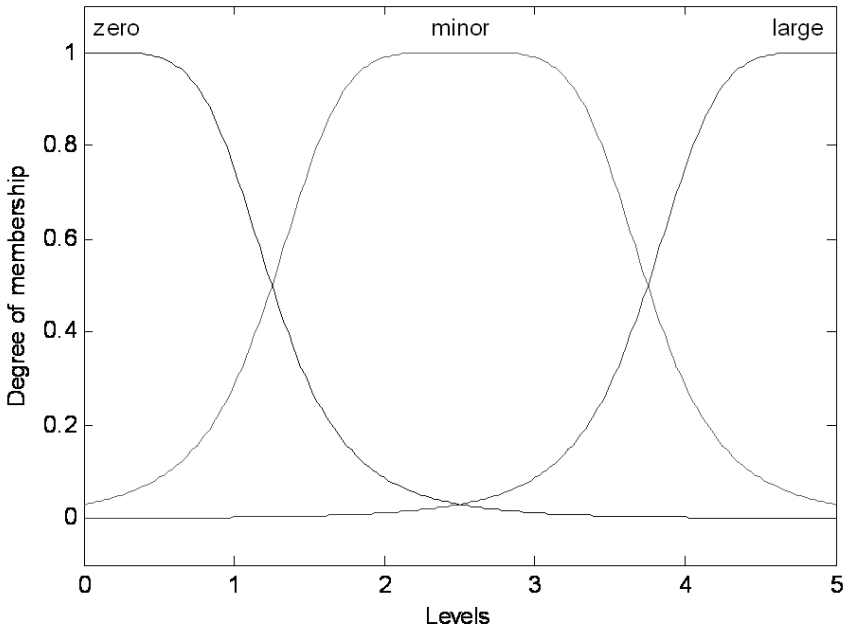

Figure 5.6 Fuzzy set to required level changes mapping

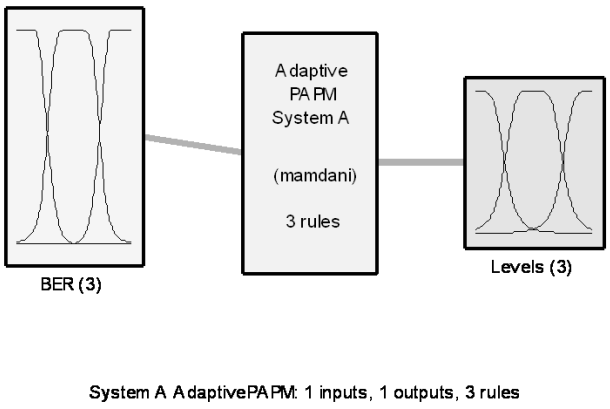

Figure 5.7 Block diagram of adaptive PAPM fuzzy system (system A)

In Figure 5.7, the fuzzy control system obtained including 1 input (BER variation) and 1 output (required level change). There were 3 membership functions for both the input and output (numbered). The input and output values were compared in Figure 5.8.

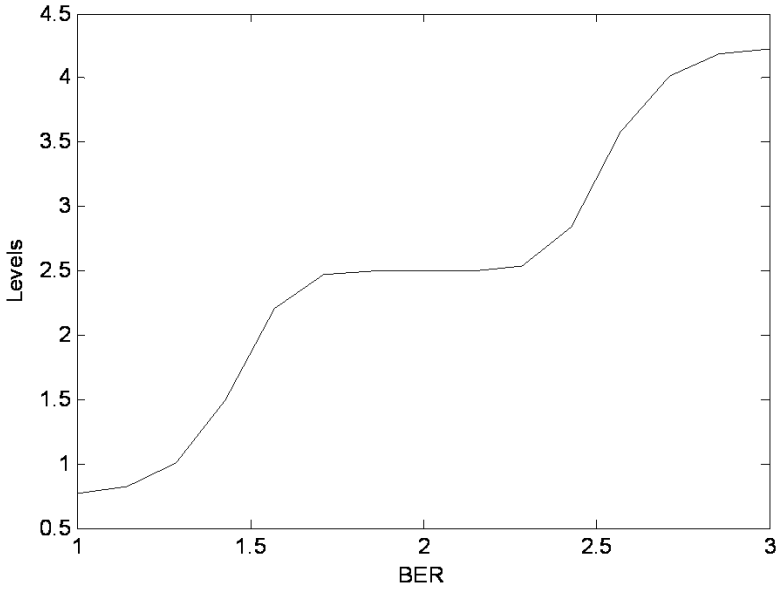

Figure 5.8 Fuzzy system inputs/outputs for system A

From Figure 5.8, the relationship between BER variation and the required level change was similar to a step function. The fuzzy system gave level change instructions according to the channel status, e.g. the BER variations. Detailed parameters of system A can be found in Appendix V-2.

5.3.3 BER Variation and Change Rate to Modulation Level

BER variation can be considered to have a variation rate, which provided a priority for the modulation level and order adaptation. The change rate was defined in the range [0, 1], with two membership functions representing ‘slow’ and ‘fast’. Updating the fuzzy rules for system A in the previous section, the new fuzzy system rules can be expressed as following, with this system named B.

1. If BER Variation is Minor then Level Change is Zero
2. If BER Variation is Moderate and Rate is Fast then Level Change is Large
3. If BER Variation is Moderate or Rate is Slow then Level Change is Small
4. If BER Variation is Severe and Rate is Fast then Level Change is Large
5. If BER Variation is Severe or Rate is Fast then Level Change is Large

In system B, ‘Rate’ is how fast the BER changes. The first rules was same as in system A, rule 2 to 5 was the joint impact between BER variation and the rate change. The fuzzy inference process for system B was shown in Figure 5.9 [115].

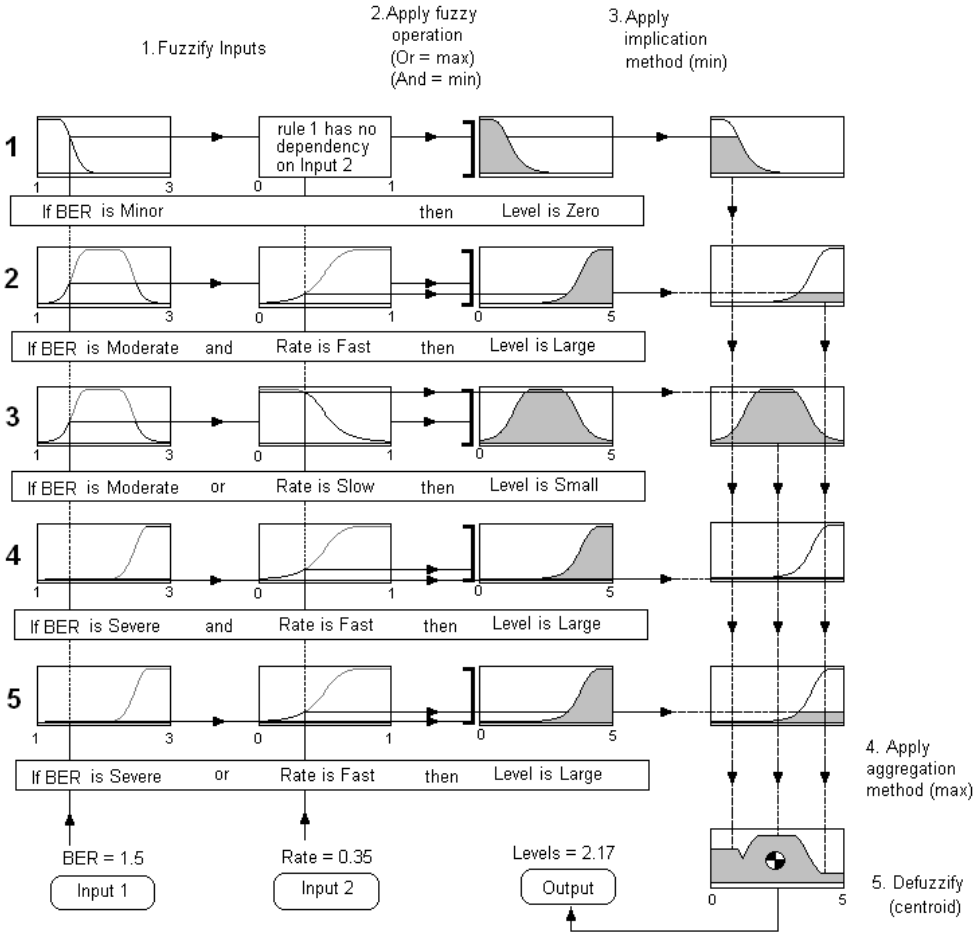

Figure 5.9 Fuzzy inference process for system B
(figure produced with reference to [110])

In Figure 5.9, BER = 1.5 and Rate = 0.35 were chosen as sample inputs. The inputs were first mapped to the FS using MF. The resulting FSs then followed the fuzzy operator to get antecedent values for each rule. The consequent value of each rule can be obtained by the implication operation (min operator). The output FS can then be calculated by applying the aggregation operator (max operator) to the consequent value. The required modulation level change can be obtained by defuzzifying the aggregated FS using the centroid operation. The required level change was 2.17. The modulation order and level can then be adjusted by continually applying the fuzzy interference process according to obtained channel

state information, e.g. BER variation and its rate of changes. The block diagram for the system B was outlined in Figure 5.10.

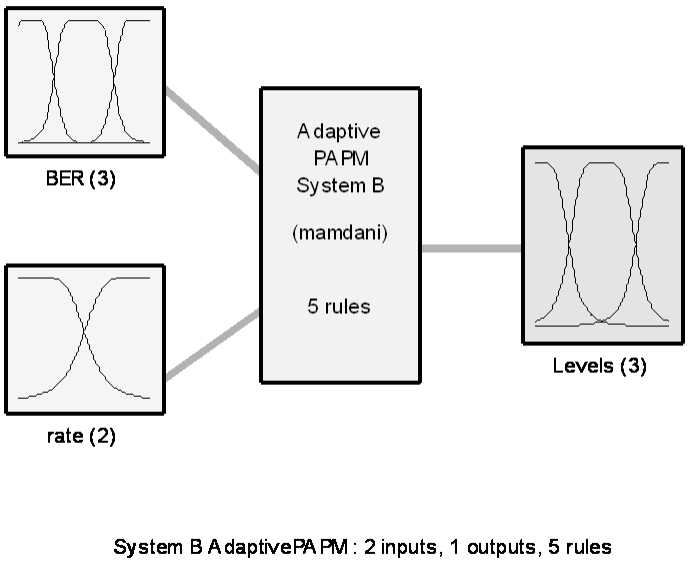

Figure 5.10 Block diagram of adaptive PAPM fuzzy system (system B)

In Figure 5.10, system B included two inputs and one output, BER variation and level change included three MFs while rate contained two MFs (numbered).

Both system A and system B were Mamdani type fuzzy inference model, where the output MF's applied centroid calculation [116]. This was different from the Takagi-Sugeno-Kang (TSK) model where the output MFs were either linear or constant [117]. Comparing these two models, the TSK model was more computational efficient and thus fit better in optimisation and adaptive control systems. While the Mamdani model was efficient in capturing the expert knowledge but was computational inefficient, thus can be used for a well known

system modelling where expert knowledge was available. The input/output for system B is shown in Figure 5.11.

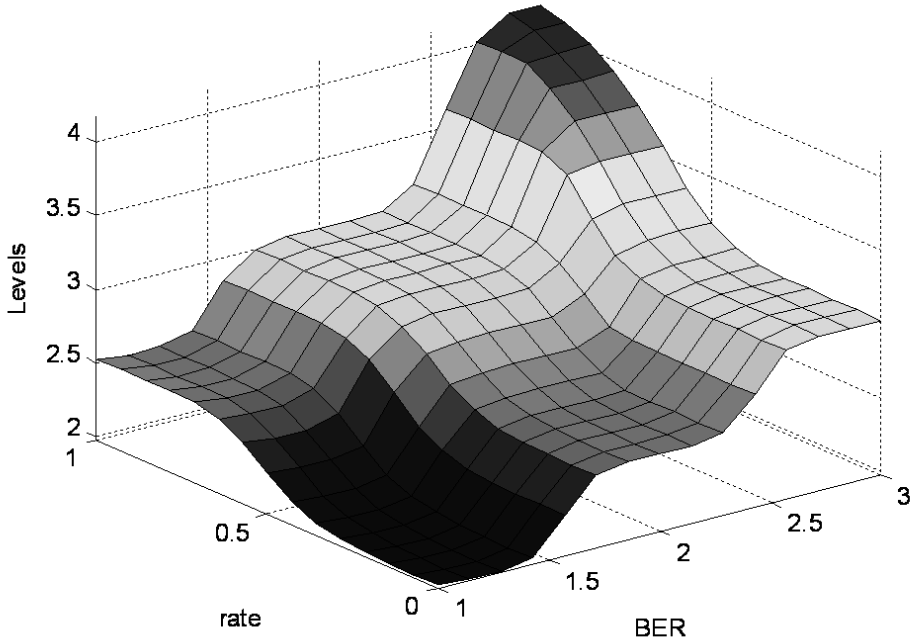

Figure 5.11 Fuzzy system inputs/outputs for system B

In Figure 5.11, the two inputs variables were the BER variation and the change rate. The system B calculated the outputs (required level change) by validating inputs values against the fuzzy rules. For example, by applying rule 4, the 'required level change' value reached maximum when BER=3 and rate =1. According to this mapping, system level change requirements were functions of the input BER and change rate. Detailed parameters of system B can be found in Appendix V-3.

5.4 ANFIS Model

5.4.1 System Structure

The adaptive neuro-fuzzy inference system (ANFIS) refered to a fuzzy system combined with a neural network algorithm [118]. The membership function parameters of an ANFIS can be trained by learning algorithms. In contrast to the Mamdani model, ANFIS was based on the TSK model [119]. Its rules were based on a constant or linear output and take the form:

$$If\ X\ and\ Y\ then\ Z = aX + bY + c \tag{5.2}$$

where X, Y were inputs, Z is system output and a, b, c are constants. The output was weighted by a rule weight (firing strength) w of the rule. The final output was the weighted average of all system outputs and took the form $\sum_i^N w_i z_i \,/\, \sum_i^N w_i$, where N is the number of rules [115]. An example ANFIS rule operation can be illustrated in the following Figure 5.12.

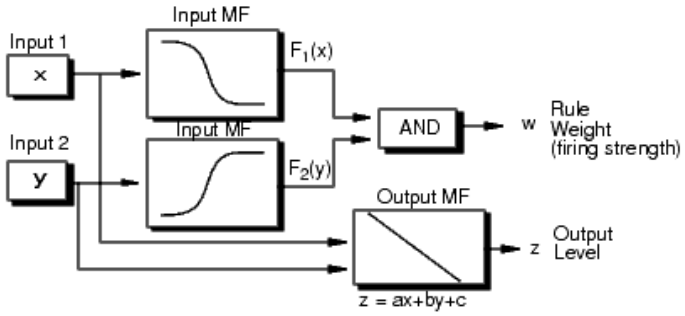

Figure 5.12 ANFIS rule operation example (figure adapted from [110])

In Figure 5.12, $F_1(x)$ and $F_1(y)$ were membership functions for input 1 and input 2, since the final output was averaged over all output values using weight w. By

changing w, the output of the system can be adjusted to better fit the model data sets [120].

The ANFIS system can employ either back propagation gradient descent or combined least-squares and the back propagation method (hybrid) to obtain the FIS structure [115]. The benefits included a more sophisticated system structure best fit to the data sets, no need to understand system behaviour prior modelling (black box) and flexible system adjustment methods for updating parameters [119].

5.4.2 Adaptive Model Identification

ANFIS was especially useful when the input and output data were available for a fuzzy system, e.g. modulation adaptation instructions for a specific channel set up. Without prior knowledge of the membership functions, the ANFIS model can identify a good approximation to the fuzzy inference system by learning the known data set of that unknown system [111]. The previously developed fuzzy system B can be used to demonstrate the benefits of the ANFIS model.

Obtain training and checking data from fuzzy system B, the obtained data set containing 100 input and output pairs. The detailed data sets can be found in Appendices V-4 and V-5. The training data and checking data were identical to the fuzzy inference system yet had different ranges to provide comparability.

5.4.3 Singleton Data Set

The input data for training and checking the ANFIS system can be grouped into two categories. Singleton and 2-D recursive matrix data sets, where singleton data

set was obtained by sampling the BER variation and the rate change value along its range linearly. The resulting output data was calculated from line values in the input space. The singleton data sets can be used to determine the rough shape of the unknown system, e.g. the output along a specific direction within the valid input data sets. The singleton data sets can miss some of the system structures as it offered less coverage of the input space.

5.4.4 2-D Recursive Data Set

The 2-D Recursive data set was obtained by fixing values of one system input and listing all values of other inputs. By repeating this process again to the next fixing values of the chosen input, the 2-D recursive data set was obtained. The 2-D recursive data set included all data values according to the chosen input data range. It can provide a better approximation to the unknown system compared to singleton data sets. The generation process of the 2-D recursive data set was more complex than the singleton data sets. The comparison between singleton and 2-D recursive process was shown in Figure 5.13.

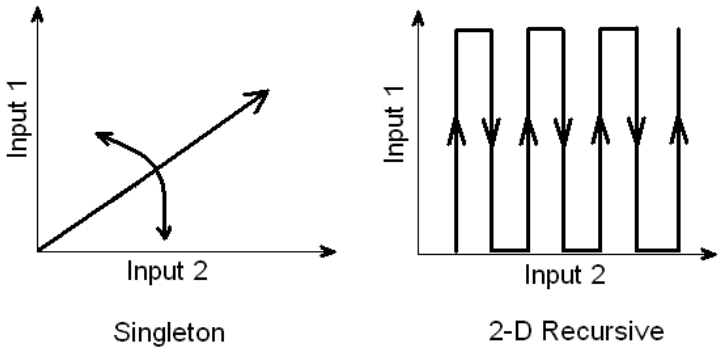

Figure 5.13 Comparison of single ton and 2-D recursive data set generation

5.4.5 Training the ANFIS Model

The ANFIS models were trained using singleton and 2-D recursive data sets; the data sets were generated by a resolution of 100 elements with a BER variation range [1, 3] and a rate range [0, 1]. The following Figure 5.14 showed comparisons between the two data set used for training the ANFIS model.

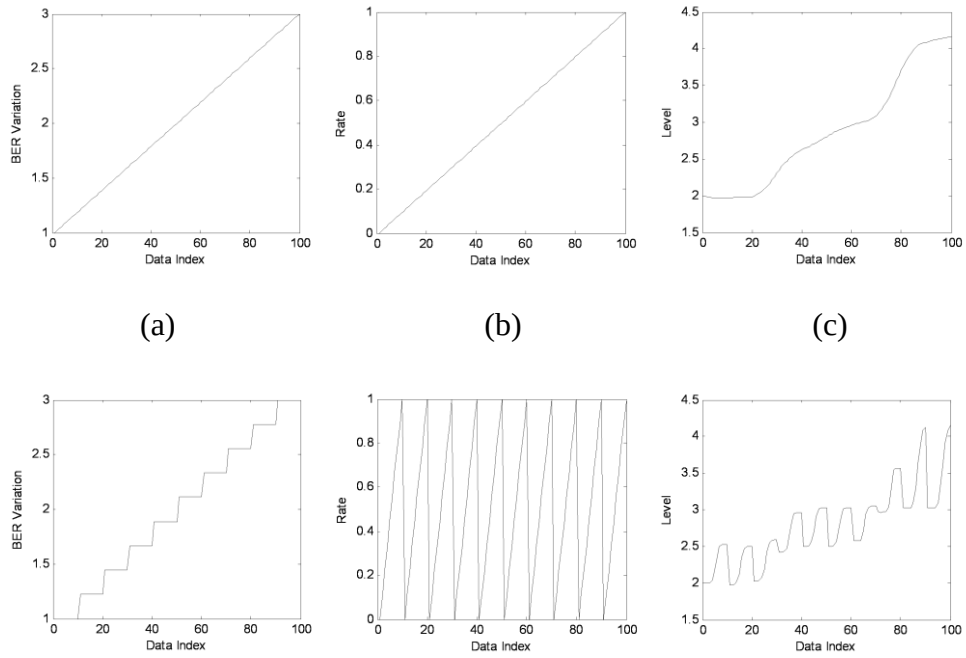

Figure 5.14 Singleton (a) BER variation (b) Rate value (c) Output levels and recursive (d) BER variation (e) Rate value (f) Output levels

In Figure 5.14, the recursive data set covered more area than the singleton set as in (e) and (f). In this test case, one of the inputs (rate) was chosen as the recursive variable. The approximation accuracy of the trained ANFIS system can be improved if all inputs were chosen as the recursive variable. The complexity of the data set generation was also increased by a factor of $M_{dr} \times N_{ti}!$, where N_{ti} is total number of input variables and M_{dr} is the data set resolution number. When

the total input numbers were relatively small (e.g. less than 10), it can be efficient to use $(N_{ti} - 1)$ number of input variables as recursive data set [120].

5.4.6 Results Comparison

The ANFIS system can be trained using four methods: 1. Back propagation gradient descent (BPGD) only; 2. BPGD and one pass of least squared estimate (LSE); 3.BPGD and LSE; 4. Sequential LSE. According to Jang [120], the hybrid training method (third method) can provide best performance compared to other method in terms of calculation complexity and accuracy. In this section, the hybrid training method was used for training the ANFIS system along with the BPGD method for comparison. The system parameters used for training can be found in Table 5.3.

Table 5.3 ANFIS system training parameters

Parameter Name	Value
Epochs	20
MF numbers	[3 3]
Method used	Hybrid BPGD
Data partition	Grid partition
Data resolution	100
Data structure	2 input 1 output

The training results can be found in following Figure 5.15 – Figure 5.20.

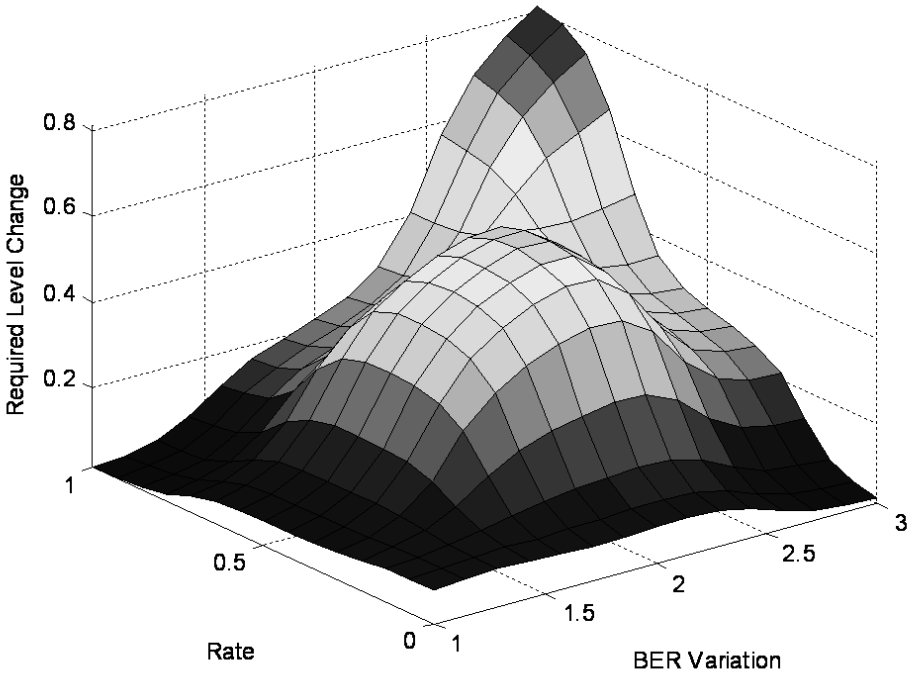

Figure 5.15 ANFIS trained by BPGD on singleton data set

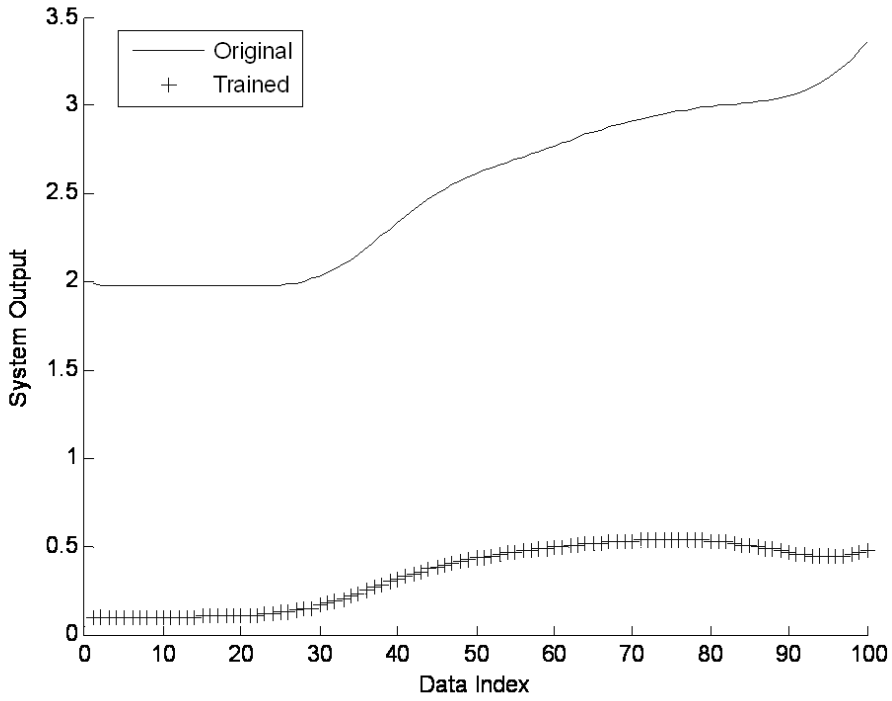

Figure 5.16 Training error of BPGD on singleton data set

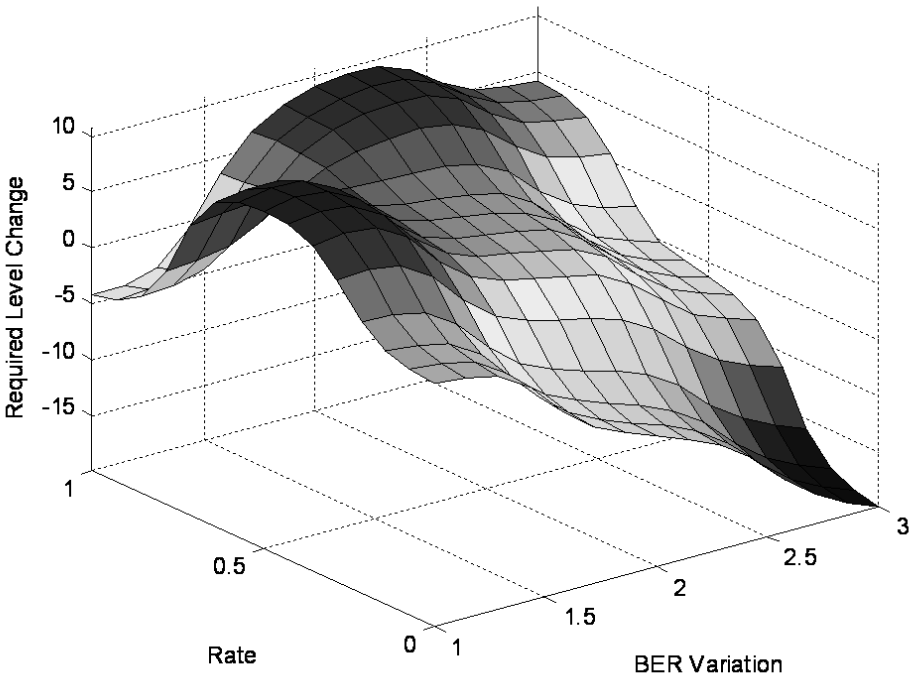

Figure 5.17 ANFIS trained by hybrid on singleton data set

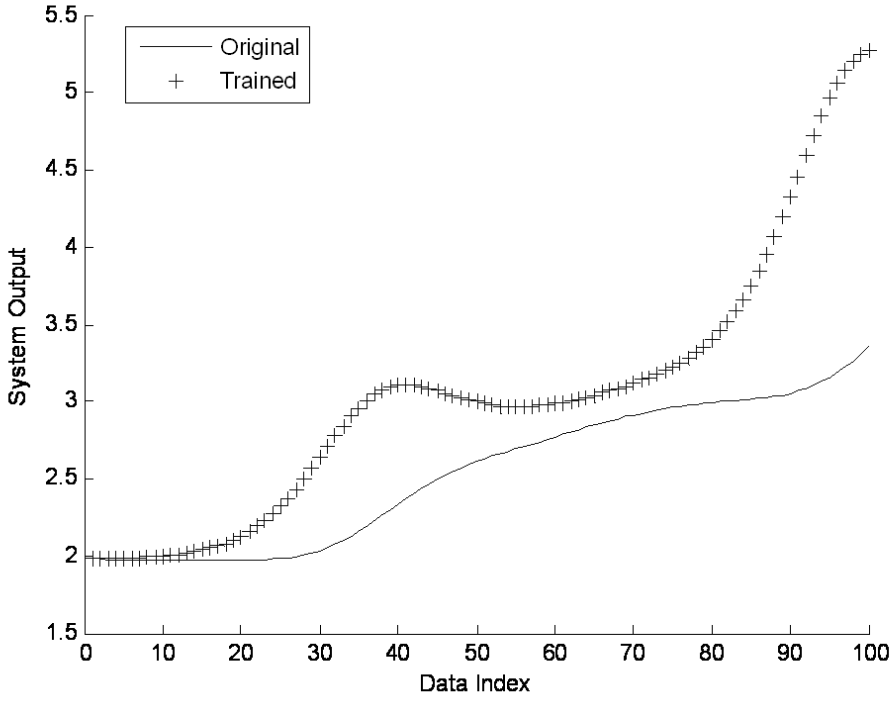

Figure 5.18 Training error of hybrid on singleton data set

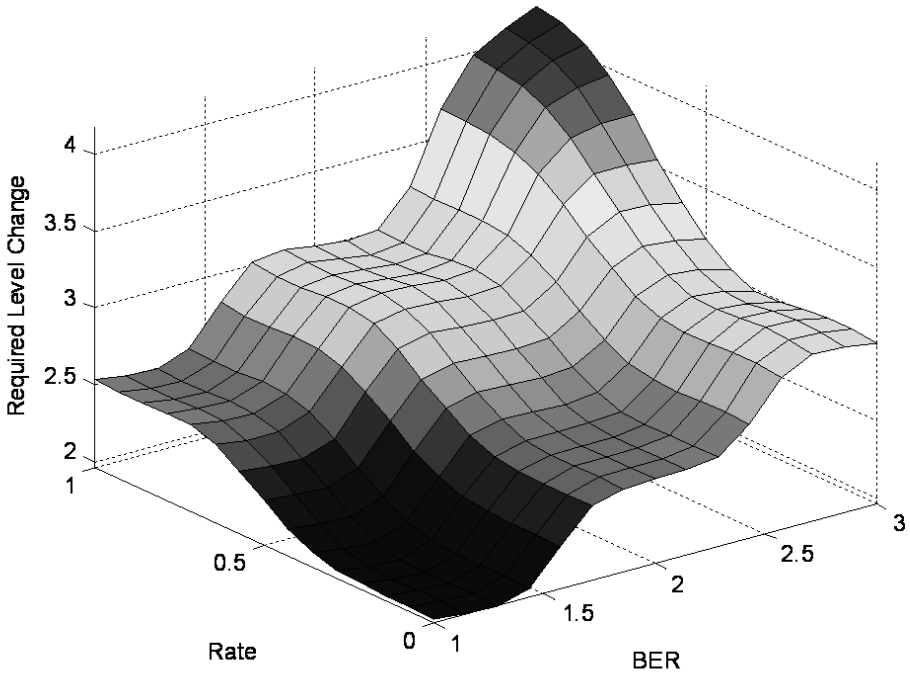

Figure 5.19 ANFIS trained by hybrid on recursive data set

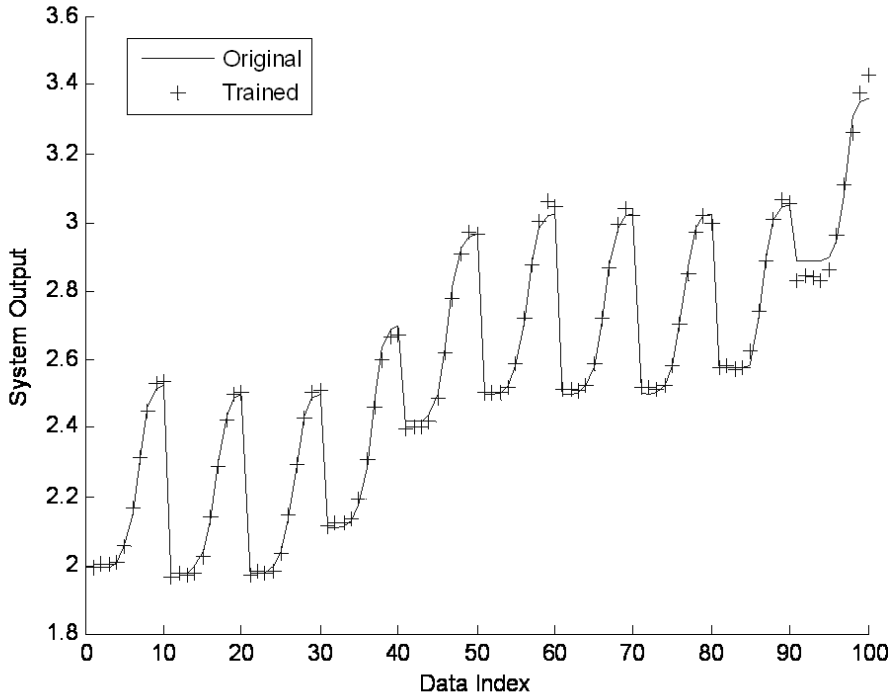

Figure 5.20 Training error of hybrid on recursive data set

Figure 5.15 and Figure 5.17 were for the ANFIS system trained using BPGD, hybrid on a singleton data set. Figure 5.19 was for the trained ANFIS system by employing the hybrid method on recursive data set. Figure 5.16, Figure 5.18 and Figure 5.20 illustrated the respective training errors. Comparing Figure 5.15 with Figure 5.17, it can be seen that the hybrid method captured more system information than the BPGD method. However, the training errors of both methods were high since they were limited by the singleton data set as reflected in Figure 5.16 and Figure 5.18. Comparing Figure 5.19 with Figure 5.11, the recursive data set captured most system structure information from the training data, and was identical to the system it approximated. According to Figure 5.20, the training error of the recursive data set was negligible compared with ANFIS system obtained using singleton data set.

5.5 Summary and Conclusions

Summary

In this chapter, the general field of AI was briefly introduced. This had led to the description and justification of FL control for an adaptive modulation system. Example fuzzy inference systems were developed to assist adaptive modulation scheme updating system parameters. The FL system benefited from system simplicity and flexibility compared with other control methods.

Employing the neuro-fuzzy approach via ANFIS was also demonstrated. This can be used to model unknown system model when given sufficient input/output data. By adjusting system parameters using different learning algorithms, ANFIS can provide excellent approximation to the unknown system. This was particularly

useful for system under different interference. An FL controlled modulation scheme can compensate for system impairments by adaptively selecting optimised modulation parameters, thus maximising system throughput and contributing to system stability and robustness.

Conclusions

The artificial intelligence control methodologies were combined with adaptive modulation schemes. Fuzzy logic control was selected as a viable control process that provided simple yet powerful control functionality. Simulation results confirmed the characteristics of the obtained fuzzy-controlled-adaptive-modulation schemes. By equipping the newly developed adaptive modulation schemes, communication systems can provide flexible yet efficient adaptations for improving transmission throughput.

The new concept exploited some exciting features, such as the ability to balance between power and bandwidth requirements, increased immunity to different types of interferences by optimising modulation parameters, ability to update control patterns through training. This certainly can attract more attentions from the mobile device design engineers, and contribute to the developments on more efficient modulation schemes for the optical wireless industry.

Chapter 6

Reliable Communication System

6.1 Introduction

The reliability or robustness of a communication system usually referred to the ability to maintain certain system performances under interferences [29]. As discussed in Chapter 2, the optical wireless channel can be easily affected by channel uncertainty. For example, distance between transmitter and receiver, distance from ambient light source or optical propagation path changes can result in BER variation. Using the adaptive modulation model and FL control concept developed in Chapter 4 and Chapter 5, different system interference can be addressed within the context of system reliability. In this chapter, the utility of the adaptive modulation schemes that employ FL control were further demonstrated.

6.2 System Reliability

The system reliability was analysed under three types of interferences:

1. Variable ISI representing geometry change between transmitter and receiver;
2. Variable ambient light noise with a constant ISI, representing the background illumination intensity change (or distance change between background illumination source and communication system);
3. Variable ISI and the ambient light noise, both conditions changing.

6.2.1 Variable ISI

As discussed in Chapter 4, the ceiling height H can be used to reflect the impact of the ISI on the channel; it can also be treated as distance variable to model the geometry change between the transmitter and receiver. Here an adaptive M-n-PAPM system operating with M=1 and n=4 was considered. This was equivalent to 4-PPM, which was adopted by the IrDA standards [89]. Ceiling heights of 1m, 2m and 3m were considered and the BERs obtained for a range of data rates up to 140Mb/s were shown in Figure 6.1. Detailed procedures and Matlab programs can be found in Appendix VI-4. What was apparent from the figure being that for low data rates (up to 20Mb/s), the effects of H variation on the BER were negligible. However, as the data rate increased, the impact of H variation upon BER increased significantly. Moreover, the concomitant simulation time noticeably increased with H, and took up to 30 minutes for H=3m, which was over 10 times as long as the corresponding case at 10Mb/s.

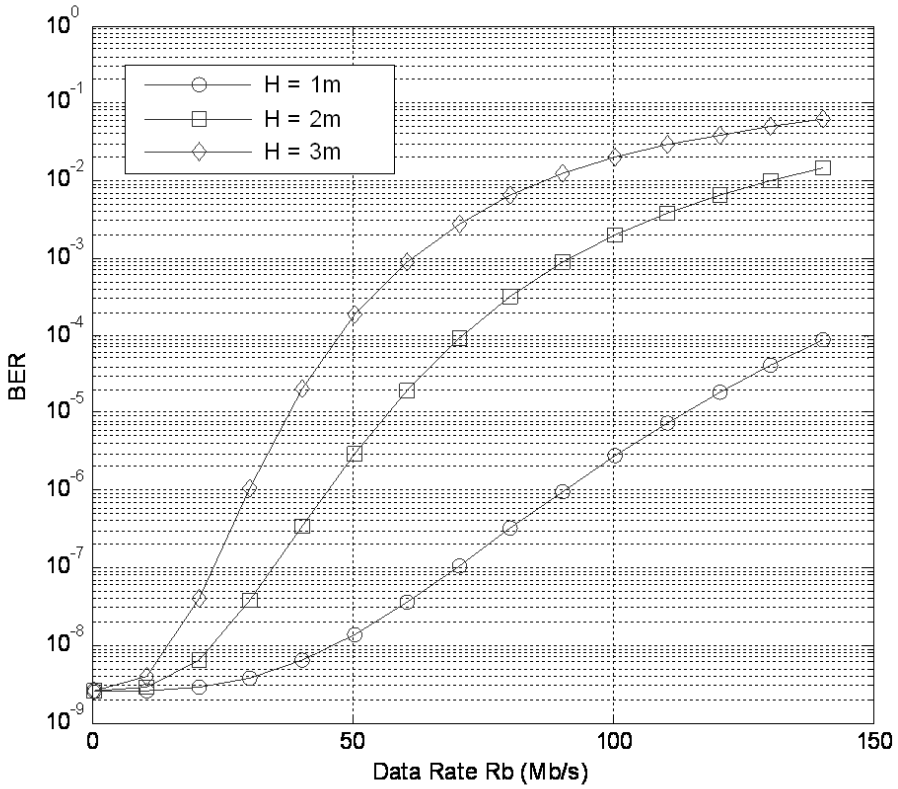

Figure 6.1 BER and data rate performance for M-n-PPM (M=1, n=4) modulation scheme with variable H and no ambient light interference

From Figure 6.1, it can be seen that the variation of H can affect BER performance at different data rate. Since the background ambient light noise was not considered, the factors contributing to the BER variation were thus purely the consequences of channel geometry variations. In contrast to other approaches to combat the ISI variation, the adaptive modulation system in this work can change its modulation parameters to provide compensations for H variation. In this case, *n* can be updated to find a match. Considering M-n-PAPM (M=1, n=4) with a data rate of 50.5 Mb/s as a benchmark, the adaptation search results was shown in Table 6.1

Table 6.1 System parameters for adaptive M-n-PAPM modulation with variable H and no ambient light noise

H value (m)		1	2	3
BER Rb=50.5Mb/s, M=1, n=4		1.4×10^{-8}	2.9×10^{-6}	1.8×10^{-4}
M=1, n=5	BER	3.0×10^{-12}	3.4×10^{-8}	1.8×10^{-5}
	Data rate (Mb/s)	46.9	46.9	46.9
	Simulation time (s)	0.6	3.1	3.1
M=1, n=6	BER	3.1×10^{-16}	3.9×10^{-10}	2.1×10^{-6}
	Data rate (Mb/s)	43.5	43.5	43.5
	Simulation time (s)	1.1	6.6	6.5
M=1, n=2	BER	2.5×10^{-3}	1.0×10^{-2}	2.9×10^{-2}
	Data rate (Mb/s)	50.5	50.5	50.5
	Simulation time (s)	0.08	0.1	0.5
M=2, n=4	BER	1.0×10^{-3}	4.0×10^{-3}	2.3×10^{-2}
	Data rate (Mb/s)	75.8	75.8	75.8
	Simulation time (s)	1.2	1.2	9.3

In the table, various combinations of M and n values were listed and improved or evenly matched system parameters were marked with light shading. Compared to the benchmark, when H increased from 1m to 3m, BER can be maintained or improved by increasing n thus increasing the pulse slot numbers within a symbol. However, this came at a cost of reduced data rate, for instance it can be seen that the data rate dropped to 46.9 Mb/s and 43.5 Mb/s for n = 5 and n = 6 respectively, representing 7% and 14% data rate losses for these cases. As would be expected, the reverse happened when the n value decreased as the system was trading bandwidth as *n* increased to decrease BER. As an example, using an *n* value of 2

maintains the data rate with H variation but offered a BER that was much worse than the original one, e.g. for M=1, n=2 and H=2m, the BER was only 1.0×10^{-2}, which was unlikely to be tolerated by any system requirements. It was interesting to note that when the amplitude level was increased, the data rate can be improved significantly, e.g. when M=2, n=4, data rate improved to 75.8Mb/s which was nearly 50% improvement compared to the original 50.5Mb/s. This was due to the fact that the amplitude modulation was more bandwidth efficient. The increased data rate was a consequence of reduced bandwidth requirements. Yet this also came at a cost of more power consumption and reduced achievable BER, which offset the benefit from the data rate increase. Moreover, the increased noise susceptibility was absent from this scenario as the ambient noise was ignored, the room was 'dark'. It can be observed that the simulation time was proportional to the H and M values.

From Table 6.1 and the discussion above, when variable ISI was the main source of system degradation, the adaptive modulation system can reduce the consequent BER variation by increasing number of pulse positions within a symbol sequence. This came at a cost of data rate loss and a trade off was necessary between loss of data rate and BER.

6.2.2 Variable Ambient Light Noise with Constant ISI

As discussed in Chapter 4, the background ambient light can be quantified by the ambient light to signal ratio (ASR). By changing the ASR value, different ambient light noise interference can be applied to the adaptive modulation system. Considering the same adaptive M-n-PAPM modulation system from the previous

section, for constant ISI (H=1), the effect of ambient light noise can be simulated, with the results illustrated in Figure 6.2. It can be observed that when the ASR value increased, the lower data rates were most affected. For example, a system operating at a data rate of 10.5 Mb/s can only achieve a BER of 3.1×10^{-2} when *n* was increased to 10. This was a severe degradation compared to the case when n = 1. The ambient light interference had a much smaller impact on the higher data rates in comparison to the lower data rates. The simulation time of different ASR values were comparable so this was different from the case with variable H, which suggested simulation time was identical with H values.

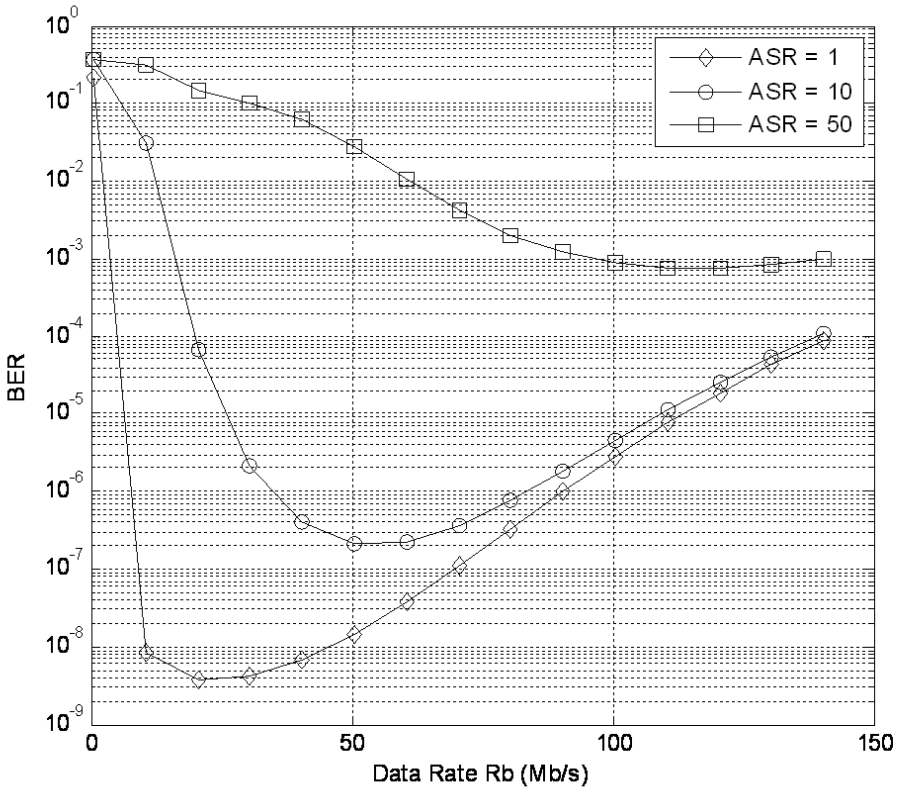

Figure 6.2 BER and data rate performance for M-n-PPM (M=1, n=4) modulation scheme with variable ASR and constant ISI (H=1m)

In Figure 6.2, when the ASR increased, the BER of system operating at lower data rates increased significantly. Although higher data rate were also affected by high

ASR, the degradation were less severe compared to the lower data rates. It can also be noticed that for a given ASR, there was a data rate value that can minimise achievable BER which can be denoted by R_{b_minBER}. When the ASR increased, R_{b_minBER} increased accordingly; here the resulting R_{b_minBER} values were 20.5Mb/s, 50.5Mb/s and 120.5Mb/s for ASR values of 1, 10 and 50 respectively.

Taking a data rate of 50.5 Mb/s as a benchmark again, the adaptive M-n-PAPM parameters can be updated to find an optimum combination to reduce the BER. Similar to the variable ISI case, the pulse position numbers and amplitude levels can be adjusted and detailed simulation results can be found in Table 6.2

Table 6.2 System parameters for adaptive M-n-PAPM modulation with variable ASR and constant ISI (H=1m)

ASR value		1	10	50
BER Rb=50.5Mb/s, M=1, n=4		1.4×10^{-8}	2.9×10^{-6}	1.8×10^{-4}
M=1, n=5	BER	3.3×10^{-12}	3.5×10^{-10}	1.9×10^{-2}
	Data rate (Mb/s)	46.9	46.9	46.9
	Simulation time (s)	1.2	1.3	1.2
M=1, n=6	BER	3.1×10^{-16}	2.0×10^{-13}	1.2×10^{-2}
	Data rate (Mb/s)	43.5	43.5	43.5
	Simulation time (s)	2.3	2.3	2.3
M=1, n=2	BER	2.6×10^{-3}	3.5×10^{-3}	4.4×10^{-2}
	Data rate (Mb/s)	50.5	50.5	50.5
	Simulation time (s)	0.1	0.1	0.1
M=2, n=4	BER	6.9×10^{-3}	8.3×10^{-2}	1.8×10^{-2}
	Data rate (Mb/s)	75.8	75.8	75.8
	Simulation time (s)	2.4	1.9	1.2

This table illustrated similar results to those shown in Table 6.1, suggesting that the interference induced by the ambient light noise can be reduced by changing pulse position values. System improvements were marked with light shading. Compared to the variable ISI case, the simulation time was shorter and comparable between different ASR values except for the M = 2 and n = 4 combinations. By actively choosing system parameters, the adaptive modulation can maintain the desired communication link requirements under variation of the background ambient noise.

Comparing results obtained in Table 6.1 and Table 6.2, by changing the pulse position values, the bandwidth requirements and thus the achievable system data rate can be adjusted. When increasing the pulse position orders, the occupied period of the 'on' chip within a pulse sequence was reduced, thus the periodic ambient light noise contribution can be reduced compared to lower order pulse position modulation systems. Higher order pulse position systems can lead to lower power consumption and better immunity for both ISI and ambient light noise interference. The combined contribution from both pulse position and amplitude was thus a balance among different system parameters. This can be further investigated in the following section.

6.2.3 BER and Data Rate Optimisation

From previous sections, it can be seen that by applying the adaptive modulation scheme, the impact of both channel interference introduced by ISI and background ambient light noise can be substantially reduced. In this section, the performance of the adaptive modulation was analysed when the optical wireless channel was affected by contributions from both types of interferences. As observed in previous sections, the modulation system operated at a given ISI and ambient light noise condition exhibited a minimum BER at data rate R_{b_minBER}. Compared to the initial system parameters, the task of the adaptive modulation was to adapt its pulse position and amplitude levels to achieve the required BER value while maximising data throughput. The detailed system parameter of the noise scenarios can be found in Table 6.3 below.

Table 6.3 Initial system parameters for adaptive M-n-PAPM (M=1, n=4) modulation with H=1 and ASR=50

Parameters		Value
4-PPM (M=1, n=4)	Minimum BER	7.4×10^{-4}
	R_{b_minBER} (Mb/s)	120.5
	Simulation Time (s)	27.9

In order to find the optimum combination of pulse position and amplitude level, exhaustive search can be used with a limit on the maximum amplitude level of 2 and pulse position values allowed within [2, 16]. Four candidate search results can be found in Table 6.4

Table 6.4 System parameters for adaptive M-n-PAPM (M=1, n=4) modulation with H=1 and ASR=50 using exhaustive search

Parameters		Value
4-PPM (M=1, n=4)	Minimum BER	7.4×10^{-4}
	R_{b_minBER} (Mb/s)	120.5
	Simulation Time (s)	27.9
2-4-PAPM (M=2, n=4)	Minimum BER	2.2×10^{-4}
	R_{b_minBER} (Mb/s)	180.8
	Simulation Time (s)	56.2
2-8-PAPM (M=2, n=8)	Minimum BER	1.3×10^{-8}
	R_{b_minBER} (Mb/s)	100.5
	Simulation Time (s)	298
2-9-PAPM (M=2, n=9)	Minimum BER	7.3×10^{-10}
	R_{b_minBER} (Mb/s)	93.1
	Simulation Time (s)	217.5

From this table, when H=1, ASR=50, the minimum BER achieved for a 4-PPM (M=1, n=4) modulation scheme was 7.4×10^{-4} with a data rate of 120.5Mb/s. The BER was not acceptable when compared to the 10^{-9} requirements. However, by increasing the pulse position number, 2-8-PAPM and 2-9-PAPM achieved improved BER values of 1.3×10^{-8} and 7.3×10^{-10} with a reduced data rate of 100.5Mb/s and 93.1Mb/s, respectively. The 2-4-PAPM scheme achieved a higher data rate of 180.8Mb/s but the BER performance was not as good as the other two candidates. The BER performance of all data rate steps was shown in Figure 6.3.

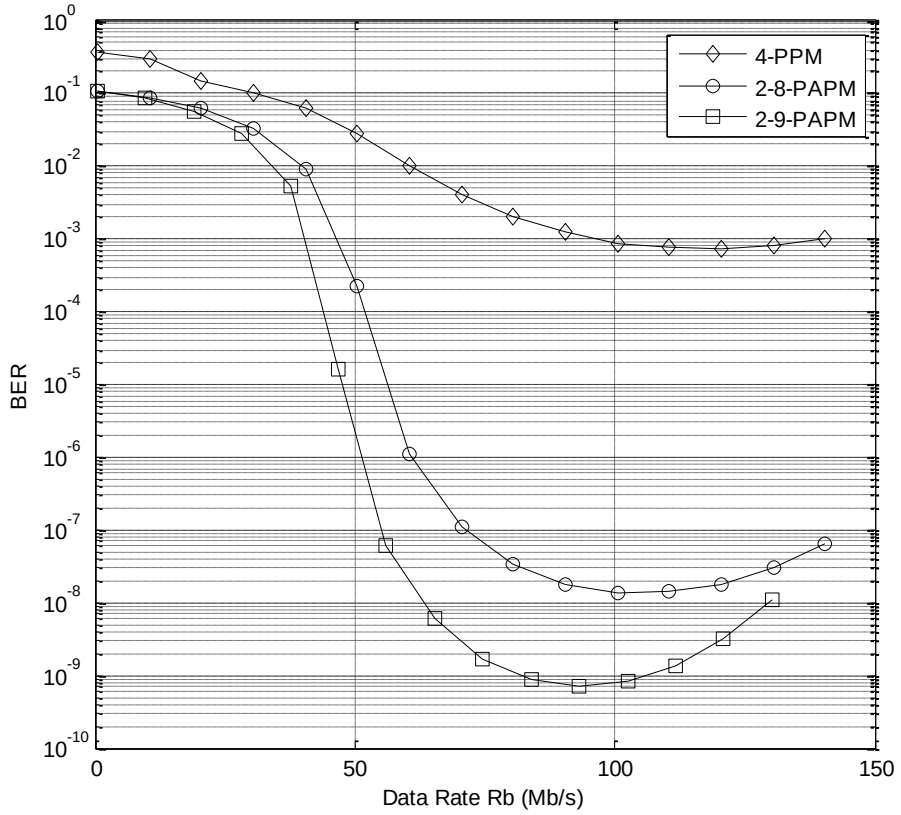

Figure 6.3 BER and data rate performance for candidate adaptive M-n-PPM modulation scheme with ASR=50 and H=1m

From above figure, for specific system degradation, the adaptive modulation scheme can be optimised according to different system requirements (in this test case, finding the optimum BER). The SNR to BER performance can be compared

to the case where no system adaptation was performed (4-PPM). This can be found in Figure 6.4.

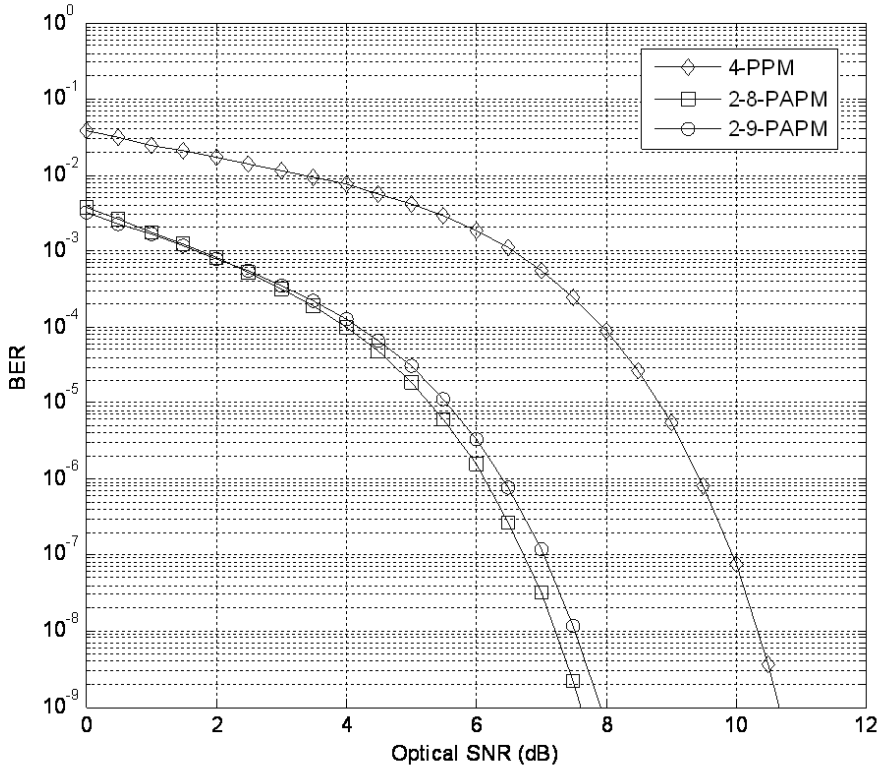

Figure 6.4 SNR to BER performance for candidate adaptive M-n-PPM modulation scheme with ASR=50 and H=1m

In Figure 6.4, the candidate modulation schemes reduced the optical SNR by at least 3dB to achieve a BER of 10^{-9} compared to modulation without adaptation. The 2-9-PAPM required 0.3dB more power compared to 2-8-PAPM. This was a result of balancing between pulse positions and amplitude levels. In this way the adaptive M-n-PAPM modulation schemes can utilise the benefits from both PAM and PPM modulation schemes. Depending on system requirements, the adaptive modulation can thus provide robustness under channel uncertainty with negligible impact on system performance.

An FL control system can be set up for the adaptive modulation system discussed in previous sections. This system was named C and its rules can be expressed as follows:

1. If H=1 and ASR=11 then M=1 and n=5
2. If H=1 and ASR=10 then M=1 and n=6
3. If H=1 and ASR=50 then M=2 and n=9

Where H is ceiling height, ASR is the ambient light noise to signal ratio, M and n were the resulting amplitude level and pulse position change values. The system had two inputs (H and ASR) and two outputs (M and n). Detailed fuzzy system construction was similar to that in Chapter 5 and can be found in Appendix VI-1, the original fuzzy system mapping can be found in Figure 6.5

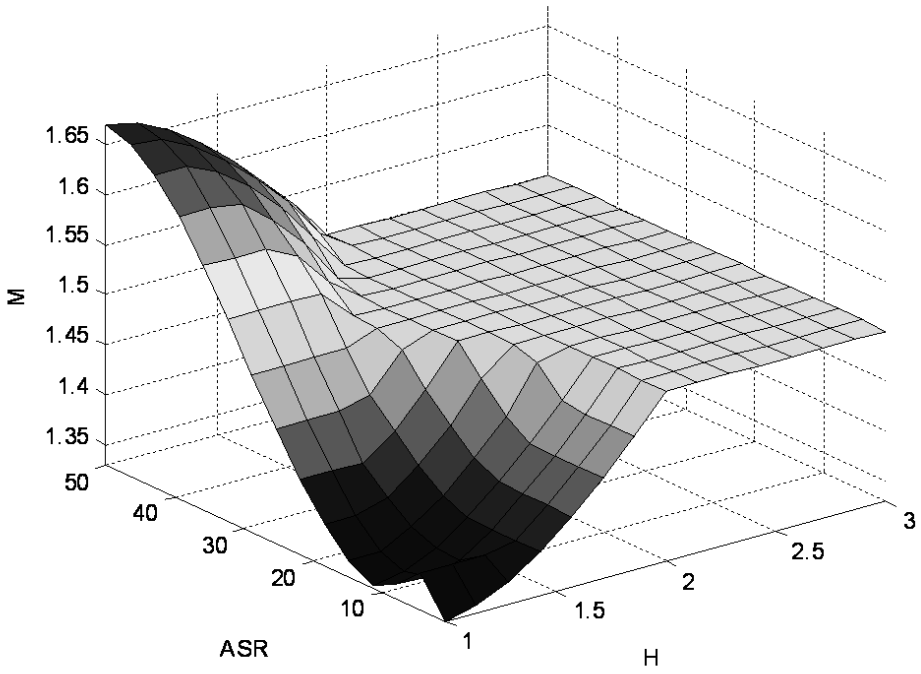

Figure 6.5 Fuzzy system inputs/outputs for system C

By using sample data from system C, an ANFIS model (System D) can be obtained in Figure 6.6 and with a training error shown in Figure 6.7

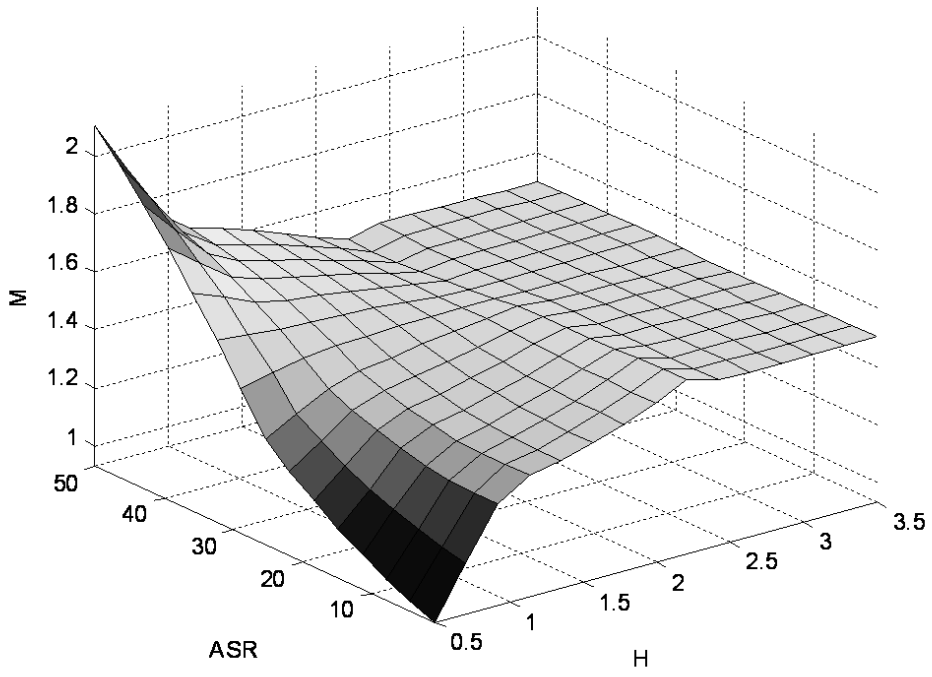

Figure 6.6 ANFIS trained using hybrid with recursive data set (system D)

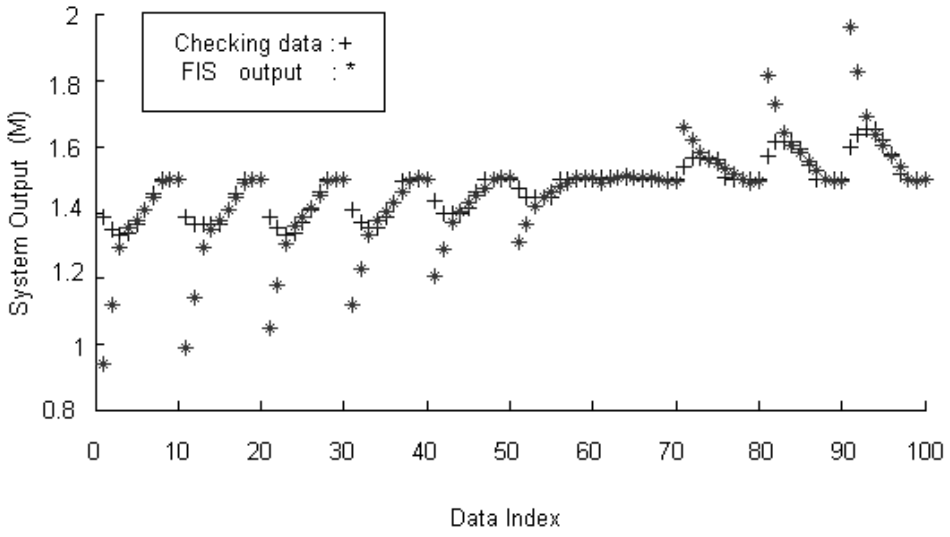

Figure 6.7 Training errors of system D

In Figure 6.5, system C can be used to give instructions for a 4-PPM modulation system under different interferences. Since the simulation time increased with channel geometry and amplitude level, the simulation can be done prior to system installation to reduce response time. This can be realised by simulating a wide range of degradation scenarios and storing the adaptive control instructions on the system memory chips. When the system was deployed in the designated working environment, the optimum modulation parameters can be adapted according to the preset instructions. For applications that required optimisation or robustness under a specific interference, the adaptation instructions can be optimised particularly for that requirement to better suit the designated environment. Detailed parameter of system D and the training data can be found in Appendices VI-2 and VI-3

The FL control system can realise system adaptation with just three rules applied to fuzzy interference process. This showed the simple yet powerful approach the FL method can provide for system design. From Figure 6.6 and Figure 6.7, the ANFIS model can identify the required control pattern by learning from training data set of an unknown system. This was extremely useful when the control patterns were complex and no prior knowledge of the system design was available.

6.3 Summary and Conclusions

Summary

The performances of the adaptive modulation system were discussed in the presence of combined effects of ISI and background ambient noises. From the analysis, both factors must be taken into account when validating modulation

schemes for optical wireless communication systems. It was demonstrated that by adaptively adjusting modulation parameters, the BER degradation caused by multipath ISI and background ambient light noise variation can be reduced. The adaptive modulation can be used to combat channel uncertainty and was capable of providing excellent BER improvement under different channel impairments. System parameters can be optimised for specific channel impairments. The ANFIS model was demonstrated to be an excellent viable technique to identify the unknown system control pattern.

By equipping the adaptive modulation scheme with fuzzy control technique, robust communication systems can be developed. The obtained system can maintain system stability through modulation optimisation under degradation, thus a reliable communication system structure can be realised for the optical wireless channel.

Conclusions

The fuzzy-logic-controlled-adaptive-modulation-schemes were validated under different types of interferences, simulation results showed the new schemes were effective for reducing the system degradation. Depending on the interference patterns, significant improvements can be achieved by validating the possible combinations of modulation parameters. Modulation optimisation models can be developed for specific and general applications. Previous developed system control patterns can be used as references for new channel environment. The capability of realising reliable communication through the fuzzy logic controlled adaptive modulation can be observed.

Chapter 7

Conclusions and Future Work

7.1 Conclusions

This chapter concluded the thesis with main findings from the discussions in previous chapters. The main task of this thesis was to identify areas where optical wireless communication can be better employed by the adaptive modulation techniques discussed in this thesis.

As stated in Chapter 1, the optical wireless channel can offer attractive benefits over the RF channel. Optical wireless communication became an important complement for the communication systems. The system architecture grew more complicated and sophisticated. This resulted more demand for channel throughput and robustness.

In Chapter 2, the unique channel model for the optical wireless communication was discussed. Channel topologies and propagation model were demonstrated. Most important, the interference artificial light model was described.

In Chapter 3, candidate modulation schemes for the optical wireless channel were discussed. Comparisons between modulation schemes were carried out.

In Chapter 4, the adaptive modulation technique was proposed. System adaptation under different channel impairments were analysed together with modulation schemes without adaptation. The results showed substantial improvements for channel impaired by ISI and ambient background noise.

In Chapter 5, the fuzzy logic control method was applied to the adaptive modulation scheme. The control model used in the test case showed the capability of the fuzzy logic control process. The ANFIS model developed was validated using different data set from the system, and provided excellent approximation to model the unknown control pattern though training.

Chapter 6 demonstrated further the proposed adaptive modulation schemes under different channel degradation by using the fuzzy logic control model developed in Chapter 5. By parameter optimisation, the adaptive modulation improved system throughput and can be further exploit for reliable communication applications.

The main arguments of this thesis were based on the modulation optimisation. The following contributions were made:

1. System performances under combined multipath ISI and background ambient light noise were validated using different modulation schemes. Discussions were extended to include any order multilevel modulation schemes. Computer programs were developed to simulate system performance under different degradations.

2. The adaptive modulation scheme was proposed and validated according to the requirements of optical wireless communication systems. Comparisons of the adaptive scheme with other schemes showed that the proposed system can better exploit the throughput capacity under certain system degradations.

3. Fuzzy Logic control modules were developed for the adaptive modulation scheme. The system can achieve self adaptation by using fuzzy inference methods, which benefited in a simple system structure compared to other artificial intelligence systems. The ANFIS model was very efficient in pattern identification.

7.2 Future Work

The system model developed in this project can be further investigated. This includes the follows:

1. The ultimate channel capacity of the optical wireless channel remains an open question. Although the channel capacity has been extensively discussed in the literature, general expressions for the ultimate optical channel capacity still remain open. Further investigation on this topic will help the researchers to better understand the optical wireless channel.

2. The possibility of the adaptive modulation can indeed be further explored. As the discussions were based on utilising the PAPM as the candidate modulation scheme. Yet using the same analytical model, other modulation schemes, such as the spectral efficient AB-QAM and throughput improving DAPPM can also be investigated in terms of adaptability under channel uncertainty.

3. The fuzzy logic control algorism developed in this thesis can be further investigated. As the efficient control mechanism will provide the communication system with more accurate instructions for adapting system parameters. Applications on different system requirements can also be analysed using this model.

APPENDIX

Appendix II-1 Parameters and Geometry for Simulation (Unblocked)

Parameter	Value
Room Dimensions (metre) (length ×width ×height)	5×3×2
Coordination System Geometry	X (North to South) Y (East to West) Z (Floor Ceiling)
ρ North (reflectivity) %	0.58
ρ South	0.56
ρ West	0.12
ρ East	0.30
ρ Ceiling	0.69
ρ Floor	0.09
Coordinate (0 0 0)	South East Floor Corner
Transmitter Location (metre)	(3 0.8 2)
Transmitter Elevation and Azimuth (degree)	(-90 0)
Transmitter Lobe Order	1
Receiver Location (metre)	(2 2 0.8)
Receiver Elevation and Azimuth (degree)	(60 0)
Receiver Werea (cm^2)	1
Receiver FOV (degree)	70
Transmitted Optical Power (Watts)	1
Time Step (ns)	0.2
Resolution (K=1 bounces)	30
Resolution (K=2 bounces)	8
Resolution (K=3 bounces)	4

Appendix II-2 Parameters and Geometry for Simulation (Blocked)

Parameter	Value
Room Dimensions (metre) (length × width × height)	5 ×3 ×2
Coordination System Geometry	X (North to South) Y (East to West) Z (Floor Ceiling)
ρ North (reflectivity) %	0.58
ρ South	0.56
ρ West	0.12
ρ East	0.30
ρ Ceiling	0.69
ρ Floor	0.7
Coordinate (0 0 0)	South East Floor Corner
Transmitter Location (metre)	(3 0.8 2)
Transmitter Elevation and Azimuth (degree)	(-90 0)
Transmitter Lobe Order	1
Receiver Location (metre)	(2 2 0.8)
Receiver Elevation and Azimuth (degree)	(60 0)
Receiver Werea (cm^2)	1
Receiver FOV (degree)	70
Transmitted Optical Power (Watts)	1
Time Step (ns)	0.2
Resolution (K=1 bounces)	30
Resolution (K=2 bounces)	8
Resolution (K=3 bounces)	4
Separator Corner Point (X Y Z)	(2.5 0 0)
Separator Dimensions (length width height)	(0.2 1 1.9)
Separator Reflectivity (north south; west east; ceiling floor)	(0.8 0.8; 0 0; 0 0)

Appendix III-1 Derivation of PAPM BER

Derivation of $p_j = \int_{-\infty}^{B_j} P_{x_j} dx_j = \int_{-\infty}^{B_j} \frac{1}{\sigma\sqrt{2\pi}} e^{-\frac{x_j{}^2}{2\sigma}} dx_j = 1 - Q\left(\frac{B_j}{\sigma}\right)$

$$p_j = \int_{-\infty}^{B_j} P_{x_j} dx_j$$

Since probability density function of $P_{x_j} = \frac{1}{\sigma\sqrt{2\pi}} e^{-\frac{x_j{}^2}{2\sigma^2}}$

$$p_j = \int_{-\infty}^{B_j} \frac{1}{\sigma\sqrt{2\pi}} e^{-\frac{x_j{}^2}{2\sigma^2}} dx_j$$

$$p_j = \frac{1}{\sigma}\frac{1}{\sqrt{2\pi}} \int_{-\infty}^{B_j} e^{-\frac{x_j{}^2}{2\sigma^2}} dx_j$$

According to reversing limit of integration $\int_a^b f(x)dx = -\int_b^a f(x)dx$

$$p_j = -\frac{1}{\sigma}\frac{1}{\sqrt{2\pi}} \int_{B_j}^{-\infty} e^{-\frac{x_j{}^2}{2\sigma^2}} dx_j \quad (s)$$

Make $u = -\frac{x_j}{\sigma}$, $dx_j = -du\sigma = -\sigma du$ and replace x_j and dx_j in (s)

$$p_j = \frac{1}{\sqrt{2\pi}} \int_{\frac{-B_j}{\sigma}}^{+\infty} e^{-\frac{u^2}{2}} du \quad (s1)$$

Since Q function Q(x) is defined as

$$Q(x) = \frac{1}{\sqrt{2\pi}} \int_{x}^{\infty} e^{-\frac{u^2}{2}} du$$

Replace (s1) with Q(x) and (s1) becomes

$$p_j = Q\left(-\frac{B_j}{\sigma}\right)$$

Since $Q(-x) = 1 - Q(x)$

$$p_j = 1 - Q\left(\frac{B_j}{\sigma}\right)$$

Thus

$$p_j = \int_{-\infty}^{B_j} P_{x_j} dx_j = 1 - Q\left(\frac{B_j}{\sigma}\right)$$

Thus

$$p_j = \int_{-\infty}^{B_j} P_{x_j} dx_j = \int_{-\infty}^{B_j} \frac{1}{\sigma\sqrt{2\pi}} e^{-\frac{{x_j}^2}{2\sigma}} dx_j = 1 - Q\left(\frac{B_j}{\sigma}\right)$$

Appendix IV-1 Matlab program for calculating adaptive factor for PAM, PPM and M-n-PAPM

In this program, there were four parts, which counted for OOK, L-PAM, L-PPM, and M-n-PAPM schemes respectively. This can be shown in the following:

```
%OOK
%Moderate
sook=(qfuncinv(1e-7)/qfuncinv(1e-9))^2; %Calsulate OOK noise ratio
Rook=4; %data rate
Rookf=Rook/sook %data rate for new BER
pause
Rook=250; % data rate
Rookf=Rook/sook % data rate for new BER


%Severe
sook=(qfuncinv(1e-4)/qfuncinv(1e-7))^2; %calculate OOK Noise Ratio
Rook=4; % data rate
Rookf=Rook/sook %data rate for new BER

pause
Rook=250; % data rate
Rookf=Rook/sook % data rate for new BER



%L_PAM
LPAM=[2:4]; %L-PAM modulation order
Ratio=(LPAM-1)./(sqrt(log2(LPAM))); % L-PAM adaptive factor ratio expression
%Calculate L-PAM adaptive ratio factor
for n=1:3,
   for M=1:3,
      Ratio2(n,M)=(Ratio(n)/Ratio(M))^2;
   end
end
%Moderate
   %Calculate L-PAM noise ratio
   sm=(qfuncinv(1e-7)/qfuncinv(1e-9))^2;
   %Calculate combined ratio factor
   optimum(i,j)=Ratio2(i,j)*sm;
   optimum =(round(optimum.*10))./10; %keeping one digit after decimal
   optimum2=(optimum-1);% compare to the constant value 1
   %convert diagonal value to 10, make it less identical to other values
```

```
for ii=1:3,
   for jj=1:3,
      if  ii==jj
         optimum2(ii,jj)=10;
      end
   end
end
   find_minimum_value(abs(optimum2)) % find miminum adaptive compare ratio
factor and its location

%Severe
   %repeat above process but with new sm value
   sm=(qfuncinv(1e-4)/qfuncinv(1e-7))^2;

%data rate
%Moderate
   Ri=250;
   Rpam_m=Ri*Ratio2(2,3)*sm;

%Severe
   ss=(qfuncinv(1e-4)/qfuncinv(1e-7))^2;
   %data rate
   Ri=250;
   Rpam_s=Ri*Ratio2(2,3)*ss;




%LPPM

LPPM=[2:4];% Calculate L-PPM modulation order
Ratioppm=(LPPM.*log2(LPPM)); % Calculate L-PPM Ratio Factor

for n=1:3,
   for M=1:3,
      Ratioppm2(n,M)=(Ratioppm(n)/Ratioppm(M));
   end
end
%Moderate

   sm_ppm=(qfuncinv(1e-7)/qfuncinv(1e-9))^2; % Moderate BER Ratio
   optimum_ppm=Ratioppm2*sm_ppm; % Moderate Data rate value matrix
   optimum_ppm2 =(round(optimum_ppm.*100))./100; %keeping one digit after
decimal
   optimum3_ppm=(optimum_ppm2-1);% compare to the constant value 1
   %convert diagonal value to 10, make it less identical to other values
```

```
for ii=1:3,
   for jj=1:3,
      if  ii==jj
         optimum2_ppm(ii,jj)=10;
      end
   end
end


   find_minimum_value(abs(optimum2_ppm)) % find miminum adaptive compare ratio factor and its location



   %Severe

   sm_ppm=(qfuncinv(1e-4)/qfuncinv(1e-7))^2;
   %repeat same process but with sm_ppm new values


%data rate
   Rppm_i=250;
   Rppm_m=Rppm_i*Ratioppm2(2,3)*sm_ppm;

%Severe

   ss=(qfuncinv(1e-4)/qfuncinv(1e-7))^2;

   Rppm_i=250;
   Rppm_s=Rppm_i*Ratioppm2(2,3)*sm_ppm;







%M-n-PPM

% Calculate M-n-PAPM ratio modulation matrix
M=2;
for i=1:3,
      Ratiopapm(i)=(M+1)^2./((i+1).*log2(M.*(i+1)));
end

M=3;
for i=4:6,
      Ratiopapm(i)=(M+1)^2./((i-2).*log2(M.*(i-2)));
```

```
end

M=4;
for i=7:9,
      Ratiopapm(i)=(M+1)^2./((i-5).*log2(M.*(i-5)));
end
%Find adaptive ratio factor table 4.8 for M-n-PAPM
for j=1:9,
   for k=1:9,
      Ratio_papm_2(j,k)=Ratiopapm(j)./Ratiopapm(k);
   end
end
%Find the optimum adaptive ratio factor
%First convert the diagonal value to 10, make it less significant

for ii=1:9,
   for jj=1:9,
      if  ii==jj
         Ratio_papm_2(ii,jj)=10;
      end

   end
end

%Moderate condition for M-n-PAPM

   NRatio_mod_papm=(qfuncinv(1e-7)/qfuncinv(1e-9))^2;
   % Calculate the data rate value matrix
   optimum_papm =Ratio_papm_2*NRatio_mod_papm;
   % Find the adaptive factor matrix
   optimum_papm2 = optimum_papm -1;

%Convert diagonal back to 1 for table presentation

   optimum_ppm2 =(round(optimum_ppm.*100))./100; %keeping one digit after
decimal
   optimum3_ppm=(optimum_ppm2-1);% compare to the constant value 1

optimum_papm_Fig=optimum_papm2;

for i1=1:9,
      for j1=1:9,
         if i1==j1
            optimum_papm_Fig(i1,j1)=0;
         end
      end
end


%take absolute value
```

```
optimum_papm3=abs(optimum_papm2);

%Find the minimum Value

papm_min=min(min(optimum_papm3));

%Find the initial and final levels
for i2=1:9,
   for j2=1:9,
      if  optimum_papm(i2,j2)==min(min(optimum_papm3))
         n_i=i2;
         n_f=j2;
      end

   end
end



%Severe condition for M-n-PAPM

   sm_papm=(qfuncinv(1e-4)/qfuncinv(1e-7))^2;
%repeat process with new sm_papm value
%data rate

   Rpapm_i=250;
   Rpapm_m=Rpapm_i* Ratio_papm_2(n_i,n_f)*sm_papm;


%Severe

   Rppm_i=250;
   Rppm_s=Rppm_i*Ratioppm2(2,3)*sm_papm;
```

Appendix IV-2 Procedures and Matlab program for obtaining Figure 4.3

Recall the following equation (3.5) and equation (3.9)

$$B_{L-PAM} = \frac{R_b}{log_2 L} = \frac{1}{log_2 L} B_{OOK} \quad (3.5)$$

$$P_{L-PAM} = \frac{L-1}{\sqrt{log_2 L}} P_{OOK} \quad (3.9)$$

In order to get normalised power and bandwidth for L-PAM, first the normalized power and bandwidth equation can be obtained using above equation (3.5) and equation (3.9), divide equation (3.5) with bandwidth requirement of OOK modulation scheme and divide equation (3.9) with power requirement of OOK modulation scheme the expression for normalised bandwidth and power requirements for L-PAM scheme can be obtained as following:

Normalised L-PAM bandwidth requirements

$$= \frac{B_{L-PAM}}{B_{OOK}} = \frac{R_b}{log_2 L} = \frac{1}{log_2 L} \quad \text{(IV-2 a)}$$

Normalised L-PAM power requirements

$$= \frac{P_{L-PAM}}{P_{OOK}} = \frac{L-1}{\sqrt{log_2 L}} \quad \text{(IV-2 b)}$$

Relate equation (IV-2 b) to the OOK power requirement in dB is then

$$= 10log_{10}(\frac{P_{L-PAM}}{P_{OOK}}) = 5log_{10}(\frac{P_{L-PAM}}{P_{OOK}})^2 = 5log_{10}(\frac{L-1}{\sqrt{log_2 L}})^2 = 5log_{10}(\frac{(L-1)^2}{log_2 L}) \quad \text{(IV-2 c)}$$

Where L is the amplitude levels of L-PAM scheme, equation (IV-2 a) is the x-axis and equation (IV-2 c) is the y-axis. Take the L value from 2 to 16 with step 1, the combined normalised power and bandwidth can be obtained. The Matlab program thus is the following:

```
%L-PAM
L=[2:16];
x=1./log2(L);%bandwidth normalised to OOK
y=5*log10(((L-1).*(L-1))./(log2(L)));%power normalised to OOK
plot(x,y,'o:');
grid on
```

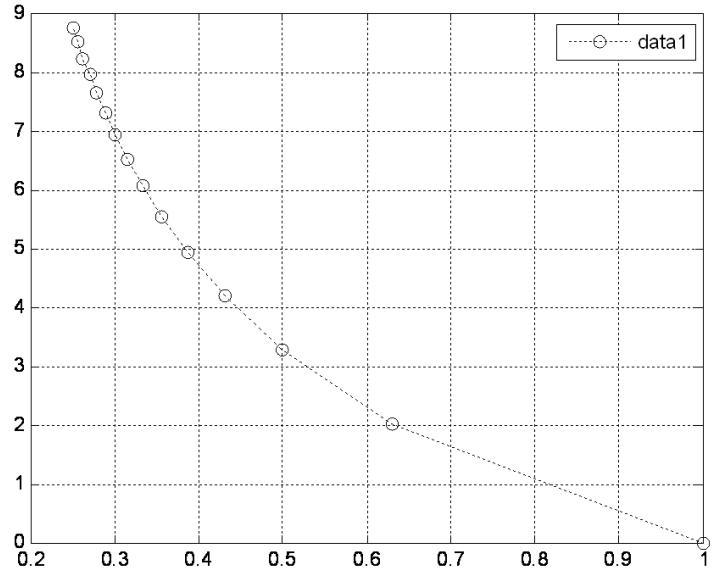

Increase x-axis range to 1.2, and add legends, Figure 4.3 can be obtained

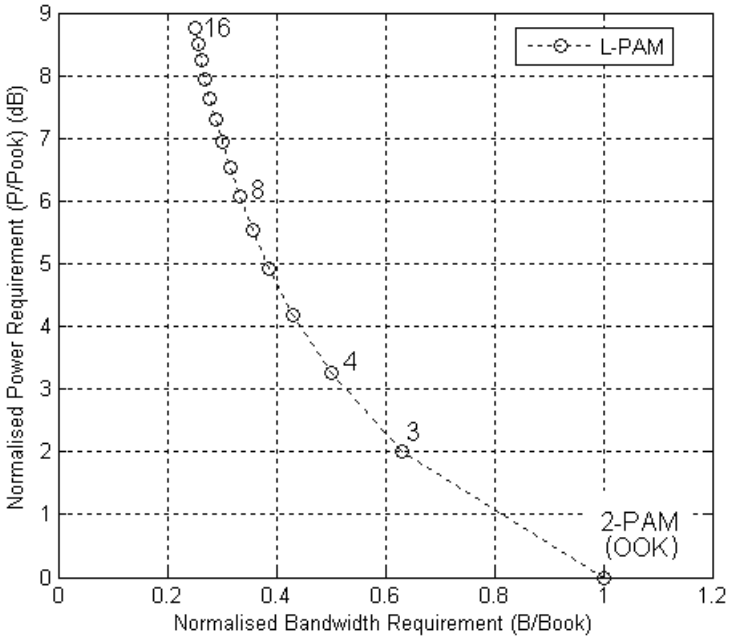

Appendix IV-3 Procedures and Matlab program to obtain Figure 4.5

According to equation (3.10) and equation (3.11)

$$P_{L-PPM} = \sqrt{\frac{2}{Llog_2 L}} P_{OOK} \tag{3.10}$$

$$B_{L-PPM} = \frac{L}{log_2 L} B_{OOK} \tag{3.11}$$

Normalized power and bandwidth requirement of L-PPM to OOK scheme as following:

$$\frac{P_{L-PPM}}{P_{OOK}} = \sqrt{\frac{2}{Llog_2 L}} \tag{IV-3 a}$$

$$\frac{B_{L-PPM}}{B_{OOK}} = \frac{L}{log_2 L} \tag{IV-3 b}$$

Relate equation (IV-3 a) to the OOK power requirement in dB is then

$$= 10log_{10}\left(\frac{P_{L-PPM}}{P_{OOK}}\right) = 5log_{10}\left(\frac{P_{L-PPM}}{P_{OOK}}\right)^2 = 5log_{10}\left(\sqrt{\frac{2}{Llog_2 L}}\right)^2$$

$$= 5log_{10}\left(\frac{2}{Llog_2 L}\right) = -5log_{10}\left(\frac{Llog_2 L}{2}\right) = -5log_{10}(0.5Llog_2 L) \tag{IV-3 c}$$

Where L is the slots number of L-PPM scheme, equation (IV-3 c) is the y-axis and equation (IV-3 b) is the x-axis. Increase L value from 2 to 16, the combined normalised power and bandwidth can be obtained. The Matlab program thus is the following:

```
%L-PPM
L=[2:16];
x=L./log2(L);
y=-5*log10(0.5*L.*log2(L));
plot(x,y,'s:');
grid on
```

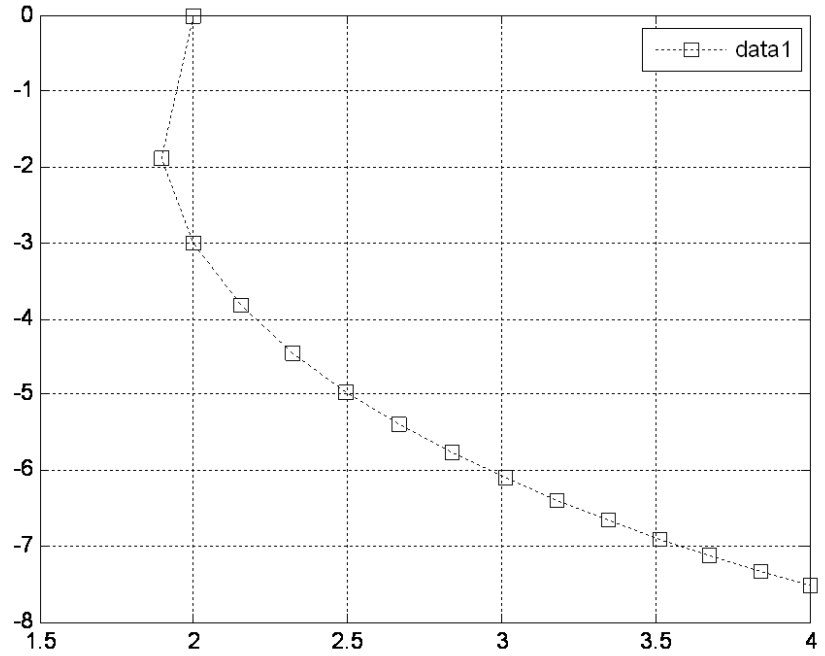

Add legends and labels to the above figure, Figure 4.5 can then be obtained

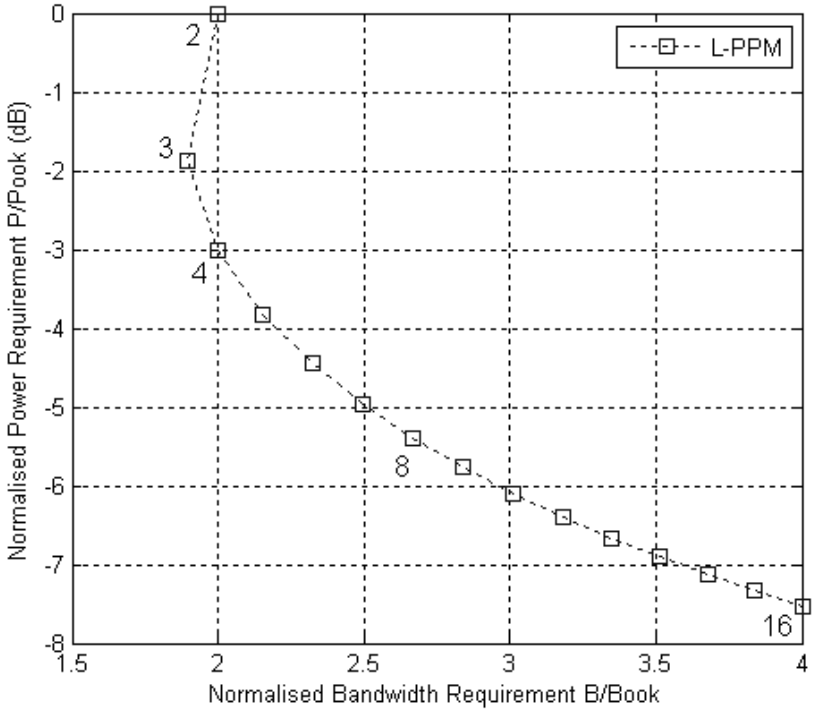

Appendix IV-4 Procedures and Matlab program to obtain Figure 4.7

According to equation (3.12) and equation (3.13), the bandwidth and power requirements of M-n-PAPM scheme were:

$$B_{M-n-PAPM} = \frac{n}{log_2 nM} B_{OOK} \tag{3.12}$$

$$P_{M-n-PAPM} = \sqrt{\frac{2M^2}{nlog_2 nM}} P_{OOK} \tag{3.13}$$

Normalized power and bandwidth requirement of M-n-PAPM to OOK scheme as following:

$$\frac{P_{M-n-PAPM}}{P_{OOK}} = \sqrt{\frac{2M^2}{nlog_2 nM}} \tag{IV-4 a}$$

$$\frac{B_{M-n-PAPM}}{B_{OOK}} = \frac{n}{log_2 nM} \tag{IV-4 b}$$

Relate equation (IV-4 a) to the OOK power requirement in dB is then

$$10log_{10}(\frac{P_{M-n-PPM}}{P_{OOK}}) = 5log_{10}(\frac{P_{M-n-PPM}}{P_{OOK}})^2 = 5log_{10}(\sqrt{\frac{2M^2}{nlog_2 nM}})^2 = 5log_{10}(\frac{2M^2}{nlog_2 nM}) \tag{IV-4 c}$$

Where M and n is the amplitude level and slots number of M-n-PAPM scheme respectively, equation (IV-4 c) is the y-axis and equation (IV-4 b) is the x-axis. Increase M and n value from 2 to 16, this is done by fix one of M or n value first and increase the other unfixed variable from 2 to 16, repeat this process, then the combined normalised power and bandwidth can be obtained. Together with the normalised power and bandwidth requirements of L-PAM, L-PPM and OOK for references, the Matlab program can be found as the following:

```
L=[2:16]; define variable for L-PAM and L-PPm

%L-PAM
xx=1./log2(L);
yy=5*log10(((L-1).*(L-1))./(log2(L)));


%L-PPM
x=L./log2(L);
y=-5*log10(0.5*L.*log2(L));

%OOK
%the reference of OOK is the point (1.0) as the OOK bandwidth and power
%requirement is normalised by other scheme

plot(xx,yy,'o:',x,y,'s:',1,0,'v'); %plot the normalised power and bandwidth
                                   %requirements of L-PAM, L-PPM and OOK
                                   %for reference
hold on

%M-n-PAPM

      for M = 2:16 %fix M value
         for n = 2:16 %repeat calculation for the entire range of n
            xpp=n./log2(n*M);
            ypp=5*log10(2*M.*M./(n*log2(n*M)));
            plot(xpp,ypp,'k.:');
            grid on
         end
      end

hold off
```

the following figure can then be obtained.

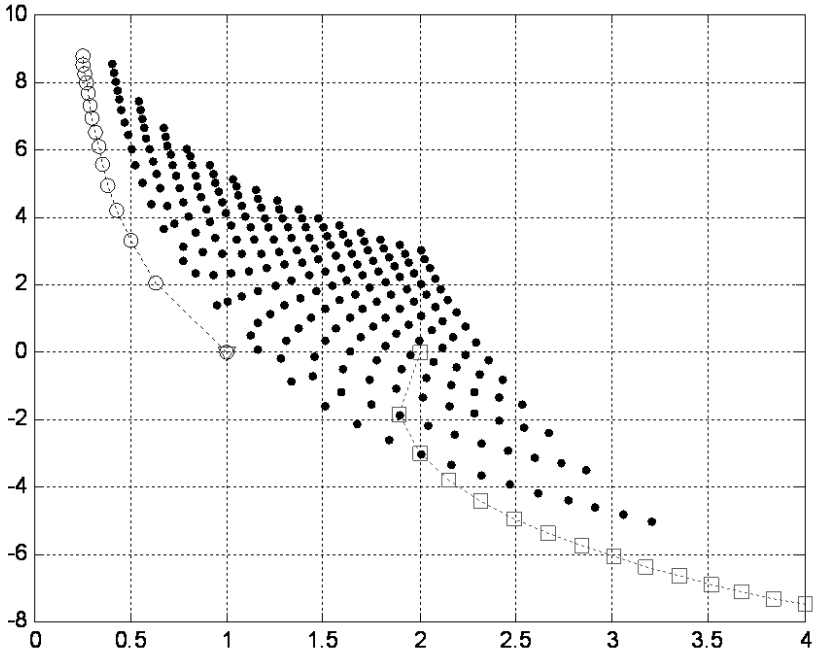

Add legends and labels to the above figure, Figure 4.7 can then be obtained

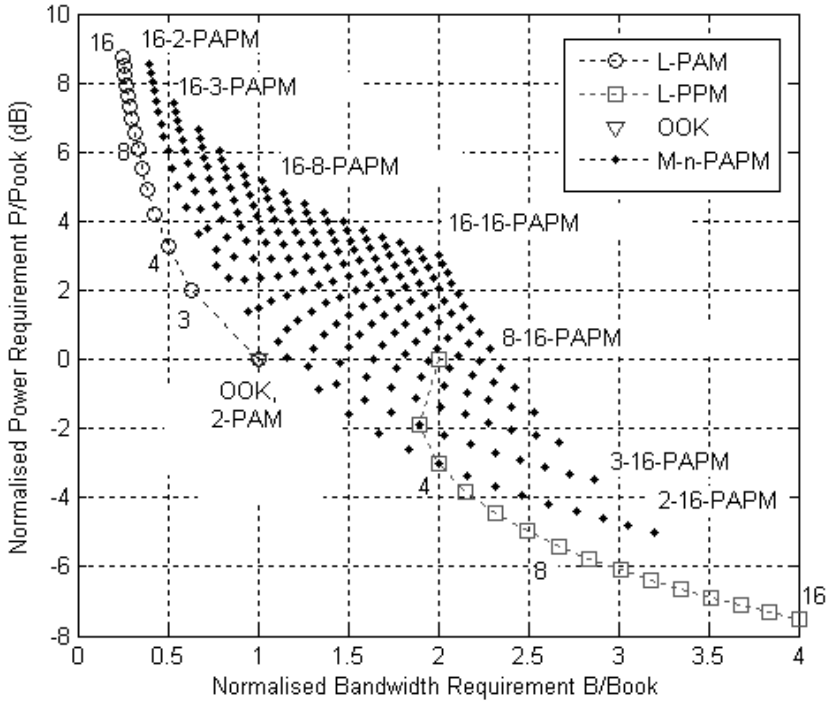

Appendix IV-5 Procedures and Matlab program to obtain Figure 4.9

The SNR vs BER performance of OOK and L-PAM can be simulated using equation (3.23) and (3.26) derived in Chapter 3 respectively.

$$BER_{OOK} = \frac{1}{T_i}\int_{t}^{t+T_i}\left(\frac{1}{2}\right)^{k}\left[\sum_{\substack{b\\ b_0=0}} Q\left(S_\sigma(1-S^1-V_k)\right) + \sum_{\substack{b\\ b_0=1}} Q\left(S_\sigma(S^0+V_k-1)\right)\right]dt \tag{3.23}$$

where

$$S^0 = \lambda\sum_{j=0}^{k-1} b_{k-j}h_j\,, \qquad S^1 = \lambda\sum_{j=1}^{k-1} b_{k-j}h_j\,, \qquad V_k = ASR = m/\bar{E}$$

$$BER_{L\_PAM} = \frac{1}{T_i}\int_{t}^{t+T_i}\frac{1}{(M+1)^k}\left[\sum_{\substack{b\\ b_0=0}} Q\left(S_\sigma\left(\tilde{\theta}_0 - S - V_k\right)\right) + \sum_{\substack{b\\ 0<a<A}} Q\left(S_\sigma\left(\tilde{\theta}_a - S - V_k\right)\right) + \sum_{\substack{b\\ 0<a<A}} Q\left(S_\sigma\left(S + V_k - \tilde{\theta}_{a-1}\right)\right) + \sum_{\substack{b\\ b_0=A}} Q\left(S_\sigma\left(S + V_k - \tilde{\theta}_{A-1}\right)\right)\right]dt \tag{3.26}$$

Where $\tilde{\theta}$ represents the thresholds for different levels, V_k is ASR, $S_\sigma = SNR_0 = R\bar{P}\sqrt{2T_c/N_0}$ is the defined optical SNR, $S = \lambda\sum_{j=0}^{k-1} b_{k-j}h_j$ is the convolved signal after the optical wireless channel. The detection threshold θ_i make 'hard decision' on received pulses. For a received pulse sequence, there were three types

of possibilities: 1. Detection success; 2.Over detection failure; 3. Under detection failure. Over detection failure occurs when received powers exceed detection thresholds, and under detection failure was caused by received signal power not enough to the detection thresholds. The detection thresholds can be demonstrated in the following figure:

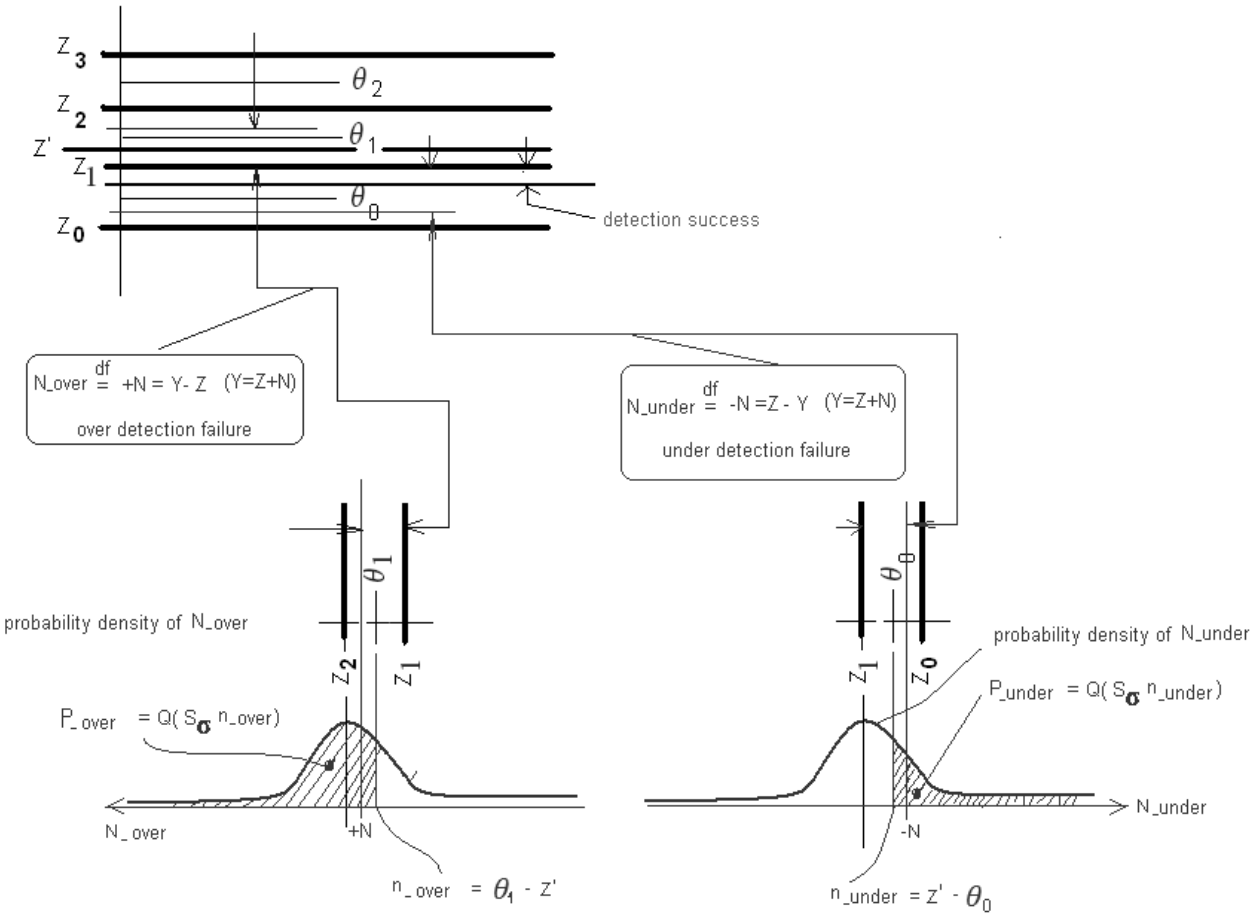

To simulate the BER, the following variables need to be considered:

1. Ceiling height

The ceiling height can be used to reflect the severities of the multipath ISI interference, the impulse response model used was the ceiling bouncing model, the ceiling height here is H=1m.

2. Amplitude levels

Since 2-PAM has two possible levels of amplitudes and this is in line with the definition of OOK. By changing the variable 'Amax' in main_PAM_SNR_BER.m, different amplitude levels L-PAM schemes can be simulated.

3. Data rate

Data rate Rb, for Figure 4.9, the link is operating at 1Mbps.

4. Ambient light interference factor (for fluorescent light driven by electronic ballast).

The artificial light interference is not considered in Figure 4.9, thus the ambient light factor was not enabled. The interference model can be enabled by setting 'amInteferenceSummationPoints' in main_PAM_SNR_BER.m to values greater than 1.

5. SNR values

The SNR value in dB can be set to an initial range of [0, 20]. The SNR values ranges need to be given before simulating the BER. Depending on the simulation carried out, the SNR value range can be updated.

The following functions were developed to simulate the BER, detailed programs were listed after the function descriptions.

Function Descriptions:

1. main_PAM_SNR_BER	Main function for calculating the BER for given conditions, set initial values of variables, e.g. ceiling height, data rate, modulation order, interference ratio from artificial light interference.

2. am_prepwere	Sub function for initialise the artificial interference model of the fluorescent light driven by electronic ballast discussed in Chapter 2
3. am_vi	Sub function to calculate ambient light average energy contribution over time t2-t1 starting from time t1. Returns: 1/dt*Integral_over amV by dt. Purpose: calculate noise applied to one chip:
4. betaPortion	Sub function to calculate werea under the impulse response h function of the ceiling bounce model over interval [k*step,k*step+step]
5. convolve	Sub function to calculate outputPulses = inputPulses * beta starting from element "start" in array outputPulses, where * is a discrete convolution
6. erfh	Sub function that works in two modes: When erfScale<0, returns flipped horizontally Heaviside Function. Otherwise, flips horizontally and shrinks erf by erfScale times.
7. simulateThresholding	Sub function to find BER for given channel over all chip sequences, all noise events, and all ambient light events.

Matlab Program Details:

1. main_PAM_SNR_BER.m

```
%Calculate BER for L-PAM with ISI, and ambient light.
Tic %simulation time start
%Rbindex=1;
%for Rb=1e6:4e6:100e6
%for ceilingHeight=1:20

%============================
% Noise Model Selection
%----------------------------
global shotNoisePresented
shotNoisePresented=1
global amInteferenceSummationPoints;
%global ambientLightPresented
%ambientLightPresented=0
%Set this parameter to 1 to disable ambient light:
%To enable ambient light, set this parameter to number of points over
%which averaging via interference interval is desired:
```

```
%Accracy is proportional to this number:
amInteferenceSummationPoints=1;

%============================

%============================
% Default parameters
%----------------------------
%global ceilingHeight
global Amax
global L
global Rb
global Bandwidth
global SNR
global amSAR
global amInterferencePeriodTi
        ceilingHeight=1 %Height of the room.
        Amax=2 %Number of non-zero amplitude levels.
        L=1 %Maximum number of chips in symbol
        Bandwidth=100E6;
        %Rb=Bandwidth*log2(Amax);
        SNR=0:0.5:20; %Signal To Noise Ratio, db
        amInterferencePeriodTi=25.0e-6 %In seconds.
        amSAR=10 %Signal to Ambient light Ratio.  = amSAR = 1/K w
        %here K is parameter from [Wong at all].

global OOK_threshold; %In units of minumum non-zero chip.
        OOK_threshold=0.5
        %============================

        %============================
        %Derivative parameters:
        global a %ISI length parameter in chips. Parameter of h-function.
        global SN %SNR not in dB form:
        global T %Chip length, seconds.
        global avLength %Average number of chips in symbol.
        global aphabetCount %Number of symbols in alphabet
        global M %Bits per symbol
        global bitsPerChip
        global scaled_chip_length %T/a
        global tapsNumber %"Memory" of multipath channel.
        global beta  %Discretized h., Array
        global bh %Convolution b*h, Array
        global lambda %(min non-zero Intensity)/average Intensity:
        %============================


        %============================
        % Prepwere parameters
        %----------------------------
```

```
        a=2.0*ceilingHeight/300000000.0
        avLength=L
        aphabetCount=1;
        for i=1:L
        aphabetCount=aphabetCount*(Amax+1);
        end
        aphabetCount

        M=log(aphabetCount)/log(2.0)
        lambda=2.0/Amax

%Part II:
    bitsPerChip=M/avLength
        T=bitsPerChip/Bandwidth%chip duration
        scaled_chip_length=T/a %

    %-------------------------------------------------------
    %estimation of size of sequence beta:
    %Consider only significant remnants of impulse from the past
    %and neglect small remnants from too distant past, it can be
    %estimated rigidly based on preset accuracy
    %- - - - - - - - - - - - - - - - - - - - - - - - - - -
    accuracyEps=1.0e-3 %preset accuracy 0.001 is a good choice,
   %although can go further
    hThresholdTs= (1.0/accuracyEps)^(1.0/6.0) - 1;
    if hThresholdTs<1.0
      hThresholdTs=1.0
    end
    hThresholdTs

    %mark temporary variable with "w":
    wtapsNumber = hThresholdTs/scaled_chip_length
    tapsNumber  = (floor(wtapsNumber)) + 1 %1 is taken for safety.
    %tapsNumber sets a number of elements in arrary b, that is , a
    %number of most distant chip from the past if to assign number
    %0 to current symbol and count backward in time

        %Convert SN from dB to numbers:
        SN=exp( SNR/10.0*log(10.0))

    %Adjust x-scale adopted in MatLab for erfc:
    SN=SN/sqrt(2.0);
    %============================

    beta=[1:tapsNumber];
    bh=[1:tapsNumber+L];
    %Create beta:
                for k=1:tapsNumber
                        beta(k)=betaPortion(k-1, scaled_chip_length);
          end
```

```
    beta %display beta value
    q=[1:tapsNumber];

    am_prepwere();
    %simulateThresholding();
    b=simulateThresholding();
    %b(ceilingHeight)=simulateThresholding();
    %b(Rbindex)=simulateThresholding();
    %Rbindex=Rbindex+1;
    %plot(Rb,b,'bs-');
    semilogy(SNR,b,'kv-');
    %hold on;
    %plot(Rb,b,'bv-');
    %hold on;
    %end
    %Rb=1:4:100;
    %plot(log2(Amax)*Rb,b,'rv-');
    hold on;

toc % Calculation time finish
```

2. am_prepwere.m

```
%=========================================
    %  Ambient light from fluorescent light driven by electronic ballast
%=========================================

function am_prepwere()

    global am_b
    am_b=[1:20];
    global am_c
    am_c=[1:20];
    global am_zeta
    am_zeta=[1:20];
    global am_fi
    am_fi=[1:20];
    global am_d %shifted from 0 to 1
    am_d=[1:13];
    global am_teta %shifted from 0 to 1
    am_teta=[13];
    global am_A1_reciprocal
    global am_A2_reciprocal
    %Fundamental frequency of high frequency component in (7), Hz:
    global am_fh
    global PI2
    am_A1_reciprocal=1.0/5.9;
    am_A2_reciprocal=1.0/2.1;
    am_fh=37.5E3;
```

```
PI2=2*pi;

log10 = log(10);

for i=1:20
        am_b(i)=exp(  log10*(  -13.1*log(100*i-50) +27.1  )/20       );
        am_c(i)=exp(  log10*(  -20.8*log(100*i) + 92.4    )/20       );
        end
        %Table I:Amplitude and phase parameters for low-frequency
        %components.
amAux=[ 1, 4.65, 0.00, 11, 1.26, 6.00,   2, 2.86, 0.08, 12, 1.29, 6.17,
        3, 5.43, 6.00, 13, 1.28, 5.69,   4, 3.90, 5.31, 14, 0.63, 5.37,
        5, 2.00, 2.27, 15, 6.06, 4.00,   6, 5.98, 5.70, 16, 5.49, 3.69,
        7, 2.38, 2.07, 17, 4.45, 1.86,   8, 4.35, 3.44, 18, 3.24, 1.38,
        9, 5.87, 5.01, 19, 2.07, 5.91,   10, 0.70, 6.01, 20, 0.87, 4.88
];
for ii=1:10
        for jj=1:2
          j=jj-1;
                pos=(ii-1)*6+j*3+1;
                i=ii+10*j;
                am_zeta(i)=amAux(pos+1);
             am_fi(i)=amAux(pos+2);
           end
        end
    %Check results matrix
for i=1:10
        j=i+10;
        end
        %Wong et al Table II. Amplitude and phase parameters for high-
        %frequency components.
amAux2=[  0, -22.22, 5.09, 6, -39.30, 3.55, 1,   0.00, 0.00, 7, -42.70, 4.15,
        2, -11.50, 2.37, 8, -46.40, 1.64,  3, -30.00, 5.86, 9, -48.10, 4.51,
        4, -33.90, 2.04, 10, -53.10, 3.55, 5, -35.30, 2.75, 11, -54.90, 1.78];
    for ii=1:6
          for jj=1:2
                j=jj-1;
              pos=(ii-1)*6+j*3+1;
              i=ii+6*j;
              am_d(i)=amAux2(pos+1);
              am_teta(i)=amAux2(pos+2);
           end
        end
```

3. am_vi.m

```
%=========================================
    %  Artificial light interference model
%=========================================

%Calculate ambient light average energy contribution over time t2-t1 starting
```

```
   %from time t1.
   %Returns: 1/dt*Integral_over amV by dt.
   %Purpose: calculate noise applied to one chip:

function retv=am_vi(t1, dt)
   global am_b
   global am_c
   global am_zeta
   global am_fi
   global am_d
   global am_teta
   global am_A1_reciprocal
   global am_A2_reciprocal;
   %Fundamental frequency of high frequency component in (7), Hz:
   global am_fh
   global PI2

        %Calculate member 1 in (7), RPm.
        sum1=dt;

        %Calculate member 2:
        sum2=0.0;
for i=1:20
        a0=PI2*100*i;
        a1=a0-PI2*50;
        delta0=a0*dt*0.5;
        delta1=a1*dt*0.5;
        alpha1=a1*t1+am_zeta(i)+delta1;
        alpha0=a0*t1+am_fi(i)+delta0;
        sum2 = sum2+am_b(i)*2.0*(  ...
                sin(delta1)*cos(alpha1)/a1+...
                sin(delta0)*cos(alpha0)/a0...
                                        );
end
        sum2=sum2*am_A1_reciprocal;
        %Calculate member 3:
        a1=PI2*am_fh;
        delta=a1*dt*0.5;
        alpha=a1*t1+am_teta(1)+delta;
        sum3=am_d(1)*2.0*sin(delta)*cos(alpha)/a1;
for i=1:11
        a1=PI2*2*i*am_fh;
        alpha=a1*t1+am_teta(i+1)+delta;
        sum3 = sum3 + am_d(i+1)*sin(delta)*cos(alpha)/a1;
end
        sum3=sum3*am_A2_reciprocal;
        sum=(sum1+sum2+sum3)/dt;
        %Total Ambient Light Interference over period dt

retv=sum;
```

```
end
```

4. betaPortion.m

```
%Returns werea under h-function over interval [k*step,k*step+step]:
%
function retv=betaPortion(k, step)
t=k*step;%start time1
power=t+1;
value1=1/((power)^6);%calculate impulse response of time1
t=t+step;%time increment
power=t+1;
retv=value1-1/((power)^6);%calculate integration impulse response of time2-time1
end
```

5. convolve.m

```
%Calculates outputPulses = inputPulses * beta starting from element "start " in
%array outputPulses
%where * is a discrete convolution:
function retv=convolve(start, inputPulses, outputPulses)
        global tapsNumber
        global beta
        nOut=size(outputPulses,2);
        nIn=size(inputPulses,2);
        for k=start:nOut
           s=0.0;
           for j=1:tapsNumber
                 tail=k-j+1;
                 if(tail<1 || tail>nIn)
                break;
              end
                        s=s+inputPulses(tail)*beta(j);
                        end
                        outputPulses(k)=s;
                 end
          retv=outputPulses;
         end
```

6. erfh.m

```
%Works in two modes:
%When erfScale<0, returns flipped horizontally Heaviside Function.
%Otherwise, flips horizontally and shrinks erf by erfScale times.
function retv=erfh(x,erfScale)
        if(erfScale<0)
```

```
%In Heviside Mode:
      if(x>=0)
        retv=0;
          else
        retv=1;
      end
else
      retv=0.5*erf(-(x*erfScale))+0.5;
   end
end
```

7. simulateThresholding.m

```
%Finds BER for given channel over all chip sequences, all noise events, and all
%ambient light events.

function retv=simulateThresholding()

      tapsSimulationLimit=31;
      global a
      global shotNoisePresented
      global amSAR
      global amInteferenceSummationPoints
      global amInterferencePeriodTi
      global Amax
      global OOK_threshold
      global SN
      global b
      global bh
      global S
      global tapsNumber
      global lambda
            global scaled_chip_length

            if tapsSimulationLimit<=tapsNumber
                  sprintf('Taps Number limit exceeded.')
         return;
      end
      %tapsLimit:
      tL=min(tapsSimulationLimit,tapsNumber);
      unitEventsCount=1;
      eventsCount=1;
      for i=1:tL
         unitEventsCount=2*unitEventsCount;
         eventsCount=eventsCount*(Amax+1);
      end

      unitEventsCount
      eventsCount
```

```
    EVENTS_MEASURE_LIMIT=1000000;
    if eventsCount>EVENTS_MEASURE_LIMIT
        message='Stat. events limit exceeded'
        EVENTS_MEASURE_LIMIT
        eventsCount
            return;
    end

    teta=lambda*OOK_threshold%teta=lambda/2  for OOK lambda=1/2 for PAM,
    %lambda=2/A
    amK=1.0/amSAR % define ambient light to signal ratio amK

amInterferenceStep=amInterferencePeriodTi/amInteferenceSummationPoints;
BAmb=0.0;%set initial value
    for iXAm=0:amInteferenceSummationPoints-1

        t=amInterferenceStep*iXAm;

        B=0.0;  %initial BER value
        Bup=0.0;
        Bdown=0.0;
        k=tL-1; %Probe slot to count statistics.
        for e=0:unitEventsCount-1
                %------------------------------
                %Generate signal of units:
                mask=e;
                weight=1;
           for slot=0:tL-1
           ampl=rem(mask,2); %ampl=bitand(uint32(mask),uint32(1));
%http://www.mathworks.com/access/helpdesk/help/techdoc/index.html?/access/helpdesk/help/techdoc/ref/bitshift.html&http://www.mathworks.com/access/helpdesk/help/techdoc/ref/bitand.html
                if ampl>0
             weight=weight*Amax;
             end
                b(k-slot+1)=ampl;
              mask=mask-ampl;
              mask=mask/2; %mask=bitshift(mask,-1)
%http://www.mathworks.com/access/helpdesk_r13/help/techdoc/ref/uint8.html
           end
        %------------------------------
           for iW=0:weight-1
        %--------------------------------------------
           %Decompose iW and assign amplitudes to a signal  of units:
              weightS=iW;
              for j=1:tL
                 i=tL-j;
                        if(b(i+1)>0)
                                reminder=rem(weightS,Amax);
```

```
                        b(i+1)=reminder+1;
                        weightS=(weightS-reminder)/Amax;
                    end
                end
                  %---------------------------------------------
                bh=convolve(k+1,b,bh);
                %bh(k+1)=bh(k+1)
                S=lambda*bh(k+1);
                Z=S; %no ambient light yet (default value)
                if amInteferenceSummationPoints>1 %add ambient noise if
                %parameter >1
                Z=Z+amK*am_vi(t, scaled_chip_length*a);
                end

                bk=b(k+1);        %shortcut for b matrix
                nUp=1.0*(lambda*bk+teta-Z);     %noise Up
                nDown=1.0*(Z-(lambda*bk-teta)); %noise Down

                SNRf=SN; %SNR factor
                if(~shotNoisePresented) %no shot noise case
                  SNRf=-1;
                end

                up=0.0;%initial value for up noise contribution
                down=0.0;%initial value for down noise contribution
                %We have three principal cases, bk=0, bk=A, bk in the middle.
                if(0==bk)
                  up=erfh(nUp,SNRf);
                elseif(Amax==bk)
                  down=erfh(nDown,SNRf);
                else
                  down=erfh(nDown,SNRf);
                  up=erfh(nUp,SNRf);
                end
                Bup=Bup+up;%Total Bup noise contribution
                   B=B+up;%add up Bup noise contribution to total noise
                Bdown=Bdown+down;%Total Bdown noise contribution
                   B=B+down;%add up Bdown noise contribution to total noise
              end % iW
            end %for e
            B=B/eventsCount
            Bup=Bup/eventsCount
            Bdown=Bdown/eventsCount
            BAmb=BAmb+B/amInteferenceSummationPoints;
          end
% for(int iXAm=0; iXAm<amInteferenceSummationPoints; iXAm++){
          BAmb
          retv=BAmb;
        end
```

Appendix IV-6 Procedures and Matlab program for Figure 4.10

The procedures and Matlab functions used to obtain the BER vs ceiling height was same as the sample in Appendix IV-5, thus will not be repeated. The updated main_PAM_SNR_BER function was listed after the variable list. The following variables need to be considered:

1. Ceiling height H

In order to find the variation of BER caused by multipath ISI, the ceiling height considered here was within the range [0,20] meters. Since the interference from artificial light not considered here, the room is 'dark'. The contributions from the ceiling height change will not cause significant variation in BER. A 'for' loop was used to calculate each BER under different ceiling height H values.

2. Amplitude levels Amax

Amax =1.

3. Data rate Rb

For the case in Figure 4.10, Rb = 1Mbps.

4. SNR

According to Figure 4.9, the OOK and 2-PAM will need 7dB SNR to achieve a BER of 10^{-7}, thus the SNR used for investigate the ceiling height change was set at 7dB.

The updated function **main_PAM_SNR_BER** can be found in the following:

main_PAM_SNR_BER

```
%Simulation for BER vs Ceiling height H
Tic %program start

for ceilingHeight=1:20

%============================
% Sub Model Usage
%----------------------------
      global shotNoisePresented
      shotNoisePresented=1
      global amInteferenceSummationPoints;
      %global ambientLightPresented
      %ambientLightPresented=0
        %Set this parameter to 1 to disable ambient light:
        %To enable ambient light, set this parameter to number of points over
         %which
        %averaging via interference interval is desired:
        %Accracy is proportional to this number:
      amInteferenceSummationPoints=1;
%============================

%============================
% Default parameters
%----------------------------
%global ceilingHeight
global Amax
global L
global Rb
global SNR
global amSAR
global amInterferencePeriodTi
        Amax=1 %Number of non-zero amplitude levels.
        L=1 %Maximum number of chips in symbol
        Rb=1E6
        SNR=7 %Signal To Noise Ratio, db
        amInterferencePeriodTi=25.0e-6 %In seconds.
        amSAR=5 %Signal to Ambient light Ratio.  = amSAR = 1/K where K is
        parameter from [Wong at all].

global OOK_threshold; %In units of minumum non-zero chip.
        OOK_threshold=0.5
%============================

%============================
%Derivative parameters:
global a %ISI length parameter in chips. Parameter of h-function.
global SN %SNR not in dB form:
global T %Chip length, seconds.
global avLength %Average number of chips in symbol.
```

```
global aphabetCount %Number of symbols in alphabet
global M %Bits per symbol
global bitsPerChip
global scaled_chip_length %T/a
global tapsNumber %"Memory" of multipath channel.
global beta  %Discretized h., Array
global bh %Convolution b*h, Array
global lambda %(min non-zero Intensity)/average Intensity:
%============================

%============================
%Default parameters
%---------------------------
      a=2.0*ceilingHeight/300000000.0

      avLength=L
      aphabetCount=1;
      for i=1:L
         aphabetCount=aphabetCount*(Amax+1);
      end
      aphabetCount

      M=log(aphabetCount)/log(2.0)
      lambda=2.0/Amax

      %Part II:
      bitsPerChip=M/avLength
      T=bitsPerChip/Rb
      scaled_chip_length=T/a

      %-------------------------------------------------------
      %estimation of size of sequence beta:
      %- - - - - - - - - - - - - - - - - - - - - - - - - - -
      accuracyEps=1.0e-3
      hThresholdTs= (1.0/accuracyEps)^(1.0/6.0) - 1;
      if hThresholdTs<1.0
        hThresholdTs=1.0
      end
      hThresholdTs

      wtapsNumber = hThresholdTs/scaled_chip_length
      tapsNumber  = (floor(wtapsNumber)) + 1 %1 is taken for safety.


                  %Convert SN from dB to numbers:
                  SN=exp( SNR/10.0*log(10.0) )

      %Adjust x-scale adopted in MatLab for erfc:
      SN=SN/sqrt(2.0);
            %============================
```

```
                beta=[1:tapsNumber];
bh=[1:tapsNumber+L];
%Create beta:
                for k=1:tapsNumber
                        beta(k)=betaPortion(k-1, scaled_chip_length);
            end
        beta

        am_prepwere();
        simulateThresholding();

        b(ceilingHeight)=simulateThresholding();


end
        plot(b,'bv-');

        toc %program end
```

Appendix IV-7 Procedures and Matlab Program for Figure 4.11

To simulate BER vs data rate comparison for OOK and 2-PAM, the analytical model was same as in Appendix IV-5. Data rate variation range within [0, 300], the SNR value was chosen to achieve a BER of 10^{-8}. The main function were also updated and listed following the variable list.

1. Data Rate

Rb within range [1, 300] Mbps, increase step 20Mbps.

2. Ceiling height

H=3.5m

3. Amplitude levels

Amax=1

4. SNR value

As demonstrated in Figure 4.9, OOK and 2-PAM need 7.5dB to achieve a BER of 10^{-8} in the experiment setup. Thus SNR=7.5 dB

Updated main function main_PAM_BER_Rb listed as following:

```
%BER vs data rate for OOK and 2-PAM.
Tic %program start
Rbindex=1;
b=0;
for Rb=1e6:20e6:3e8
%for ceilingHeight=1:20

%============================
% Noise Model Selection
%----------------------------

global shotNoisePresented
shotNoisePresented=1
global amInteferenceSummationPoints;
```

```
%global ambientLightPresented
%ambientLightPresented=0
%Set this parameter to 1 to disable ambient light:
%To enable ambient light, set this parameter to number of points over which
%averaging via interference interval is desired:
%Accracy is proportional to this number:
amInteferenceSummationPoints=1;

%============================

%============================
% Default parameters
%----------------------------

global Amax
global L
global SNR
global amSAR
global amInterferencePeriodTi
        ceilingHeight=3.5 %Height of the room.
        Amax=1 %Number of non-zero  amplitude levels.
        L=1 %Maximum number of chips in symbol
        SNR=7.5 %Signal To Noise Ratio, db
        amInterferencePeriodTi=25.0e-6 %In seconds.
        amSAR=1 %Signal to Ambient light Ratio.  = amSAR = 1/K where K is
                        %parameter from [Wong at all].

global OOK_threshold; %In units of minumum non-zero chip.
        OOK_threshold=0.5
%============================

%============================
%Derivative parameters:
global a %ISI length parameter in chips. Parameter of h-function.
global SN %SNR not in dB form:
global T %Chip length, seconds.
global avLength %Average number of chips in symbol.
global aphabetCount %Number of symbols in alphabet
global M %Bits per symbol
global bitsPerChip
global scaled_chip_length %T/a
global tapsNumber %"Memory" of multipath channel.
global beta  %Discretized h., Array
global bh %Convolution b*h, Array
global lambda %(min non-zero Intensity)/average Intensity:
%============================


%============================
% Prepwere parameters
```

```
%----------------------------
    a=2.0*ceilingHeight/3e8

    avLength=L
    aphabetCount=1;
    for i=1:L
    aphabetCount=aphabetCount*(Amax+1);
    end
    aphabetCount

    M=log(aphabetCount)/log(2.0)
    lambda=2.0/Amax

    %Part II:
    bitsPerChip=M/avLength
    T=bitsPerChip/Rb%chip duration
     scaled_chip_length=T/a

    %-------------------------------------------------------
    %estimation of size of sequence beta:
    %Consider only significant remnants of impulse from the past
    %and neglect small remnants from too distant past, it can be
    %estimated rigidly based on preset accuracy
    %- - - - - - - - - - - - - - - - - - - - - - - - - - - -
    accuracyEps=1.0e-3 %preset accuracy 0.001 is a good choice,
                       %although can go further
    hThresholdTs= (1.0/accuracyEps)^(1.0/6.0) - 1;
    if hThresholdTs<1.0
      hThresholdTs=1.0
    end
    hThresholdTs
    %mark temporary variable with "w":
    wtapsNumber = hThresholdTs/scaled_chip_length
    tapsNumber  = (floor(wtapsNumber)) + 1 %1 is taken for safety.

    %-------------------------------------------------------

    %Convert SN from dB to numbers:
       SN=exp( SNR/10.0*log(10.0))

    %Adjust x-scale adopted in MatLab for erfc:
    SN=SN/sqrt(2.0);
       %============================

       beta=[1:tapsNumber];
    bh=[1:tapsNumber+L];
    %Create beta:
                for k=1:tapsNumber
                        beta(k)=betaPortion(k-1, scaled_chip_length);
          end
```

```
        beta %display beta value

        am_prepwere();
        b(Rbindex)=simulateThresholding();
        Rbindex=Rbindex+1;
end
        Rb=1:20:300;
        semilogy(Rb,b,'rv-');
        hold on;
        toc %simulation end
```

Appendix IV-8 Procedures and Matlab Program for Figure 4.12

Figure 4.12 can be obtained using equation (3.35) and equation (3.36).

$$P_{success} = \int_{G^-}^{G^+} P_y \prod_j \left(1 - Q\left(\frac{B_j}{\sigma}\right)\right) dy \tag{3.35}$$

$$P_{de} = 1 - Pcd = \frac{1}{T_i} \int_{dt}^{T_i} \frac{1}{C} \sum_{C} (1 - P_{success}) \tag{3.36}$$

The L-PPM modulation scheme can be treated as a special M-n-PAPM with M=1. The L-PPM employed MAP detection and can be demonstrated in the following figure:

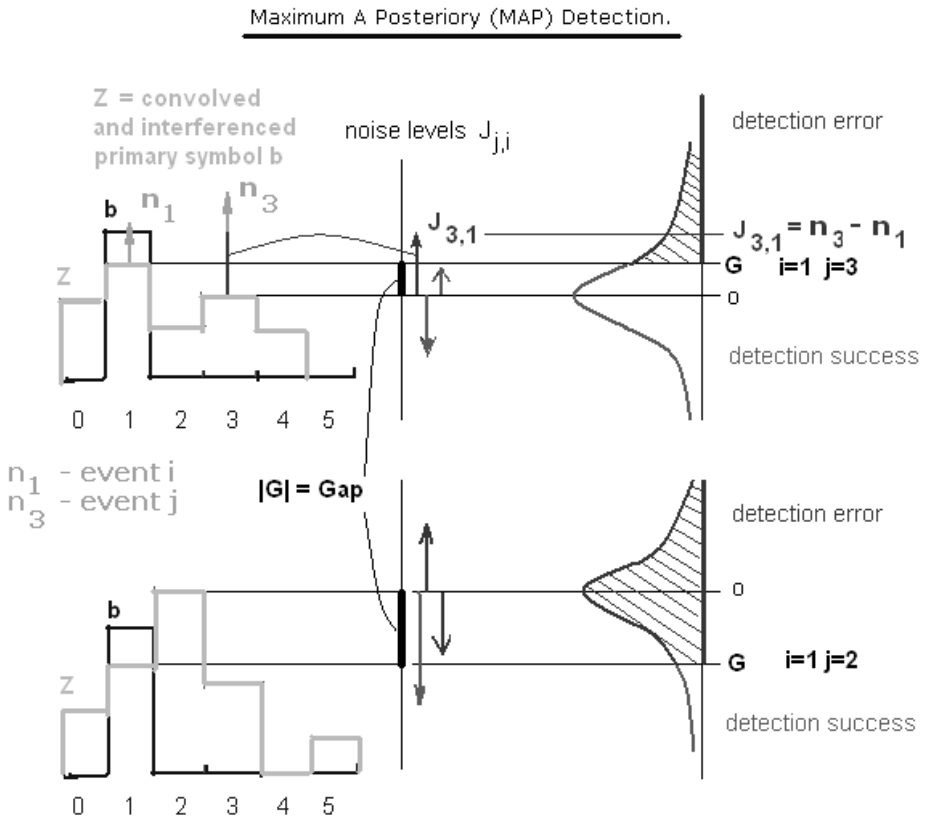

From above figure, received symbol can be recognised when noise contribution N was not significant, that is, the noise not leading the value of wrong peak j greater than value of correct peak i. When the received signal power exceed amplitude level G, symbol error occurs, and when received signal power less than level G, success detection is G=$Z_i - Z_j$.

In order to simulate the BER for L-PPM scheme, Matlab program was written and details were listed in the next section. The functions for L-PPM were listed as following:

1. main_PPM
2. am_prepwere
3. am_vi
4. betaPortion
5. convolve
6. erfh
7. simulatePPM

Function 2,3,4,5 and 6 were as same as the case for L-PAM, since these were common functions. The simulation variables for Figure 4.12 listed as following:

1. Data rate

Data rate for this case in the range of 1Mbps to 300Mbps, step is 10Mbps.

2. Ceiling height

Ceiling height H=3.5m

3. Pulse position slots number

L=2

4. SNR

Similar to L-PAM case, when no artificial light interference was considered, the 2-PPM requires 6dB to achieve BER of 10^{-8}.

Function 1 and 7 were different from L-PAM, and were listed below:

1. Function **main_PPM**

```
%Calculate BER for PPM with ISI and ambient light.
Tic %simulation time start

%for ceilingHeight=1:20
Rbindex=1;
for Rb=1e6:10e6:300e6
%============================
% Noise Model Selection
%----------------------------


global shotNoisePresented
shotNoisePresented=1
global amInteferenceSummationPoints;
%global ambientLightPresented
%ambientLightPresented=0

    % Ambient light noise
    amInteferenceSummationPoints=1;
    %   amInteferenceSummationPoints.
    %       If this parameter>1 then ambient noise is taken into account,
    %       and this parameter is number of integration points.
    %       Set this parameter to 1 to disable ambient light.
    %       Integration accracy is proportional to this parameter.
            %============================

            %============================
            % Default parameters
            %----------------------------
            global Amax
            global L
            global Rb
            global SNR
            global amSAR
            global amInterferencePeriodTi
            ceilingHeight=3.5%Height of the room.
            Amax=1 %Number of non-zero  amplitude levels.
            L=2 %Maximum number of chips in symbol
            %Rb=1e6
            %SNR=7
    SNR=6 %Signal To Noise Ratio, db
    amInterferencePeriodTi=25.0e-6 %In seconds.
    amSAR=0.05 %Signal to Ambient light Ratio.  amSAR = 1/K where K is
                    %parameter from [Wong et al].
            %============================
```

```
%============================
%Derivative parameters:
global a %ISI length parameter in chips. Parameter of h-function.
global SN %SNR not in dB form:
global T %Chip length, seconds.
 global avLength %Average number of chips in symbol.
global aphabetCount %Number of symbols in alphabet
global M %Bits per symbol
global bitsPerChip
global scaled_chip_length %T/a
global tapsNumber %"Memory" of multipath channel.
 global beta  %Discretized h., Array
  global lambda %(min non-zero Intensity)/average Intensity:
%============================


%============================
% Prepwere parameters
%---------------------------
a=2.0*ceilingHeight/300000000.0

avLength=L
  aphabetCount=L

M=log(aphabetCount)/log(2.0)
 lambda=L

%Part II:
 bitsPerChip=M/avLength
T=bitsPerChip/Rb

scaled_chip_length=T/a


%-------------------------------------------------------
%estimation of size of sequence beta:
%- - - - - - - - - - - - - - - - - - - - - - - - - - - -
accuracyEps=1.0e-3
hThresholdTs= (1.0/accuracyEps)^(1.0/6.0) - 1;
if hThresholdTs<1.0
  hThresholdTs=1.0
end
hThresholdTs
%mark temporary variable with "w":
wtapsNumber = hThresholdTs/scaled_chip_length
tapsNumber  = (floor(wtapsNumber)) + 1 %1 is taken for safety.


%Convert SN from dB to numbers:
SN=10.^(SNR/10);
```

```
        %============================

            beta=[1:tapsNumber];
    %Create beta:
            for k=1:tapsNumber
                beta(k)=betaPortion(k-1, scaled_chip_length);
        end
    beta %beta value

    am_prepwere();
    simulatePPM();

    b(Rbindex)=simulatePPM();

    Rbindex=Rbindex+1;

end
    Rb=1:10:300;
    semilogy(Rb,b,'kd-');
    hold on;

toc   %simulation time end
```

7. Function **simulatePPM**

```
%Finds P - symbol error probability (symbol error rate)
%for given channel over all chip sequences, all noise events, and all ambient light
events.
%It can be observed that BER=P/M.
%P is denoted as BAmb.


function retv=simulatePPM()

    global a
    global shotNoisePresented
    global amSAR
    global amInteferenceSummationPoints
    global amInterferencePeriodTi
    global Amax
    global L
    global M
    global SN
    global T
    global S
    global tapsNumber
    global lambda
```

```
global scaled_chip_length

    %-------------------------------------------------
    %Prevent errors:
    %- - - - - - - - - - - - - - - - - - - - - - - -
    tapsSimulationLimit=10000;
        if tapsSimulationLimit<=tapsNumber
            message='Taps Number limit exceeded.'
       return;
    end
    if L<2
      message='Incorrect value: L<2.'
      return;
    end
    %- - - - - - - - - - - - - - - - - - - - - - - -
    %Prevent errors:
    %-------------------------------------------------

    SNR2=SN/sqrt(2.0);  %Jump is built up "with" two noise events.
    %Adjust x-scale adopted in MatLab for erfc:
    SNR2=SNR2/sqrt(2.0);

    %First, find out number of preceding symbols:
    sslots=0;
    %take enough slots to cover ISI tapsNumber:
        while sslots*L<tapsNumber
      sslots=sslots+1;
    end

    %Recalculated taps number occupied by preceding symbols:
    pastTaps=sslots*L;

    %Recalculate tapsNumber including primary symbol:
        symTapsNumber=pastTaps+L;

    b=[1:symTapsNumber];
        bh=[1:symTapsNumber];
        %Ambient contribution to primary symbol chips:
        V=[1:L];

    %Find out number of all combination of preceding symbols:
    symbol_events=1;
        for i=1:sslots
            symbol_events=symbol_events*L;
        end

    %Now, symbol_events=L^sslots
    %set limit to 1E6, this can be changed to larger value
        PPMSymbolSimulationLimit=1000000;
        %Protect against long calculations:
```

```
            if PPMSymbolSimulationLimit<=symbol_events
                    sprintf('Symbol Slots Limit exceeded.');
      symbol_events
      PPMSymbolSimulationLimit
                    return;
    end

    %artificial noise factor
    amK=1.0/amSAR;

    weight_ISI_NOISE=1.0/symbol_events/L/(L-1);

    BAmb=0.0;

amInterferenceStep=amInterferencePeriodTi/amInteferenceSummationPoints;
    for iXAm=0:amInteferenceSummationPoints-1

        tt=amInterferenceStep*iXAm;
        BB=0.0; %"BER under integration sign" by time.

        %Prepwere ambient contributions to current symbol:
        for i=0:L-1
                V(i+1)=amK*am_vi(tt+T*i, T);
        end


        for e=0:symbol_events-1

%-------------------------------------
%Generate symbols and chip sequences.
%- - - - - - - - - - - - - - - - - - -
                mask=symbol_events;
            for slot=0:sslots-1
                sym=rem(mask,L);
              mask=mask-sym;
              mask=mask/L;
              for i=0:L-1
                b(slot*L+i+1)=0;
                if sym==i
                  b(slot*L+i+1)=Amax;
                end
              end
            end
%- - - - - - - - - - - - - - - - - - -
%Generate symbols and chip sequences.
%-------------------------------------

            %Cycle through primary chips:
            for i=0:L-1
              %Fill primary symbol's chips with zeros:
```

```
                for k=0:L-1
              b(sslots*L+k+1)=0;
            end
            %Make i-th primary chip non-zero:
               b(sslots*L+i+1)=Amax;


            %Calculate convolved chips for primary symbol:
            %from pastTaps+1 to pastTaps+L:
                  bh=convolve(pastTaps+1,b,bh);

            Zi=lambda*bh(pastTaps+i+1);

            if amInteferenceSummationPoints>1
              Zi=Zi+V(i+1);
            end

            %Cycle through competing chips:
            for j=0:L-1
                  if(i==j)%repeated chips
                continue;%finish loop
               end
               Zj=lambda*bh(pastTaps+j+1);
               if amInteferenceSummationPoints>1 %Ambient noise present
                 Zj=Zj+V(j+1);
               end
               G=Zi-Zj;
               SNRf=SNR2; %SNR factor
               if ~shotNoisePresented
                 SNRf=-1;
               end
               BB=BB+erfh(G,SNRf);
                  end
         end % Cycle through primary chips:
            % for i=0:L-1
      end % for(e
      BAmb=BAmb+weight_ISI_NOISE*BB;
   end % for iXAm=0 ..
   BAmb=BAmb/amInteferenceSummationPoints
   retv=BAmb;
end
```

Appendix IV-9 Procedures to obtain Figure 4.13

Figure 4.13 was a zoomed version of Figure 4.12, the purpose is to verify the data rate value that started to cause sharp rise in BER. This also verified the analytical results discussed for L-PPM modulation scheme. The procedures and Matlab programs were same as Figure 4.12, thus will not repeat.

Appendix V-1 Fuzzy Set Logic Operation [116]

Fuzzy Set Operations	Operator Expressions
Equality	$\mu_A(u) = \mu_B(u),\ u \in U$
Union	$\mu_{A\cup B}(u) = \max\{\mu_A(u), \mu_B(u)\}$, for all $u \in U$
Intersection	$\mu_{A\cap B}(u) = \min\{\mu_A(u), \mu_B(u)\}$, for all $u \in U$
Complement	$\mu_{\bar{A}}(u) = 1 - \mu_A(u),\ u \in U$
Normalization	$\mu_{NORM(A)}(u) = \mu_A(u) / \max(\mu_A(u)),\ u \in U$
Concentration	$\mu_{CON(A)}(u) = (\mu_A(u))^2,\ u \in U$
Dilation	$\mu_{DIL(A)}(u) = (\mu_A(u))^{0.5},\ u \in U$
Intensification	$\mu_{INT(A)}(u) = \begin{cases} 2(\mu_A(u))^2 & for \quad 0 \le \mu_A(u) \le 0.5 \\ 1 - 2(1-\mu_A(u))^2 & for \quad 0.5 \le \mu_A(u) \le 1 \end{cases}$
Algebraic Product	$\mu_{A\bullet B}(u) = \mu_A(u) \bullet \mu_B(u)$, for all $u \in U$
Bounded Sum	$\mu_{A\oplus B}(u) = \min\{1, \mu_A(u) + \mu_B(u)\}$, for all $u \in U$
Bounded Product	$\mu_{A\oplus B}(u) = \max\{0, \mu_A(u) + \mu_B(u) - 1\}$, for all $u \in U$
Drastic Product	$\mu_{A\otimes B}(u) = \begin{cases} \mu_A(u) & for \quad \mu_B(u) = 1 \\ \mu_B(u) & for \quad \mu_A(u) = 1 \\ 0 & for \quad \mu_A(u), \mu_B(u) < 1 \end{cases}$

Appendix V-2 Fuzzy Model Construction

Fuzzy System A Parameters

1.	Name	AdaptivePAPM01
2.	Type	mamdani
3.	Inputs/Outputs	[1 1]
4.	NumInputMFs	3
5.	NumOutputMFs	3
6.	NumRules	3
7.	AndMethod	min
8.	OrMethod	max
9.	ImpMethod	min
10.	AggMethod	max
11.	DefuzzMethod	centroid
12.	InLabels	BER
13.	OutLabels	Levels
14.	InRange	[1 3]
15.	OutRange	[0 5]
16.	InMFLabels	Minor
17.		Morderate
18.		Severe
19.	OutMFLabels	zero
20.		minor
21.		large
22.	InMFTypes	gauss2mf
23.		gbellmf
24.		gauss2mf
25.	OutMFTypes	gbellmf
26.		gbellmf
27.		gbellmf
28.	InMFParams	[0.033 0.87 0.1934 1.315]
29.		[0.46 3.28 1.993 0]
30.		[0.185 2.659 0.168 3.413]
31.	OutMFParams	[1.25 2.5 -2.776e-017 0]
32.		[1.25 2.5 2.5 0]
33.		[1.25 2.5 5 0]
34.	Rule Antecedent	1 2 3
35.	Rule Consequent	1 2 3
36.	Rule Weight	1 1 1
37.	Rule Connection	1 1 1

Appendix V-3 Fuzzy Model Construction

Fuzzy system B parameters

1.	Name	AdaptivePAPM02
2.	Type	mamdani
3.	Inputs/Outputs	[2 1]
4.	NumInputMFs	[3 2]
5.	NumOutputMFs	3
6.	NumRules	5
7.	AndMethod	min
8.	OrMethod	max
9.	ImpMethod	min
10.	AggMethod	max
11.	DefuzzMethod	centroid
12.	InLabels	BER, rate
13.	OutLabels	Levels
14.	InRange	[1 3] [0 1]
15.	OutRange	[0 5]
16.	InMFLabels	Minor Morderate Severe fast slow
17.	OutMFLabels	zero small large
18.	InMFTypes	gauss2mf
19.		gbellmf
20.		gauss2mf
21.		gbellmf
22.		gbellmf
23.	OutMFTypes	gbellmf
24.	InMFParams	[0.183 1.06 0.183 1.34]
25.		[0.46 3.28 1.993 0]
26.		[0.183 2.664 0.168 3.454]
27.		[0.5152 3.13 0.998 0]
28.		[0.406 2.5 0.114 0]
29.	OutMFParams	[1.25 2.5 -2.776e-017 0]
30.		[1.25 2.5 2.5 0]
31.		[1.25 2.5 5 0]
32.	Rule Antecedent	[1 0] [2 1] [2 2] [3 1] [3 1]
33.	Rule Consequent	1 3 2 3 3
34.	Rule Weight	1 1 1 1 1
35.	Rule Connection	1 1 2 1 2

Appendix V-4 ANFIS Model Data (Singleton)

Training Data

No.	BER	rate	Level
1	1.0000	0	1.9906
2	1.0202	0.0101	1.9814
3	1.0404	0.0202	1.9767
4	1.0606	0.0303	1.9756
5	1.0808	0.0404	1.9756
6	1.1010	0.0505	1.9756
7	1.1212	0.0606	1.9756
8	1.1414	0.0707	1.9756
9	1.1616	0.0808	1.9756
10	1.1818	0.0909	1.9756
11	1.2020	0.101	1.9756
12	1.2222	0.1111	1.9757
13	1.2424	0.1212	1.9759
14	1.2626	0.1313	1.9761
15	1.2828	0.1414	1.9764
16	1.3030	0.1515	1.9769
17	1.3232	0.1616	1.9774
18	1.3434	0.1717	1.9781
19	1.3636	0.1818	1.9808
20	1.3838	0.1919	1.9874
21	1.4040	0.202	1.9989
22	1.4242	0.2121	2.0155
23	1.4444	0.2222	2.0373
24	1.4646	0.2323	2.0643
25	1.4848	0.2424	2.0964
26	1.5051	0.2525	2.133
27	1.5253	0.2626	2.1739
28	1.5455	0.2727	2.2186
29	1.5657	0.2828	2.2658
30	1.5859	0.2929	2.3129
31	1.6061	0.303	2.3584
32	1.6263	0.3131	2.4015
33	1.6465	0.3232	2.4413
34	1.6667	0.3333	2.4778
35	1.6869	0.3434	2.5106
36	1.7071	0.3535	2.5394
37	1.7273	0.3636	2.5645
38	1.7475	0.3737	2.5864
39	1.7677	0.3838	2.6059
40	1.7879	0.3939	2.6238

Checking Data

No.	BER	rate	Level
1	1.0000	0	1.9906
2	1.0152	0.0081	1.9833
3	1.0303	0.0162	1.9786
4	1.0455	0.0242	1.9762
5	1.0606	0.0323	1.9756
6	1.0758	0.0404	1.9756
7	1.0909	0.0485	1.9756
8	1.1061	0.0566	1.9756
9	1.1212	0.0646	1.9756
10	1.1364	0.0727	1.9756
11	1.1515	0.0808	1.9756
12	1.1667	0.0889	1.9756
13	1.1818	0.097	1.9756
14	1.1970	0.1051	1.9757
15	1.2121	0.1131	1.9757
16	1.2273	0.1212	1.9759
17	1.2424	0.1293	1.976
18	1.2576	0.1374	1.9763
19	1.2727	0.1455	1.9766
20	1.2879	0.1535	1.977
21	1.3030	0.1616	1.9774
22	1.3182	0.1697	1.978
23	1.3333	0.1778	1.9786
24	1.3485	0.1859	1.9795
25	1.3636	0.1939	1.982
26	1.3788	0.202	1.9868
27	1.3939	0.2101	1.9943
28	1.4091	0.2182	2.0046
29	1.4242	0.2263	2.0179
30	1.4394	0.2343	2.0342
31	1.4545	0.2424	2.0535
32	1.4697	0.2505	2.0757
33	1.4848	0.2586	2.1008
34	1.5000	0.2667	2.1285
35	1.5152	0.2747	2.1588
36	1.5303	0.2828	2.1914
37	1.5455	0.2909	2.2261
38	1.5606	0.299	2.2624
39	1.5758	0.3071	2.2991
40	1.5909	0.3152	2.3355

41	1.8081	0.404	2.6404
42	1.8283	0.4141	2.6565
43	1.8485	0.4242	2.673
44	1.8687	0.4343	2.6903
45	1.8889	0.4444	2.7086
46	1.9091	0.4545	2.7276
47	1.9293	0.4646	2.7472
48	1.9495	0.4747	2.7673
49	1.9697	0.4848	2.7876
50	1.9899	0.4949	2.8077
51	2.0101	0.5051	2.8272
52	2.0303	0.5152	2.8461
53	2.0505	0.5253	2.8641
54	2.0707	0.5354	2.8812
55	2.0909	0.5455	2.8973
56	2.1111	0.5556	2.9123
57	2.1313	0.5657	2.9263
58	2.1515	0.5758	2.939
59	2.1717	0.5859	2.9508
60	2.1919	0.596	2.9615
61	2.2121	0.6061	2.9713
62	2.2323	0.6162	2.9805
63	2.2525	0.6263	2.9892
64	2.2727	0.6364	2.9982
65	2.2929	0.6465	3.0077
66	2.3131	0.6566	3.0188
67	2.3333	0.6667	3.0321
68	2.3535	0.6768	3.0489
69	2.3737	0.6869	3.0702
70	2.3939	0.697	3.097
71	2.4141	0.7071	3.1303
72	2.4343	0.7172	3.1709
73	2.4545	0.7273	3.2188
74	2.4747	0.7374	3.2755
75	2.4949	0.7475	3.34
76	2.5152	0.7576	3.4113
77	2.5354	0.7677	3.486
78	2.5556	0.7778	3.5625
79	2.5758	0.7879	3.6374
80	2.5960	0.798	3.7095
81	2.6162	0.8081	3.7769
82	2.6364	0.8182	3.839
83	2.6566	0.8283	3.8952
84	2.6768	0.8384	3.9455

41	1.6061	0.3232	2.3709
42	1.6212	0.3313	2.4052
43	1.6364	0.3394	2.4378
44	1.6515	0.3475	2.469
45	1.6667	0.3556	2.4983
46	1.6818	0.3636	2.5258
47	1.6970	0.3717	2.5505
48	1.7121	0.3798	2.5732
49	1.7273	0.3879	2.5939
50	1.7424	0.396	2.613
51	1.7576	0.404	2.6308
52	1.7727	0.4121	2.6476
53	1.7879	0.4202	2.6636
54	1.8030	0.4283	2.679
55	1.8182	0.4364	2.6939
56	1.8333	0.4444	2.7087
57	1.8485	0.4525	2.7237
58	1.8636	0.4606	2.7393
59	1.8788	0.4687	2.7552
60	1.8939	0.4768	2.7714
61	1.9091	0.4848	2.7876
62	1.9242	0.4929	2.8037
63	1.9394	0.501	2.8195
64	1.9545	0.5091	2.8348
65	1.9697	0.5172	2.8498
66	1.9848	0.5253	2.8641
67	2.0000	0.5333	2.8779
68	2.0152	0.5414	2.891
69	2.0303	0.5495	2.9035
70	2.0455	0.5576	2.9152
71	2.0606	0.5657	2.9263
72	2.0758	0.5737	2.9365
73	2.0909	0.5818	2.9461
74	2.1061	0.5899	2.9549
75	2.1212	0.598	2.9631
76	2.1364	0.6061	2.9705
77	2.1515	0.6141	2.9773
78	2.1667	0.6222	2.9835
79	2.1818	0.6303	2.989
80	2.1970	0.6384	2.9942
81	2.2121	0.6465	2.9989
82	2.2273	0.6545	3.0034
83	2.2424	0.6626	3.0076
84	2.2576	0.6707	3.012

85	2.6970	0.8485	3.9902
86	2.7172	0.8586	4.0294
87	2.7374	0.8687	4.0537
88	2.7576	0.8788	4.0658
89	2.7778	0.8889	4.0774
90	2.7980	0.899	4.0883
91	2.8182	0.9091	4.0987
92	2.8384	0.9192	4.1085
93	2.8586	0.9293	4.1178
94	2.8788	0.9394	4.1267
95	2.8990	0.9495	4.1349
96	2.9192	0.9596	4.1425
97	2.9394	0.9697	4.1497
98	2.9596	0.9798	4.1563
99	2.9798	0.9899	4.1625
100	3.0000	1	4.1682

85	2.2727	0.6788	3.0166
86	2.2879	0.6869	3.0217
87	2.3030	0.6949	3.0277
88	2.3182	0.703	3.0349
89	2.3333	0.7111	3.0437
90	2.3485	0.7192	3.0545
91	2.3636	0.7273	3.0679
92	2.3788	0.7354	3.0842
93	2.3939	0.7434	3.1039
94	2.4091	0.7515	3.1273
95	2.4242	0.7596	3.1548
96	2.4394	0.7677	3.1866
97	2.4545	0.7758	3.2228
98	2.4697	0.7838	3.2638
99	2.4848	0.7919	3.3097
100	2.5000	0.8	3.3599

Appendix V-5 ANFIS Model Data (2-D Recursive)

Training Data

No.	BER	rate	Level
1	1	0	1.9906
2	1	0.1111	1.9908
3	1	0.2222	1.9996
4	1	0.3333	2.0406
5	1	0.4444	2.1503
6	1	0.5556	2.3575
7	1	0.6667	2.4959
8	1	0.7778	2.5245
9	1	0.8889	2.5264
10	1	1	2.5264
11	1.2222	0	1.9755
12	1.2222	0.1111	1.9757
13	1.2222	0.2222	1.9844
14	1.2222	0.3333	2.0251
15	1.2222	0.4444	2.133
16	1.2222	0.5556	2.3359
17	1.2222	0.6667	2.4709
18	1.2222	0.7778	2.4984
19	1.2222	0.8889	2.5
20	1.2222	1	2.5
21	1.4444	0	2.0283
22	1.4444	0.1111	2.0285
23	1.4444	0.2222	2.0373
24	1.4444	0.3333	2.0791
25	1.4444	0.4444	2.1934
26	1.4444	0.5556	2.4122
27	1.4444	0.6667	2.5572
28	1.4444	0.7778	2.5837
29	1.4444	0.8889	2.5852
30	1.4444	1	2.5852
31	1.6667	0	2.4176
32	1.6667	0.1111	2.4177
33	1.6667	0.2222	2.4273
34	1.6667	0.3333	2.4778
35	1.6667	0.4444	2.6326
36	1.6667	0.5556	2.8468
37	1.6667	0.6667	2.9456
38	1.6667	0.7778	2.963
39	1.6667	0.8889	2.9639
40	1.6667	1	2.9639

Checking Data

No.	BER	rate	Level
1	1	0	1.9906
2	1	0.0889	1.9908
3	1	0.1778	1.9938
4	1	0.2667	2.0104
5	1	0.3556	2.0553
6	1	0.4444	2.1503
7	1	0.5333	2.3152
8	1	0.6222	2.4583
9	1	0.7111	2.5149
10	1	0.8	2.5255
11	1.1667	0	1.9755
12	1.1667	0.0889	1.9756
13	1.1667	0.1778	1.9786
14	1.1667	0.2667	1.9952
15	1.1667	0.3556	2.0397
16	1.1667	0.4444	2.133
17	1.1667	0.5333	2.2946
18	1.1667	0.6222	2.4343
19	1.1667	0.7111	2.4893
20	1.1667	0.8	2.4993
21	1.3333	0	1.9755
22	1.3333	0.0889	1.9756
23	1.3333	0.1778	1.9786
24	1.3333	0.2667	1.9952
25	1.3333	0.3556	2.0397
26	1.3333	0.4444	2.133
27	1.3333	0.5333	2.2946
28	1.3333	0.6222	2.4343
29	1.3333	0.7111	2.4893
30	1.3333	0.8	2.4993
31	1.5	0	2.1079
32	1.5	0.0889	2.108
33	1.5	0.1778	2.1111
34	1.5	0.2667	2.1285
35	1.5	0.3556	2.1769
36	1.5	0.4444	2.2854
37	1.5	0.5333	2.4799
38	1.5	0.6222	2.6365
39	1.5	0.7111	2.6869
40	1.5	0.8	2.6953

41	1.8889	0	2.5
42	1.8889	0.1111	2.5001
43	1.8889	0.2222	2.5098
44	1.8889	0.3333	2.5607
45	1.8889	0.4444	2.7086
46	1.8889	0.5556	2.9123
47	1.8889	0.6667	3.0068
48	1.8889	0.7778	3.0234
49	1.8889	0.8889	3.0244
50	1.8889	1	3.0244
51	2.1111	0	2.5
52	2.1111	0.1111	2.5001
53	2.1111	0.2222	2.5098
54	2.1111	0.3333	2.5607
55	2.1111	0.4444	2.7086
56	2.1111	0.5556	2.9123
57	2.1111	0.6667	3.0068
58	2.1111	0.7778	3.0234
59	2.1111	0.8889	3.0244
60	2.1111	1	3.0244
61	2.3333	0	2.5773
62	2.3333	0.1111	2.5772
63	2.3333	0.2222	2.5773
64	2.3333	0.3333	2.5787
65	2.3333	0.4444	2.7213
66	2.3333	0.5556	2.9343
67	2.3333	0.6667	3.0321
68	2.3333	0.7778	3.0493
69	2.3333	0.8889	3.0503
70	2.3333	1	3.0503
71	2.5556	0	2.9671
72	2.5556	0.1111	2.9669
73	2.5556	0.2222	2.967
74	2.5556	0.3333	2.9737
75	2.5556	0.4444	3.0343
76	2.5556	0.5556	3.2329
77	2.5556	0.6667	3.5408
78	2.5556	0.7778	3.5625
79	2.5556	0.8889	3.5637
80	2.5556	1	3.5637
81	2.7778	0	3.0245
82	2.7778	0.1111	3.0244
83	2.7778	0.2222	3.0245
84	2.7778	0.3333	3.0317

41	1.6667	0	2.4176
42	1.6667	0.0889	2.4176
43	1.6667	0.1778	2.4209
44	1.6667	0.2667	2.4398
45	1.6667	0.3556	2.4983
46	1.6667	0.4444	2.6326
47	1.6667	0.5333	2.8107
48	1.6667	0.6222	2.9211
49	1.6667	0.7111	2.9573
50	1.6667	0.8	2.9635
51	1.8333	0	2.5
52	1.8333	0.0889	2.5
53	1.8333	0.1778	2.5033
54	1.8333	0.2667	2.5224
55	1.8333	0.3556	2.5808
56	1.8333	0.4444	2.7087
57	1.8333	0.5333	2.878
58	1.8333	0.6222	2.9834
59	1.8333	0.7111	3.0181
60	1.8333	0.8	3.024
61	2	0	2.5
62	2	0.0889	2.5
63	2	0.1778	2.5033
64	2	0.2667	2.5224
65	2	0.3556	2.5807
66	2	0.4444	2.7086
67	2	0.5333	2.8779
68	2	0.6222	2.9833
69	2	0.7111	3.018
70	2	0.8	3.0239
71	2.1667	0	2.5
72	2.1667	0.0889	2.5
73	2.1667	0.1778	2.5033
74	2.1667	0.2667	2.5224
75	2.1667	0.3556	2.5808
76	2.1667	0.4444	2.7087
77	2.1667	0.5333	2.8781
78	2.1667	0.6222	2.9835
79	2.1667	0.7111	3.0181
80	2.1667	0.8	3.0241
81	2.3333	0	2.5773
82	2.3333	0.0889	2.5772
83	2.3333	0.1778	2.5772
84	2.3333	0.2667	2.5774

85	2.7778	0.4444	3.097
86	2.7778	0.5556	3.3066
87	2.7778	0.6667	3.636
88	2.7778	0.7778	3.9102
89	2.7778	0.8889	4.0774
90	2.7778	1	4.1202
91	3	0	3.0245
92	3	0.1111	3.0244
93	3	0.2222	3.0245
94	3	0.3333	3.0317
95	3	0.4444	3.097
96	3	0.5556	3.3066
97	3	0.6667	3.636
98	3	0.7778	3.9102
99	3	0.8889	4.0774
100	3	1	4.1682

85	2.3333	0.3556	2.5833
86	2.3333	0.4444	2.7213
87	2.3333	0.5333	2.8985
88	2.3333	0.6222	3.0078
89	2.3333	0.7111	3.0437
90	2.3333	0.8	3.0498
91	2.5	0	2.8849
92	2.5	0.0889	2.8848
93	2.5	0.1778	2.8848
94	2.5	0.2667	2.8855
95	2.5	0.3556	2.8951
96	2.5	0.4444	2.9437
97	2.5	0.5333	3.0737
98	2.5	0.6222	3.307
99	2.5	0.7111	3.3522
100	2.5	0.8	3.3599

Appendix VI-1 Fuzzy Model Construction

Fuzzy System C Parameters

1.	Name	System C
2.	Type	mamdani
3.	Inputs/Outputs	[2 2]
4.	NumInputMFs	[3 3]
5.	NumOutputMFs	[2 9]
6.	NumRules	3
7.	AndMethod	min
8.	OrMethod	max
9.	ImpMethod	min
10.	AggMethod	max
11.	DefuzzMethod	centroid
12.	InLabels	H
13.		ASR
14.	OutLabels	M
15.		n
16.	InRange	[1 3]
17.		[1 50]
18.	OutRange	[1 2]
19.		[2 10]
20.	InMFLabels	1 2 3 1 10 50
21.	OutMFLabels	1 2 3 5 7 4 2 6 8 9 10
22.	InMFTypes	trimf
23.	OutMFTypes	trimf
24.	InMFParams	[0 1 2 0] [1 2 3 0] [2 3 4 0] [-9 1 10 0] [1 10 50 0] [10 50 90 0]
25.	OutMFParams	[0 1 2 0] [1 2 3 0] [2 3 4 0] [4 5 6 0] [6 7 8 0] [3 4 5 0]
26.		[1 2 3 0] [5 6 7 0] [7 8 9 0] [8 9 10 0] [8 9 10 0] [9 10 11 0]
27.	Rule Antecedent	[1 1]
28.		[1 2]
29.		[1 3]
30.	Rule Consequent	[1 2]
31.		[1 6]
32.		[2 8]
33.	Rule Weight	1 1 1
34.	Rule Connection	1 1 1

Membership Functions of Input / Output and Surface plot

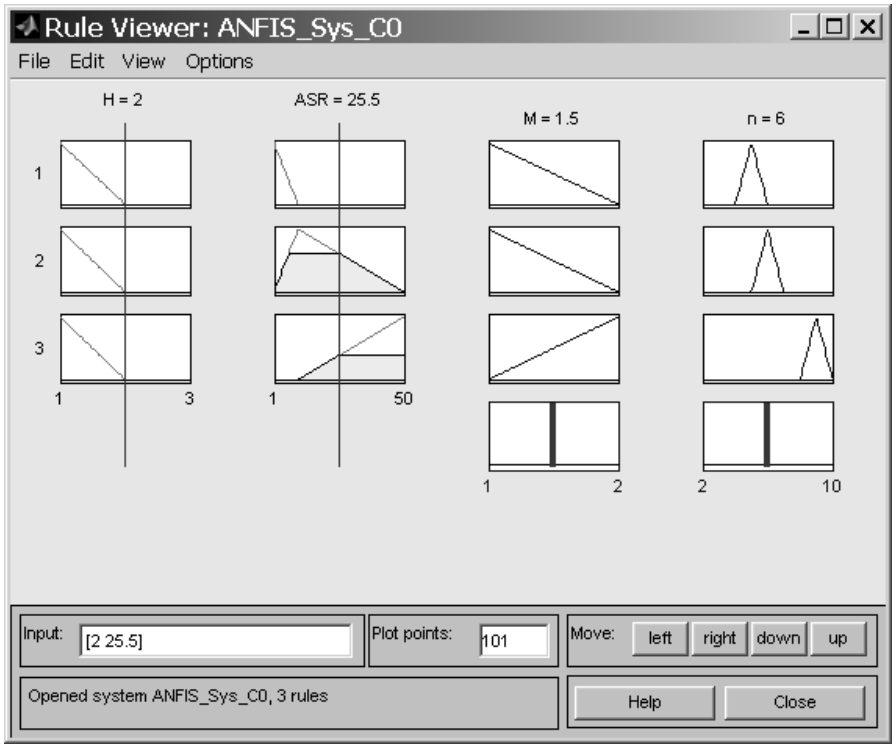

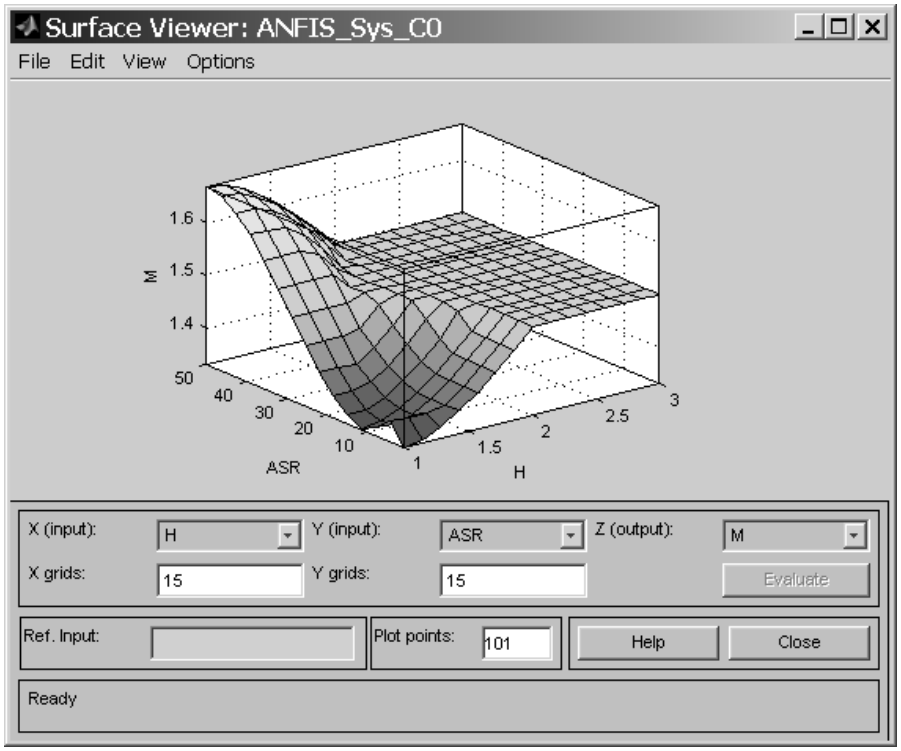

FIS Structures and 3 Rules

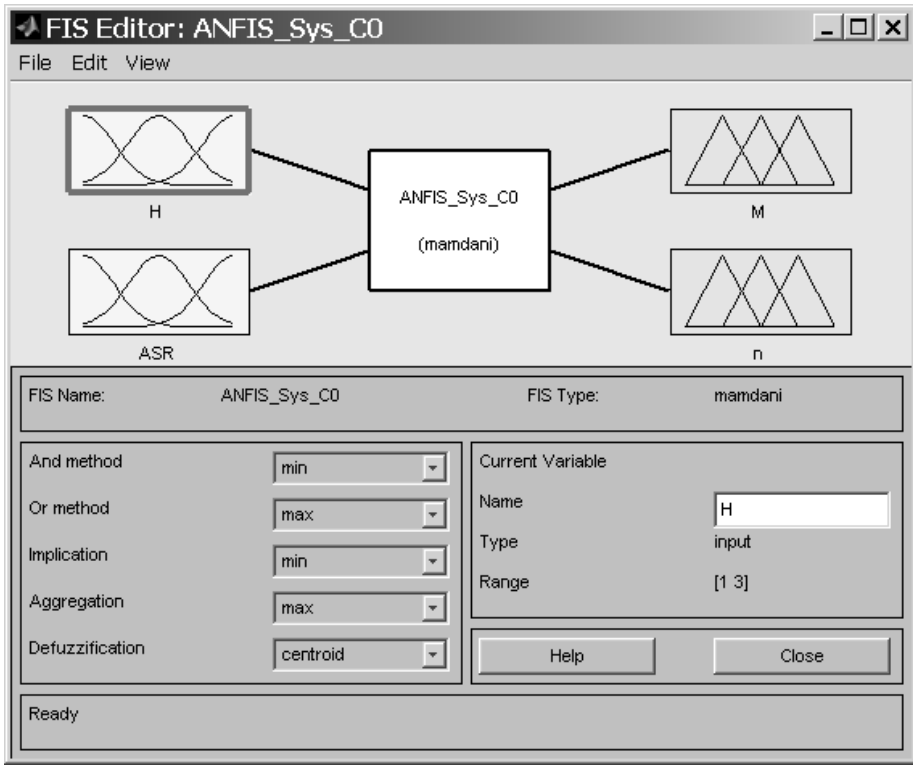

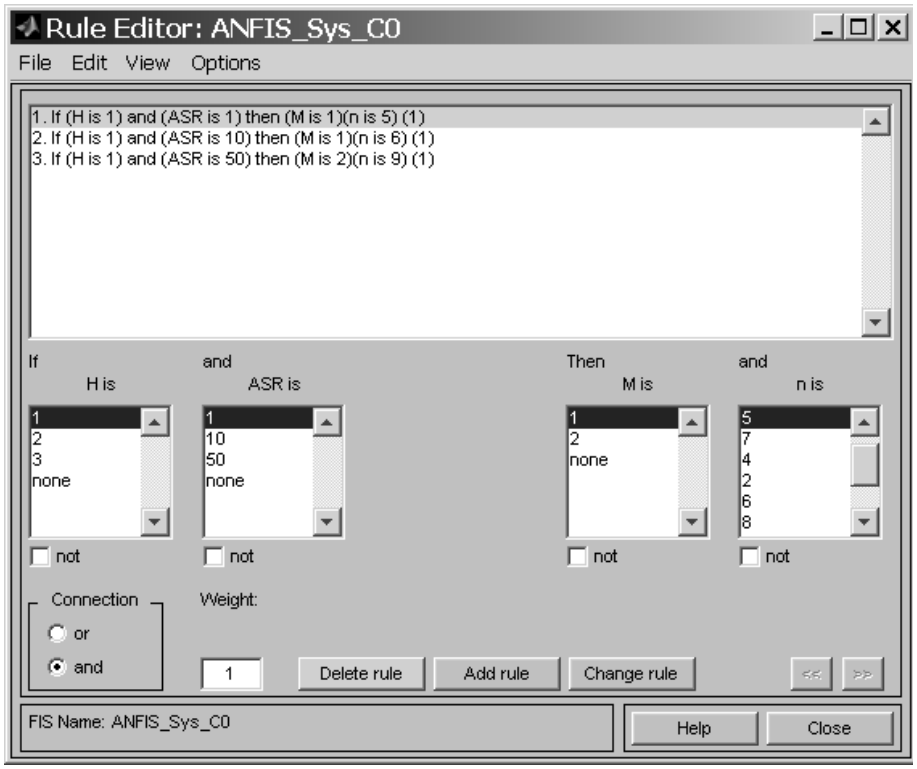

Appendix VI-2 Fuzzy Model Construction

Fuzzy System D Parameters

1.	Name	ANFIS System D
2.	Type	sugeno
3.	Inputs/Outputs	[2 1]
4.	NumInputMFs	[3 3]
5.	NumOutputMFs	9
6.	NumRules	9
7.	AndMethod	prod
8.	OrMethod	probor
9.	ImpMethod	prod
10	AggMethod	sum
11	DefuzzMethod	wtaver
12	InLabels	input1
13		input2
14	OutLabels	output
15	InRange	[0.5 3.5]
16		[1 50]
17	OutRange	[1.33 1.67]
18	InMFLabels	in1mf1 in1mf2 in1mf3 in2mf1 in2mf2 in2mf3
19	OutMFLabels	out1mf1 out1mf2 out1mf3 out1mf4 out1mf5
20		out1mf6 out1mf7 out1mf8 out1mf9
21	InMFTypes	trimf
22	OutMFTypes	linear
23	InMFParams	[-0.25 0.9883 2.265 0] [1.002 2.236 3.502 0] [2.211 3.498 4.75 0]
24		[-23.5 1 25.5 0] [0.9998 25.5 50 0] [25.5 50 74.5 0]
25	OutMFParams	[0.8147 0.04792 0.4771 0]
26		[0.2715 0.05442 -0.2307 0]
27		[-0.8405 0.04764 0.1414 0]
28		[0.898 0.0609 -0.5483 0]
29		[0.2619 0.06082 -0.6229 0]
30		[-0.8571 0.06336 0.2343 0]
31		[0.9153 0.07682 -1.781 0]
32		[0.2681 0.07687 -1.401 0]
33		[-0.8753 0.07592 0.7658 0]
34	Rule Antecedent	[1 1] [1 2] [1 3] [2 1] [2 2] [2 3] [3 1] [3 2] [3 3]
35	Rule Consequent	1 2 3 4 5 6 7 8 9
36	Rule Weight	1 1 1 1 1 1 1 1 1
37	Rule Connection	1 1 1 1 1 1 1 1 1

Appendix VI-3 ANFIS Training Data (2-D Recursive) for System D

Training Data

1	1.0000	1	1.33
2	1.2800	1	1.35
3	1.5600	1	1.4
4	1.8300	1	1.46
5	2.1100	1	1.5
6	2.3900	1	1.5
7	2.6700	1	1.5
8	2.9400	1	1.5
9	3.2200	1	1.5
10	3.5000	1	1.5
11	1.0000	6.44	1.37
12	1.2800	6.44	1.37
13	1.5600	6.44	1.4
14	1.8300	6.44	1.46
15	2.1100	6.44	1.5
16	2.3900	6.44	1.5
17	2.6700	6.44	1.5
18	2.9400	6.44	1.5
19	3.2200	6.44	1.5
20	3.5000	6.44	1.5
21	1.0000	11.89	1.33
22	1.2800	11.89	1.35
23	1.5600	11.89	1.4
24	1.8300	11.89	1.46
25	2.1100	11.89	1.5
26	2.3900	11.89	1.5
27	2.6700	11.89	1.5
28	2.9400	11.89	1.5
29	3.2200	11.89	1.5
30	3.5000	11.89	1.5
31	1.0000	17.33	1.36
32	1.2800	17.33	1.37
33	1.5600	17.33	1.42
34	1.8300	17.33	1.5
35	2.1100	17.33	1.5
36	2.3900	17.33	1.5
37	2.6700	17.33	1.5
38	2.9400	17.33	1.5
39	3.2200	17.33	1.5
40	3.5000	17.33	1.5
41	1.0000	22.78	1.41

Checking Data

1	0.5000	2	1.39
2	0.7200	2	1.35
3	0.9400	2	1.33
4	1.1700	2	1.34
5	1.3900	2	1.37
6	1.6100	2	1.41
7	1.8300	2	1.46
8	2.0600	2	1.5
9	2.2800	2	1.5
10	2.5000	2	1.5
11	0.5000	6.78	1.39
12	0.7200	6.78	1.36
13	0.9400	6.78	1.36
14	1.1700	6.78	1.36
15	1.3900	6.78	1.37
16	1.6100	6.78	1.41
17	1.8300	6.78	1.46
18	2.0600	6.78	1.5
19	2.2800	6.78	1.5
20	2.5000	6.78	1.5
21	0.5000	11.56	1.39
22	0.7200	11.56	1.35
23	0.9400	11.56	1.33
24	1.1700	11.56	1.34
25	1.3900	11.56	1.37
26	1.6100	11.56	1.41
27	1.8300	11.56	1.46
28	2.0600	11.56	1.5
29	2.2800	11.56	1.5
30	2.5000	11.56	1.5
31	0.5000	16.33	1.41
32	0.7200	16.33	1.37
33	0.9400	16.33	1.35
34	1.1700	16.33	1.35
35	1.3900	16.33	1.38
36	1.6100	16.33	1.43
37	1.8300	16.33	1.5
38	2.0600	16.33	1.5
39	2.2800	16.33	1.5
40	2.5000	16.33	1.5
41	0.5000	21.11	1.44

42	1.2800	22.78	1.41
43	1.5600	22.78	1.46
44	1.8300	22.78	1.5
45	2.1100	22.78	1.5
46	2.3900	22.78	1.5
47	2.6700	22.78	1.5
48	2.9400	22.78	1.5
49	3.2200	22.78	1.5
50	3.5000	22.78	1.5
51	1.0000	28.22	1.48
52	1.2800	28.22	1.48
53	1.5600	28.22	1.5
54	1.8300	28.22	1.5
55	2.1100	28.22	1.5
56	2.3900	28.22	1.5
57	2.6700	28.22	1.5
58	2.9400	28.22	1.5
59	3.2200	28.22	1.5
60	3.5000	28.22	1.5
61	1.0000	33.67	1.55
62	1.2800	33.67	1.55
63	1.5600	33.67	1.51
64	1.8300	33.67	1.5
65	2.1100	33.67	1.5
66	2.3900	33.67	1.5
67	2.6700	33.67	1.5
68	2.9400	33.67	1.5
69	3.2200	33.67	1.5
70	3.5000	33.67	1.5
71	1.0000	39.11	1.61
72	1.2800	39.11	1.61
73	1.5600	39.11	1.55
74	1.8300	39.11	1.5
75	2.1100	39.11	1.5
76	2.3900	39.11	1.5
77	2.6700	39.11	1.5
78	2.9400	39.11	1.5
79	3.2200	39.11	1.5
80	3.5000	39.11	1.5
81	1.0000	44.56	1.65
82	1.2800	44.56	1.64
83	1.5600	44.56	1.59
84	1.8300	44.56	1.51
85	2.1100	44.56	1.5

42	0.7200	21.11	1.4
43	0.9400	21.11	1.4
44	1.1700	21.11	1.4
45	1.3900	21.11	1.41
46	1.6100	21.11	1.46
47	1.8300	21.11	1.5
48	2.0600	21.11	1.5
49	2.2800	21.11	1.5
50	2.5000	21.11	1.5
51	0.5000	25.89	1.47
52	0.7200	25.89	1.45
53	0.9400	25.89	1.45
54	1.1700	25.89	1.45
55	1.3900	25.89	1.45
56	1.6100	25.89	1.5
57	1.8300	25.89	1.5
58	2.0600	25.89	1.5
59	2.2800	25.89	1.5
60	2.5000	25.89	1.5
61	0.5000	30.67	1.5
62	0.7200	30.67	1.51
63	0.9400	30.67	1.51
64	1.1700	30.67	1.51
65	1.3900	30.67	1.51
66	1.6100	30.67	1.5
67	1.8300	30.67	1.5
68	2.0600	30.67	1.5
69	2.2800	30.67	1.5
70	2.5000	30.67	1.5
71	0.5000	35.44	1.54
72	0.7200	35.44	1.57
73	0.9400	35.44	1.57
74	1.1700	35.44	1.57
75	1.3900	35.44	1.56
76	1.6100	35.44	1.51
77	1.8300	35.44	1.5
78	2.0600	35.44	1.5
79	2.2800	35.44	1.5
80	2.5000	35.44	1.5
81	0.5000	40.22	1.57
82	0.7200	40.22	1.61
83	0.9400	40.22	1.62
84	1.1700	40.22	1.62
85	1.3900	40.22	1.6

86	2.3900	44.56	1.5
87	2.6700	44.56	1.5
88	2.9400	44.56	1.5
89	3.2200	44.56	1.5
90	3.5000	44.56	1.5
91	1.0000	50	1.67
92	1.2800	50	1.65
93	1.5600	50	1.6
94	1.8300	50	1.54
95	2.1100	50	1.5
96	2.3900	50	1.5
97	2.6700	50	1.5
98	2.9400	50	1.5
99	3.2200	50	1.5
100	3.5000	50	1.5

86	1.6100	40.22	1.55
87	1.8300	40.22	1.5
88	2.0600	40.22	1.5
89	2.2800	40.22	1.5
90	2.5000	40.22	1.5
91	0.5000	45	1.6
92	0.7200	45	1.64
93	0.9400	45	1.65
94	1.1700	45	1.65
95	1.3900	45	1.62
96	1.6100	45	1.58
97	1.8300	45	1.52
98	2.0600	45	1.5
99	2.2800	45	1.5
100	2.5000	45	1.5

Appendix VI-4 Equations and Matlab program for Figure 6.1

Recall equation (3.34) in Chapter 3:

$$P_{success} = \int_{G^-}^{G^+} P_y dy \prod_j \int_{-\infty}^{B_j} P_{x_j} dx_j \qquad (3.34)$$

The successful detection process for M-n-PAPM modulation can be demonstrated by the following figure:

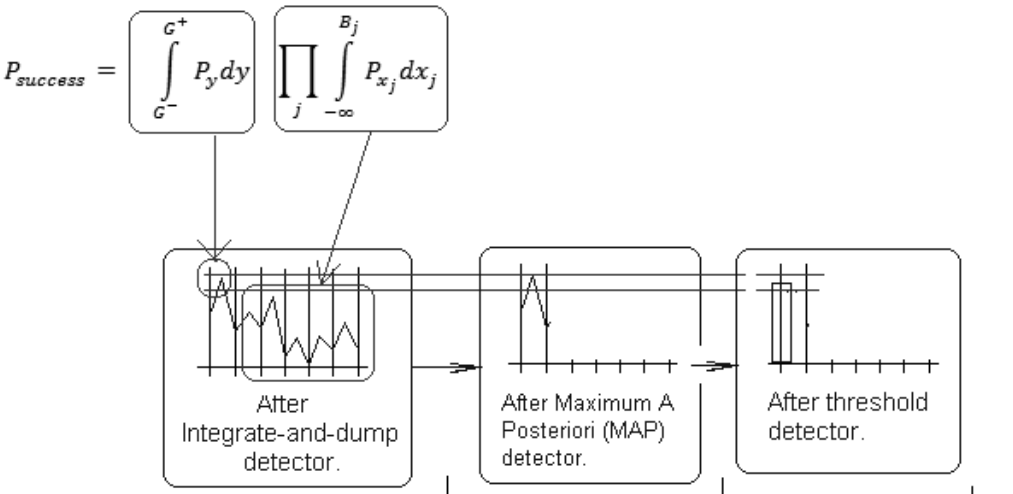

OOK	used	------	used
PAM	used	------	used
PPM	used	used	------
PAPM	used	used	used

In above figure, the PAPM pulses first gone through integrate and dump detector, the pulse with maximum amplitude can be identified, then MAP detector can map the detected pulse to its symbol sequence position (same process as PPM demodulation). The resulting pulse then feed to a threshold detector to determine its amplitude levels (same process as PAM demodulation). Thus the received PAPM pulse can be correctly detected. In equation (3.34), the first part is the probability for the primary chips, which chooses the maximum value from

incoming pulse sequences. The second part calculates the probability of the secondary pulses in the pulse sequences. To calculate the detection error of the M-n-PAPM modulation, equation (3.36) can be used. Detailed discussion on how to obtain equation (3.36) and meaning of its variables can be found in Chapter 3.

$$P_{de} = 1 - Pcd = \frac{1}{T_i}\int_{dt}^{T_i}\frac{1}{C}\sum_{C}(1 - P_{success}) \tag{3.36}$$

Combine equation (3.34) and (3.36) yields

$$P_{de} = \frac{1}{T_i}\int_{dt}^{T_i}\frac{1}{C}\sum_{C}\left(1 - \int_{G^-}^{G^+} P_y dy \prod_{j}\int_{-\infty}^{B_j} P_{x_j} dx_j\right) \tag{VI - 4 a}$$

Where $P_x = \frac{1}{\sigma\sqrt{2\pi}} e^{-\frac{x^2}{2\sigma}}$, C is the set of all possible chip sequences combinations, $C = (M \cdot n)^{(\frac{K}{n}+1)}$, M is the number of amplitude level, n is number of slot number, k is length of previous sequence length, T_i is the ambient light noise interference period, the threshold levels can be found in followings:

$$x_j < B_j = y + G_j \tag{3.30}$$

$$G^- < y < G^+ \tag{3.31}$$

Where G_j is the amplitude level gap $G_j = z_i - z_j$, G^- and G^+ were defined as following

$$G^+ = \begin{cases} \theta_m - Z_i, & m < M \\ +\infty, & m = M \end{cases}$$

$$G^- = \begin{cases} \theta_{m-1} - Z_i, & m > 0 \\ -\infty, & m = 0 \end{cases} \tag{3.32}$$

The MAP detection was same as the PPM case and combined PAPM pulse detection can be demonstrated in the following figures.

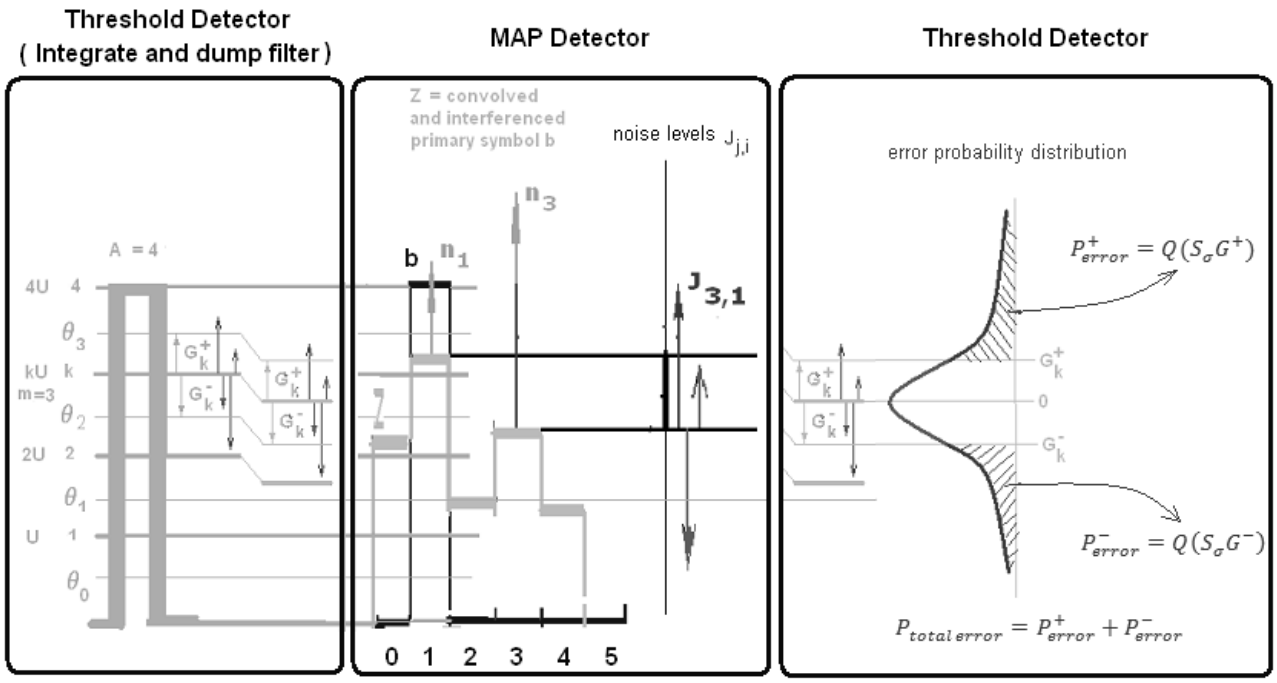

In order to simulate the BER for M-n-PAPM modulation scheme under multipath ISI and artificial light interference, a Matlab program was written with the following functions:

1. Main_PAPM_default
2. am_prepwere
3. am_vi
4. betaPortion
5. convolve
6. erfh
7. SimulatePAPM

Similar to PAM and PPM case, function 2,3,4,5,6 were public functions and same as the other two cases. Function 1 and function 7 were different and specific for PAPM scheme only. The following listed the variable used and details of function 1 and 7.

Variables

1. Data rate

Data rate range from 0Mbps to 140Mbps, step of 10Mbps.

2. Ceiling height

Three cases were considered, with H=1, 2, 3 (m)

3. M, n Value

M=1, n=4

4. SNR

SNR=6 dB

5. Artificial light factor

As artificial light was not considered for this case, thus the power ratio ASR was not enabled.

Functions details

1. Main_PAPM_default

```
%Calculate BER for PAPM with ISI, and ambient light.
tic %start timer
Rbindex=1;%data rate Rb index

b=0;%initial BER value

global Rb;

for Rb=1e6:10e6:140e6

%============================
% Noise Model Selection
%----------------------------
      global shotNoisePresented
      shotNoisePresented=1;
      global amInteferenceSummationPoints;
      %global ambientLightPresented
      %ambientLightPresented=0
        amInteferenceSummationPoints=2;
      %      If this parameter>1 then ambient noise is taken into account,
```

```
%       and this parameter is a number of integration points.
%       Set this parameter to 1 to disable ambient light.
%       Integration accracy is proportional to this parameter.
%============================

%============================
% Default parameters
%----------------------------
        global ceilingHeight
        global Amax
        global L
        global SNR
        global amSAR
        global amInterferencePeriodTi
        ceilingHeight=1; %Height of the room.
        Amax=1; %Number of non-zero  amplitude levels.
        L=4; %Maximum number of chips in symbol
        SNR=6; %Signal To Noise Ratio, db
        amInterferencePeriodTi=25.0e-6; %In seconds.
        amSAR=0.02; %Signal to Ambient light Ratio.  = amSAR = 1/K where K
                        %is similar parameter from [Wong et al].
%============================

%============================
%Derivative parameters:
global a %ISI length parameter in chips. Parameter of h-function.
global SN %SNR not in dB form:
global T %Chip length, seconds.
global avLength %Average number of chips in symbol.
global aphabetCount %Number of symbols in alphabet
global M %Bits per symbol
global bitsPerChip
global scaled_chip_length %T/a
global tapsNumber %"Memory" of multipath channel.
global beta  %Discretized h., Array
global lambda %(min non-zero Intensity)/average Intensity:
%============================

%============================
% Prepwere parameters
%----------------------------
      a=2.0*ceilingHeight/3e8;

      avLength=L;
      aphabetCount=L*Amax; %

      M=log(aphabetCount)/log(2.0);
      lambda=2*L/(Amax+1); %

      %Part II:
```

```
        bitsPerChip=M/avLength;
           T=bitsPerChip/Rb;
           scaled_chip_length=T/a;

%-------------------------------------------------------
%estimation of size of sequence beta:
%- - - - - - - - - - - - - - - - - - - - - - - - - -
        accuracyEps=1.0e-3;
        hThresholdTs= (1.0/accuracyEps)^(1.0/6.0) - 1;
        if hThresholdTs<1.0
          hThresholdTs=1.0;
        end
        hThresholdTs;
        %mark temporary variable with "w":
        wtapsNumber = hThresholdTs/scaled_chip_length;
        tapsNumber  = (floor(wtapsNumber)) + 1; %1 is taken for safety.

%Convert SN from dB to numbers:
 %SNR
SN=exp(SNR/10.0*log(10.0));
%============================

           beta=[1:tapsNumber];
        %Create beta:
           for k=1:tapsNumber
                              beta(k)=betaPortion(k-1, scaled_chip_length);
        end
        beta %display beta value
        q=[1:tapsNumber];

        %hold on
        %b=0;%Initial BER value
        am_prepwere();%prepwere Ambient Noise parameters
        b(Rbindex)=simulatePAPM();%BER value
        %b=simulatePAPM();
        %b(Rbindex)=simulatePAPM();
        Rbindex=Rbindex+1;%data rate counter
        %plot(Rb,b,'rs-');
        %semilogy(SNR,b,'rs-');
        %hold on;

end

        Rb=1:10:140;
        semilogy((Rb/(L/(log2(L*Amax)))),b,'rs-');
        hold on;
toc

%Find Data Rate with minimum BER value
```

```
for i=1:length(b)
   if b(i)==min(b)
     j=i;
   end
   %i=i+1;
end

Rmin=(Rb(j)/(L/(log2(L*Amax))));
```

7. SimulatePAPM

```
%Finds symbol error probability (symbol error rate) for PAPM
%for given channel over all chip sequences, all noise events, and all ambient light
%events.
%It can be speculated that BER_symb=BER/M     M - bits/symmbol
%In this procedure, P is denoted as BAmb.

function retv=simulatePAPM()

      global a  %impulse response parameter
      global shotNoisePresented %decision on noise value
      global amSAR %signal to artificial light power ratio
      global amInteferenceSummationPoints %resolution for artificial interferences
      global amInterferencePeriodTi %time variable applied to the lighting model
      global Amax % number of amplitude
      global L % slot number
      global M %number of bits
      global SN %signal to noise ratio
      global T % integration time period for artificial light model
      global tapsNumber %number of pulses selected
      global lambda % ratio of peak and average intensity
      global scaled_chip_length %number of chips convolved in the channel


      %Numerical integration amount:
      NIPoints=100;


      %-------------------------------------------------
      %Prevent errors:
      %- - - - - - - - - - - - - - - - - - - - - - - -
      tapsSimulationLimit=10000;
            if tapsSimulationLimit<=tapsNumber
                  message='Taps Number limit exceeded.'
        return;
      end
      if L<2
```

```
  message='Incorrect value: L<2.'
  return;
end
%- - - - - - - - - - - - - - - - - - - - - - - -
%Prevent errors:
%-----------------------------------------------

%Adjust x-scale adopted in MatLab for erfc:
sqrt2m1=1.0/sqrt(2);

%First, find out number of preceding symbols:
sslots=0;
%try to take enough slots to cover ISI tapsNumber:
      while sslots*L<tapsNumber
 sslots=sslots+1;
end

%Recalculated taps number occupied by preceding symbols:
pastTaps=sslots*L;

%Recalculate tapsNumber including primary symbol:
      symTapsNumber=pastTaps+L;
b=[1:symTapsNumber];
      bh=[1:symTapsNumber];
      %Ambient contribution to primary symbol chips:
      V=[1:L];

%Set initial value
overFlowProtector=1.0;

%-------------------------------------
%Generate symbols and chip sequences.
%- - - - - - - - - - - - - - - - - -
      AAmax=Amax;  %Number of active levels.
      %For PAM Amax+1.
      overFlowProtector=1.0*L*AAmax;
      if overFlowProtector>2.0E9
            sprintf(' L*AAmax>2E9, ~ bit limit reached.');
  L
  AAmax
  return;
      end

      symSlotWeight=L*AAmax;

%Find out number of all combinations of preceding symbols:
symbol_events=1;
      overFlowProtector=1.0;
      for i=1:sslots
            overFlowProtector=overFlowProtector*symSlotWeight;
```

```
                if overFlowProtector>2.0E9
                  sprintf('symSlotWeight^preSymbolSlots>2E9, ~ bit limit
                                                          reached.');
        L
        AAmax
        preSymbolSlots
        return;
                end
                symbol_events=symbol_events*symSlotWeight;  %total  number
of symbol_events
         end

    %symbol_events=(L*AAmax)^sslots
    %set limit to 1E6
        PPMSymbolSimulationLimit=1e6;
        %Protect against long calculations:
        if PPMSymbolSimulationLimit<=symbol_events
                sprintf('Symbol Slots Limit exceeded.');
      symbol_events
      PPMSymbolSimulationLimit
                return;
    end
    %- - - - - - - - - - - - - - - - - -
    %Generate symbols and chip sequences.
    %-----------------------------------

    %Shortcuts:
    amK=1.0/amSAR;  %Parameter K-declwered in [7, Wong, ...]

    weight_ISI_NOISE=1.0/symbol_events/(symSlotWeight*M);

    %Prepwere constants for numerical integration:
    GaussNorm=1.0/sqrt(2.0*pi);


    BAmb=0.0;%initial BER value

       amInterferenceStep=amInterferencePeriodTi/amInteferenceSummationPoi
       nts;
    for iXAm=0:amInteferenceSummationPoints-1

          tt=amInterferenceStep*iXAm;
       BB=0.0; %"BER under integration sign" by time.

       %Prepwere ambient contributions to current symbol:
       for i=0:L-1
               V(i+1)=amK*am_vi(tt+T*i, T);
       end
```

```
        for e=0:symbol_events-1

%-------------------------------------
%Generate symbols and chip sequences.
%- - - - - - - - - - - - - - - - - -
%
%   Symbol is encoded as couple data
%         (d,A) = (PostionOfPrimaryChip, AmplitudeLevelOfPrimaryChip).
%   0<=d<=L-1, 0<A<=Amax
%
%   (d,A) is encoded as number sym:
%   sym=d*Amax+(A-1)
%
%   Hence, sym has range 0<=sym<symSlotWeight=L*Amax.
%   In turn, for sequence of Lps symbols, the full number
%   of possible sequences is
%
%   symbol_events = Lps ^ symSlotWeight
%
%   Notations in program:
%     preSymbolSlots=Lps
%     primaryChip=d
%
                mask=symbol_events;%mask=symbol_events=(L*AAmax)^sslots
            for slot=0:sslots-1
                %sym=rem(mask,L);
               sym=rem(mask,symSlotWeight);                % sym=
((L*AAmax)^sslots)/(L*AAmax)=(L*AAmax)^(sslots-1);
               mask=mask-sym;%
               mask=mask/L;%


               amplitude=rem(sym,L);
               primaryChip=(sym-amplitude)/L;
               amplitude=amplitude+1;

               for i=0:L-1
                  b(slot*L+i+1)=0;
                  if primaryChip==i
                    b(slot*L+i+1)=amplitude;
                  end
               end
            end
                %- - - - - - - - - - - - - - - - - -
                %Generate symbols and chip sequences.
                %-------------------------------------

            %Cycle through primary chips:
            for i=0:L-1
               %Fill primary symbol's chips with zeros:
```

```
   for k=0:L-1
  b(sslots*L+k+1)=0;
end

for ia=1:Amax

   %Make i-th primary chip non-zero:

   b(sslots*L+i+1)=ia;


   %Calculate convolved chips for primary symbol:
   %from pastTaps+1 to pastTaps+L:
         bh=convolve(pastTaps+1,b,bh);

   Zi=lambda*bh(pastTaps+i+1);

   if amInteferenceSummationPoints>1
     Zi=Zi+V(i+1);
   end

   %threshold for PAPM detector
   Gplus=lambda*(ia+0.5)-Zi;
   Gminus=lambda*(ia-0.5)-Zi;
   %Setup integration over y.

   skipSummation = false;
   normedGplus=0.0;
   normedGminus=0.0;
   %Prepwere for integrate and avoid extreme case.
   if ~shotNoisePresented
       if Gplus<0.0 || Gminus>0.0
          skipSummation=true;
       end
   else
       normedGplus=Gplus*SN;
       normedGminus=Gminus*SN;

       %Set limits for extreme levels for PAPM:
       if 1==ia
         normedGminus=-100.0;
       end
       if Amax==ia
         normedGplus=100.0;
       end
       %Hence, when Amax==1, then limit of integration for
       %y is -oo to +oo.

       normedGplus=min(10.0,normedGplus);
             normedGminus=max(-10.0,normedGminus);
```

```
                    if normedGplus<-9.0
                      skipSummation=true;
                    end
                    if normedGminus>9.0
                      skipSummation=true;
                    end

                end
                if skipSummation
                  continue;
                end

                PSuccess=0.0;
                % start integration
                NIStep= (normedGplus-normedGminus)/NIPoints;
                for iNIy=0:NIPoints-1
                   %Take values in the middle of intervals: add 0.5 to index:
                   y=(iNIy+0.5)*NIStep+normedGminus;% start integration from
normedGminus to normedGplus with step = NIStep
                   yWeight=GaussNorm*exp(-y.*y*0.5).*NIStep;


                   %Cycle through competing chips:
                   PRODUCT=1.0;%initial Product operator value
                   for j=0:L-1
                        if i==j %avoid case where Zi=Zj
                        continue;
                      end
                      Zj=lambda*bh(pastTaps+j+1);
                      if amInteferenceSummationPoints>1
                        Zj=Zj+V(j+1);
                      end
                      G=Zi-Zj; %contribution from noise contribution from Zi to Zj
                      SNRf=sqrt2m1; %SNR factor
                      if ~shotNoisePresented %skip BER calculation when no shot
noise
                        SNRf=-1;
                      end
                      %Calculate correct detection of maximum
                      %pulse (primary pulse), for the first (MAP) detector, ignore
negative values (error)
                      qq=max((1-erfh(y+G*SN,SNRf)),0.0);
                      PRODUCT=PRODUCT.*qq; %Calculate all consequent
successful event using product operation
                         end %Cycle through competing chips
                   PSuccess=PSuccess+yWeight.*PRODUCT;
                end %Cycle through y-integration
                BB=BB+1.0-PSuccess;%calculate detection error
             end %Cycle through amplitude levels of primary chip.
          end % Cycle through primary chips, i=0:L-1 )
```

```
        end % cycle through u-sequence, e
        BAmb=BAmb+weight_ISI_NOISE*BB;%averaging over all possible symbole sequence combinations
    end % total ambient noise interference , start from iXAm=0
    BAmb=BAmb/amInteferenceSummationPoints % averaging interference over number of interference points
    retv=BAmb;
end
```

References:

[1] J. Beckett, "The Internet phenomenon," *Engineering Science and Education Journal* vol. 5, pp. 102-104, June 1996 1996.

[2] W. A. Gambling, "Possibilities of optical communications," *Engineering*, vol. 198, p. 776, 1964 1964.

[3] M. Macedonia, "Why digital entertainment drives the need for speed," *Computer*, vol. 33, pp. 124-127, 2000.

[4] T. S. Rappaport, "Wireless personal communications: trends and challenges," *IEEE Antennas and Propagation Magazine,* vol. 33, pp. 19-29, 1991.

[5] R. Dawson, "LED bandwidth improvement by bipolar pulsing," *IEEE Journal of Quantum Electronics,* vol. 16, pp. 697-699, Jul 1980 1980.

[6] T. H. Meng, B. M. Gordon, E. K. Tsern, and A. C. Hung, "Portable video-on-demand in wireless communication," *Proceedings of the IEEE,* vol. 83, pp. 659-680, April 1995 1995.

[7] W. A. Gambling, "The rise and rise of optical fibers," *Selected Topics in Quantum Electronics, IEEE Journal of,* vol. 6, pp. 1084-1093, 2000.

[8] P. Van der Gracht and R. Donaldson, "Communication Using Pseudonoise Modulation on Electric Power Distribution Circuits," *IEEE Transactions on Communications, [legacy, pre - 1988],* vol. 33, pp. 964-974, September, 1985 1985.

[9] T. J. Kostas, M. S. Borella, I. Sidhu, G. M. Schuster, J. Grabiec, and J. Mahler, "Real-time voice over packet-switched networks," *Network, IEEE,* vol. 12, pp. 18-27, 1998.

[10] F. R. Gfeller and U. Bapst, "Wireless in-house data communication via diffuse Infrared radiation," *Proceedings of the IEEE,* vol. 67, pp. 1474-1486, November, 1979 1979.

[11] F. Gfeller and W. Hirt, "A robust wireless Infrared system with channel reciprocity," *Communications Magazine, IEEE,* vol. 36, pp. 100-106, 1998.

[12] J. R. Barry, *Wireless Infrared communications*. Boston, Mass. ; London: Kluwer Academic, 1994.

[13] D. J. T. Heatley, D. R. Wisely, I. Neild, and P. Cochrane, "Optical wireless: the story so far," *Communications Magazine, IEEE,* vol. 36, pp. 72-74, 79-82, 1998.

[14] M. J. McCullagh, P. P. Smyth, D. R. Wisely, and P. L. Eardley, "Optical wireless LANs: applications and systems," in *IET Colloquium on Cordless Computing - Systems and User Experience* London: The Institution of Engineering and Technology, 1993, pp. 8/1-8/3.

[15] J. M. Kahn and J. R. Barry, "Wireless Infrared communications," *Proceedings of the IEEE,* vol. 85, pp. 265-298, Feb, 1997 1997.

[16] W. Hirt, M. Hassner, and N. Heise, "IrDA-VFIr (16 Mb/s): modulation code and system design," *Personal Communications, IEEE [see also IEEE Wireless Communications],* vol. 8, pp. 58-71, 2001.

[17] V. Jungnickel, T. Haustein, A. Forck, and C. v. Helmolt, "155 Mbit/s wireless transmission with imaging Infrared receiver," *Electronics Letters*, vol. 37, pp. 314-315, 1 March 2001 2001.
[18] IrDA, "Market Requirements for IrBurst," *Infrared Data Association*, September 18, 2003 September 2003.
[19] IrDA, "Marketing Requirement for UFIR," *Infrared Data Association*, October 14, 2002 October 2002.
[20] IrDA, "Proposed Changes to Infrared Data Association Serial Infrared Physical Layer Link Specification for UFIR (100Mbit/s) Addition," *Infrared Data Association*, February 21, 2005 February 2005.
[21] S. Hranilovic, *Wireless optical communication systems*. New York: Springer, 2005.
[22] R. Becher, M. Dillinger, M. Haardt, and W. Mohr, "Broadband wireless access and future communication networks," *Proceedings of the IEEE*, vol. 89, pp. 58-75, 2001.
[23] F. P. Kapron, D. B. Keck, and R. D. Maurer, "Radiation losses in glass optical fibers," *Appl. Phys. Lett.*, vol. 17, pp. 423-425, 1970.
[24] M. Cvijetic, *Optical transmission systems engineering*. Boston ; London: Artech House, 2004.
[25] N. Jayant, *Broadband last mile : access technologies for multimedia communications*. Boca Raton, FL: Taylor & Francis/CRC Press, 2005.
[26] N. P. Reid, *Fixed broadband wireless access networks and services*. New York, N.Y. ; [Great Britain]: Wiley Computer Pub., 2002.
[27] J. Newbury, "Communication requirements and standards for low voltage mains signalling," *Power Delivery, IEEE Transactions on*, vol. 13, pp. 46-52, 1998.
[28] S. Arnon, "Optimization of urban optical wireless communication systems," *Wireless Communications, IEEE Transactions on*, vol. 2, pp. 626-629, 2003.
[29] J. G. Proakis, *Digital communications*, 3rd ed. New York; London: McGraw-Hill, 1995.
[30] S. Patrick, "CableFree Virtual-Point-to-MultiPoint™ White Papers," August, 2000 (Accessed 28th May, 2007).
[31] A. J. C. Moreira, R. T. Valadas, and A. M. de Oliveira Duarte, "Performance of Infrared transmission systems under ambient light interference," *Optoelectronics, IEE Proceedings -*, vol. 143, pp. 339-346, 1996.
[32] http://www.irda.org/, accessed 20th July 2009.
[33] WHO, "2003 WHO research agenda for radio frequency fields." vol. 2009, 2003.
[34] Wikipedia, "Nervous system." vol. 2009, 2009.
[35] O. S. H. Administration, "Radiofrequency and Microwave Radiation - Health Effects." vol. 2009, 2009.
[36] Z. Ghassemlooy and A. R. Hayes, "Digital pulse interval modulation for IR communication systems - a review," *International Journal of Communication Systems*, vol. 13, pp. 519-536, 2000.
[37] S. Da-Shan and J. M. Kahn, "Differential pulse-position modulation for power-efficient optical communication," *Communications, IEEE Transactions on*, vol. 47, pp. 1201-1210, 1999.

[38] M. D. Audeh, J. M. Kahn, and J. R. Barry, "Performance of pulse-position modulation on measured non-directed indoor Infrared channels," *Communications, IEEE Transactions on,* vol. 44, pp. 654-659, 1996.

[39] J. B. Carruthers and J. M. Kahn, "Multiple-subcarrier modulation for nondirected wireless Infrared communication," *Selected Areas in Communications, IEEE Journal on,* vol. 14, pp. 538-546, April 1996 1996.

[40] L. Diana and J. M. Kahn, "Rate-adaptive modulation techniques for Infrared wirelesscommunications," in *IEEE International Conference on Communications, 1999* vol. Vol. 1 Vancouver,Canada, 6-10 June, 1999, pp. 597 - 603.

[41] J. M. Garrido-Balsells, J. M. Garrido-Balsells, A. Garcia-Zambrana, and A. Puerta-Notario, "Spectral characterisation of variable weight MPPM modulation technique," *Electronics Letters,* vol. 42, pp. 1109-1110, 2006.

[42] M. S. Leeson, "Pulse position modulation for spectrum-sliced transmission," *Photonics Technology Letters, IEEE,* vol. 16, pp. 1191-1193, 2004.

[43] H. Sugiyama and K. Nosu, "MPPM: a method for improving the band-utilization efficiency in optical PPM," *Lightwave Technology, Journal of,* vol. 7, pp. 465-472, March 1989 1989.

[44] G. E. Atkin and K. S. L. Fung, "Coded multipulse modulation in optical communication systems," *Communications, IEEE Transactions on,* vol. 42, pp. 574-582, 1994.

[45] G. C. Clark and J. B. Cain, *Error-correction coding for digital communications*. New York ; London: Plenum Press, 1981.

[46] D. C. M. Lee and J. M. Kahn, "Coding and equalization for PPM on wireless Infrared channels," *Communications, IEEE Transactions on,* vol. 47, pp. 255-260, 1999.

[47] H. Park and J. R. Barry, "Trellis-coded multiple-pulse-position modulation for wireless Infrared communications," *Communications, IEEE Transactions on,* vol. 52, pp. 643-651, 2004.

[48] P. Djahani and J. M. Kahn, "Analysis of Infrared wireless links employing multibeam transmitters and imaging diversity receivers," *Communications, IEEE Transactions on,* vol. 48, pp. 2077-2088, 2000.

[49] J. B. Carruther and J. M. Kahn, "Angle diversity for nondirected wireless Infrared communication," *Communications, IEEE Transactions on,* vol. 48, pp. 960-969, 2000.

[50] M. D. Higgins, R. J. Green, and M. S. Leeson, "A Genetic Algorithm Method for Optical Wireless Channel Control," *Lightwave Technology, Journal of,* vol. 27, pp. 760-772, 2009.

[51] G. W. Marsh, G. W. Marsh, and J. M. Kahn, "Channel reuse strategies for indoor Infrared wireless communications," *Communications, IEEE Transactions on,* vol. 45, pp. 1280-1290, 1997.

[52] V. Jungnickel, V. Pohl, S. Nonnig, and C. von Helmolt, "A physical model of the wireless Infrared communication channel," *Selected Areas in Communications, IEEE Journal on,* vol. 20, pp. 631-640, 2002.

[53] J. B. Carruthers and J. M. Kahn, "Modeling of nondirected wireless Infrared channels," *Communications, IEEE Transactions on* vol. 45, pp. 1260-1268, 1997.

[54] J. R. Barry and J. M. Kahn, "Link Design for Non-Directed Wireless Infrared Communications," *Applied Optics*, vol. 34, pp. 3764-3776, July 1995.
[55] K.-P. Ho and J. M. Kahn, "Compound Parabolic Concentrators for Narrow-Band Wireless Infrared Receivers," *Optical Engineering*, vol. 34, pp. 1385-1395, May 1995.
[56] R. Ramirez-Iniguez and R. J. Green, "Totally internally reflecting optical antennas for wireless IR communication," in *IEEE Wireless Design Conference*, Piscataway, N.J. pp. 129-132, 2002, pp. 129-132.
[57] D. C. Lee and J. M. Kahn, "Experimental 25-Mb/s Wireless Infrared Link Using 4-PPM with Scalar Decision-Feedback Equalization," *IEEE International Conference on Communications, ICC98, 1998.*, vol. 1, pp. 26-30, June 7-11, 1998.
[58] G. W. Marsh and J. M. Kahn, "Performance Evaluation of Experimental 50-Mb/s Diffuse Infrared Wireless Link using On-Off Keying with Decision-Feedback Equalization," *IEEE Transactions on Communications*, vol. 44, pp. 1496 - 1504, 1996.
[59] R. J. Green, H. Joshi, M. D. Higgins, and M. S. Leeson, "Recent developments in indoor optical wireless systems," *Communications, IET*, vol. 2, pp. 3-10, 2008.
[60] Cablefree, "Cablefree Gigabit Product," *http://www.cablefreesolutions.com/cablefreeuk/products_fso.htm*, accessed 24/07/09.
[61] R. Ramirez-Iniguez, *Optical wireless communications : IR for wireless connectivity*. Boca Raton, Fla.: CRC Press, 2008.
[62] J. J. Chaturi Singh, K.K.Tripathi, "A Review of Indoor Optical Wireless Systems," *IETE Technical Review*, vol. 19, pp. 3-17, January-April 2002.
[63] R. Ramirez-Iniguez and R. J. Green, "Indoor optical wireless communications," *IEE Colloquium on Optical Wireless Communications (Ref. No. 1999/128),*, pp. 14/1-14/7, 1999.
[64] U. Sethakaset and T. A. Gulliver, "Differential amplitude pulse-position modulation for indoor wireless optical communications " *EURASIP Journal on Wireless Communications and Networking*, vol. 2005, pp. 3-11, March 2005 2005.
[65] Z. Ghassemlooy, A. R. Hayes, N. L. Seed, and E. D. Kaluarachchi, "Digital pulse interval modulation for optical communications," *Communications Magazine, IEEE*, vol. 36, pp. 95-99, 1998.
[66] S. Hranilovic and D. A. Johns, "A multilevel modulation scheme for high-speed wireless Infrared communications," *Proceedings of the IEEE International Symposium on Circuits and Systems*, vol. VI, pp. 338-341, 1999.
[67] J. J. Grubor, V. Langer, K.-D. , "Rate-adaptive multiple sub-carrier-based transmission for broadband Infrared wireless communication," *Optical Fiber Communication Conference, 2006 and the 2006 National Fiber Optic Engineers Conference, California, USA*, p. 10, 5-10 March 2006 5-10 March 2006
[68] K. K. Wong, T. O. Farrell, and M. Kiatweerasakul, "The performance of optical wireless OOK, 2-PPM and spread spectrum under the effects of multipath dispersion and artificial light interference," *International Journal of Communication Systems*, vol. 13, pp. 551-576, 2000.

[69] A. J. C. Moreira, R. T. Valadas, and A. M. de Oliveira Duarte, "Reducing the effects of artificial light interference in wireless Infrared transmission systems," in *Optical Free Space Communication Links, IEE Colloquium on*, 1996, pp. 5/1-510.

[70] H. Park, "PhD thesis, Coded modulation and equalization for wireless Infrared communications," School of Electrical and Computer Engineering, Georgia Institute of Technology, 1997, p. 135.

[71] Y. Zeng, R. J. Green, S. B. Sun, and M. S. Leeson, "Tunable Pulse Amplitude and Position Modulation Technique for Reliable Optical Wireless Communication Channels," *Journal of Communications*, vol. 2, pp. 22-28, March 2007 2007.

[72] G. Einarsson, *Principles of Lightwave Communications*. Chichester ; New York; Brisbane; Toronto; Singapore: Wiley, 1996.

[73] C. E. Shannon, "Communication in the presence of noise," *Proceedings of the IEEE*, vol. 72, pp. 1192-1201, 1984.

[74] S. Hranilovic and F. R. Kschischang, "Capacity bounds for power- and band-limited optical intensity channels corrupted by Gaussian noise," *Information Theory, IEEE Transactions on*, vol. 50, pp. 784-795, 2004.

[75] I. Bar-David, "Communication under the Poisson regime," *Information Theory, IEEE Transactions on*, vol. 15, pp. 31-37, Jan 1969 1969.

[76] T. H. Chan, S. Hranilovic, and F. R. Kschischang, "Capacity-achieving probability measure for conditionally Gaussian channels with bounded inputs," *Information Theory, IEEE Transactions on*, vol. 51, pp. 2073-2088, 2005.

[77] A. A. Farid and S. Hranilovic, "Upper and Lower Bounds on the Capacity of Wireless Optical Intensity Channels," in *IEEE International Symposium on Information Theory, 2007. ISIT 2007.* Nice, France, 2007, pp. 2416-2420.

[78] S. Dolinar, D. Divsalar, J. Hamkins, and F. Pollara, "Capacity of Pulse-Position Modulation (PPM) on Gaussian and Webb Channels," *TMO Progress Report 42-142, Jet Propulsion Laboratory, California Institute of Technology*, 2000.

[79] www.lasersafety.org.uk/, " The Royal Society for the Prevention of Accidents," Accessed May 2008.

[80] D Hash, J Hillery, and J. White, "IR RoomNet: Model and Measurement," in *IBM Communication ITL Conference* June 1986.

[81] J. R. Barry, J. M. Kahn, W. J. Krause, E. A. Lee, and D. G. Messerschmitt, "Simulation of multipath impulse response for indoor wireless optical channels," *Selected Areas in Communications, IEEE Journal on*, vol. 11, pp. 367-379, 1993.

[82] C. R. Lomba, R. T. Valadas, and A. M. d. O. Duarte, "Efficient simulation of the impulse response of the indoor wireless optical channel," *International Journal of Communication Systems*, vol. 13, pp. 537-549, 2000.

[83] J. B. Carruthers and P. Kannan, "Iterative site-based modeling for wireless Infrared channels," *Antennas and Propagation, IEEE Transactions on*, vol. 50, pp. 759-765, 2002.

[84] J. C. M. Adriano, T. V. Rui, and A. M. d. O. Duarte, "Optical interference produced by artificial light," *Wirel. Netw.*, vol. 3, pp. 131-140, 1997.

[85] A. J. C. Moreira, R. T. Valadas, and A. M. de Oliveira Duarte, "Characterisation and modelling of artificial light interference in optical wireless communication systems," in *Personal, Indoor and Mobile Radio Communications, 1995. PIMRC'95. 'Wireless: Merging onto the Information Superhighway'., Sixth IEEE International Symposium on*, 1995, pp. 326-331 vol.1.

[86] R. Narasimhan, M. D. Audeh, and J. M. Kahn, "Effect of electronic-ballast fluorescent lighting on wireless Infrared links," *Optoelectronics, IEE Proceedings* -, vol. 143, pp. 347-354, 1996.

[87] T. Ohtsuki, "Rate-adaptive indoor Infrared wireless communication systems using repeated and punctured convolutional codes," *Communications Letters, IEEE*, vol. 4, pp. 56-58, 2000.

[88] Z. Ghassemlooy and N. M. Aldibbiat, "Multilevel Digital Pulse Interval Modulation Scheme for Optical Wireless Communications," in *Transpwerent Optical Networks, 2006 International Conference on*, 2006, pp. 149-153.

[89] IrDA, "Infrared Data Association Serial Infrared Physical Layer Specification Version 1.4," *Infrared Data Association,* May 30th 2001 May 2001.

[90] R. Narasimhan, M. D. Audeh, and J. M. Kahn, "Effect of electronic-ballast fluorescent lighting on wireless Infrared links," in *Communications, 1996. ICC 96, Conference Record, Converging Technologies for Tomorrow's Applications. 1996 IEEE International Conference on*, 1996, pp. 1213-1219 vol.2.

[91] M. D. Audeh, J. M. Kahn, and J. R. Barry, "Decision-feedback equalization of pulse-position modulation on measured nondirected indoor Infrared channels," *Communications, IEEE Transactions on,* vol. 47, pp. 500-503, 1999.

[92] Z. Ghassemlooy, W. O. Popoola, S. Rajbhandari, M. Amiri, and S. Hashemi, "A synopsis of modulation techniques for wireless Infrared communication," in *International Conference on Transpwerent Optical Networks* Rome, Italy IEEE, 2007, pp. 1-6.

[93] S. J. Chapman, *MATLAB programming for engineers*. Pacific Grove, Calif. ; London: Brooks/Cole-Thomson Learning, 2002.

[94] A. Svensson, "An Introduction to Adaptive QAM Modulation Schemes for Known and Predicted Channels," *Proceedings of the IEEE,* vol. 95, pp. 2322-2336, 2007.

[95] Y. Zeng, R. J. Green, and M. S. Leeson, "Adaptive pulse amplitude and position modulation for optical wireless channels," in *The 2nd Institution of Engineering and Technology International Conference on Access Technologies, Cambridge, UK.* , 21-22 June 2006, pp. 13-16.

[96] IrDA, "Infrared Data Association Serial Infrared Physical Layer Measurement Guidelines Version 1.2.7," *Infrared Data Association,* February 2006.

[97] J. Grubor, V. Jungnickel, and K. D. Langer, "Bit-loading for modulation-adaptive transmission in Infrared wireless indoor communication," *IET Conference Publications,* vol. 2006, pp. 9-12, 2006.

[98] P. Norvig and S. J. Russell, *Artificial intelligence : a modern approach*. Upper Saddle River, N.J: Prentice Hall, 2003.

[99] M. Negnevitsky, *Artificial intelligence : a guide to intelligent systems*: Harlow ; Addison-Wesley, 2005.
[100] J. McCarthy, "WHAT IS ARTIFICIAL INTELLIGENCE?," Computer Science Department, Stanford University, September 2007.
[101] G. Lakemeyer and P. M.I.T, *The logic of knowledge bases*. Cambridge, Mass: MIT Press, 2000.
[102] D. J. Hand, *Principles of data mining*. Cambridge, Mass. ; London: MIT Press, 2001.
[103] A. P. Engelbrecht, *Computational intelligence : an introduction*. Chichester: J. Wiley & Sons, 2002.
[104] M. Ananda Rao, *Neural networks : algorithms and applications*. Pangbourne, Eng.: Alpha Science International, 2003.
[105] D. B. Fogel, *Evolutionary computation : toward a new philosophy of machine intelligence*, 2nd ed. New York: IEEE Press, 2000.
[106] N. Forbes, *Imitation of life : how biology is inspiring computing*. Cambridge, Mass.: MIT Press, 2004.
[107] T. J. Ross, *Fuzzy logic with engineering applications*, 2nd ed. Hoboken, N.J.: John Wiley, 2004.
[108] L. A. Zadeh, *Fuzzy sets and their applications to cognitive and decision processes*: Academic Press, 1975.
[109] H. T. Nguyen and E. Walker, *A first course in fuzzy logic*. Boca Raton, FL: Chapman & Hall/CRC, 2000.
[110] L. A. Zadeh, "Fuzzy sets," *Information and Control*, vol. 8, no.3, pp. 338-353, June 1965 June 1965.
[111] D. D. e. Hellendoorn, *Fuzzy model identification : selected approaches*. Berlin ; London: Springer, 1997.
[112] T. J. Ross, J. M. Booker, and W. J. Parkinson, "Fuzzy logic and probability applications : bridging the gap," in *ASA-SIAM series on statistics and applied probability* Philadelphia, Pa.: Society for Industrial and Applied Mathematics, 2002, pp. xxiii, 409 p. 26 cm.
[113] D. Driankov, H. Hellendoorn, and M. Reinfrank, *An introduction to fuzzy control*. Berlin ; New York: Springer-Verlag, 1993.
[114] J. M. Mendel, "Fuzzy logic systems for engineering: a tutorial," *Proceedings of the IEEE*, vol. 83, pp. 345-377, 1995.
[115] Mathworks, "Matlab Tutorial on Fuzzy Inference Systems (2009a)," 2009.
[116] E. H. Mamdani, "Applications of fuzzy logic to approximate reasoning using linguistic synthesis," *IEEE Transactions on Computers*, vol. C-26, pp. 1182-1191, 1977.
[117] K. Hirota and M. Sugeno, "Industrial applications of fuzzy technology in the world," in *Advances in fuzzy systems. applications and theory ; vol.2* Singapore ; River Edge, NJ: World Scientific, 1995, p. 380p.
[118] M. A. Denai, F. Palis, and A. Zeghbib, "ANFIS based modelling and control of non-linear systems : a tutorial," in *2004 IEEE International Conference on Systems, Man and Cybernetics*, , The Hague, The Netherlands, 10-13 Oct. 2004, pp. 3433-3438.
[119] L.-X. Wang, *Adaptive fuzzy systems and control : design and stability analysis*. Englewood Cliffs, N.J. ; London: PTR Prentice Hall,, 1994.
[120] J.-S. R. Jang, "ANFIS: adaptive-network-based fuzzy inference system," *IEEE Transactions on Systems, Man and Cybernetics*, vol. 23, pp. 665-685, May/Jun 1993 1993.